CONVECTIVE HEAT AND MASS TRANSFER IN A MICROPOLAR FLUID FLOW WITH CONVECTIVE BOUNDARY CONDITION

A THESIS SUBMITTED TO
NATIONAL INSTITUTE OF TECHNOLOGY WARANGAL, (T.S.)
FOR THE AWARD OF THE DEGREE OF
DOCTOR OF PHILOSOPHY
IN
MATHEMATICS

BY
TEEGALA PRADEEPA
(Roll No. 701439)

UNDER THE SUPERVISION OF
Dr. CH. RAMREDDY

DEPARTMENT OF MATHEMATICS
NATIONAL INSTITUTE OF TECHNOLOGY
WARANGAL-506004, INDIA

MAY 2017

C E R T I F I C A T E

This is to certify that the thesis entitled " **Convective Heat and Mass Transfer in a Micropolar Fluid Flow with Convective Boundary Condition** " submitted to National Institute of Technology Warangal, for the award of the degree of ***Doctor of Philosophy***, is the bonafide research work done by **Mrs. TEEGALA PRADEEPA** under my supervision. The contents of this thesis have not been submitted elsewhere for the award of any degree.

Dr. Ch. Ramreddy
Assistant Professor
Department of Mathematics
National Institute of Technology Warangal
Telangana State, INDIA

.

DECLARATION

This is to certify that the work presented in the thesis entitled **"Convective Heat and Mass Transfer in a Micropolar Fluid Flow with Convective Boundary Condition"**, is a bonafide work done by me under the supervision of **Dr. CH. RAMREDDY** and has not been submitted elsewhere for the award of any degree.

I declare that this written submission represents my ideas in my own words and where others' ideas or words have been included, I have adequately cited and referenced the original sources. I also declare that I have adhered to all principles of academic honesty and integrity and have not misrepresented or fabricated or falsified any idea / data / fact /source in my submission. I understand that any violation of the above will be a cause for disciplinary action by the Institute and can also evoke penal action from the sources which have thus not been properly cited or from whom proper permission has not been taken when needed.

T. Pradeepa

Roll No. 701439

Date:_____

ACKNOWLEDGEMENTS

I am most grateful to God for giving me his grace to achieve all I have so far. It is a rare privilege and boon that I could associate myself for pursuing my research work with Dr. Ch. Ramreddy, Assistant Professor of Mathematics, National Institute of Technology Warangal, India. I sincerely record my gratitude for his invaluable guidance and constant encouragement throughout the preparation of this thesis and his involvement and meticulous supervision while my work was in progress. With his inimitable qualities as a good teacher, he chiseled my path towards perfection. Ever since I met him, he has been a perpetual source of motivation, inspiration, encouragement and enlightenment. He is responsible for making the period of my research work as an educative and enjoyable learning experience. The thesis would not have seen the light of the day without his unrelenting support and cooperation. I deem it a privilege to have worked under his amiable guidance. My vocabulary is inadequate to express my gratitude.

I am greatly indebted to the dynamic personalities, Prof. G. Radhakrishnamacharya and Dr. D. Srinivasacharya, Department of Mathematics for their affectionate support, encouragement and for sparing their valuable time in bringing a proper form for presentation of the results in the thesis. It is not an exaggeration to state that without thier assistance and suggestions, this thesis would not have taken this form.

I am grateful to Prof. Debashis Dutta, Head, and former Heads, Prof. K.N.S. Kasi Viswanadham and Prof. J. V. Ramana Murthy, Department of Mathematics for providing necessary help and support throughout my research period.

I take this opportunity to thank the Prof. Y. N. Reddy, Department of Mathematics for his valuable suggestions, moral support and encouragement during my stay.

I thank the members of the Doctoral Scrutiny Committee, Prof. K.N.S. Kasi Viswanadham, Dr. D. Srinivasacharya, Department of Mathematics and Prof. P. Nagashewar Rao,

Department of Chemistry for their valuable suggestions, moral support and encouragement while my work was in progress.

I place on record my gratitude to Dr. J. Pranitha and all other faculty members of the Department of Mathematics, for their constant encouragement. Also, I thank the office staff.

I express my sincere thanks to Prof. G. R. C. Reddy, Director I/c, National Institute of Technology, Warangal for awarding me Institute Fellowship (MHRD, GoI) to carry out my research work. I thank him for his kind support and encouragement at every stage of this endeavor.

I owe my special thanks to Dr. K. Kaladhar, Dr. M. Krishna Prasad, Dr. M. Upendar, Dr. O. Surender, Dr. P. Vijay, Dr. G. Madhava Rao for their support. I thank Mrs. K. Hima Bindu, Mr. Md. Shafeeurrahaman, Mr. G. Venkata Suman, Mr. Ch. Venkata Rao, P. Naveen, Mr. P. Jagadeeshwar, Mr. I. Sreenath and all other research colleagues in the Department of mathematics and my friends, who helped me during my Ph.D for being cooperative and also for making my stay in the NITW campus fruitful and enjoyable every moment.

My deepest gratitude to my Parents, T. Prasad and T. Bhagya and in-laws, M. Sundaram and M. Navamani for their continuous support and constant encouragement over the years. My thanks, choked with emotion, to my sons M. Chaitanya and M. Sandeep for their understanding and adjustment while I missed them, when I was engrossed in my research. All of their love and affection have been motivating force behind what I am today.

Finally, and most importantly, I would like to thank my husband, M. Sunil Kumar for his support, patience and understanding. Without their help and encouragement, I would not have been finished this thesis.

. T. Pradeepa

A B S T R A C T

Modeling and analysis of the dynamics of micropolar fluids continue to be an area of intensive research activity. This stems from the evidence that these types of fluids may have a large variety of engineering and industrial applications. Micropolar fluids are defined as fluids consisting of randomly oriented molecules whose fluid elements undergo translational as well as rotational motions. The heat transfer problems in a micropolar fluid related to the convective boundary condition are more extensive and it occurs in realistic situations. The mathematical model of a micropolar fluid flow involving the convective boundary condition becomes slightly more complicated leading to the complex interactions of the fluid flow, heat and mass transfer mechanisms. An attempt has been made to analyze free and mixed convective flows of micropolar fluid and/or micropolar fluid saturated porous medium in the presence or absence of suction/injection, homogeneous-heterogeneous reactions, nonlinear convection, radiation, Biot number, Soret and viscous dissipation effects. The problems considered deal with vertical plate and truncated cone geometries.

The thesis consists of FOUR parts and EIGHT chapters. *Part-I* consists of a single chapter (Chapter - 1), which provides an introduction to the concepts in micropolar fluid, convective boundary condition, porous medium and a review of the pertinent literature. *Part-II* contains four chapters (i.e. Chapters 2, 3, 4 and 5) and deals with the similarity solution of a micropolar fluid along a vertical plate subject to the convective boundary condition. Chapter 2 deals with the effects of suction/injection on a permeable vertical plate immersed in a micropolar fluid whereas chapter 3 is an extension of chapter 2 in which Darcy porous medium is considered. Chapter 4 examines the effects of homogeneous-heterogeneous reactions on the nonlinear convective flow of a micropolar fluid in the presence of thermal radiation effect. Chapter 5 is an extension of chapter 4 in which Darcy porous medium is considered in the absence of radiation effect. *Part-III* consists of two chapters (Chapters 6 and 7) and deal with non-similarity solutions for the Soret and viscous dissipation effects on micropolar fluid flow over a truncated cone with and without non-Darcy porous medium. In all the above chapters, the nonlinear governing equations and their associated boundary conditions are initially cast into dimensionless form by using similarity transformations and/or non-similarity transformations. The resulting system of equations is solved using the *Spectral Quasilinearization Method*. The influence of pertinent parameters on the non-dimensional velocity, microrotation, temperature and concentration are presented graphically. Moreover, the skin friction, wall couple stress, heat and mass transfer rates are studied quantitatively and qualitatively. The final *Part-IV* consists of only one chapter (Chapter - 8) which gives a summary, overall conclusions and scope for future work.

NOMENCLATURE

$\overline{a}, \overline{b}$	Concentrations of the chemical species A and B
a_0	Positive constant
A, B	Chemical species
b	Forchheimer constant
Bi	Biot number
$\mathcal{B}$	Buoyancy ratio
C	Concentration
C_w	Wall concentration
C_∞	Ambient concentration
C_p	Specific heat capacity
D	Solutal diffusivity
D_A, D_B	Diffusion coefficients
Da	Darcy number
f	Reduced stream function
f_w	Suction/Injection parameter
g^*	Gravitational acceleration
g	Dimensionless microrotation
Gr	Thermal Grashof number
h_f	Convective heat transfer coefficient
h, h_1	Reduced concentrations of the chemical species A and B
j	Micro-inertia density
$\mathcal{J}$	Dimensionless micro-inertia density
k	Thermal conductivity
k_c, k_s	Reaction rate constants
K	Measures the strength of the homogeneous reaction
K_p	Permeability of the medium
K_s	Measures the strength of the heterogeneous (surface) reaction
k^*	Mean absorption coefficient
L	Characteristic length
M_w	Dimensionless wall couple stress
m_w	Wall couple stress
$Nu_{\overline{x}}$	Local Nusselt number
n	Material constant
Pr	Prandtl number
R	Radiation parameter
$Re_{\overline{x}}$	Local Reynolds number
Re	Reynolds number
r	Radius of truncated cone
Sc	Schmidt number
Sr	Soret number

$Sh_{\overline{x}}$	Local Sherwood number
T	Temperature
T_f	Convective wall temperature
T_∞	Ambient temperature
$\overline{u}$, $\overline{v}$	Velocity components in $\overline{x}$ and $\overline{y}$ directions
$\overline{u}_e$	Free stream velocity
U_∞	Reference velocity
x_0	Leading edge distance of a truncated cone
$\overline{x}$, $\overline{y}$	Coordinates along and normal to the plate
x, y	Dimensionless coordinates along and normal to the plate

Greek Symbols

α	Thermal diffusivity
α_1, β	Gyration viscosity parameters
β_1, β_2	Coefficients of thermal expansion
γ	Spin-gradient viscosity
δ	Ratio of diffusion coefficient
ϵ	Porosity
ε	Viscous dissipation parameter
η	Similarity variable
θ	Dimensionless temperature
ϕ	Dimensionless concentration
κ	Vortex viscosity
λ	Mixed convection parameter
μ	Dynamic viscosity
ν	Kinematic viscosity
ξ	Streamwise coordinate
ρ	Density of the fluid
σ^*	Stefan-Boltzmann constant
τ_w	Wall shear stress
ψ	Stream function
$\overline{\omega}$, ω	Components of microrotation

Subscripts

w	Wall condition.
∞	Ambient condition.

Superscript

$\prime$	Differentiation with respect to η.

Contents

[1]Case(a):Published in "**Advances in High Energy Physics**"2015 (2015) 1–16, Case(b):Published in "**Journal of Applied Analysis and Computation**"6(2) (2016) 254–270

[2]Case(a):Published in "**Procedia Engineering**" 127 (2015) 235–243,
Case(b) Published in "**Advanced Science Engineering and Medicine**" 7 (2015) 234–245

[3]Case(a):Published in "**Nonlinear Engineering**" 5(3) (2016) 193–204.,
Case(b) Accepted in "**Proc. Natl. Acad. Sci., India, Sect. A Phys. Sci**"

[4]Case(a): Published in "**Frontiers in Heat and Mass Transfer**" (2017) DOI: 10.5098/hmt.8.6,

Case(b) Published in "**Open Engineering**", 6 (2016) 106–119

[5]Case(a): Published in "**Int. J. Appl. Comput. Math**", DOI: 10.1007/s40819-016-0227-y (2016)
Case(b) Accepted in "**International Journal of Nonlinear Sciences and Numerical Simulation**"

[6]Case(a): Accepted in "**Special Topics and Reviews in Porous Media**",
Case(b) Communicated to "**Journal of Engineering Thermophysics**"

Part I

INTRODUCTION

Chapter 1

Preliminaries and Review

1.1 Introduction

The science of fluid dynamics encompasses the motion of gases and liquids, the forces those are responsible for this motion and the interaction of the fluid with solids. This field stands central to various branches of science and engineering, and touches almost every aspect of our daily life. Fluid dynamics, one way or another, impacts defense, transportation, manufacturing, environment, medicine, energy, etc. From predicting the aerodynamic behavior of moving vehicles to the movement of biological fluids in the human body, weather predictions, cooling of electronic components, performance of micro-fluidic devices, all demand a detailed understanding of the subject of fluid dynamics and a substantial research, thereof.

Due to the complexity of the subject and a breadth of its applications, fluid dynamics is proven to be a highly exciting and challenging subject of modern sciences. The quest for deeper understanding of the subject has not only inspired the development of the subject itself, but has also led to the progress in the supporting areas, such as, applied mathematics, numerical computing and experimental techniques. A large number of problems in fluid

dynamics have claimed the attention of mathematicians, physicists and engineers for many years. As a result, an enormous body of established results has accumulated steadily but remains scattered in the literature.

The mechanism of heat transfer is the passage of thermal energy from a hot to a cold body. When a physical body is at a different temperature than its surroundings or another body, transfer of thermal energy between them is also known as heat transfer. It occurs through conduction, convection, radiation or any combination of these. The combined process of heat transfer by conduction and convection is referred to as the convective heat transfer. The convective mode of heat transfer is generally divided into two basic processes: free (or natural) convection and forced convection. If the fluid motion is set up by buoyancy effects resulting from density differences caused by temperature differences in the fluid, then the heat transfer is said to be free convection. On other hand, if the motion of the fluid arises from an external agent, then the process is termed as forced convection. When both free and forced convection effects are significant and neither of these can be neglected, then the process is termed as mixed convection. Both free and mixed convection processes may be divided into external flows over immersed bodies (such as flat plates, cones, cylinders and wires, spheres or other bodies), free boundary flows (such as plumes, jets and wakes), and internal flow in ducts (such as pipes, channels and enclosures).

The transport of a component in a mixture from a region of high concentration to a region of low concentration is called mass transfer. The involvement and applications of mass transfer process has gained much attention and it goes to a greater length in multiple fields such as in the industrial, biological, physical and chemical engineering processes. Mass transfer is divided into two modes: Diffusion mass transfer and Convective mass transfer. There is a close similarity between heat transfer and mass transfer in terms of the transport rate equation and transport conservation equation. The convective mass transfer is analogous to convective heat transfer and occurs between a moving mixture of fluid species and an exposed solid surface. Coupled heat and mass transport constitute a major area of research in modern fluid dynamics. Such flow arises in electronic cooling, drying processes, manufacture of electric cable insulations, curing of plastics, solar energy system and purification processes.

A Newtonian fluid is a fluid that exhibits a viscosity that remains constant regardless of any external stress that is placed upon it, such as mixing or a sudden application of force. One example is water, since it flows the same way, in spite of whether it is left alone or agitated vigorously. Another way to describe these fluids is that obey Newton′s law relating shear stress and shear rate with a simple material property (the viscosity). The viscosity dependent on basic thermodynamic variables such as temperature, concentration and pressure, but independent of flow parameters such as shear rate and time. This can be contrasted with non-Newtonian fluids, which can become thicker or thinner when stress is applied. A great deal of involvement has been brought forth to illustrate the nonlinear relationship between the rate of strain and stress in non-Newtonian fluid models. But there is no single fluid flow model which undoubtedly exhibits all the properties of real fluids. Therefore, during the last century, several fluid models are proposed to characterize the real fluid behaviour. Among these, micropolar fluid introduced by Eringen [32] has distinct features, such as the micro inertial effect, the presence of couple stresses, body couples and non-symmetric stress tensor.

1.2 Micropolar Fluids

Micropolar fluids are a subclass of microfluids and deal with a class of fluids which exhibit some microscopic effects arising from the local structure and micro-motion of the fluid elements. Compared to the classical Newtonian fluids, the flow motion of micropolar fluids is distinguished by two supplementary variables, (i.e.,) the spin vector responsible for the micro-rotation, and the microinertia tensor which describes the distribution of atoms and molecules inside the fluid elements in addition to the velocity vector. Physically, micropolar fluids are the fluids that comprise of rigid randomly oriented (spherical) particles suspended in a viscous medium where the deformation of the particles is ignored. Some common examples of micropolar fluids are sediments in rivers, human blood, liquid crystal, drug suspension in pharmacology, plasma, colloidal fluids, etc. These fluids have immense applications in diverse areas such as engineering sciences, lubrication theory, short waves for heat conducting

fluids, boundary layer theory, etc. A deep monograph to the micropolar fluid theory and its applications has been reported by Ariman *et al.* [5, 6], Lukaszewicz [51] and Eremeyev *et al.* [31].

The governing equations of micropolar fluids are represented in terms of the velocity and microrotation vectors associated with each particle present in the fluid medium. The governing equations of micropolar fluid dynamics [32] are

$$\frac{d\rho}{dt} + \rho(\nabla \cdot \overrightarrow{q}) = 0 \tag{1.1}$$

$$\rho \, \frac{d\overrightarrow{q}}{dt} = \rho \overrightarrow{f} - \nabla p + \kappa(\nabla \times \overrightarrow{\omega}) - (\mu + \kappa)[\nabla \times (\nabla \times \overrightarrow{q})] + (\lambda_1 + 2\mu + \kappa) \, \nabla(\nabla \cdot \overrightarrow{q}) \tag{1.2}$$

$$\rho j \, \frac{d\overrightarrow{\omega}}{dt} = \rho \overrightarrow{l} - 2k\overrightarrow{\omega} + \kappa \nabla \times \overrightarrow{q} - \gamma[\nabla \times (\nabla \times \overrightarrow{\omega})] + (\alpha_1 + \beta + \gamma)\nabla(\nabla \cdot \overrightarrow{\omega}) \tag{1.3}$$

where $\overrightarrow{q}$ is the velocity vector, $\overrightarrow{\omega}$ is the microrotation vector, p is the fluid pressure, ρ is the density of the fluid, j is the microgyration parameter, t is the time variable, $\overrightarrow{f}$ is the body force per unit mass and $\overrightarrow{l}$ is the body couple per unit mass. Also, the material constants $\{\lambda_1, \mu, \kappa\}$ and $\{\alpha_1, \beta, \gamma\}$ denote the viscosity and gyroviscosity coefficients respectively, and satisfy the following inequalities

$$\kappa \geq 0, \; 2\mu + \kappa \geq 0, \; 3\alpha_1 + \beta + \gamma \geq 0, \; 3\lambda_1 + 2\mu + \kappa \geq 0, \quad |\gamma| \geq 0, \; \gamma \geq |\beta_1|$$

The force stress tensor τ_{ij} and couple stress tensor m_{ij} of a micropolar fluid are given by

$$\tau_{i,j} = (-p + \lambda_1 \, (\nabla . \overrightarrow{q})) \, \delta_{ij} + (2\mu + \kappa) \, e_{ij} + \kappa \, \varepsilon_{ijm} \, (\Omega_m - \omega_m) \tag{1.4}$$

$$m_{ij} = \alpha_1 \, (\nabla . \overrightarrow{\omega}) \, \delta_{ij} + \beta \, \omega_{i,j} + \gamma \, \omega_{j,i} \tag{1.5}$$

where ω_i and $2\Omega_i$ are the components of microrotation and vorticity vector respectively. δ_{ij} is the Kronecker delta, e_{ij}'s are the components of the rate of strain, comma indicates covariant differentiation and ε_{ijm} is the Levi-Civita symbol. The boundary conditions are considered for microrotation such that there is no relative spin on the boundary and this condition is the generalization of classical no-slip condition to require that the fluid particles

nearest to a solid boundary stick to it neither translating nor rotating.

In the special case where the fluid has constant physical properties, no external body forces exist and for steady state flow, the conservation equations can be extremely simplified. Apart from the previous case, when $\kappa = \alpha_1 = \beta = \gamma = 0$ and with vanishing $\overrightarrow{l}$, the gyration vector disappears and angular momentum equation (1.3) vanishes identically and the equation (1.2) reduces to the classical Navier-Stokes equations. Also it may be noticed that in the case of zero vortex viscosity ($\kappa = 0$) only, the velocity vector $\overrightarrow{q}$ and the microrotation vector $\overrightarrow{\omega}$ are decoupled and the global motion is unchanged by the microrotation.

1.3 Porous Medium

A porous medium may be defined as a solid matrix containing holes either connected or non-connected, dispersed within the medium in a regular or random manner provided such holes occur frequently in the medium. If these pores are saturated with a fluid, then the solid matrix with the fluid is called a fluid-saturated porous medium. This type of analysis in porous media plays an important role in many fields of science and engineering, for instance, petroleum engineering, ground water hydrology, agricultural engineering and soil mechanics. But, the flow of the fluid in a saturated porous material is possible only when some of the pores are interconnected.

To study the motion of fluids through porous media, one must have sufficient understanding of the governing equations for the fluid flow through the porous media. Owing to the intricate structure of the porous medium, several models have proposed in order to explain mathematical and physical aspects of porous media. Among these, the Darcy model and a series of its modifications have attained much acceptance. Further, the boundary layer assumptions have been successfully applied to these models and much work over the last few decades has been done on them for a wide variety of geometries.

Darcy Model

The governing equation of fluid motion in a vertical porous column was first given by Darcy [24] in 1856. It represents a balance of viscous force, gravitational force and pressure gradient. In mathematical form, it is given as

$$\overrightarrow{q} = -\frac{K_p}{\mu}(\nabla P - \rho\, g) \tag{1.6}$$

where $\overrightarrow{q}$ is the space averaged velocity (or Darcian velocity), K_p is the (intrinsic) permeability of the medium, μ is the coefficient of viscosity, P is the pressure, ρ is the density of the fluid and g is the body force per unit volume. For one-dimensional flow and low porosity system, the above law appears to provide good agreement with experimental results. As this model does not take inertial effects into consideration, it is valid only for seepage flows, i.e., for flows with low Reynolds number ($O(Re) < 1$).

Darcy-Brinkman Model

It is assumed that the flow through an anisotropic porous medium with high permeability must reduce to the viscous flow in a limit. In viewing this, Brinkman felt the need to account for the viscous force exerted by a flowing fluid on a dense swarm of spherical particles embedded in a porous mass and added the term $\mu'\,\nabla^2 V$ to balance the pressure gradient. Here μ' is the effective viscosity given by $\mu' = \mu(1-2.5(1-\epsilon))$. The validity of the Brinkman model is restricted to the high porosity medium (as confirmed by the experiments) and its governing equation is given by

$$-\left[\nabla P - \rho g\right] = \frac{\mu}{K_p}\overrightarrow{q} - \mu'\nabla^2\overrightarrow{q} \tag{1.7}$$

Darcy-Forchheimer Model

In 1901, Forchheimer conducted experiments and proposed that inertial effects can be accounted for by the addition of the square of velocity in the momentum equation. The

modification to Darcy′s equation is

$$\left[1+\frac{\rho\, c\,\sqrt{K_p}}{\mu}|\overrightarrow{q}|\right]\overrightarrow{q}=-\frac{K_p}{\mu}\left[\nabla P-\rho g\right] \tag{1.8}$$

where c is the dimensionless form drag coefficient and it varies with the nature of the porous medium. The coefficients of Darcy and Forchheimer terms contain both fluid properties and the microstructure of the porous medium. Several other models are found in the literature related to porous media and the validity and limitations of these models are well discussed in the text book by Nield and Bejan [74].

1.4 Convective Boundary Condition

It can be seen from the literature that several investigators have considered convective heat transfer problems with either wall temperature or heat flux in Newtonian and/or non-Newtonian fluids. But, these conditions cannot explain the supply of heat with a finite heat capacity to the convecting fluid through a bounding surface. To explain this, a novel mechanism for the heating process has drawn the attention of many researchers, known as the Convective Boundary Condition (CBC) (for more details see Aziz [8]). Further, the heat transfer with a convective boundary condition is more general and realistic, especially with respect to various engineering and industrial processes including material drying, laser pulse heating and transpiration cooling. Also, it occurs when a solid substrate is in contact with the fluid at a different temperature and involves relative motion between the fluid and the substrate. The magnitude of heat exchange is described in terms of Newton's law of cooling, for which the relevant constitutive property of the system is the convective heat transfer coefficient. The convective boundary condition for heat transfer involves equating Fourier's law of conduction at the solid surface with Newton's law of cooling in the fluid.

$$-k\frac{\partial T}{\partial y}=h_f(T_f-T) \tag{1.9}$$

1.5 Spectral Quasi-linearization Method

The governing equations of convective heat and mass transfer in Newtonian and/or non-Newtonian fluids are essentially coupled and non-linear differential equations. Generally, these non-linear differential equations cannot be solved analytically, so recourse must be made to a numerical approach. Several methods are available to solve these nonlinear differential equations namely, shooting method, local similarity and non-similarity method, finite difference method, finite element methods, cubic spline collocation method, spectral methods etc. Among these, the *Spectral Quasi-linearization Method* is one of the efficient and accurate spectral method introduced by Motsa [61]. It is developed by combining two methods viz., quasi-linearization method and Chebyshev spectral collocation method. This method has several desirable features that make it appropriate for the solution of differential equations. In this section, the spectral quasi-linearization method (SQLM) is presented for solving the differential equation. The brief details of the SQLM are as follows:

Quasi-linearization Method

Quasi-linearization method (QLM) is a generalization of the Newton-Rhapson method initiated by Bellman and Kalaba [16] to solve nonlinear ordinary and partial differential equations. To obtain the QLM iteration scheme, the nonlinear component of a differential equation is linearized using the multi-variable Taylor series expansion. To develop the QLM, we consider a system of m nonlinear ordinary differential equations with m unknowns $z_i(\eta)$ for $i = 1, 2, ..., m$, where η is the independent variable. The system of equations can be written as a sum of its linear component ($\mathcal{L}$) and nonlinear component ($\mathcal{N}$) as

$$\mathcal{L}\left[z_1(\eta), z_2(\eta), ..., z_m(\eta)\right] + \mathcal{N}\left[z_1(\eta), z_2(\eta), ..., z_m(\eta)\right] = 0 \tag{1.10}$$

Define vector Z_i to be the vector of derivatives of the variable z_i with respect to the independent variable η, that is

$$Z_i = \left[z_i^{(0)}, z_i^{(1)}, ..., z_i^{(n_i)}\right] \tag{1.11}$$

where $z_i^{(0)} = z_i$ and $z_i^{(p)}$ is the p^{th} derivative of z_i with respect to η and $n_i\,(i = 1, 2, ..., m)$ is the higher order derivative of the variable z_i appearing in the system of equations. In addition, we define $\mathcal{L}_i$ and $\mathcal{N}_i$ to be the linear and non-linear operators respectively, that operate on the Z_i for $i = 1, 2, ..., m$. With these definitions, the Eq.(1.10) can be written as

$$\mathcal{L}_i\left[Z_1, Z_2, ..., Z_m\right] + \mathcal{N}_i\left[Z_1, Z_2, ..., Z_m\right] = \sum_{j=1}^{m}\sum_{p=0}^{n_i} \alpha_{ij}^{[p]} z_j^{(p)} + \mathcal{N}_i\left[Z_1, Z_2, ..., Z_m\right] = 0 \qquad (1.12)$$

where $\alpha_{ij}^{[p]}$ are the constant coefficient of $z_j^{(p)}$, the derivative of $z_j\,(j = 1, 2, ..., m)$ that appears in the i^{th} equation for $i = 1, 2, ..., m$.

Again, assume that the Eq.(1.10) is to be solved subject to separated two-point boundary conditions which are expressed as

$$\sum_{j=1}^{m}\sum_{p=0}^{n_j-1} \beta_{v,j}^{[p]} z_j^{(p)}(a) = K_{a,v}, \qquad v = 1, 2, ..., m_a \qquad (1.13)$$

$$\sum_{j=1}^{m}\sum_{p=0}^{n_j-1} \gamma_{\sigma,j}^{[p]} z_j^{(p)}(b) = K_{b,\sigma}, \qquad \sigma = 1, 2, ..., m_b \qquad (1.14)$$

where $\beta_{v,j}^{[p]}$, $\gamma_{\sigma,j}^{[p]}$ are the constant coefficients of $z_j^{(p)}$ in the boundary conditions and m_a, m_b are the total number of prescribed boundary conditions at $\eta = a$ and $\eta = b$ respectively.

Assume that the solution $z_i(\eta)$ of Eq.(1.12) at the $(r+1)^{th}$ iteration is $z_{i,r+1}(\eta)$. If the solution at the previous iteration $z_{i,r}(\eta)$ is sufficiently close to $z_{i,r+1}(\eta)$, then the nonlinear component $\mathcal{N}_i$ of the Eq.(1.12) can be linearised using one term Taylor series for multiple variables so that the Eq.(1.12) can be approximated as

$$\mathcal{L}_i\left[Z_{1,r+1}, ..., Z_{m,r+1}\right] + \mathcal{N}_i\left[...\right] = \sum_{j=1}^{m}\sum_{p=0}^{n_i} \left(z_{j,r+1}^{(p)} - z_{j,r}^{(p)}\right) \frac{\partial \mathcal{N}_i}{\partial z_j^{(p)}}\left[...\right] = 0 \qquad (1.15)$$

where

$$\left[...\right] = \left[Z_{1,r}, Z_{2,r}, ..., Z_{m,r}\right] \qquad (1.16)$$

Equation (1.15) can be re-written as

$$\mathcal{L}_i\left[Z_{1,r+1},...,Z_{m,r+1}\right]+\sum_{j=1}^{m}\sum_{p=0}^{n_i}z_{j,r+1}^{(p)}\frac{\partial\mathcal{N}_i}{\partial Z_j^{(p)}}\left[...\right]=\sum_{j=1}^{m}\sum_{p=0}^{n_i}z_{j,r}^{(p)}\frac{\partial\mathcal{N}_i}{\partial z_j^{(p)}}\left[...\right]-\mathcal{N}_i\left[...\right] \tag{1.17}$$

The above equation can be solved using any numerical method. But, in this work the Chebyshev spectral collocation method is used and the resulting method is called the spectral quasi-linearization method ($SQLM$).

Chebyshev Spectral Collocation Method

The Chebyshev spectral collocation method ([25, 101, 18]) is based on the Chebyshev polynomials defined on the interval [-1, 1]. To solve the problems using this method, one has to first transform the domain $[a, b]$ of the problem to $[-1, 1]$ by using the following transformation

$$(b-a)\tau=2\eta-(a+b),\ \ -1\leq\tau\leq1 \tag{1.18}$$

Discretize the domain [-1, 1] using the Gauss-Lobatto collocation points given by

$$\tau_j=\cos\frac{\pi j}{\overline{N}},\quad\ j=0,1,2,...,\overline{N} \tag{1.19}$$

where $\overline{N}$ is the number of collocation points used. The function Z_i is approximated at the collocation points as follows

$$z_i(\tau)=\sum_{k=0}^{\overline{N}}z_i(\tau_k)T_k(\tau_j) \tag{1.20}$$

where T_k is the k^{th} Chebyshev polynomial defined by $T_k(\tau)=\cos[k\cos^{-1}\tau]$

The derivatives of the variables at the collocation points are represented as

$$\frac{d^r z_i}{d\eta^r}=\sum_{k=0}^{\overline{N}}\left[\frac{2}{b-a}\mathbf{D}_{kj}\right]^r z_i(\tau_k) \tag{1.21}$$

where r is the order of differentiation and $\mathbf{D}$ being the Chebyshev spectral differentiation

matrix whose entries are defined as

$$\left.\begin{aligned}
&\mathbf{D}_{00} = \tfrac{2\overline{N}^2+1}{6} \\
&\mathbf{D}_{jk} = \tfrac{c_j}{c_k}\tfrac{(-1)^{j+k}}{\tau_j-\tau_k}, \;\; j \neq k; \;\; j,k = 0,1,2\cdots,\overline{N}, \\
&\mathbf{D}_{kk} = -\tfrac{\tau_k}{2(1-\tau_k{}^2)}, \;\; k = 1,2\cdots,\overline{N}-1, \\
&\mathbf{D}_{NN} = -\tfrac{2\overline{N}^2+1}{6}
\end{aligned}\right\} \tag{1.22}$$

Substituting Eqs.(1.19)-(1.22) into the given equation leads to the system of matrix equation as follows

$$\mathbf{A}_{i-1}\mathbf{X}_i = \mathbf{R}_{i-1} \tag{1.23}$$

where A_{i-1} is a square matrix of size $(\overline{N}+1)\times(\overline{N}+1)$, while X_i and R_{i-1} are column vectors of size $(\overline{N}+1)\times 1$. After incorporating the boundary conditions, the solution of the system of equations can be written as

$$\mathbf{X}_i = \mathbf{A}_{i-1}^{-1}\mathbf{R}_{i-1} \tag{1.24}$$

Combined Finite Difference and Spectral Method

In the previous subsection, a brief description of the spectral quasi-linearisation method (SQLM) is provided to solve the system of ordinary differential equations (ODE's). In this subsection, the extension of the SQLM is presented briefly to solve the system of partial differential equations (PDE's). Since the finite difference methods are known to converge more slowly than spectral methods, combining these two methods one would compromise the rapid convergence of problems. The combination of spectral method and finite difference method is used to approximate solutions of the system of non-linear partial differential equations. This modification of the SQLM utilizes the spectral method to discretize derivatives in space and implicit finite difference method to discretize in a streamwise coordinate. Further, this spectral method in space improves the accuracy of the results using few grid points and then it improves the computational time of the finite difference method.

1.6 Literature Review

The study of free and mixed convection due to a heated or cooled vertical flat plate provides one of the most basic scenarios for heat and mass transfer theory and thus is of considerable theoretical and practical interest. Free convection of heat and mass transfer occurs simultaneously in the fields of design of chemical processing equipment, formation and dispersion of fog, distributions of temperature, moisture over agricultural fields and groves of fruit trees. It also occurs in the context of damage of crops due to freezing and pollution of the environment. The phenomenon of mixed convection occurs in many technical and industrial problems such as electronic devices cooled by fans, nuclear reactors cooled during an emergency shutdown, a heat exchanger placed in a low-velocity environment, solar collectors and so on.

Convective boundary layer flow over a vertical flat plate is probably the first buoyancy convective problem which has been studied and it has been a very popular research topic for many years. Merkin [56] considered the boundary layer flow over a semi-infinite vertical plate in a uniform stream in the presence of buoyancy forces. The mixed convective boundary layer flow on a vertical surface has been studied by Lloyd and Sparrow [50]. Kafoussias and Williams [44] analyzed the steady laminar mixed convective flow over an isothermal vertical plate by considering the temperature dependent viscosity. Aboeldahab and Elbarbary [1] examined the effect of Hall current on the free convective flow of an electrically conducting viscous fluid along a semi-infinite vertical plate. An exhaustive monograph on free and mixed convective heat and mass transfer characteristics has been given in the textbook by Bejan [15].

Convective flow over a vertical surface embedded in a viscous fluid saturated porous medium is one of the fundamental and classical problems in the heat and mass transfer theory. It has attracted a great deal of interest from many investigators owing to their wide applications, such as in geothermal systems, energy-storage units, heat insulation, heat exchangers for the packed bed, drying technology, catalytic reactors and nuclear waste repositories, etc. The literature relevant to the convective flows in Darcy and non-Darcy

porous medium has been reported in the textbooks by Ingham and Pop [41], Nield and Bejan [74], Vafai [102] and also see the citations therein.

The heat transfer problems involving the convective boundary condition appears in realistic situations, where heat transfer occurs at the bounding surface to or from a fluid flowing on the surface at a known temperature and a known heat transfer coefficient, e.g. in heat exchangers, condensers and re-boilers. To explore it, several investigators have analyzed the fluid flow problems in the presence of convective boundary condition. Ishak [42] studied the effects of suction and injection on steady laminar boundary layer flow over a permeable surface with the convective boundary condition. Effect of Biot number on the mixed convective flow of an electrically conducting fluid along a vertical plate embedded in a porous medium has been considered by Makinde and Aziz [55]. Recently, Rahman *et al.* [82] considered the mixed convective boundary layer flow along a vertical plate with the convective boundary condition.

In wide range, most of the researchers considered the effect of buoyancy force by assuming that the temperature and density vary linearly (it is known as linear Boussinesq approximation or simply Boussinesq approximation). However, there are several reasons for the density-temperature relationship to become non-linear, for instance, when the temperature difference between the surface of the body and the ambient fluid becomes significantly large. In this case, non-linear density and temperature variations in the buoyancy force term may exert a strong influence on the flow field and heat transfer characteristics (for details see Barrow and Rao [11]). This physical concept has an unavoidable applications in geothermal and engineering processes such as pore water convection near salt domes, cooling of electric equipment, and the residual warm water discharged from a geothermal power plant. In view of the above said applications, Partha [77] developed a mathematical model on non-Darcy porous medium with a temperature-concentration dependent density relation, in which it can be observed that with an increase in nonlinear temperature and concentration parameters, the heat and mass transfer varies extensively depending on Darcy and non-Darcy porous medium. Prasad *et al.* [81] scrutinized the natural convective flow along a vertical flat plate in a non-Darcy porous medium with the nonlinear density-temperature variation under pre-

scribed constant surface temperature. The convective flow of nonlinear density-temperature relationship over an impulsive stretching sheet has been examined by Motsa *et al.* [62] (and also see the citations therein).

In the recent past, several investigators have concentrated on convective transport phenomena in different fluids with first and higher order chemical reaction effects, owing to the realistic applications in engineering and industrial processes. Rout *et al.* [89] analyzed the effects of heat source and chemical reaction on magneto-hydrodynamic flow over a moving vertical plate subject to the convective boundary condition. There are several chemically reacting systems which involve both homogeneous and heterogeneous reactions. Applications of this process occur in catalysis, biochemical systems, drying processes, combustion processes, metallurgical flows, cooling towers, etc. Generally, the interaction between the homogeneous reaction in the bulk of the fluid and heterogeneous reactions occurring on some catalytic surfaces are very complex and involved in the production and consumption of reactant species at different rates both within the fluid and on the catalytic surfaces.

In view of the above said applications, Merkin [59] presented a model for homogeneous-heterogeneous reactions in a uniform stream flow over a flat surface in which the heterogeneous reaction takes place by the first-order process and the homogeneous reaction by the cubic autocatalysis method. The boundary layer flow near the stagnation point over a stretching sheet with the homogeneous and heterogeneous reactions has been studied by Bachok *et al.* [9]. Kameswaran *et al.* [46] analyzed the effect of homogeneous and heterogeneous reactions on the stagnation point in a nanofluid flow due to stretching or shrinking sheet. Nandkeolyar *et al.* [70] discussed the effects of MHD and internal heat generation on heat and mass transport in a nanofluid in the presence of homogeneous-heterogeneous reactions. The effects of homogeneous and heterogeneous reactions in the viscoelastic fluid flow towards a melting stretching sheet with variable thickness have been examined by Hayat *et al.* [39]. But from the literature, it seems that a very limited work has been reported on the homogeneous and heterogeneous reactions in non-Newtonian fluid flows.

Radiative heat transfer flow is very important in manufacturing industries for the design of reliable equipments, nuclear plants, gas turbines and various propulsion devices for aircraft,

missiles, satellites and space vehicles. Also, the effect of thermal radiation on convective flows is important in the context of space technology and processes involving high temperature. To study these applications, Hossain and Takhar [40] considered the combined free and forced convective boundary layer flow along a heated vertical plate with the radiation effect. The effect of radiation on laminar free convective flow along a vertical porous plate in a porous medium has been investigated by Raptis [84]. Makinde [53] discussed the free convective boundary layer flow past a moving vertical porous plate in the presence of thermal radiation.

Several investigators have shown much attention to non-Newtonian fluids in view of their applications in various aspects of industrial processing, design of equipment, chemical and allied processes such as cosmetics, synthetic polymers, biological fluids, synthetic lubricants etc. These fluids reveal complex rheological nature which is not accomplished by Newtonian fluids. Among the non-Newtonian fluids, the micropolar fluid is the one which takes care about the rotation of fluid particles by means of independent kinematic vector known as the microrotation vector. The subject of convective flow of a micropolar fluid has been studied by several investigators due to its immense applications in engineering problems such as solar energy collecting devices, material processing and passive cooling of nuclear reactors. The boundary layer flow over a semi-infinite flat plate is considered for deep understanding of the micropolar fluid theory and its application to low concentration suspension flow by Ahmadi[3]. Hayat *et al.* [38] presented the study on the laminar mixed convective flow of micropolar fluid over a non-linear stretching sheet. Yacob and Ishak [104] discussed the micropolar fluid flow past stretching or shrinking sheet in the presence of convective boundary condition and obtained the dual solutions. Srinivasacharya and RamReddy [97] analyzed the effects of double stratification on the mixed convective flow of an incompressible micropolar fluid along a vertical plate and hence noted that the effect of the stratification on temperature is the formation of a region with a temperature deficit (i.e., a negative dimensionless temperature).

The analysis of convective transport phenomena over various surface geometries embedded in a micropolar fluid saturated porous medium has been provided by several researchers due to its tremendous applications in discrete aspects of engineering, scientific and indus-

trial applications like porous rocks, foams and foamed solids, aerogel, alloys, polymer blends, micro-emulsions, cooling of molten metals and so on. In view of these applications, Hassanien *et al.* [36] proposed a mathematical model for the natural convective flow over a permeable semi-infinite plate embedded in a porous medium saturated by a micropolar fluid. The effect of stratification on natural convection over a continuously moving plate immersed in a non-Darcian porous medium has been presented by Beg *et al.* [13]. Srinivasacharya and RamReddy [94] investigated the effect of double stratification on free convection along a vertical plate in a micropolar fluid saturated non-Darcy porous medium. The hydro-magnetic boundary layer flow of a micropolar fluid over a stretching surface through a non-Darcy porous medium, considering a variable permeability, has been discussed by Aiyesimi *et al.* [4].

The occurrence of diffusion flux due to temperature gradient is known as Soret or thermal-diffusion effect. In most of the studies related to heat and mass transfer process, Soret effect is neglected on the basis that it is of a smaller order of magnitude than the effects described by Fourier's and Fick's laws. This Soret effect can play an important role in many natural activities, viz., in the underlying physics of the solar ponds, the demographics of an ocean and also convection in stars (See Ingham and Pop [41]). Also, it has been utilized for isotope separation and in a mixture between gases with very light molecular weight (H_2, He) and of medium molecular weight (N_2, air)[26]. Due to the significant applications of Soret effect, several authors analyzed the Newtonian and Non-Newtonian fluids through different geometries. Kafoussias and Williams [45] discussed the mixed convective flow over a vertical plate under the influence of Soret and Dufour effects. Although, the Soret effect on heat and mass transfer in a micropolar fluid is important, little work is noticed in the literature. Srinivasacharya and RamReddy [95] analyzed the effects of thermal-diffusion and diffusion-thermo on micropolar fluid flow over a vertical plate (for more details, see the citations therein).

During the motion of fluid particles, the viscosity of the fluid converts some kinetic energy into thermal energy. This process, which is caused due to viscosity is irreversible and is known as viscous dissipation. It may arise in free convection in several devices which

are treated with large deceleration or operate at a high rotative speed [33]. In spite of the huge literature available on viscous dissipation, here we have provided some of the useful and related studies only. El-Aziz [28] discussed the effect of viscous dissipation on the laminar mixed convective flow of a micropolar fluid over an exponentially stretching sheet. Effects of slip velocity and thermal slip boundary condition on micropolar fluid flow along a moving vertical surface in the presence of viscous dissipation have been studied by Mutlag *et al.* [67]. Muthuraj *et al.* [65] presented a mathematical model to explore the combined effects of viscous dissipation and cross-diffusion on MHD mixed convective fully developed flow of a micropolar fluid in a vertical channel and also provided usefulness of the study.

Self similarity of solution of PDE's has allowed their reduction to ODE's which often simplifies the investigation. In the recent past, many researchers focused on different procedures for obtaining the similarity solutions of the convective transport phenomena problems arising in fluid dynamics, aerodynamics, plasma physics, meteorology and some branches of engineering. One such procedure is *Lie group analysis*, also known as symmetry analysis, initiated by Sophus Lie. The very idea of self-similarity is connected with the study of the structure of PDE's using the notion of symmetry group. It determines point transformations which map a given differential equation to itself and it combines almost all known exact integration techniques (Ref.[76, 75, 17]). It provides a potent, sophisticated and systematic tool for generating the invariant solutions of the system of nonlinear partial differential equations (PDE's) with relevant initial or boundary conditions. A special form of Lie group transformations, known as the scaling group of transformation, has been suggested by various researchers to study convective flows of different fluids with some unavoidable limitations [see Tapanidis *et al.* [100]; Hassanien and Hamad [37]; Kandasamy *et al.* [48]; Mutlag *et al.* [66] etc, are worth observing].

The analysis of heat and mass transfer over a vertical truncated cone has attracted the interest of scientists and researchers as a consequence of their important applications in engineering and industrial processes such as cooling of electronic devices, heat exchangers, etc. Initially, the free convective flow over a truncated cone has been investigated by Na and Chiou [68]. Later, Singh *et al.* [92] studied the laminar natural convective flow over the

vertical frustum of a cone with constant wall temperature. Using the Keller-box method, a numerical solution has been provided by Yih [105] for the natural convective flow over a vertical truncated cone in a porous medium. Cheng [22] discussed the natural convective boundary layer flow over a truncated cone embedded in a porous medium saturated with a nanofluid by taking thermophoresis and Brownian motion effects. Postelnicu [80] scrutinized the laminar natural convective flow of an incompressible micropolar fluid over a truncated cone subjected to heat flux condition. Patrulescu *et al.* [78] analyzed the mathematical model for combined free and forced convective flow of nanofluid over a truncated cone by incorporating three kinds of nanoparticles and noticed that the dual solution exists for flow reversal.

This limited literature shows that the analysis of micropolar fluid flow over the vertical frustum of a cone under different conditions has not received significant attention so far. Also, it seems from the literature that the similarity solution in the case of vertical frustum of a cone does not exist by using either Lie scaling group or other transformations. Hence, one has to use appropriate non-similarity transformations to find the approximate solutions of the governing system of partial differential equations.

Owing to the important applications of the micropolar fluid with and/or without saturated porous media, the convective flow over a vertical plate and/or truncated cone has been analyzed in this thesis. In addition, the convective boundary is incorporated into the analysis. The problems that we studied are outlined in the next section.

1.7 Aim and Scope

The objective of the present thesis is to develop the numerical solution for convective heat and mass transfer in a micropolar fluid flow with the convective boundary condition. The study focuses on the attributes of various effects such as suction/injection, mixed convection, Darcy and non-Darcy (Forchheimer), nonlinear convection, radiation, homogeneous-heterogeneous reactions, Soret and viscous dissipation. The problems considered in this thesis deal with

a semi-infinite vertical plate and/or a vertical truncated cone for the two cases: (i) free convection (ii) mixed convection.

1.8 Outline of the Thesis

This thesis is arranged in four sections with a total of eight chapters. *Part I* consists of single chapter (i.e., Chapter-1). It is introductory in nature and gives motivation to the investigations carried out in the thesis. A survey of pertinent literature is presented to show the significance of the problems considered. The basic equations governing the flow, heat and mass transfers of a micropolar fluid and details of the numerical method (spectral quasi-linearization method) are given.

Part II presents the similarity solution of a micropolar fluid flow along a vertical plate in the presence of convective boundary condition. This part consists of four chapters (i,e., Chapters 2-5). In these chapters, Lie scaling group of transformations are applied to get the similarity representation to the system of partial differential equations and then the resulting systems of equations are solved numerically by the spectral quasi-linearization method. A quantitative comparison of the numerical results with previously published results has been done for special cases and the results are found to be in good agreement. The details of these chapters are given below.

In Chapter-2, the similarity solution of a micropolar fluid along a permeable vertical plate with the convective boundary condition is obtained. The effects of physical parameters on the velocity, microrotation, temperature, concentration, skin friction, wall couple stress, heat and mass transfer rates along a vertical plate are given and the salient features are discussed.

The effects of Biot number on the free and mixed convective flow along a permeable vertical plate in a micropolar fluid saturated porous medium, are examined in Chapter-3. The effects of Biot number, Darcy and micropolar parameters on the fluid flow are exhibited graphically and quantitatively in the presence of suction and injection.

In Chapter-4, the significance of nonlinear temperature-dependent density relation and convective boundary condition on the convective flow of an incompressible micropolar fluid with the homogeneous-heterogeneous reactions, is analyzed. The effects of various parameters on the velocity, microrotation, temperature, concentration are presented through graphs. Moreover, the skin friction and wall couple stress coefficients, heat and mass transfer rates are presented in tabular form.

Chapter-5 discusses the effects of homogeneous-heterogeneous reactions on nonlinear convective flow of a micropolar fluid along a semi-infinite vertical plate embedded in a Darcy porous medium under the convective boundary condition. The velocity, microrotation, temperature and concentration profiles are exhibited graphically. Further, the local skin-friction coefficient, wall couple stress coefficient, heat and mass transfer rates are explored quantitatively for various values of the coupling number, Biot number, Darcy parameter, nonlinear convection parameter, homogeneous and heterogeneous reaction parameters.

Part III deals with the non-similarity solution for the convective flow over a truncated cone immersed in a micropolar fluid with and without saturated porous medium subject to the convective boundary condition. This consists of two chapters (i,e., Chapters 6-7) in which the governing non-linear partial differential equations in dimensional form are transformed to non-dimensional, non-linear partial differential equations by making use of appropriate non-similarity transformations. The extended spectral quasi-linearization method is employed to solve the system of non-similar, coupled partial differential equations. The obtained results are checked against previously published work on special cases of the problem and are found to be in excellent agreement. The details of these chapters are given below.

In the presence of convective boundary condition, the non-similarity solution for the convective flow of a micropolar fluid over a truncated cone is provided in Chapter-6. In addition, the Soret and viscous dissipation effects are taken into account. The effects of viscous dissipation, coupling number, Biot number and Soret number on the velocity, microrotation, temperature and concentration are presented graphically. Moreover, the non-dimensional skin friction, wall couple stress, Nusselt and Sherwood numbers against the stream-wise coordinate for various values of pertinent flow parameters are also analyzed through graphs.

In Chapter-7, the effects of Soret and viscous dissipation on the convective flow of micropolar fluid over a truncated cone embedded in a non-Darcy porous medium under the convective boundary condition, are discussed. The effects of various parameters, namely, micropolar, viscous dissipation, Biot number, Forchheimer number and Soret number on physical quantities of the fluid flow are explored in detail and some interesting results have been obtained.

The spectral quasi-linearisation method is used to solve the resultant system of nonlinear ordinary/partial differential equations in all the chapters (i.e., Chapters 2-7). The governing equations are linearised by using the quasi-linearisation method and then solved by applying the Chebyshev spectral collocation method [18]. In addition to these two methods, the implicit finite difference method has been utilised in Chapters - 6 and 7.

Finally, *Part IV* consists of single chapter (i.e., Chapter-8). The main conclusions of the earlier chapters are recorded and the directions in which further investigations may be carried out are indicated in this chapter.

List of references is given at the end of the thesis. The references are arranged in an alphabetical order and according to this order, citations appear in the text.

Considerable part of the work in the thesis is published/accepted for publication in reputed journals. The remaining part is communicated for possible publications. The details are presented below.

List of Papers Published

1. "Similarity solution for free convection flow of a micropolar fluid under convective boundary condition via Lie scaling group transformations", *Advances in High Energy Physics*, Vol. 2015, pp. 1–16, (2015).

2. "Numerical study of mixed convection flow of a micropolar fluid towards permeable vertical plate with convective boundary condition", *Journal of Applied Analysis and Computation*, Vol. 6(2), pp. 254–270, (2016).

3. "The effect of suction/injection on free convection in a micropolar fluid saturated porous medium under convective boundary condition", *Procedia Engineering*, Vol. 127, pp. 235–243, (2015).

4. "Numerical solution for mixed convection in a Darcy porous medium saturated with a micropolar fluid under convective boundary condition using spectral quasi-linearization method", *Advanced Science, Engineering and Medicine*, Vol. 7, pp. 234–245, (2015).

5. "Spectral quasi-linearisation method for nonlinear thermal convection flow of a micropolar fluid under convective boundary condition", *Nonlinear Engineering*, Vol. 5(3), pp. 193–204, (2016).

6. "Spectral quasi-linearization method for homogeneous-heterogeneous reactions on nonlinear convection flow of micropolar fluid saturated porous medium with convective boundary condition", *Open Engineering*, Vol. 6, pp. 106–119, (2016).

7. "Non-similarity solution of micropolar fluid flow over a truncated cone with Soret and viscous dissipation effects using spectral quasi-linearization method", *Int. J. Appl. Comput. Math*, DOI: 10.1007/s40819-016-0227-y, (2017).

8. "Influence of convective boundary condition on nonlinear thermal convection flow of a micropolar fluid saturated porous medium with homogeneous-heterogeneous reactions", *Frontiers in Heat and Mass Transfer*, 8 - 003006, pp.1-10, (2017) DOI: 10.5098/hmt.8.6, (2017).

List of Papers Accepted

9. "Influence of homogeneous-heterogeneous reactions on nonlinear convection in micropolar fluid under convective boundary condition", Accepted for publication in *Proc. Natl. Acad. Sci., India, Sect. A Phys. Sci*, (2017).

10. "Non-similarity solutions for viscous dissipation and Soret effects in micropolar fluid over a truncated cone with convective boundary condition: spectral quasilinearization

approach", Accepted for publication in *International Journal of Nonlinear Sciences and Numerical Simulation*, (2017).

11. "A spectral method approach for role of soret and viscous dissipation over a truncated cone in a micropolar fluid saturated non-Darcy porous medium", Accepted in *Special Topics and Reviews in Porous Media*, (2017).

List of Papers Communicated

12. "Micropolar fluid flow over a vertical truncated cone in a porous medium with convective boundary condition: A Darcy-Forchheimer model", Communicated to *Journal of Engineering Thermophysics*.

Part II

CONVECTIVE TRANSPORT ALONG A SEMI-INFINITE VERTICAL PLATE IN A MICROPOLAR FLUID

Chapter 2

Similarity Solution of Micropolar Fluid Flow along a Permeable Vertical Plate with Convective Boundary Condition[1]

2.1 Introduction

Convective boundary condition plays a vital role in the mechanism of supplying heat to the convecting fluid through a bounding surface with a confined heat capacity, because of its universal and realistic nature, particularly in diverse technologies and industrial operations such as transpiration cooling process, textile drying, laser pulse heating etc. In view of these applications, Bataller [12] analyzed the thermal radiation effect on Blasius and Sakiadis flows under the convective boundary condition. Aziz [8] provided the similarity solution for thermal boundary layer flow over a flat plate in a uniform stream of fluid with the convective boundary condition. In the presence of an internal heat generation and convective boundary

[1]Case(a):Published in "**Advances in High Energy Physics**"2015 (2015) 1–16, Case(b):Published in "**Journal of Applied Analysis and Computation**"6(2) (2016) 254–270

condition, the local similarity solution for the free convective heat transfer from a moving vertical plate has been given by Makinde [54].

One of the best established theories of fluids with microstructure is the theory of micropolar fluids. It has received a good deal of attention due to the obvious reasons that Newtonian fluids cannot explain successfully the attributes of fluids with a substructure. Physically, the micropolar fluids may be treated as fluids consisting of rigid randomly oriented spherical particles suspended in a viscous medium where the deformation of the particles is ignored. The analysis of free and mixed convective flows of a micropolar fluid along a vertical plate has received considerable interest from both theoretical and practical point of view. Jena and Mathur [43] considered the mixed convective flow of an incompressible micropolar fluid from an isothermal vertical plate. Rees and Pop [87] discussed the free convective flow of a micropolar fluid along a vertical flat plate (For more details, see the citations therein).

From the literature survey, it seems that the problem of convective heat and mass transport along a permeable vertical plate in a micropolar fluid with the convective boundary condition has not been investigated so far. Hence, the aim of the present chapter is to identify the similarity solution of a micropolar fluid flow along a permeable vertical plate with the convective boundary condition. But, this type of mathematical modeling becomes slightly more complicated leading to the complex interactions of the flow, heat, and mass transfer mechanisms. In spite of this complexity, the similarity representation of the system of non-dimensional equations is obtained using Lie group transformations and then the similarity solution to the reduced system of non-dimensional equations is obtained using the spectral quasi-linearisation method. Also, the influence of important parameters, namely, Biot number, micropolar and suction/injection parameters on the physical quantities of the flow, heat and mass transfer rates, are analyzed in different flow situations.

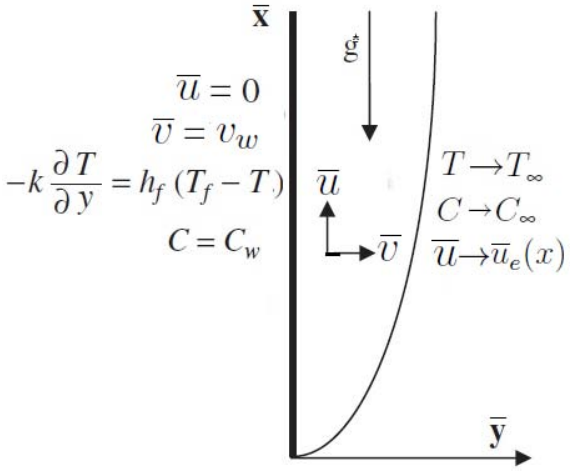

Figure 2.1: Physical model and coordinate system.

2.2 Mathematical Formulation

Consider the steady, laminar and two dimensional flow of an incompressible micropolar fluid along a permeable vertical plate. The velocity of the external/outer flow is taken in the form $\overline{u}_e(x)$, whereas the free stream temperature and concentration are assumed to be T_∞ and C_∞ respectively. Choose the coordinate system such that the $\overline{x}$-axis is along the vertical plate and $\overline{y}$-axis is normal to the plate. The physical model of the problem is shown in Fig. (2.1). The suction/injection velocity distribution is assumed to be v_w. The plate is either heated or cooled from left by convection from a fluid of temperature T_f with $T_f > T_\infty$ corresponding to a heated surface and $T_f < T_\infty$ corresponding to a cooled surface respectively. On the wall, the concentration is taken to be constant and is given by C_w.

By employing linear Boussinesq approximation and standard boundary layer assumptions, the governing equations for the micropolar fluid [3, 43] are given by

$$\frac{\partial \overline{u}}{\partial \overline{x}} + \frac{\partial \overline{v}}{\partial \overline{y}} = 0 \tag{2.1}$$

$$\rho\left(\overline{u}\frac{\partial \overline{u}}{\partial \overline{x}} + \overline{v}\frac{\partial \overline{u}}{\partial \overline{y}}\right) = (\mu + \kappa)\frac{\partial^2 \overline{u}}{\partial \overline{y}^2} + \rho\overline{u}_e\frac{d\overline{u}_e}{d\overline{x}} + \kappa\frac{\partial \overline{\omega}}{\partial \overline{y}} + \rho g^*\left[\beta_T(\overline{x})(T - T_\infty) + \beta_C(\overline{x})(C - C_\infty)\right] \tag{2.2}$$

$$\rho j\left(\overline{u}\frac{\partial \overline{\omega}}{\partial \overline{x}} + \overline{v}\frac{\partial \overline{\omega}}{\partial \overline{y}}\right) = \gamma\frac{\partial^2 \overline{\omega}}{\partial \overline{y}^2} - \kappa\left(2\overline{\omega} + \frac{\partial \overline{u}}{\partial \overline{y}}\right) \tag{2.3}$$

$$\overline{u}\frac{\partial T}{\partial \overline{x}} + \overline{v}\frac{\partial T}{\partial \overline{y}} = \alpha \frac{\partial^2 T}{\partial \overline{y}^2} \tag{2.4}$$

$$\overline{u}\frac{\partial C}{\partial \overline{x}} + \overline{v}\frac{\partial C}{\partial \overline{y}} = D \frac{\partial^2 C}{\partial \overline{y}^2} \tag{2.5}$$

where $\overline{u}$ and $\overline{v}$ are the velocity components in $\overline{x}$ and $\overline{y}$ directions respectively, T is the temperature, C is the concentration, $\overline{\omega}$ is the component of microrotation whose direction of rotation lies in the $\overline{x}\,\overline{y}$-plane, g^* is the acceleration due to gravity, ρ is the density, μ is the dynamic coefficient of viscosity, $\beta_T(\overline{x})$ is the coefficient of thermal expansion, $\beta_C(\overline{x})$ is the coefficient of solutal expansion, κ is the vortex viscosity, j is the micro-inertia density, γ is the spin-gradient viscosity, α and D are the thermal and solutal diffusivities of the medium respectively.

The boundary conditions are

$$\overline{u} = 0,\ \ \overline{v} = v_w,\ \ \overline{\omega} = -n\frac{\partial \overline{u}}{\partial \overline{y}},\ \ -k\frac{\partial T}{\partial \overline{y}} = h_f(T_f - T),\ \ C = C_w \quad \text{at} \quad \overline{y} = 0 \tag{2.6a}$$

$$\overline{u} = \overline{u}_e(x),\ \ \overline{\omega} = 0,\ \ T = T_\infty,\ \ C = C_\infty \quad \text{as} \quad \overline{y} \to \infty \tag{2.6b}$$

where, the subscripts w and ∞ indicate the conditions at the wall and the outer edge of the boundary layer respectively, h_f is the convective heat transfer coefficient, k is the thermal conductivity of the fluid and n is a material constant ($0 \leq n \leq 1$). Generally, when $n = 0$, Eq.(2.6) yields $\overline{\omega} = 0$ and this represents the case of concentrated particle flows in which the micro-elements close to the wall are not able to rotate. The case corresponding to $n = 1/2$ results in the vanishing of antisymmetric part of stress tensor and represents weak concentrations. The particle spin is equal to fluid vorticity at the boundary for the fine particle suspensions. The case corresponding to $n = 1$ is representative of turbulent boundary layer flows [3]. Thus, for $n = 0$, particles are not free to rotate near the surface, whereas, as n increases from 0 to 1, the microrotation term gets augmented and induces flow enhancement. Further, the assumption $\gamma = \left(\mu + \frac{\kappa}{2}\right) j$ is incorporated to allow the field equations to predict the correct behavior in the limiting case when the microstructure effects become negligible and the total spin $\overline{\omega}$ reduces to the angular velocity [3]. The same symbols are used throughout the thesis unless otherwise specified.

In this chapter, two types (cases) of problems are considered: (a) free/natural convection and (b) mixed convection.

2.2.1 Case(a): Natural Convection

The flow is assumed to be a natural convection which is caused by buoyancy forces only without any external agent, and hence the velocity of the external flow becomes zero ($i.e., \overline{u}_e = 0$). Initially, we introduce the following dimensionless variables

$$\left.\begin{aligned} x = \frac{\overline{x}}{L},\ y = \frac{\overline{y}}{L}\mathrm{Gr}^{1/4},\ u = \frac{L}{\nu \mathrm{Gr}^{1/2}}\overline{u},\ v = \frac{L}{\nu \mathrm{Gr}^{1/4}}\overline{v}, \\ \omega = \frac{L^2}{\nu \mathrm{Gr}^{3/4}}\overline{\omega},\ \theta = \frac{T - T_\infty}{T_f - T_\infty},\ \phi = \frac{C - C_\infty}{C_w - C_\infty}, \end{aligned}\right\} \tag{2.7}$$

where $\mathrm{Gr} = \dfrac{g^* \beta_{T_0}(T_f - T_\infty)L^3}{\nu^2}$ is the Grashof number.

Later, the stream function ψ is introduced to satisfy the continuity equation (2.1) identically by

$$u = \frac{\partial \psi}{\partial y}, \quad v = -\frac{\partial \psi}{\partial x}. \tag{2.8}$$

Substituting (2.7) and (2.8) into Eqs.(2.2)-(2.5), we get the following momentum, angular momentum, energy and concentration equations

$$\frac{\partial \psi}{\partial y}\frac{\partial^2 \psi}{\partial x \partial y} - \frac{\partial \psi}{\partial x}\frac{\partial^2 \psi}{\partial y^2} - \left(\frac{1}{1-N}\right)\frac{\partial^3 \psi}{\partial y^3} - \left(\frac{N}{1-N}\right)\frac{\partial \omega}{\partial y} - \frac{\beta_T(x)}{\beta_{T_0}}\theta - \frac{\beta_C(x)(C_w - C_\infty)}{\beta_{T_0}(T_f - T_\infty)}\phi = 0 \tag{2.9}$$

$$\frac{\partial \psi}{\partial y}\frac{\partial \omega}{\partial x} - \frac{\partial \psi}{\partial x}\frac{\partial \omega}{\partial y} - \left(\frac{2-N}{2-2N}\right)\frac{\partial^2 \omega}{\partial y^2} + \left(\frac{N}{1-N}\right)\left[2\omega + \frac{\partial^2 \psi}{\partial y^2}\right] = 0 \tag{2.10}$$

$$\frac{\partial \psi}{\partial y}\frac{\partial \theta}{\partial x} - \frac{\partial \psi}{\partial x}\frac{\partial \theta}{\partial y} - \frac{1}{\mathrm{Pr}}\frac{\partial^2 \theta}{\partial y^2} = 0 \tag{2.11}$$

$$\frac{\partial \psi}{\partial y}\frac{\partial \phi}{\partial x} - \frac{\partial \psi}{\partial x}\frac{\partial \phi}{\partial y} - \frac{1}{\mathrm{Sc}}\frac{\partial^2 \phi}{\partial y^2} = 0 \tag{2.12}$$

In usual definitions, ν is the kinematic viscosity, $\mathrm{Pr} = \dfrac{\nu}{\alpha}$ is the Prandtl number, $\mathrm{Sc} = \dfrac{\nu}{D}$ is the Schmidt number, $N = \dfrac{\kappa}{\mu + \kappa}$ $(0 \le N < 1)$ is the coupling number [23] and the micro-inertia

density is taken to be $j = \dfrac{L^2}{\mathrm{Gr}^{1/2}}$.

Now, the boundary conditions (2.6) become

$$\frac{\partial \psi}{\partial y} = 0, \;\; \frac{\partial \psi}{\partial x} = f_w, \;\; \omega = -n\frac{\partial^2 \psi}{\partial y^2}, \;\; \frac{\partial \theta}{\partial y} = -\mathrm{Bi}(1-\theta), \;\; \phi = 1 \quad \text{at} \quad y = 0 \tag{2.13a}$$

$$\frac{\partial \psi}{\partial y} = 0, \;\; \omega = 0, \;\; \theta = 0, \;\; \phi = 0 \quad \text{as} \quad y \to \infty \tag{2.13b}$$

where $f_w = -\dfrac{L}{\nu \mathrm{Gr}^{1/4}}\, v_w$ is the suction/injection parameter. It is worth mentioning that f_w determines the transpiration rate at the surface. Further, $f_w > 0$ represents suction, $f_w < 0$ indicates injection and $f_w = 0$ corresponds to an impermeable surface. $\mathrm{Bi} = \dfrac{h_f\, L}{k\, \mathrm{Gr}^{1/4}}$ is the Biot number and physically, it is the ratio of internal thermal resistance of the plate to the boundary layer thermal resistance of the hot fluid at the bottom of the surface.

Similarity representation via Lie scaling group transformations

A one-parameter Lie scaling group of transformations, which is a simplified form of Lie group transformation, is selected as (For Ref. See [90])

$$\begin{aligned} \Gamma : x^* = x\, e^{\varepsilon\, \alpha_1},\; y^* = y\, e^{\varepsilon\, \alpha_2},\; \psi^* = \psi\, e^{\varepsilon\, \alpha_3},\; \omega^* = \omega\, e^{\varepsilon\, \alpha_4}, \\ \theta^* = \theta\, e^{\varepsilon\, \alpha_5},\; \phi^* = \phi\, e^{\varepsilon\, \alpha_6},\; \beta_T^* = \beta_T\, e^{\varepsilon\, \alpha_7},\; \beta_C^* = \beta_C\, e^{\varepsilon\, \alpha_8} \end{aligned} \tag{2.14}$$

Here $\varepsilon \neq 0$ is the parameter of the group and $\alpha_i's$ are arbitrary real numbers, whose interrelationship will be determined by our analysis. Transformations in Eq.(2.14) may be treated as a point transformation, transforming the coordinates as given below:

$$(x,\, y,\, \psi,\, \omega,\, \theta,\, \phi,\, \beta_T,\, \beta_C) = (x^*,\, y^*,\, \psi^*,\, \omega^*,\, \theta^*,\, \phi^*,\, \beta_T^*,\, \beta_C^*)$$

Investigating the relationship among the exponents $\alpha's$ such that

$$\Delta_j \left[x^*,\, y^*,\, u^*,\, v^*,\, ...,\, \frac{\partial^3 \psi^*}{\partial y^{*3}}\right] = H_j \left[x,\, y,\, u,\, v,\, ...,\, \frac{\partial^3 \psi}{\partial y^3};\, a\right] \Delta_j \left[x,\, y,\, u,\, v,\, ...,\, \frac{\partial^3 \psi}{\partial y^3}\right],\; (j = 1, 2, 3, 4)$$

This is the requirement that the differential forms Δ_1, Δ_2, Δ_3 and Δ_4 are conformally invariant under the transformation Eq.(2.14). Substituting the transformations Eq.(2.14) into Eqs.(2.9)-

(2.12), the following equations are obtained

$$\Delta_1 = e^{\varepsilon(\alpha_1+2\alpha_2-2\alpha_3)}\left(\frac{\partial\psi^*}{\partial y^*}\frac{\partial^2\psi^*}{\partial x^*\partial y^*} - \frac{\partial\psi^*}{\partial x^*}\frac{\partial^2\psi^*}{\partial y^{*2}}\right) - \frac{\beta_T^*}{\beta_{T_0}}e^{-\varepsilon(\alpha_5+\alpha_7)}\theta^* \tag{2.15a}$$

$$-\left(\frac{1}{1-N}\right)e^{\varepsilon(3\alpha_2-\alpha_3)}\frac{\partial^3\psi^*}{\partial y^{*3}} - \left(\frac{N}{1-N}\right)e^{\varepsilon(\alpha_2-\alpha_4)}\frac{\partial\omega^*}{\partial y^*} - \frac{\beta_C^*(C_w-C_\infty)}{\beta_{T_0}(T_f-T_\infty)}e^{-\varepsilon(\alpha_6+\alpha_8)}\phi^* = 0$$

$$\Delta_2 = e^{\varepsilon(\alpha_1+\alpha_2-\alpha_3-\alpha_4)}\left(\frac{\partial\psi^*}{\partial y^*}\frac{\partial\omega^*}{\partial x^*} - \frac{\partial\psi^*}{\partial x^*}\frac{\partial\omega^*}{\partial y^*}\right) - \left(\frac{2-N}{2-2N}\right)e^{\varepsilon(2\alpha_2-\alpha_4)}\frac{\partial^2\omega^*}{\partial y^{*2}} + \tag{2.15b}$$

$$\left(\frac{N}{1-N}\right)\left(2\omega^* e^{-\varepsilon\,\alpha_4} + e^{\varepsilon(2\alpha_2-\alpha_3)}\frac{\partial^2\psi^*}{\partial y^{*2}}\right) = 0$$

$$\Delta_3 = e^{\varepsilon(\alpha_1+\alpha_2-\alpha_3-\alpha_5)}\left(\frac{\partial\psi^*}{\partial y^*}\frac{\partial\theta^*}{\partial x^*} - \frac{\partial\psi^*}{\partial x^*}\frac{\partial\theta^*}{\partial y^*}\right) - \frac{1}{\mathrm{Pr}}e^{\varepsilon(2\alpha_2-\alpha_5)}\left(\frac{\partial^2\theta^*}{\partial y^{*2}}\right) = 0 \tag{2.15c}$$

$$\Delta_4 = e^{\varepsilon(\alpha_1+\alpha_2-\alpha_3-\alpha_6)}\left(\frac{\partial\psi^*}{\partial y^*}\frac{\partial\phi^*}{\partial x^*} - \frac{\partial\psi^*}{\partial x^*}\frac{\partial\phi^*}{\partial y^*}\right) - \frac{1}{\mathrm{Sc}}e^{\varepsilon(2\alpha_2-\alpha_6)}\left(\frac{\partial^2\phi^*}{\partial y^{*2}}\right) = 0 \tag{2.15d}$$

Now, the boundary conditions (2.13) become

$$e^{\varepsilon(\alpha_2-\alpha_3)}\frac{\partial\psi^*}{\partial y^*} = 0,\;\; e^{\varepsilon(\alpha_1-\alpha_3)}\frac{\partial\psi^*}{\partial x^*} = f_w,\;\; e^{-\varepsilon\alpha_4}\omega^* = -ne^{\varepsilon(2\alpha_2-\alpha_3)}\frac{\partial^2\psi^*}{\partial y^{*2}},$$

$$e^{\varepsilon(\alpha_2-\alpha_5)}\frac{\partial\theta^*}{\partial y^*} = -\mathrm{Bi}(1-e^{-\varepsilon\alpha_5}\theta^*),\;\; e^{-\varepsilon\alpha_6}\phi^* = 1 \quad \text{at} \quad y^* = 0 \tag{2.16a}$$

$$e^{\varepsilon(\alpha_2-\alpha_3)}\frac{\partial\psi^*}{\partial y^*} = 0,\;\; e^{-\varepsilon\alpha_4}\omega^* = 0,\;\; e^{-\varepsilon\alpha_5}\theta^* = 0,\;\; e^{-\varepsilon\alpha_6}\phi^* = 0 \quad \text{as} \quad y^* \to \infty \tag{2.16b}$$

From the Lie group analysis, it can be observed that the system remains invariant under the group transformation Γ. To maintain this invariant nature, equating the exponents of Eqs. (2.15)-(2.16), we get

$$\left.\begin{aligned}
&\alpha_1+2\alpha_2-2\alpha_3 = 3\alpha_2-\alpha_3 = \alpha_2-\alpha_4 = -\alpha_5-\alpha_7 = -\alpha_6-\alpha_8;\\
&\alpha_1+\alpha_2-\alpha_3-\alpha_4 = 2\alpha_2-\alpha_4 = -\alpha_4 = 2\alpha_2-\alpha_3;\\
&\alpha_1+\alpha_2-\alpha_3-\alpha_5 = 2\alpha_2-\alpha_5; \alpha_1+\alpha_2-\alpha_3-\alpha_6 = 2\alpha_2-\alpha_6;\\
&\alpha_1-\alpha_3 = 0; -\alpha_4 = 2\alpha_2-\alpha_3; \alpha_2-\alpha_5 = 0 = -\alpha_5; \alpha_6 = 0
\end{aligned}\right\} \tag{2.17}$$

Solving the linear system of Eq.(2.17), we get the following relationship among the exponents

$$\alpha_1 = \alpha_3 = \alpha_4 = \alpha_7 = \alpha_8,\; \alpha_2 = \alpha_5 = \alpha_6 = 0 \tag{2.18}$$

Substituting (2.18) into (2.14), the set of transformations Γ reduces to

$$\left.\begin{aligned} &x^* = x\, e^{\varepsilon\,\alpha_1},\ y^* = y,\ \psi^* = \psi\, e^{\varepsilon\,\alpha_1},\ \omega^* = \omega\, e^{\varepsilon\,\alpha_1}, \\ &\theta^* = \theta,\ \phi^* = \phi,\ \beta_T^* = \beta_T\, e^{\varepsilon\,\alpha_1},\ \beta_C^* = \beta_C\, e^{\varepsilon\,\alpha_1} \end{aligned}\right\} \tag{2.19}$$

Expanding the transformations (2.19) by using the Taylor series in powers of ε, keeping the term up to the first degree (neglecting higher power of ε), we obtain

$$\left.\begin{aligned} &x^* - x = \varepsilon\,\alpha_1 x,\ y^* = y,\ \psi^* - \psi = \varepsilon\,\alpha_1\psi,\ \omega^* - \omega = \varepsilon\,\alpha_1\omega, \\ &\theta^* = \theta,\ \phi^* = \phi,\ \beta_T^* - \beta_T = \varepsilon\,\alpha_1\beta_T,\ \beta_C^* - \beta_C = \varepsilon\,\alpha_1\beta_C \end{aligned}\right\} \tag{2.20}$$

The characteristic equations to the above system (2.20) can be written as

$$\frac{dx}{\alpha_1 x} = \frac{dy}{0} = \frac{d\psi}{\alpha_1\psi} = \frac{d\omega}{\alpha_1\omega} = \frac{d\theta}{0} = \frac{d\phi}{0} = \frac{d\beta_T}{\alpha_1\beta_T} = \frac{d\beta_C}{\alpha_1\beta_C} \tag{2.21}$$

Solving the above characteristic equations, the similarity transformations are obtained as follows

$$\eta = y,\ \ \psi = xf(\eta),\ \ \omega = xg(\eta), \beta_T = \beta_{T_0} x,\ \ \beta_C = \beta_{C_0} x,\ \ \theta = \theta(\eta),\ \ \phi = \phi(\eta) \tag{2.22}$$

where β_{T_0} and β_{C_0} are the constant thermal and solutal expansion coefficients.

Using (2.22) in Eqs.(2.9)-(2.12), we get the following system of similarity equations

$$\left(\frac{1}{1-N}\right) f''' + ff'' - f'^2 + \left(\frac{N}{1-N}\right) g' + \theta + \mathcal{B}\phi = 0 \tag{2.23}$$

$$\left(\frac{2-N}{2-2N}\right) g'' + fg' - f'g - \left(\frac{N}{1-N}\right)(2g + f'') = 0 \tag{2.24}$$

$$\frac{1}{\mathrm{Pr}}\theta'' + f\theta' = 0 \tag{2.25}$$

$$\frac{1}{\mathrm{Sc}}\phi'' + f\phi' = 0 \tag{2.26}$$

where the primes indicate differentiation with respect to η alone and $\mathcal{B} = \dfrac{\beta_{C_0}(C_w - C_\infty)}{\beta_{T_0}(T_f - T_\infty)}$ is the buoyancy ratio.

Boundary conditions (2.13) in terms of f, g, θ and ϕ become

$$f(0) = f_w,\ f'(0) = 0,\ g(0) = -nf''(0),\ \theta'(0) = -\mathrm{Bi}[1-\theta(0)],\ \phi(0) = 1, \tag{2.27a}$$

$$f'(\infty) \to 0,\ g(\infty) \to 0,\ \theta(\infty) \to 0,\ \phi(\infty) \to 0 \tag{2.27b}$$

Skin friction, Wall couple stress, Heat and Mass transfer coefficients

The wall shear stress and the wall couple stress are

$$\tau_w = \left[(\mu+\kappa)\frac{\partial \overline{u}}{\partial \overline{y}} + \kappa\overline{\omega}\right]_{\overline{y}=0} \quad \text{and} \quad m_w = \gamma\left[\frac{\partial \overline{\omega}}{\partial \overline{y}}\right]_{\overline{y}=0} \tag{2.28a}$$

and the heat and mass transfer rates along the plate respectively, are given by

$$q_w = -k\left[\frac{\partial T}{\partial \overline{y}}\right]_{\overline{y}=0} \quad \text{and} \quad q_m = -D\left[\frac{\partial C}{\partial \overline{y}}\right]_{\overline{y}=0} \tag{2.29a}$$

The non-dimensional skin friction $C_f = \dfrac{2\tau_w}{\rho\overline{u}_*^2}$, wall couple stress $M_w = \dfrac{m_w}{\rho\overline{u}_*^2\overline{x}}$, local Nusselt number $Nu_{\overline{x}} = \dfrac{q_w\overline{x}}{k(T_f - T_\infty)}$ and local Sherwood number $Sh_{\overline{x}} = \dfrac{q_m\overline{x}}{D(C_w - C_\infty)}$, are given by

$$\left.\begin{aligned} &C_f\mathrm{Gr}_{\overline{x}}^{1/4} = 2\left(\frac{1-nN}{1-N}\right)f''(0), \quad M_w\mathrm{Gr}_{\overline{x}}^{1/2} = \left(\frac{2-N}{2-2N}\right)g'(0), \\ &\frac{Nu_{\overline{x}}}{\mathrm{Gr}_{\overline{x}}^{1/4}} = -\theta'(0), \quad \frac{Sh_{\overline{x}}}{\mathrm{Gr}_{\overline{x}}^{1/4}} = -\phi'(0) \end{aligned}\right\} \tag{2.30}$$

where $\overline{u}_*$ is the characteristic velocity and $\mathrm{Gr}_{\overline{x}} = \dfrac{g^*\beta_{T_0}(T_f - T_\infty)\overline{x}^3}{\nu^2}$ is the local Grashof number.

Numerical Solution

The governing Eqs.(2.23)-(2.26) along with the boundary conditions (2.27) are solved numerically using the spectral quasi-linearization method (for more details, one can refer the works of Motsa *et al.* [63, 64]). The following procedure includes main steps of the spectral quasi-linearization method.

Assume that the solutions f_r, g_r, θ_r and ϕ_r of Eqs.(2.23)-(2.26) at the $(r+1)^{th}$ iteration are f_{r+1},

g_{r+1}, θ_{r+1} and ϕ_{r+1}. If the solutions at the previous iteration are sufficiently close to the solutions at the present iteration, then the nonlinear components of Eqs.(2.23)-(2.26) can be linearised using one–term Taylor series of multiple variables so that the Eqs.(2.23)-(2.26) give the following iterative sequence of linear differential equations

$$\left(\frac{1}{1-N}\right) f'''_{r+1} + a_{1,r}\, f''_{r+1} + a_{2,r}\, f'_{r+1} + a_{3,r}\, f_{r+1} + \left(\frac{N}{1-N}\right) g'_{r+1} + \theta_{r+1} + \mathcal{B}\,\phi_{r+1} = R_{1,r} \quad (2.31)$$

$$\left(\frac{2-N}{2-2N}\right) g''_{r+1} + b_{3,r}\, g'_{r+1} + b_{4,r}\, g_{r+1} + b_{1,r}\, f'_{r+1} + b_{2,r}\, f_{r+1} - \left(\frac{N}{1-N}\right) f''_{r+1} = R_{2,r} \quad (2.32)$$

$$\frac{1}{\mathrm{Pr}}\,\theta''_{r+1} + c_{1,r}\, f_{r+1} + c_{2,r}\,\theta'_{r+1} = R_{3,r} \quad (2.33)$$

$$\frac{1}{\mathrm{Sc}}\,\phi''_{r+1} + d_{1,r}\, f_{r+1} + d_{2,r}\,\phi'_{r+1} = R_{4,r} \quad (2.34)$$

where the coefficients $a_{s_1,r}(s_1 = 1, 2, 3)$, $b_{s_2,r}(s_2 = 1, 2, .., 4)$, $c_{s_3,r}(s_3 = 1, 2)$, $d_{s_4,r}(s_4 = 1, 2)$ and $R_{s_5,r}(s_5 = 1, 2, .., 4)$ are known functions (calculated from previous iterations) and are defined as

$$a_{1,r} = f_r,\ a_{2,r} = -2\, f'_r,\ a_{3,r} = f''_r,\ R_{1,r} = f_r\, f''_r - (f'_r)^2,$$

$$b_{1,r} = -g_r,\ b_{2,r} = g'_r,\ b_{3,r} = f_r,\ b_{4,r} = -f'_r - \left(\frac{2N}{1-N}\right),\ R_{2,r} = f_r\, g'_r - f'_r\, g_r,$$

$$c_{1,r} = \theta'_r,\ c_{2,r} = f_r,\ R_{3,r} = f_r\,\theta'_r,\ d_{1,r} = \phi'_r,\ d_{2,r} = f_r,\ R_{4,r} = f_r\,\phi'_r$$

subject to the boundary conditions

$$f_{r+1}(0) = f_w,\ f'_{r+1}(0) = 0,\ g_{r+1}(0) = -n\, f''_{r+1}(0),\ \theta'_{r+1}(0) = -\mathrm{Bi}(1 - \theta_{r+1}(0)), \quad (2.35a)$$

$$\phi_{r+1}(0) = 1$$

$$f'_{r+1}(\infty) = 0,\ g_{r+1}(\infty) = 0,\ \theta_{r+1}(\infty) = 0,\ \phi_{r+1}(\infty) = 0 \quad (2.35b)$$

The system of equations (2.31) to (2.34) constitute a linear system of coupled differential equations with variable coefficients and hence, it can be solved iteratively using any numerical method for $r = 1, 2, 3, ...$ In this work, as will be discussed below, the Chebyshev pseudo–spectral method is used to solve the system of equations (2.31) to (2.34). Starting from the following set of initial approximations

$$f_0(\eta) = f_w - (\eta + 1)e^{-\eta} + 1,\ g_0(\eta) = -n(1-\eta)\, e^{-\eta},\ \theta_0(\eta) = \frac{\mathrm{Bi}}{\mathrm{Bi}+1} e^{-\eta},\ \phi_0(\eta) = e^{-\eta}$$

the system of equations (2.31) to (2.34) is solved iteratively for $f_{r+1}(\eta)$, $g_{r+1}(\eta)$, $\theta_{r+1}(\eta)$, $\phi_{r+1}(\eta)$ when $r = 0, 1, 2,...$ For this, the equations are discretized using the Chebyshev spectral collocation method as follows:

The unknown functions are approximated by the Chebyshev interpolating polynomials in such way that they are collocated at the Gauss–Lobatto collocation points defined as

$$\tau_j = \cos\frac{\pi j}{\overline{N}}, \quad j = 0, 1, 2, ..., \overline{N} \tag{2.36}$$

where $\overline{N}$ is the number of collocation points.

The physical region $[0, \infty)$ is transformed into the region $[-1, 1]$ using the domain truncation technique in which the problem is solved on the interval $[0, \eta_\infty]$ instead of $[0, \infty)$. This leads to the mapping

$$\frac{\eta}{\eta_\infty} = \frac{\tau + 1}{2}, \quad -1 \leq \tau \leq 1 \tag{2.37}$$

where η_∞ is the scaling parameter used to invoke the boundary condition at infinity.

The functions f_{r+1}, g_{r+1}, θ_{r+1} and ϕ_{r+1} are approximated at the collocation points by

$$\left.\begin{aligned} f_{r+1}(\tau) = \sum_{k=0}^{\overline{N}} f_{r+1}(\tau_k)T_k(\tau_j),\ g_{r+1}(\tau) = \sum_{k=0}^{\overline{N}} g_{r+1}(\tau_k)T_k(\tau_j), \\ \theta_{r+1}(\tau) = \sum_{k=0}^{\overline{N}} \theta_{r+1}(\tau_k)T_k(\tau_j),\ \phi_{r+1}(\tau) = \sum_{k=0}^{\overline{N}} \phi_{r+1}(\tau_k)T_k(\tau_j), \quad j = 0, 1, 2, ..., \overline{N} \end{aligned}\right\} \tag{2.38}$$

where T_k is the k^{th} Chebyshev polynomial defined as

$$T_k(\tau) = \cos[k\ \cos^{-1}(\tau)] \tag{2.39}$$

The derivatives of the variables at the collocation points are represented as

$$\left.\begin{aligned} \frac{d^p f_{r+1}}{d\eta^p} = \sum_{k=0}^{\overline{N}} \mathbf{D}_{lk}^p f_{r+1}(\tau_k),\ \frac{d^p g_{r+1}}{d\eta^p} = \sum_{k=0}^{\overline{N}} \mathbf{D}_{lk}^p g_{r+1}(\tau_k), \\ \frac{d^p \theta_{r+1}}{d\eta^p} = \sum_{k=0}^{\overline{N}} \mathbf{D}_{lk}^p \theta_{r+1}(\tau_k),\ \frac{d^p \phi_{r+1}}{d\eta^p} = \sum_{k=0}^{\overline{N}} \mathbf{D}_{lk}^p \phi_{r+1}(\tau_k), \quad l = 0, 1, ..., \overline{N} \end{aligned}\right\} \tag{2.40}$$

where p is the order of the derivative and $\mathbf{D} = \dfrac{2\mathcal{D}}{\eta_\infty}$ is the Chebyshev spectral differentiation matrix

and its entries are clearly defined in the text book by Canuto *et al.* [18].

Substitution of Eqs.(2.36)-(2.40) into Eqs.(2.31)-(2.34) leads to the following matrix equation

$$A\,X = R \tag{2.41}$$

subject to the boundary conditions

$$\left.\begin{aligned} &f_{r+1}(\tau_{\overline{N}}) = f_w,\ \sum_{k=0}^{\overline{N}} \mathbf{D}_{\overline{N}k} f_{r+1}(\tau_k) = 0,\ g_{r+1}(\tau_{\overline{N}}) = -n \sum_{k=0}^{\overline{N}} \mathbf{D}^2_{\overline{N}k} f_{r+1}(\tau_k), \\ &\sum_{k=0}^{\overline{N}} \mathbf{D}_{\overline{N}k} \theta_{r+1}(\tau_k) - \mathrm{Bi}\,\theta_{r+1}(\tau_{\overline{N}}) = -\mathrm{Bi},\ \phi_{r+1}(\tau_{\overline{N}}) = 1, \\ &\sum_{k=0}^{\overline{N}} \mathbf{D}_{0k} f_{r+1}(\tau_k) = 0,\ g_{r+1}(\tau_0) = 0,\ \theta_{r+1}(\tau_0) = 0,\ \phi_{r+1}(\tau_0) = 0 \end{aligned}\right\} \tag{2.42}$$

In Eq.(2.41), A is $(4\overline{N}+4)\times(4\overline{N}+4)$ square matrix, X and R are $(4\overline{N}+4)\times 1$ column vectors, which are defined as

$$A = \begin{bmatrix} A_{11} & A_{12} & A_{13} & A_{14} \\ A_{21} & A_{22} & A_{23} & A_{24} \\ A_{31} & A_{32} & A_{33} & A_{34} \\ A_{41} & A_{42} & A_{43} & A_{44} \end{bmatrix},\ X = \begin{bmatrix} \mathbf{F}_{r+1} \\ \mathbf{G}_{r+1} \\ \Theta_{r+1} \\ \Phi_{r+1} \end{bmatrix},\ R = \begin{bmatrix} \mathbf{R}_1 \\ \mathbf{R}_2 \\ \mathbf{R}_3 \\ \mathbf{R}_4 \end{bmatrix} \tag{2.43}$$

where

$$\begin{aligned} &A_{11} = \left(\tfrac{1}{1-N}\right)\mathbf{D}^3 + \mathrm{diag}[a_{1,r}]\mathbf{D}^2 + \mathrm{diag}[a_{2,r}]\mathbf{D} + \mathrm{diag}[a_{3,r}],\ A_{12} = \left(\tfrac{N}{1-N}\right)\mathbf{D},\ A_{13} = \mathbf{I},\ A_{14} = \mathcal{B}\mathbf{I}, \\ &A_{21} = -\left(\tfrac{N}{1-N}\right)\mathbf{D}^2 + \mathrm{diag}[b_{1,r}]\mathbf{D} + \mathrm{diag}[b_{2,r}],\ A_{22} = \left(\tfrac{2-N}{2-2N}\right)\mathbf{D}^2 + \mathrm{diag}[b_{3,r}]\mathbf{D} + \mathrm{diag}[b_{4,r}], \\ &A_{23} = \mathbf{0},\ A_{24} = \mathbf{0},\ A_{31} = \mathrm{diag}[c_{1,r}],\ A_{32} = \mathbf{0},\ A_{33} = \tfrac{1}{\mathrm{Pr}}\mathbf{D}^2 + \mathrm{diag}[c_{2,r}]\,\mathbf{D},\ A_{34} = \mathbf{0}, \end{aligned}$$

$$\begin{aligned} &A_{41} = \mathrm{diag}[d_{1,r}],\ A_{42} = \mathbf{0},\ A_{43} = \mathbf{0},\ A_{44} = \tfrac{1}{\mathrm{Sc}}\mathbf{D}^2 + \mathrm{diag}[d_{2,r}]\mathbf{D}, \\ &\mathbf{R}_1 = R_{1,r},\quad \mathbf{R}_2 = R_{2,r},\quad \mathbf{R}_3 = R_{3,r},\quad \mathbf{R}_4 = R_{4,r} \\ &\mathbf{F} = [f_{r+1}(\tau_0), f_{r+1}(\tau_1), ..., f_{r+1}(\tau_{\overline{N}})]^T,\ \ \mathbf{G} = [g_{r+1}(\tau_0), g_{r+1}(\tau_1), ..., g_{r+1}(\tau_{\overline{N}})]^T, \\ &\Theta = [\theta_{r+1}(\tau_0), \theta_{r+1}(\tau_1), ..., \theta_{r+1}(\tau_{\overline{N}})]^T,\ \ \Phi = [\phi_{r+1}(\tau_0), \phi_{r+1}(\tau_1), ..., \phi_{r+1}(\tau_{\overline{N}})]^T \end{aligned}$$

Here $\mathbf{I}$, $\mathbf{0}$ and diag[ ] are identity, zero and diagonal matrices respectively, all are of size $(\overline{N}+1)\times(\overline{N}+1)$. The subscript $\mathbf{r}$ denotes the iteration number.

After modifying the matrix system (2.41) to incorporate boundary condition (2.42), the solution is obtained as

$$X = A^{-1} R \tag{2.44}$$

Results and Discussion

It may be pointed out that the present problem reduces to free convective heat transfer in a micropolar fluid along an impermeable vertical plate without the convective boundary condition when $f_w = 0$, Bi $\to \infty$ and $\mathcal{B} = 0$. Also in the limiting case as $N \to 0$, the governing equations reduce to the corresponding equations of a free convective heat and mass transfer in a viscous fluid. In order to validate the code generated, for the special case of $N = 0$, $n = 0$, $\mathcal{B} = 0$, Pr $= 1$, Bi $\to \infty$ and $f_w = 0$, the results of the present problem have been compared with those of Merkin [57], Nazar*et al.* [72] and Molla *et al.* [60] and it is found that they are in good agreement [Tab. (2.1)]. The values of heat transfer rate, for $n = 0.5$, $\mathcal{B} = 0$, Pr $= 1$, Bi $\to \infty$ and $f_w = 0$, agree well with that of Nazar *et al.* [72] as shown in Tab. (2.2). To study the effects of coupling number N, suction/injection parameter f_w, Biot number Bi and material parameter n, computations have been carried out for $\mathcal{B} = 1.0$, Pr $= 0.71$ and Sc $= 0.22$.

The effects of coupling number N on the dimensionless velocity, microrotation, temperature and concentration are illustrated in Figs. 2.2(a)-2.2(d), for fixed values of other parameters. The coupling number N characterizes the coupling of linear and rotational motion arising from the motion of the fluid particles. In the case of $N = 0$ (i.e., as κ tends to zero), the micro-polarity is absent and the fluid become non-polar fluid. For large values of N, the effect of microstructure becomes significant, whereas, for small value of N, the individuality of the substructure is not significant. As N increases, it is found from Fig. 2.2(a) that the maximum velocity decreases in amplitude and the location of the maximum velocity moves farther away from the wall. Since $N \to 0$ corresponds to a viscous fluid, the velocity in case of a micropolar fluid is less compared to that of a viscous fluid case. Initially, the microrotation profile tends to become flat and then approaches to their free stream values far away from the wall with the increase of coupling number [Fig. 2.2(b)]. An increment in the value of N implies a higher vortex viscosity of the fluid which promotes the microrotation of a micropolar fluid. It is seen from Figs. 2.2(c) and 2.2(d) that the thickness of the thermal and concentration boundary layers of the fluid increase with an increase

in coupling number N. Hence, temperature and concentration in case of the micropolar fluid are more than those of the viscous fluid case.

The variation of Biot number Bi on the non-dimensional velocity, microrotation, temperature and concentration are displayed in Figs. 2.3(a)-2.3(d), for fixed values of other parameters. Generally, the fluid velocity is zero at plate surface and increases gradually away from plate to free stream value satisfying boundary conditions. It is interesting to note that an increase in the intensity of convective surface heat transfer Bi produces a significant enhancement in the fluid velocity within the momentum boundary layer. It can be observed from Fig. 2.3(b) that as Bi increases, the microrotation profile shows reverse rotation near the two boundaries. When Bi = 0, the plate is totally insulated, internal thermal resistance of the plate is extremely high and no convective heat transfer to the cold fluid on the upper part of the plate takes place. Also, the convective heating increases with Biot number and the case of Bi $\to \infty$ gives the isothermal surface which is clearly seen from the Fig. 2.3(c), where $\theta(0) = 1$. In fact, a higher Biot number indicates higher internal thermal resistance of the plate than the boundary layer thermal resistance. The fluid temperature is maximum at the plate surface and decreases exponentially to zero value far away from the plate satisfying boundary conditions. As a consequence, an increment in the Biot number leads to increase the fluid temperature efficiency. From Fig. 2.3(d), it is clear that the concentration of fluid decreases with the increase of Bi.

The influence of suction or injection parameter f_w on the dimensionless velocity, microrotation, temperature and concentration is depicted in Figs. 2.4(a)-2.4(d). Here, $f_w > 0$ represents suction and $f_w < 0$ denotes injection. From Fig. 2.4(a), the lower velocity is noticed in the case of suction when compared to the injection case. It can be observed from Fig. 2.4(b) that microrotation shows reverse rotation near two boundaries for both suction and injection parameter. From Fig. 2.4(c), it can be noticed that the temperature of the fluid is more in the case of injection, but less in the suction case when compared with the impermeable surface ($f_w = 0$). From Fig. 2.4(d), it can be observed that the concentration of fluid is more with the injection, but less with suction in comparison to the impermeable surface ($f_w = 0$). As a finale, the temperature and concentration are more in the case of injection, but less in suction case [Figs. 2.4(c) and 2.4(d)].

The variations of $C_f \mathrm{Gr}_{\overline{x}}^{1/4}$, $M_w \mathrm{Gr}_{\overline{x}}^{1/2}$, $\dfrac{Nu_{\overline{x}}}{\mathrm{Gr}_{\overline{x}}^{1/4}}$ and $\dfrac{Sh_{\overline{x}}}{\mathrm{Gr}_{\overline{x}}^{1/4}}$, which are proportional to the coefficients of skin-friction, wall couple stress, Nusselt and Sherwood numbers, are shown in Tab. (2.3). An

Table 2.1: *Comparison of* $-\theta'(0)$ *for free convective flow along a vertical flat plate in Newtonian fluid.*

Merkin [57]	Nazar *et al.* [72]	Molla *et al.* [60]	Present
0.4214	0.4214	0.4214	0.4214313

Table 2.2: *Comparison of* $-\theta'(0)$ *for the free convective flow of a micropolar fluid with the results obtained by Nazar* et al. *[72] for different values of coupling number* N*.*

N	Nazar *et al.* [72]	Present
0.00	0.4214	0.4214
0.33	0.3991	0.3990
0.50	0.3834	0.3834
0.60	0.3709	0.3709
0.66	0.3608	0.3608
0.75	0.3447	0.3447

increase in the value of coupling number N, results in higher skin friction and lower wall couple stress, heat and mass transfer rates. This may be beneficial in flow, temperature and concentration control of polymer processing. Thus, the presence of microscopic effects arising from the local structure and micromotion of the fluid elements reduces the heat and mass transfer rates. It can be noticed from this table that the skin-friction, wall couple stress, heat and mass transfer rates enhance with Bi for fixed values of other parameters. It is also noted that the skin-friction, wall couple stress, Nusselt and Sherwood number are less in the injection case, but more in suction case when compared to the impermeable surface. Finally, the skin friction reduces but the wall couple stress, heat and mass transfer rates increase with a material parameter n [Tab. (2.3)].

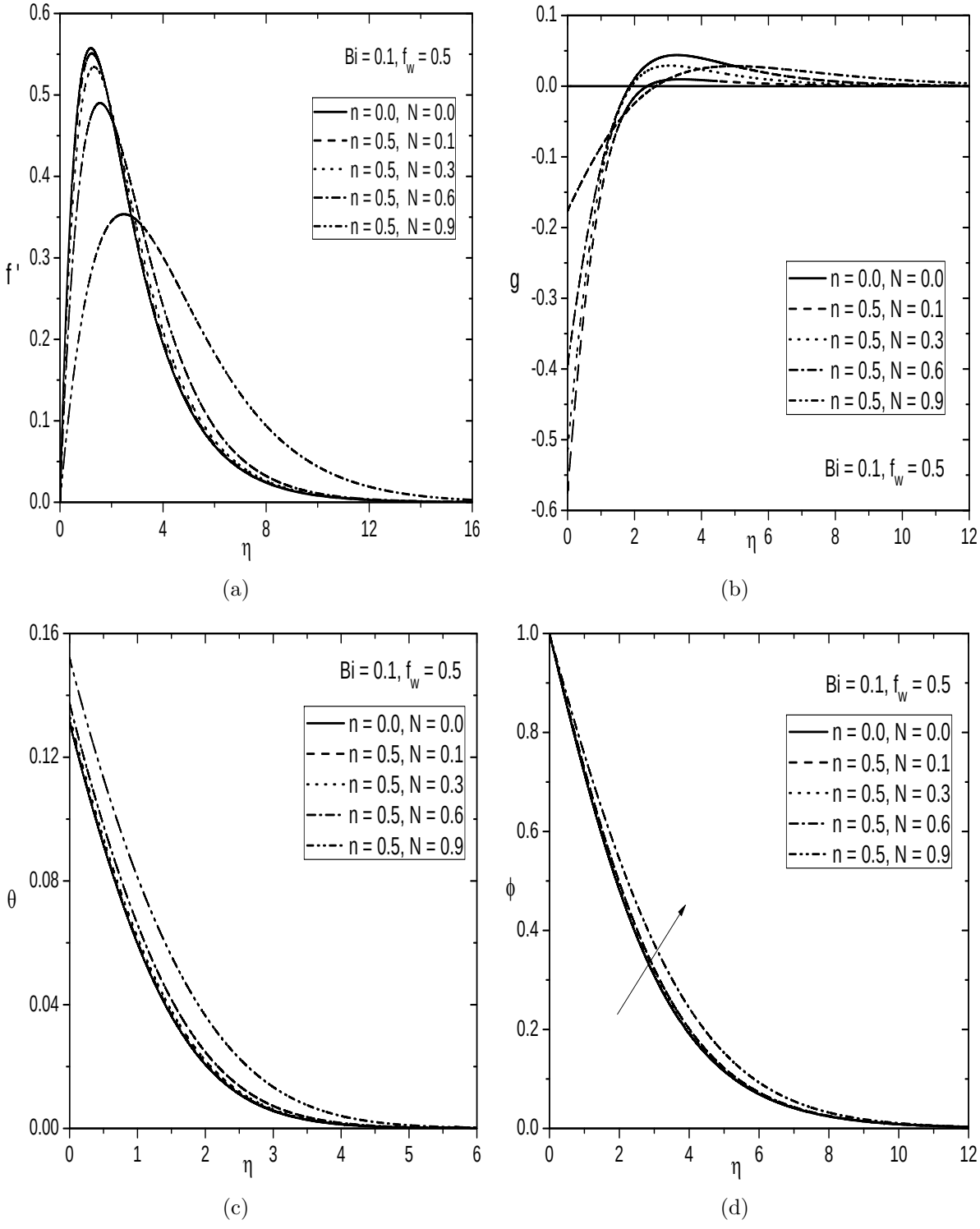

Figure 2.2: *Variation of N on (a)Velocity, (b)Microrotation, (c)Temperature and (d)Concentration profiles.*

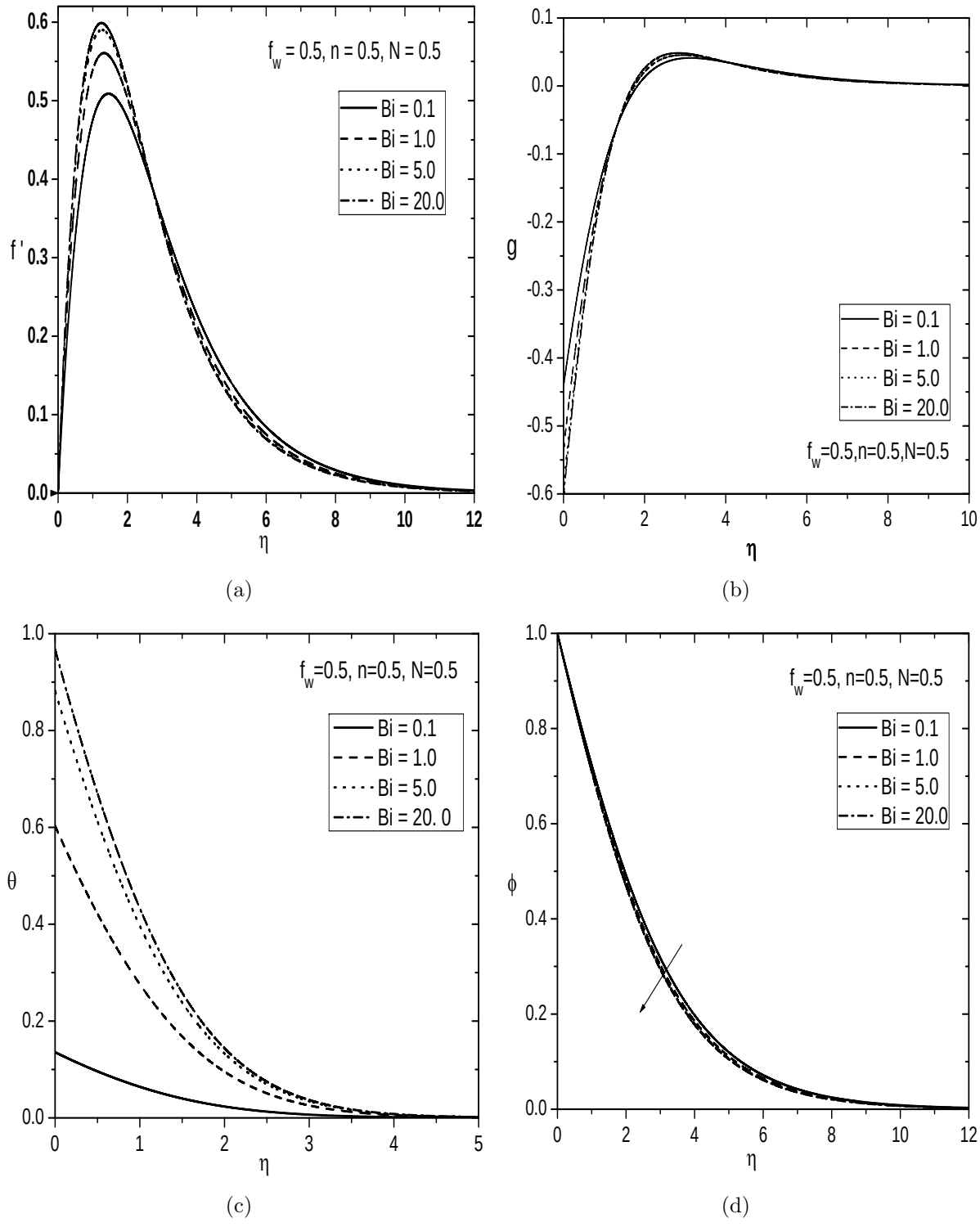

Figure 2.3: *Variation of Bi on (a)Velocity, (b)Microrotation, (c)Temperature and (d)Concentration profiles.*

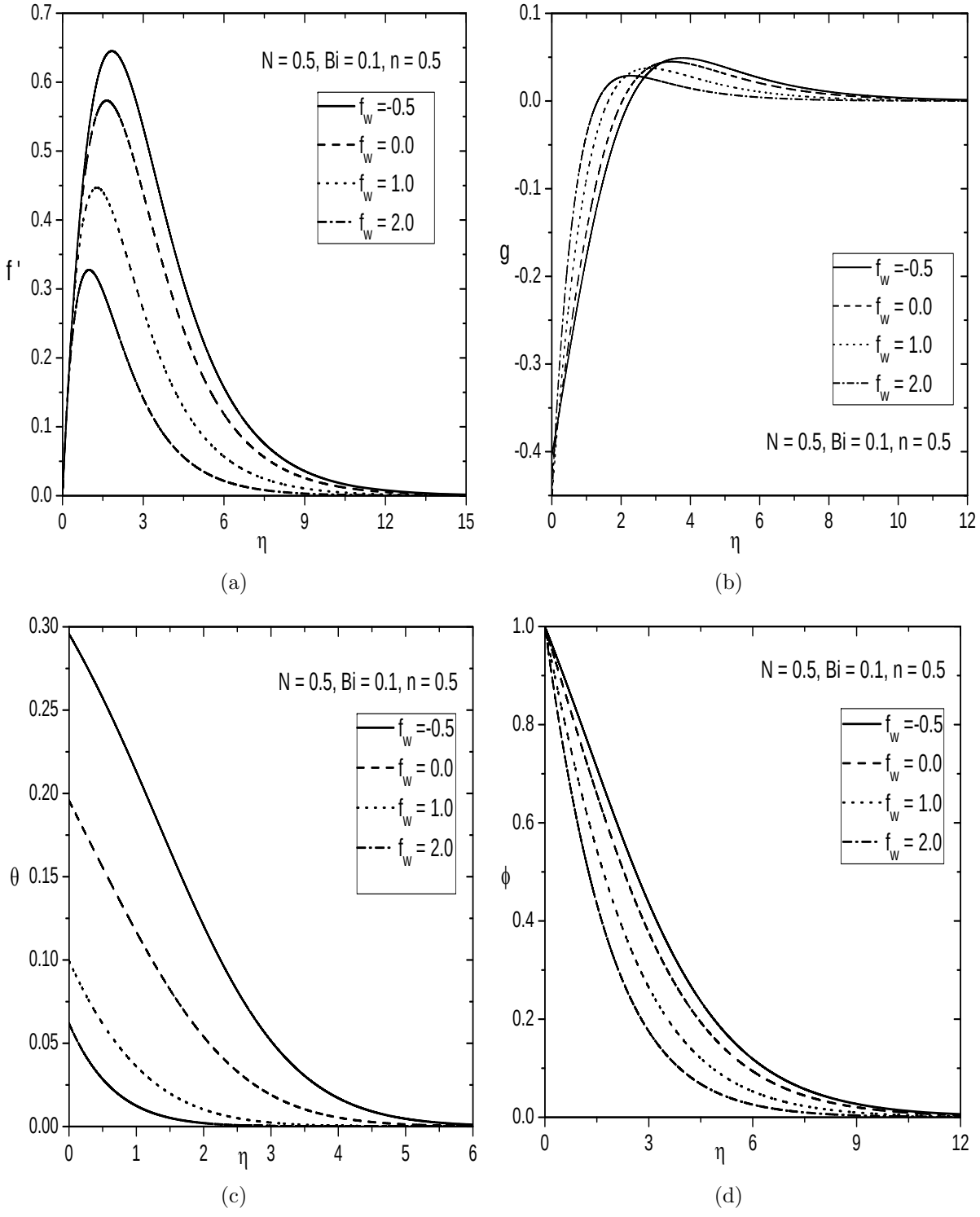

Figure 2.4: *Variation of f_w on (a)Velocity, (b)Microrotation, (c)Temperature and (d)Concentration profiles.*

Table 2.3: *Variation of skin friction, wall couple stress, Nusselt and Sherwood number for different values of micropolar parameter N, Biot numbers Bi, suction/injection parameter f_w and material parameter n.*

N	Bi	f_w	n	$C_f \mathrm{Gr}_{\overline{x}}^{1/4}$	$M_w \mathrm{Gr}_{\overline{x}}^{1/2}$	$\frac{Nu_{\overline{x}}}{\mathrm{Gr}_{\overline{x}}^{1/4}}$	$\frac{Sh_{\overline{x}}}{\mathrm{Gr}_{\overline{x}}^{1/4}}$
0.1	0.1	0.5	0.5	2.424227	0.63279	0.086824	0.301042
0.3	0.1	0.5	0.5	2.502716	0.639966	0.086672	0.298137
0.5	0.1	0.5	0.5	2.647987	0.630863	0.086437	0.293402
0.7	0.1	0.5	0.5	2.943561	0.603879	0.086006	0.284419
0.9	0.1	0.5	0.5	3.874631	0.550891	0.084799	0.258482
0.5	0.1	0.5	0.5	2.647987	0.630863	0.086437	0.293402
0.5	1.0	0.5	0.5	3.211755	0.805879	0.396928	0.30332
0.5	5.0	0.5	0.5	3.533141	0.908078	0.590276	0.30864
0.5	20.0	0.5	0.5	3.629791	0.939137	0.650654	0.310198
0.5	0.1	-0.5	0.5	2.426265	0.336219	0.070426	0.18013
0.5	0.1	0.0	0.5	2.530014	0.465429	0.08043	0.232171
0.5	0.1	1.0	0.5	2.737553	0.820899	0.090042	0.362603
0.5	0.1	0.5	0.0	2.916655	-0.289339	0.086161	0.286993
0.5	0.1	0.5	0.5	2.647987	0.630863	0.086437	0.293402

2.2.2 Case(b): Mixed Convection

The flow is assumed to be a mixed convection, which arises from both buoyancy forces and external flow with velocity $[\bar{u_e}(x)]$. We introduce the following dimensionless variables

$$\left.\begin{aligned} x = \frac{\overline{x}}{L},\ y = \frac{\overline{y}}{L} Re^{1/2},\ u = \frac{\overline{u}}{U_\infty},\ v = \frac{\overline{v}}{U_\infty} Re^{1/2}, \\ u_e = \frac{\overline{u}_e}{U_\infty},\ \omega = \frac{L^2}{\nu Re^{3/2}} \overline{\omega},\ \theta = \frac{T - T_\infty}{T_f - T_\infty},\ \phi = \frac{C - C_\infty}{C_w - C_\infty} \end{aligned}\right\} \tag{2.45}$$

where U_∞ is the reference velocity and $Re = \dfrac{U_\infty L}{\nu}$ is the global Reynold's number.

Substituting (2.45) and (2.8) into Eqs.(2.2)-(2.5), the momentum, angular momentum, energy, and concentration equations are obtained as follows

$$\frac{\partial \psi}{\partial y} \frac{\partial^2 \psi}{\partial x \partial y} - \frac{\partial \psi}{\partial x} \frac{\partial^2 \psi}{\partial y^2} - \left(\frac{1}{1 - N} \right) \frac{\partial^3 \psi}{\partial y^3} - \left(\frac{N}{1 - N} \right) \frac{\partial \omega}{\partial y} - u_e \frac{du_e}{dx}$$

$$- \frac{g^* \beta_T(\overline{x})(T_f - T_\infty)}{\nu^2 Re^2} \theta - \frac{g^* \beta_C(\overline{x})(C_w - C_\infty)}{\nu^2 Re^2} \phi = 0 \tag{2.46}$$

$$\frac{\partial\psi}{\partial y}\frac{\partial\omega}{\partial x}-\frac{\partial\psi}{\partial x}\frac{\partial\omega}{\partial y}-\left(\frac{2-N}{2-2N}\right)\frac{\partial^2\omega}{\partial y^2}+\left(\frac{N}{1-N}\right)\left(2\omega+\frac{\partial^2\psi}{\partial y^2}\right)=0 \tag{2.47}$$

$$\frac{\partial\psi}{\partial y}\frac{\partial\theta}{\partial x}-\frac{\partial\psi}{\partial x}\frac{\partial\theta}{\partial y}-\frac{1}{Pr}\frac{\partial^2\theta}{\partial y^2}=0 \tag{2.48}$$

$$\frac{\partial\psi}{\partial y}\frac{\partial\phi}{\partial x}-\frac{\partial\psi}{\partial x}\frac{\partial\phi}{\partial y}-\frac{1}{Sc}\frac{\partial^2\phi}{\partial y^2}=0 \tag{2.49}$$

Now, the boundary conditions (2.6) become

$$\frac{\partial\psi}{\partial y}=0,\ \ \frac{\partial\psi}{\partial x}=f_w,\ \ \omega=-n\frac{\partial^2\psi}{\partial y^2},\ \ \frac{\partial\theta}{\partial y}=-Bi(1-\theta),\ \ \phi=1 \quad \text{at} \quad y=0 \tag{2.50a}$$

$$\frac{\partial\psi}{\partial y}=u_e,\ \ \omega=0,\ \ \theta=0,\ \ \phi=0 \quad \text{as} \quad y\to\infty \tag{2.50b}$$

where $f_w=-\dfrac{Re^{1/2}}{U_\infty}\,v_w$ is the suction/injection parameter, $Bi=\dfrac{h_f\,L}{k\,Re^{1/2}}$ is the Biot number and the micro-inertia density is taken as $j=\dfrac{L^2}{Re}$.

Similarity representation via Lie scaling group transformations

A one-parameter scaling group of transformations, which is a simplified form of Lie group transformation, is selected as ([48])

$$\left.\begin{aligned}&\Gamma: x^*=x\,e^{\varepsilon\,\alpha_1},\ y^*=y\,e^{\varepsilon\,\alpha_2},\ \psi^*=\psi\,e^{\varepsilon\,\alpha_3},\ \omega^*=\omega\,e^{\varepsilon\,\alpha_4},\ \theta^*=\theta\,e^{\varepsilon\,\alpha_5},\\&\phi^*=\phi\,e^{\varepsilon\,\alpha_6},\ \beta_T^*=\beta_T\,e^{\varepsilon\,\alpha_7},\ \beta_C^*=\beta_C\,e^{\varepsilon\,\alpha_8},\ u_e^*=u_e\,e^{\varepsilon\,\alpha_9}\end{aligned}\right\} \tag{2.51}$$

Here $\varepsilon\neq 0$ is the parameter of the group and $\alpha's$ are arbitrary real numbers, not all simultaneously zero. Eqs.(2.46)- (2.49) along with the boundary conditions (2.50) will remain invariant under the group of transformations in Eq.(2.51) if α_i's hold following relationships

$$\left.\begin{aligned}&\alpha_1+2\alpha_2-2\alpha_3=3\alpha_2-\alpha_3=\alpha_2-\alpha_4=-\alpha_5-\alpha_7=-\alpha_6-\alpha_8=\alpha_1-2\alpha_9;\\&\alpha_1+\alpha_2-\alpha_3-\alpha_4=2\alpha_2-\alpha_4=-\alpha_4=2\alpha_2-\alpha_3;\\&\alpha_1+\alpha_2-\alpha_3-\alpha_5=2\alpha_2-\alpha_5;\alpha_1+\alpha_2-\alpha_3-\alpha_6=2\alpha_2-\alpha_6;\\&\alpha_1-\alpha_3=0;-\alpha_4=2\alpha_2-\alpha_3;\alpha_2-\alpha_5=0=-\alpha_5;\alpha_6=0;\alpha_2-\alpha_3=-\alpha_9\end{aligned}\right\} \tag{2.52}$$

Using the procedure explained in the previous case, the following similarity transformations are obtained by using the Lie scaling group transformations

$$\eta = y,\ \psi = xf(\eta),\ \omega = xg(\eta),\ u_e = x,\ \beta_T = x\beta_{T_0},\ \beta_C = x\beta_{C_0},\ \theta = \theta(\eta),\ \phi = \phi(\eta) \tag{2.53}$$

Using (2.53) in Eqs.(2.46)-(2.49), the similarity equations are obtained as follows

$$\left(\frac{1}{1-N}\right) f''' + ff'' + 1 - f'^2 + \left(\frac{N}{1-N}\right) g' + \lambda(\theta + \mathcal{B}\phi) = 0 \tag{2.54}$$

$$\left(\frac{2-N}{2-2N}\right) g'' + fg' - f'g - \left(\frac{N}{1-N}\right)(2g + f'') = 0 \tag{2.55}$$

$$\frac{1}{Pr}\theta'' + f\theta' = 0 \tag{2.56}$$

$$\frac{1}{Sc}\phi'' + f\phi' = 0 \tag{2.57}$$

where $\lambda = \dfrac{Gr}{Re^2}$ is the mixed convection parameter. Notice that $\lambda > 0$ and $\lambda < 0$ correspond to aiding flow and opposing flow respectively, whereas $\lambda = 0$ produces forced convective flow problem.

Boundary conditions (2.50) in terms of f, g, θ and ϕ become

$$f(0) = f_w,\ f'(0) = 0,\ g(0) = -nf''(0),\ \theta'(0) = -Bi[1 - \theta(0)],\ \phi(0) = 1 \tag{2.58a}$$

$$f'(\infty) = 1,\ g(\infty) = 0,\ \theta(\infty) = 0,\ \phi(\infty) = 0 \tag{2.58b}$$

The non-dimensional skin friction $C_f = \dfrac{2\tau_w}{\rho\overline{u}_e^2}$, wall couple stress $M_w = \dfrac{m_w}{\rho\overline{u}_e^2\overline{x}}$, local Nusselt number $Nu_{\overline{x}} = \dfrac{q_w\overline{x}}{k(T_f - T_\infty)}$ and local Sherwood number $Sh_{\overline{x}} = \dfrac{q_m\overline{x}}{D(C_w - C_\infty)}$, are given by

$$\left.\begin{aligned} &C_f Re_{\overline{x}^{1/2}} = 2\left(\frac{1-nN}{1-N}\right) f''(0), \qquad M_w Re_{\overline{x}} = \left(\frac{2-N}{2-2N}\right) g'(0) \\ &\frac{Nu_{\overline{x}}}{Re_{\overline{x}^{1/2}}} = -\theta'(0), \qquad \frac{Sh_{\overline{x}}}{Re_{\overline{x}^{1/2}}} = -\phi'(0) \end{aligned}\right\} \tag{2.59}$$

where $Re_{\overline{x}} = \dfrac{\overline{u}_e\overline{x}}{\nu}$ is the local Reynold's number.

Table 2.4: *Comparison of $f''(0)$ and $-\theta'(0)$ for mixed convection along a vertical flat plate in Newtonian fluids ([58]; [73]).*

λ	$f''(0)$			$-\theta'(0)$		
	Merkin [58]	Nazar *et al.* [73]	Present	Merkin [58]	Nazar *et al.* [73]	Present
-1.0	0.6489	0.6497	0.648861	0.5067	0.5071	0.506658
-0.6	0.8963	0.8971	0.896272	0.5357	0.5360	0.535659
-0.2	1.1241	1.1250	1.124101	0.5597	0.5601	0.559725
0.0	1.2326	1.2336	1.232588	0.5705	0.5708	0.570462
0.6	1.5416	1.5428	1.541593	0.5990	0.5993	0.598949
1.0	1.7367	1.7380	1.736681	0.6156	0.6160	0.615581
3.0	2.6259	2.6282	2.625893	0.6817	0.6822	0.681721
5.0	3.4230	3.4264	3.422943	0.7315	0.7320	0.731504

Results and Discussion

The governing non-linear ordinary differential equations (2.54)-(2.57) together with the boundary conditions (2.58) are solved numerically using the spectral quasi-linearization method, which is explained in the previous case. In order to validate the code generated, for the special case of $N = 0$, $n = 0$, $\lambda = 0$, $Bi \to \infty$ and $f_w = 0$, the results of the present problem have been compared with those of Merkin [58] and Nazar *et al.* [73] and it is found that they are in good agreement [Tab. (2.4)]. In order to study the effects of coupling number N, suction/injection parameter f_w, Biot number Bi and material parameter n on the various flow profiles in both opposing and aiding flow cases explicitly, computations have been carried for $\mathcal{B} = 1.0$, $Pr = 0.71$ and $Sc = 0.22$.

The influence of coupling number N on the dimensionless velocity, microrotation, temperature and concentration is illustrated in Figs. 2.5(a)-2.5(d) for both the cases of aiding and opposing flows and for fixed values of other parameters. Physically, the coupling number N characterizes the coupling of linear and rotational motion arising from the micro-motion of the fluid molecules. As N increases, it is found from Fig. 2.5(a) that the maximum velocity decreases for both aiding and opposing flow situations. It is significant to mention that the velocity of the micropolar fluid is less compared to that of the viscous fluid case. It can be noted from Fig. 2.5(b) that the microtation profile tends to become flat initially, and then tend to their free stream values far away from the wall with an increase in values of N. Likewise, an increment in the values of N, implies a higher vortex viscosity of the fluid, which promotes the microrotation of a micropolar fluid. Figs.

2.5(c) and 2.5(d) reveal that the temperature and concentration of the fluid increases with the increase of coupling number N for both aiding and opposing flow situations. The temperature and concentration of the micropolar fluid are more than those of the viscous fluid.

The effects of Biot number on the dimensionless velocity, microrotation, temperature and concentration are depicted in Figs. 2.6(a)-2.6(d) for both aiding and opposing flows cases and for fixed values of other parameters. Generally, the fluid velocity is zero at the plate surface and rises gradually away from the plate to the free stream value satisfying the boundary conditions. It is interesting to observe that an increase in the strength of convective surface heat transfer Bi produces a substantial enhancement in the fluid velocity within the momentum boundary layer in the aiding flow. But, the reverse tendency is true in the case of opposing flow situation. As Bi increases, the microrotation shows reverse rotation near the two limits as displayed in Fig. 2.6(b). In fact, the higher values of Biot number indicates higher internal thermal resistance of the plate than the boundary layer thermal resistance. For both aiding and opposing flow situations, the fluid temperature is maximum at the plate surface and decreases exponentially to zero value far away from the plate satisfying the boundary conditions. As a consequence, an increment in Biot number leads to increase in the fluid temperature, which is shown in Fig. 2.6(c). From Fig. 2.6(d), a slight reduction is seen in concentration boundary layer thickness with increasing values of Bi in the case of aiding flow situation whereas, a reverse nature is observed in the opposing flow situation.

For both aiding and opposing flow situations, the effects of f_w on the non-dimensional velocity, microrotation, temperature and concentration are exhibited in Figs. 2.7(a)-2.7(d) for fixed values of other parameters. From Fig. 2.7(a), it can be noticed that the velocity is less in the case of injection as compared to the suction case for aiding flow situation, but it shows the reverse trend for opposing flow situation. It can be seen from Fig. 2.7(b) that the microrotation is completely negative within the boundary layer. Also, it shows reverse rotation near the two boundaries for both suction and injection cases. From Fig. 2.7(c), it can be noticed that for both aiding and opposing flow situations, the temperature of the fluid is more in the case of injection, whereas it is less in the case of suction in comparison with the impermeable surface ($f_w = 0$). It is seen from Fig. 2.7(d) that the absorption of the fluid is more with injection case, whereas less with suction case when compared to the impermeable surface case ($f_w = 0$) for both aiding and opposing flow situations. The temperature and concentration are more in the case of injection as compared to the case of suction as displayed in Figs. 2.7(c) and 2.7(d).

The variations of local skin-friction, wall couple stress, rate of heat and mass transfers, is shown in Tab. (2.5) for both cases of aiding and opposing flows. It indicates that the skin friction is higher for the micropolar fluid as compared to that of the viscous fluid ($n = 0$, $N = 0$) in both cases of aiding and opposing flows. Micropolar fluids offer more resistance (resulting from vortex viscosity) to the fluid motion. The results also indicate that for both situations of aiding and opposing flows, larger values of the coupling number N leads to lower the wall couple stress, heat and mass transfer rates. Further, it can be noticed that the heat and mass transfer rates are more for a viscous fluid when compared with that of a micropolar fluid. This is because that as N increases, the thermal and solutal boundary layer thickness become larger, thus giving rise to a small value of local heat and mass transfer rates. In opposing flow, the skin friction, wall couple stress and mass transfer rate reduce, but the heat transfer rate enhances. However, in aiding flow case, the skin friction, wall couple stress, heat and mass transfer rates increase with the increase of Biot number. For both opposing and aiding flow situations, the skin friction, wall couple stress, heat and mass transfer rates are more in suction case than compared with those values in injection case. As the material constant (n) increases, the skin friction reduces, but the wall couple stress, heat and mass transfer rates enhances for both opposing and aiding flows.

Table 2.5: *Effects of skin friction, wall couple stress, heat and mass transfer coefficients for varying values of mixed convection parameter, micropolar parameter, Biot number, suction/injection parameter and material constant*

λ	N	Bi	f_w	n	$C_f Re_{\overline{x}^{1/2}}$	$M_w Re_{\overline{x}}$	$\frac{Nu_{\overline{x}}}{Re_{\overline{x}^{1/2}}}$	$\frac{Sh_{\overline{x}}}{Re_{\overline{x}^{1/2}}}$
-0.3	0.0	1.0	0.5	0.0	2.457608	0	0.419258	0.374096
-0.3	0.5	1.0	0.5	0.5	2.950299	0.592078	0.411817	0.363764
-0.3	0.9	1.0	0.5	0.5	5.402849	0.446797	0.386531	0.3267
1.0	0.0	1.0	0.5	0.0	4.911863	0	0.447789	0.417825
1.0	0.5	1.0	0.5	0.5	5.629340	1.462654	0.438512	0.404909
1.0	0.9	1.0	0.5	0.5	9.307047	1.275809	0.406981	0.357578
-0.5	0.5	0.1	0.5	0.5	2.756776	0.53627	0.087375	0.359461
-0.5	0.5	1.0	0.5	0.5	2.464685	0.446769	0.405662	0.35496
-0.5	0.5	5.0	0.5	0.5	2.280918	0.391248	0.595771	0.352041
1.0	0.5	0.1	0.5	0.5	5.18669	1.308037	0.088515	0.400014
1.0	0.5	1.0	0.5	0.5	5.62934	1.462654	0.438512	0.404909
1.0	0.5	5.0	0.5	0.5	5.92276	1.566396	0.680407	0.408067
-0.2	0.25	0.1	-0.3	0.5	1.998619	0.278709	0.077558	0.252597
-0.2	0.25	0.1	0.0	0.5	2.335069	0.416304	0.082618	0.297167
-0.2	0.25	0.1	2.0	0.5	5.21101	2.685523	0.094208	0.638161
1.0	0.25	0.1	-0.5	0.5	3.802504	0.698301	0.080986	0.294422
1.0	0.25	0.1	0.0	0.5	4.128077	0.906629	0.084617	0.33504
1.0	0.25	0.1	2.0	0.5	6.909385	3.703693	0.094314	0.656918
-0.3	0.5	1.0	0.5	0.0	3.214136	-0.447122	0.4066	0.356919
-0.3	0.5	1.0	0.5	0.5	2.950299	0.592078	0.411817	0.363764
1.0	0.5	1.0	0.5	0.0	6.248153	-0.626214	0.432237	0.395818
1.0	0.5	1.0	0.5	0.5	5.62934	1.462654	0.438512	0.404909

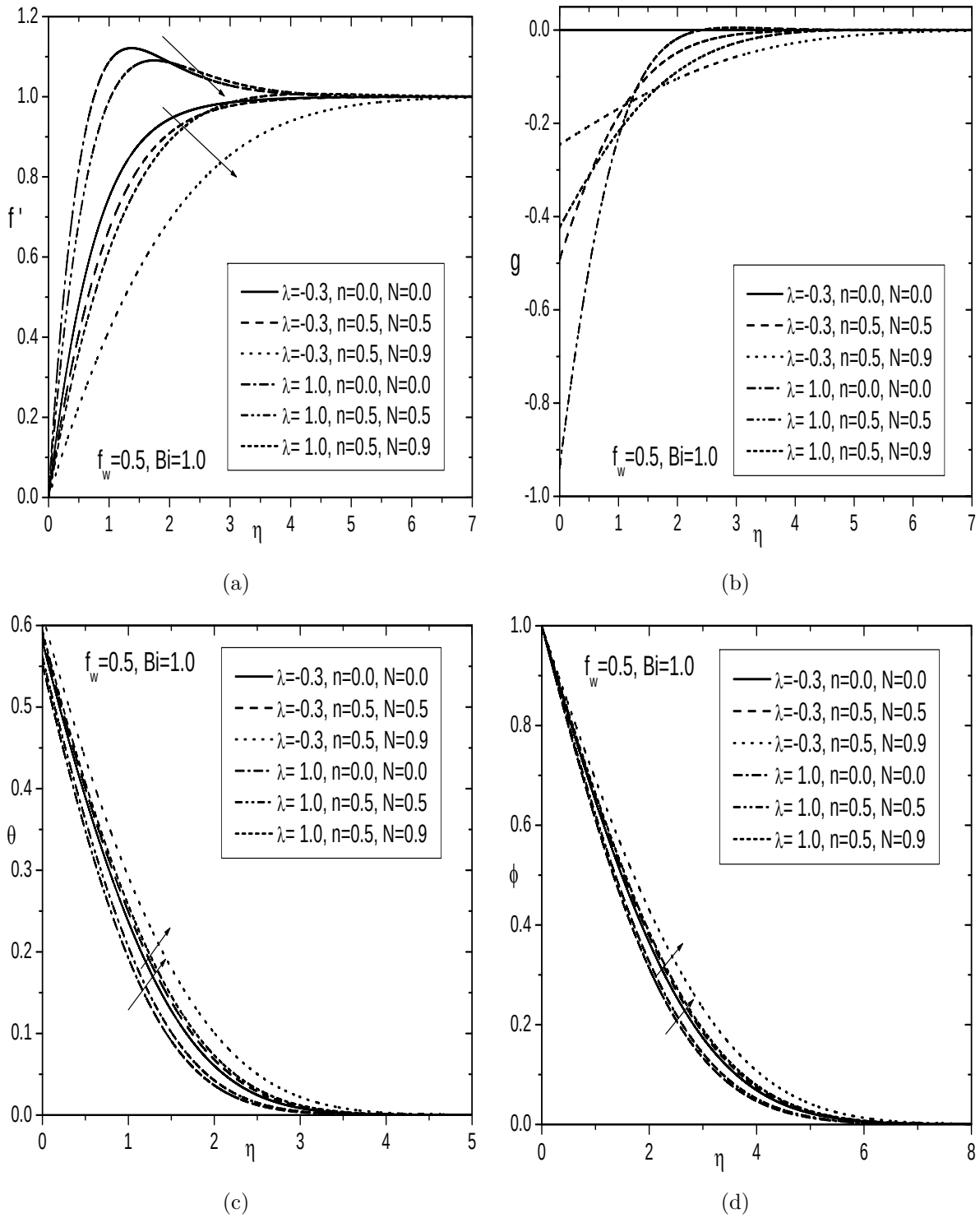

Figure 2.5: *Variation of N on (a)Velocity, (b)Microrotation, (c)Temperature and (d)Concentration profiles*

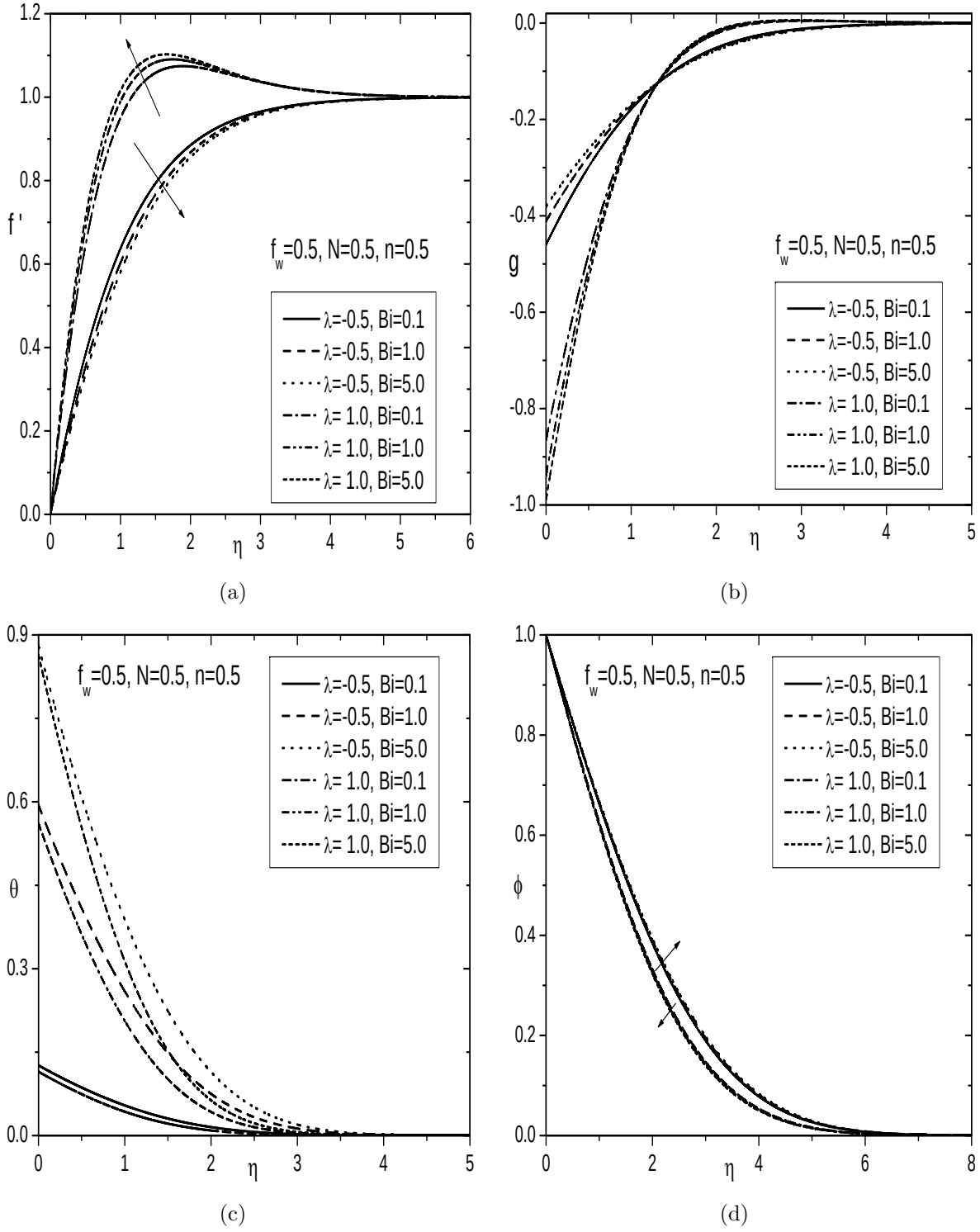

Figure 2.6: *Variation of Bi on (a)Velocity, (b)Microrotation, (c)Temperature and (d)Concentration profiles*

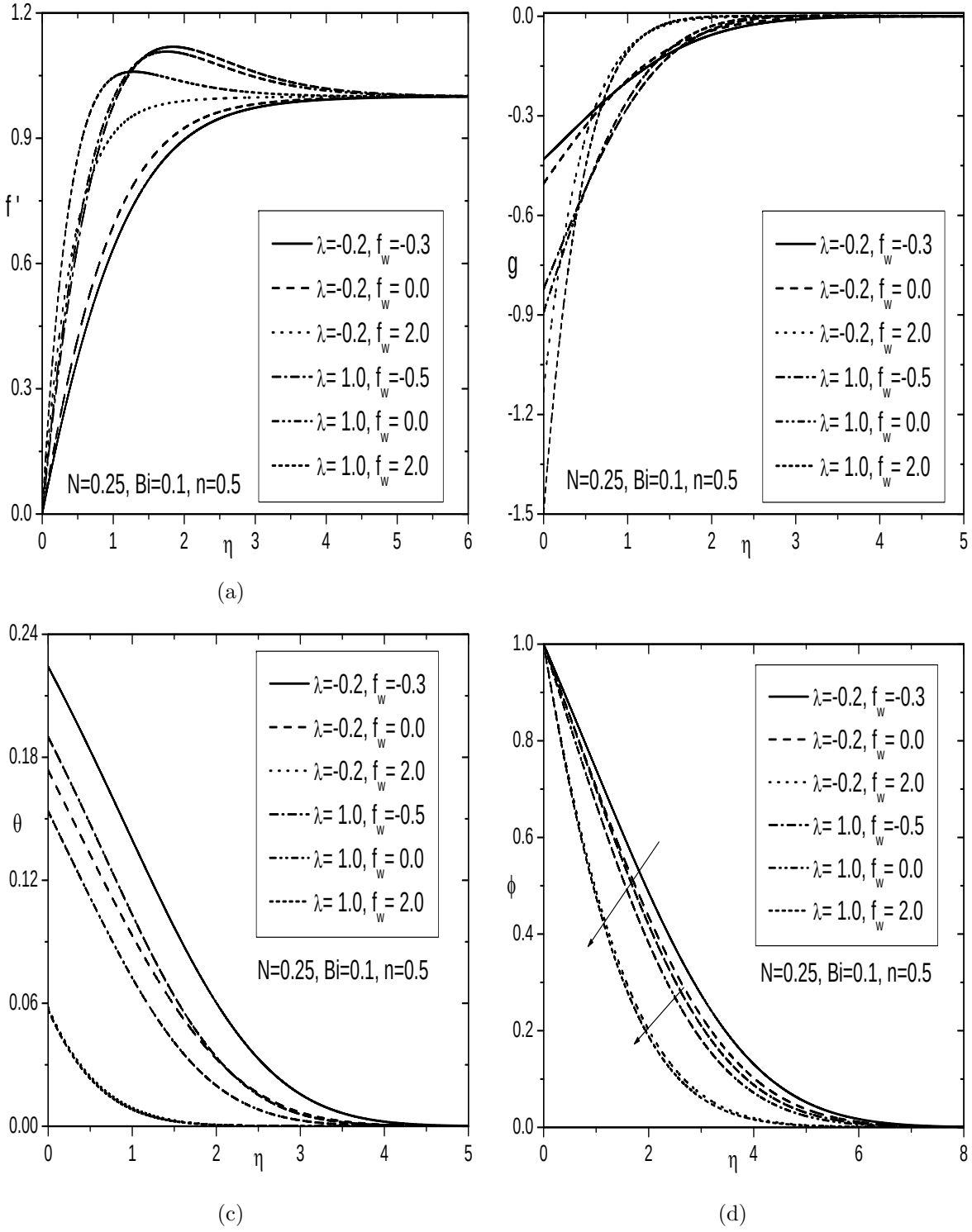

Figure 2.7: *Variation of f_w on (a)Velocity, (b)Microrotation, (c)Temperature and (d)Concentration profiles*

2.3 Conclusions

In this chapter, the similarity solution of a micropolar fluid flow along a permeable vertical plate under the convective boundary condition is obtained in two cases, namely, (a) natural convection and (b) mixed convection. Following are the important conclusions:

The velocity distribution is less near the plate and far away from the plate it shows reverse trend with the increase of coupling number in case(a), but the velocity decreases in case(b). For both cases (a) and (b), the temperature, concentration and skin friction increase, but wall couple stress, heat and mass transfer rates decrease with the increase of coupling number. An increase in Biot number leads to increase of the velocity near the plate whereas, far away from the plate it decreases. The temperature, skin friction, wall couple stress, heat and mass transfer rates enhance but the concentration reduce in case(a). However, for case (b), the velocity, skin friction, wall couple stress and mass transfer rate increase, but the concentration decreases in the aiding flow whereas, they show a reverse trend in the opposing flow. Further, for both opposing and aiding flows, the temperature and heat transfer rate increase with the increase of Biot number. In both case(a) and case(b), the skin friction, wall couple stress, heat and mass transfer rates are more, but temperature and concentration are less in suction compared to that of injection except for velocity in case(a). As the material parameter n increases, the skin friction decreases, but the wall couple stress, heat and mass transfer rates increase.

Chapter 3

Free and Mixed Convection along a Permeable Vertical Plate Embedded in a Porous Medium Saturated with Micropolar Fluid[1]

3.1 Introduction

The study of convective heat and mass transfer embedded in a porous medium arises in a number of important applications, including food processing, pollutant dispersion in aquifers, storage of nuclear waste material, a heat exchanger placed in a low-velocity environment, solar energy collecting devices, air conditioning of a room, etc. Comprehensive review of convective heat and mass transfer in a Darcy and non-Darcy porous medium can be found in the books by Ingham and Pop [41], Nield and Bejan [74] and Vafai [102].

The boundary layer flow of convective transport in a micropolar fluid saturated porous medium has gained the attention of several researchers due to its significant applications in the context

[1]Case(a):Published in "**Procedia Engineering**" 127 (2015) 235–243,
Case(b) Published in "**Advanced Science Engineering and Medicine**" 7 (2015) 234–245

of industrial manufacturing processes, discrete aspects of engineering, and also geothermal extraction. In view of the above said applications, Chamkha *et al.* [19] investigated the double diffusive natural convective boundary layer flow of a micropolar fluid over a vertical plate embedded in a uniform porous medium in the presence of chemical reaction. Bakier [10] discussed the influence of thermophoresis and radiation on the free convective flow of a micropolar fluid through saturated non-Darcy porous medium. Srinivasacharya and RamReddy [96] analyzed the mixed convective flow of an incompressible micropolar fluid in a doubly stratified non-Darcy porous medium subjected to the uniform wall temperature and concentration. Though the similarity representation of the system of governing equations for the convective flow of a micropolar fluid is essential to get invariant solutions, it has not received much attention.

In this chapter, the problem of free and mixed convective flows along a permeable vertical plate in a micropolar fluid saturated Darcy porous medium, is considered. In addition, the convective boundary condition is prescribed on the surface of the vertical plate. As in the previous chapter, the governing equations and their associated boundary conditions are initially cast into dimensionless forms by similarity variables, which are obtained using the scaling group of transformations, and then solved numerically using the spectral quasi-linearization method. The present study mainly focused on exploring the effects of micropolar parameter, Darcy number, mixed convection parameter, and convective heat transfer parameter on the physical quantities of the flow for both suction and injection cases. Further, the numerical data for the skin-friction, wall couple stress, heat and mass transfer rates are shown in the tabular form.

3.2 Mathematical Formulation

Consider the steady, two dimensional and laminar convective flow of an incompressible micropolar fluid over a permeable vertical plate in a Darcy porous medium. The $\overline{x}$-axis is taken along the vertical plate and $\overline{y}$-axis is normal to the plate as displayed in Fig. 3.1. This chapter is an extension of chapter-2 by considering the microplar fluid saturated porous medium. In addition to assumptions made in chapter-2, the following assumptions are taken into account in the analysis: (i) the porous medium is isotropic and homogeneous, (ii) the properties of the fluid and porous medium are constant except for the density variation required by the Boussinesq approximation and (iii) the fluid and the porous medium are in local thermodynamic equilibrium. Under these

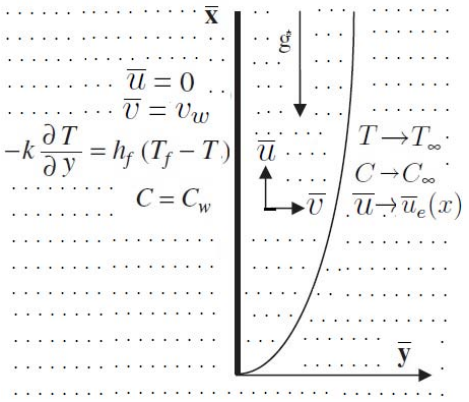

Figure 3.1: *Physical model and coordinate system*

assumptions, and using the Darcy model and Dupuit-Forchheimer relationship [74], the governing equations describing the micropolar fluid are:

$$\frac{\partial \overline{u}}{\partial \overline{x}} + \frac{\partial \overline{v}}{\partial \overline{y}} = 0 \tag{3.1}$$

$$\frac{\rho}{\epsilon^2}\left(\overline{u}\frac{\partial \overline{u}}{\partial \overline{x}} + \overline{v}\frac{\partial \overline{u}}{\partial \overline{y}}\right) = \frac{1}{\epsilon}(\mu+\kappa)\frac{\partial^2 \overline{u}}{\partial \overline{y}^2} + \rho \overline{u}_e \frac{d\overline{u}_e}{d\overline{x}} + \kappa\frac{\partial \overline{\omega}}{\partial \overline{y}} + \rho g^* \left(\beta_T(x)(T - T_\infty) + \beta_C(x)(C - C_\infty)\right) - \frac{\mu}{K_p}(\overline{u} - \overline{u}_e) \tag{3.2}$$

$$\frac{\rho j}{\epsilon}\left(\overline{u}\frac{\partial \overline{\omega}}{\partial \overline{x}} + \overline{v}\frac{\partial \overline{\omega}}{\partial \overline{y}}\right) = \gamma\frac{\partial^2 \overline{\omega}}{\partial \overline{y}^2} - \kappa\left(2\overline{\omega} + \frac{1}{\epsilon}\frac{\partial \overline{u}}{\partial \overline{y}}\right) \tag{3.3}$$

$$\overline{u}\frac{\partial T}{\partial \overline{x}} + \overline{v}\frac{\partial T}{\partial \overline{y}} = \alpha\frac{\partial^2 T}{\partial \overline{y}^2} \tag{3.4}$$

$$\overline{u}\frac{\partial C}{\partial \overline{x}} + \overline{v}\frac{\partial C}{\partial \overline{y}} = D\frac{\partial^2 C}{\partial \overline{y}^2} \tag{3.5}$$

where $\overline{u}$ and $\overline{v}$ are the Darcy velocity components in $\overline{x}$ and $\overline{y}$ directions respectively, ϵ is the porosity and K_p is the (intrinsic) permeability of the medium.

The boundary conditions are

$$\overline{u} = 0,\ \ \overline{v} = v_w,\ \ \overline{\omega} = -n\frac{\partial \overline{u}}{\partial \overline{y}},\ \ -k\frac{\partial T}{\partial \overline{y}} = h_f(T_f - T),\ \ C = C_w \quad \text{at} \quad \overline{y} = 0 \tag{3.6a}$$

$$\overline{u} = \overline{u}_e(x),\ \ \overline{\omega} = 0,\ \ T = T_\infty,\ \ C = C_\infty \quad \text{as} \quad \overline{y} \to \infty \tag{3.6b}$$

In this chapter, two types (cases) of problems are considered: (a) free/natural convection and (b) mixed convection.

3.2.1 Case(a): Natural Convection

In the case of natural convection, the fluid flow is due to buoyancy forces only and hence, the velocity of the outer flow becomes zero (*ie.*, $\overline{u}_e = 0$). We introduce the following dimensionless variables

$$\left.\begin{array}{l} x = \dfrac{\overline{x}}{L},\ y = \dfrac{\overline{y}}{L}Gr^{1/4},\ u = \dfrac{L}{\nu Gr^{1/2}}\overline{u},\ v = \dfrac{L}{\nu Gr^{1/4}}\overline{v}, \\ \omega = \dfrac{L^2}{\nu Gr^{3/4}}\overline{\omega},\ \theta = \dfrac{T - T_\infty}{T_f - T_\infty},\ \phi = \dfrac{C - C_\infty}{C_w - C_\infty} \end{array}\right\} \tag{3.7}$$

In view of the continuity equation (3.1), we introduce the stream function ψ by

$$u = \frac{\partial \psi}{\partial y}, \quad v = -\frac{\partial \psi}{\partial x}. \tag{3.8}$$

Using (3.7) and (3.8) in Eqs.(3.2)-(3.5), we get the following momentum, angular momentum, energy and concentration equations

$$\frac{1}{\epsilon^2}\left(\frac{\partial \psi}{\partial y}\frac{\partial^2 \psi}{\partial x\,\partial y} - \frac{\partial \psi}{\partial x}\frac{\partial^2 \psi}{\partial y^2}\right) - \frac{1}{\epsilon}\left(\frac{1}{1-N}\right)\frac{\partial^3 \psi}{\partial y^3} - \left(\frac{N}{1-N}\right)\frac{\partial \omega}{\partial y} - \frac{\beta_T}{\beta_{T_0}}\theta - \frac{\beta_C(C_w - C_\infty)}{\beta_{T_0}(T_f - T_\infty)}\phi + \frac{1}{Da\,Gr^{1/2}}\frac{\partial \psi}{\partial y} = 0 \tag{3.9}$$

$$\frac{1}{\epsilon}\left(\frac{\partial \psi}{\partial y}\frac{\partial \omega}{\partial x} - \frac{\partial \psi}{\partial x}\frac{\partial \omega}{\partial y}\right) - \left(\frac{2-N}{2-2N}\right)\frac{\partial^2 \omega}{\partial y^2} + \left(\frac{N}{1-N}\right)\left(2\omega + \frac{1}{\epsilon}\frac{\partial^2 \psi}{\partial y^2}\right) = 0 \tag{3.10}$$

$$\frac{\partial \psi}{\partial y}\frac{\partial \theta}{\partial x} - \frac{\partial \psi}{\partial x}\frac{\partial \theta}{\partial y} - \frac{1}{Pr}\frac{\partial^2 \theta}{\partial y^2} = 0 \tag{3.11}$$

$$\frac{\partial \psi}{\partial y}\frac{\partial \phi}{\partial x} - \frac{\partial \psi}{\partial x}\frac{\partial \phi}{\partial y} - \frac{1}{Sc}\frac{\partial^2 \phi}{\partial y^2} = 0 \tag{3.12}$$

where $Da = \dfrac{K_p}{L^2}$ is the Darcy number.

Now, the boundary conditions (3.6) become

$$\frac{\partial \psi}{\partial y} = 0,\ \frac{\partial \psi}{\partial x} = f_w,\ \omega = -n\frac{\partial^2 \psi}{\partial y^2},\ \frac{\partial \theta}{\partial y} = -Bi(1-\theta),\ \phi = 1 \text{ at } y = 0 \tag{3.13a}$$

$$\frac{\partial \psi}{\partial y} = 0,\ \omega = 0,\ \theta = 0,\ \phi = 0 \text{ as } y \to \infty \tag{3.13b}$$

Making use of the Lie scaling group transformations as explained in the previous chapter, the

following similarity transformations are obtained

$$\eta = y,\ \psi = xf(\eta),\ \omega = xg(\eta),\ \beta_T = x\beta_{T_0},\ \beta_C = x\beta_{C_0},\ \theta = \theta(\eta),\ \phi = \phi(\eta) \tag{3.14}$$

Using (3.14) in Eqs.(3.9)-(3.12), the similarity equations are obtained as follows

$$\frac{1}{\epsilon}\left(\frac{1}{1-N}\right)f''' + \frac{1}{\epsilon^2}ff'' - \frac{1}{\epsilon^2}f'^2 + \left(\frac{N}{1-N}\right)g' + \theta + \mathcal{B}\phi - \frac{1}{DaGr^{1/2}}f' = 0 \tag{3.15}$$

$$\left(\frac{2-N}{2-2N}\right)g'' + \frac{1}{\epsilon}fg' - \frac{1}{\epsilon}f'g - \left(\frac{N}{1-N}\right)\left(2g + \frac{1}{\epsilon}f''\right) = 0 \tag{3.16}$$

$$\frac{1}{Pr}\theta'' + f\theta' = 0 \tag{3.17}$$

$$\frac{1}{Sc}\phi'' + f\phi' = 0 \tag{3.18}$$

Boundary conditions (3.13) in terms of f, g, θ and ϕ become

$$f(0) = f_w,\ f'(0) = 0,\ g(0) = -nf''(0),\ \theta'(0) = -Bi[1-\theta(0)],\ \phi(0) = 1 \tag{3.19a}$$

$$f'(\infty) = 0,\ g(\infty) = 0,\ \theta(\infty) = 0,\ \phi(\infty) = 0 \tag{3.19b}$$

The non-dimensional skin friction C_f, wall couple stress M_w, local Nusselt number $Nu_{\overline{x}}$ and local Sherwood number $Sh_{\overline{x}}$, are given by

$$\left.\begin{aligned} &C_f Gr^{1/4} = 2\left[\frac{1-nN}{1-N}\right]f''(0),\ M_w Gr^{1/2} = \left(\frac{2-N}{2-2N}\right)g'(0), \\ &\frac{Nu_{\overline{x}}}{Gr_x^{-1/4}} = -\theta'(0),\ \frac{Sh_{\overline{x}}}{Gr_x^{-1/4}} = -\phi'(0) \end{aligned}\right\} \tag{3.20}$$

Results and Discussion

The coupled nonlinear Eqs.(3.15)-(3.18) along with the boundary conditions (3.19) are solved numerically using the spectral quasilinearisation method as explained in the previous chapter. In order to validate the code generated, for the special case of $N = 0$, $n = 0$, $Da \to \infty$, $\epsilon = 1$, $\mathcal{B} = 0$, $Pr = 1$, $Bi \to \infty$ and $f_w = 0$, the results of the present problem have been compared with those of Merkin [57], Nazar *et al.* [72] and Molla *et al.* [60] and it is found that they are in good agreement [Tab. (2.1)]. Also, the values of heat transfer rate, for $n = 0.5$, $Da \to \infty$, $\epsilon = 1$, $\mathcal{B} = 0$, $Pr = 1$,

$Bi \to \infty$ and $f_w = 0$, agree well with that of Nazar *et al.* [72] as shown in Tab. (2.2). To explore the significance of coupling number N, Darcy number Da and Biot number Bi, the computations have been carried out in the cases of suction and injection for $\mathcal{B} = 1.0$, $n = 0$, $\epsilon = 0.6$, $Pr = 0.71$ and $Sc = 0.22$.

The effects of coupling number (N) on the dimensionless velocity, microrotation, temperature and concentration profiles are illustrated in Figs. 3.2(a)-3.2(d) for both suction and injection cases and for fixed values of other parameters. The main advantage using the coupling number N in fluid flow model is that it characterizes the coupling between the linear and rotational motion emerging from the micromotion of the fluid particles. As N increases, it is found from Fig. 3.2(a) that the maximum velocity decreases in amplitude and the position of the maximum velocity moves farther away from the wall. It can be observed from Fig. 3.2(b) that initially, the microrotation profiles tends to become flat, and then approaches their free stream values far away from the wall with the increase of N. This is because an increment in the value of N implies a higher vortex viscosity of the fluid which promotes the microrotation of micropolar fluid. It is seen from Figs. 3.2(c) and 3.2(d) that with the increase of coupling number N, the thickness of thermal and concentration boundary layers of the fluid increase. It is observed from the above analysis that the results are true for both the suction and injection cases. Finally, the temperature and concentration are more in case of the micropolar fluid than those of the viscous fluid case.

Figs. 3.3(a)-3.3(d) depict the influence of Darcy number (Da) on the non-dimensional velocity, microrotation, temperature and concentration profiles in both the cases of suction and injection. With the increase of permeability, the porous matrix structure becomes less and less prominent. Thus, in the point of accumulation, as $Da \to \infty$ $\left(i.e., \dfrac{1}{Da\, Gr^{1/2}}\, f' \to 0 \right)$ along with $\epsilon = 1$, the porous medium vanishes and the present problem reduces to a purely free convective heat and mass transfer in a micropolar fluid. Fig. 3.3(a) indicates that with an increase in Da (which means a rise in permeability K_p), the velocity of the micropolar fluid enhances considerably near the wall and it shows reverse trend far away from the wall. From Fig. 3.3(b), it can be depicted that the microrotation changes its sign from negative to positive within the boundary layer. Also, it is noted that the magnitude of the microrotation increases with an increase in Darcy number. It is seen from Figs. 3.3(c) and 3.3(d) that the temperature and concentration of the fluid decrease with the increase of Darcy number. Further, it is to note that the above results are true in both the suction and injection cases.

Figs. 3.4(a)-3.4(d) display the effects of Biot number (Bi) on the dimensionless velocity, micro-rotation, temperature and concentration profiles in both the suction and injection cases for fixed values of other parameters. The fluid velocity is zero at the plate surface and increases gradually away from the plate to the free stream value satisfying the boundary conditions. It is interesting to observe that an increase in the strength of convective surface heat transfer Bi produces a substantial enhancement in the fluid velocity within the momentum boundary layer. The microrotation shows reverse rotation near the two boundaries with the increase of Bi [Fig. 3.4(b)]. The fluid temperature is maximum at the plate surface and decreases exponentially to zero value far away from the plate satisfying the boundary conditions. As a consequence, an increment in Biot number leads to enhance in the fluid temperature [Fig. 3.4(c)]. From Fig. 3.4(d), it is observed that a slight decrement in the concentration boundary layer thickness with the increase of Biot number Bi. These results shows same behaviour for both suction and injection cases.

The variations of skin-friction, wall couple stress, heat and mass transfer rates are shown in Tab.(3.1) for different values of the coupling number N, Biot number and Darcy parameter for both the cases of suction and injection. It is noticed that the skin friction of the micropolar fluid is higher than the viscous fluid ($N = 0$). The wall couple stress, heat and mass transfer rates reduces with coupling number enhancement. This may be beneficial in flow, temperature and concentration control of polymer processing. It can be observed that the skin-friction, heat and mass transfer rates increase, but the wall couple stress decreases with the increase of Bi. Also, it can be observed that the skin friction, Nusselt and Sherwood numbers enhances, but the wall couple stress reduces with the enhancement of Darcy parameter Da. It is observed from these results that the skin-friction, wall couple stress, heat and mass transfer rates show similar behaviour in both the cases of suction and injection.

Table 3.1: *Variations of skin friction, wall couple stress, Nusselt number and Sherwood number for varying values of micropolar parameter N, Biot numbers Bi and Darcy number Da in the presence of suction/injection parameter f_w.*

f_w	N	Bi	Da	$C_f Gr_{\overline{x}}^{1/4}$	$M_w Gr_{\overline{x}}^{1/2}$	$\frac{Nu_{\overline{x}}}{\mathrm{Gr}_{\overline{x}}^{1/4}}$	$\frac{Sh_{\overline{x}}}{\mathrm{Gr}_{\overline{x}}^{1/4}}$
-0.5	0	0.1	0.1	0.801568	0	0.048975	0.083206
-0.5	0.5	0.1	0.1	1.173704	-0.180042	0.046976	0.08024
-0.5	0.9	0.1	0.1	2.488803	-0.845552	0.040401	0.070989
0.5	0	0.1	0.1	0.890467	0	0.083082	0.194364
0.5	0.5	0.1	0.1	1.119873	-0.155206	0.082709	0.189986
0.5	0.9	0.1	0.1	1.838558	-0.600532	0.081669	0.177206
-0.5	0.5	0.1	0.1	1.173704	-0.180042	0.046976	0.08024
-0.5	0.5	1	0.1	1.438289	-0.214785	0.094606	0.088765
-0.5	0.5	20	0.1	1.500169	-0.222677	0.107394	0.090614
0.5	0.5	0.1	0.1	1.119873	-0.155206	0.082709	0.189986
0.5	0.5	1	0.1	1.482741	-0.189829	0.331779	0.198439
0.5	0.5	20	0.1	1.701339	-0.209863	0.494073	0.203173
-0.5	0.5	0.1	0.05	0.995963	-0.133976	0.035511	0.059373
-0.5	0.5	0.1	0.1	1.173704	-0.180042	0.046976	0.08024
-0.5	0.5	0.1	0.3	1.424426	-0.245786	0.056806	0.109738
0.5	0.5	0.1	0.05	0.842806	-0.101742	0.081594	0.168418
0.5	0.5	0.1	0.1	1.119873	-0.155206	0.082709	0.189986
0.5	0.5	0.1	0.3	1.557228	-0.241907	0.08401	0.220713

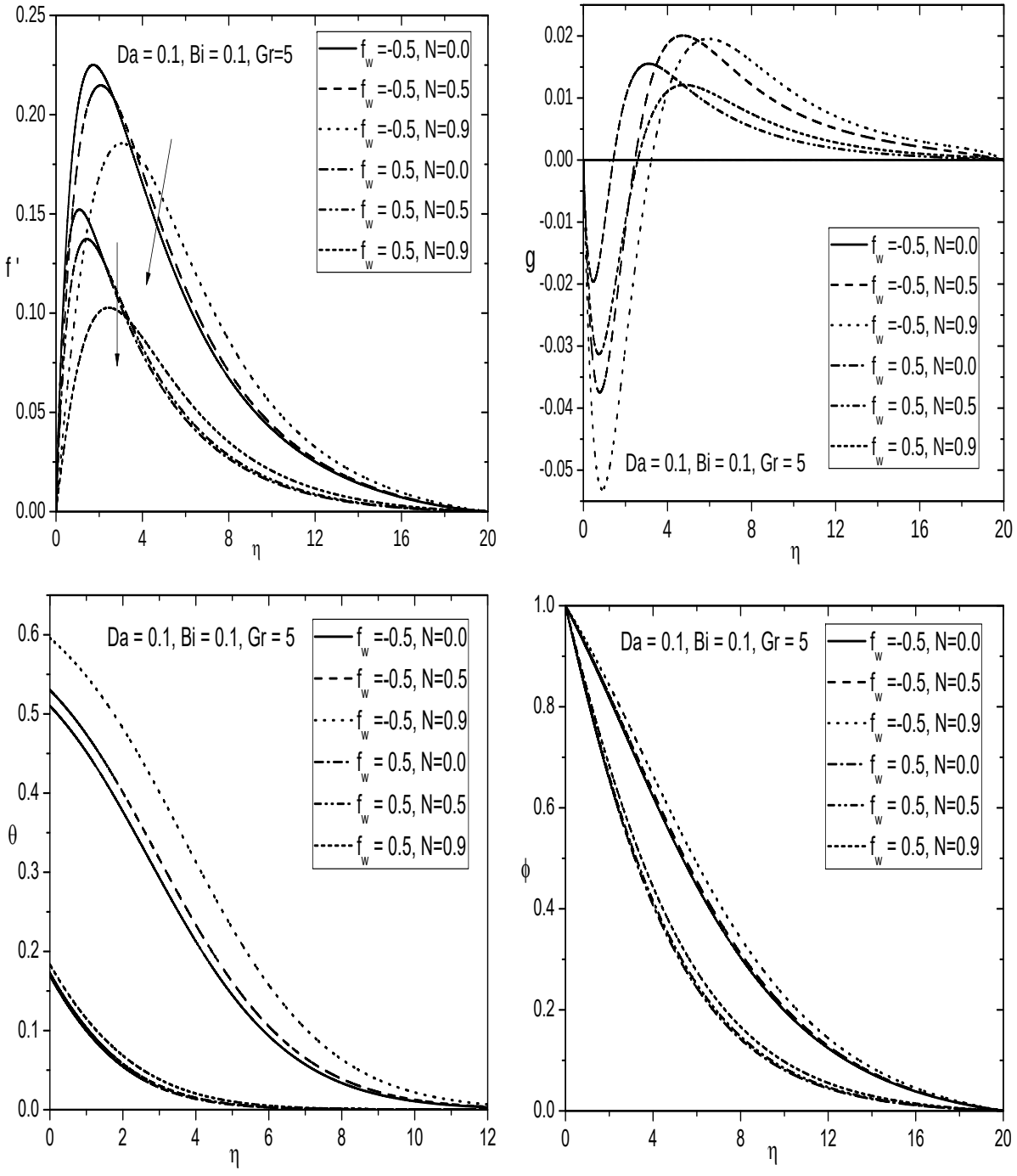

Figure 3.2: *Variation of N on (a)Velocity, (b)Microrotation, (c)Temperature and (d)Concentration profiles.*

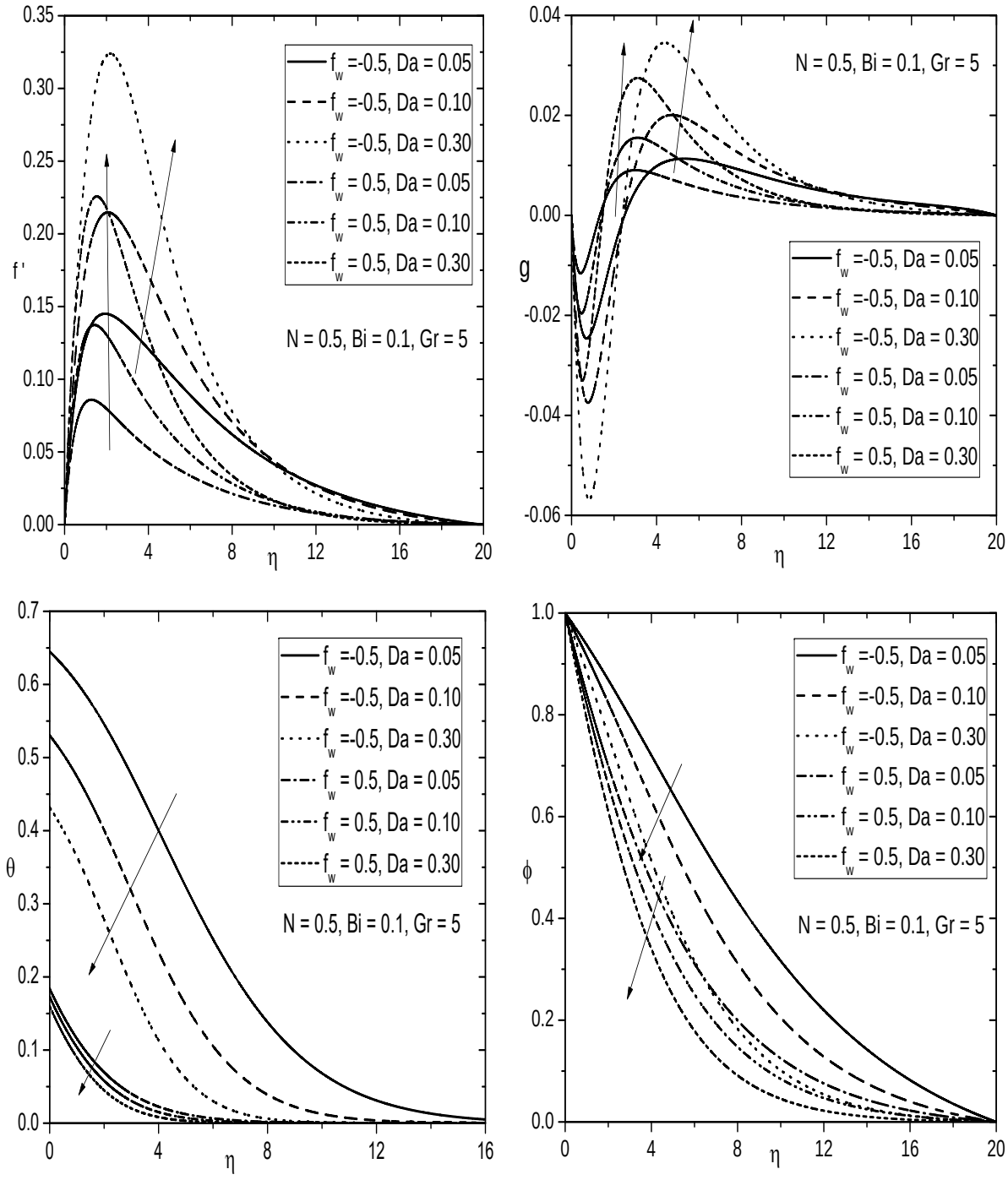

Figure 3.3: *Variation of Da on (a)Velocity, (b)Microrotation, (c)Temperature and (d)Concentration profiles.*

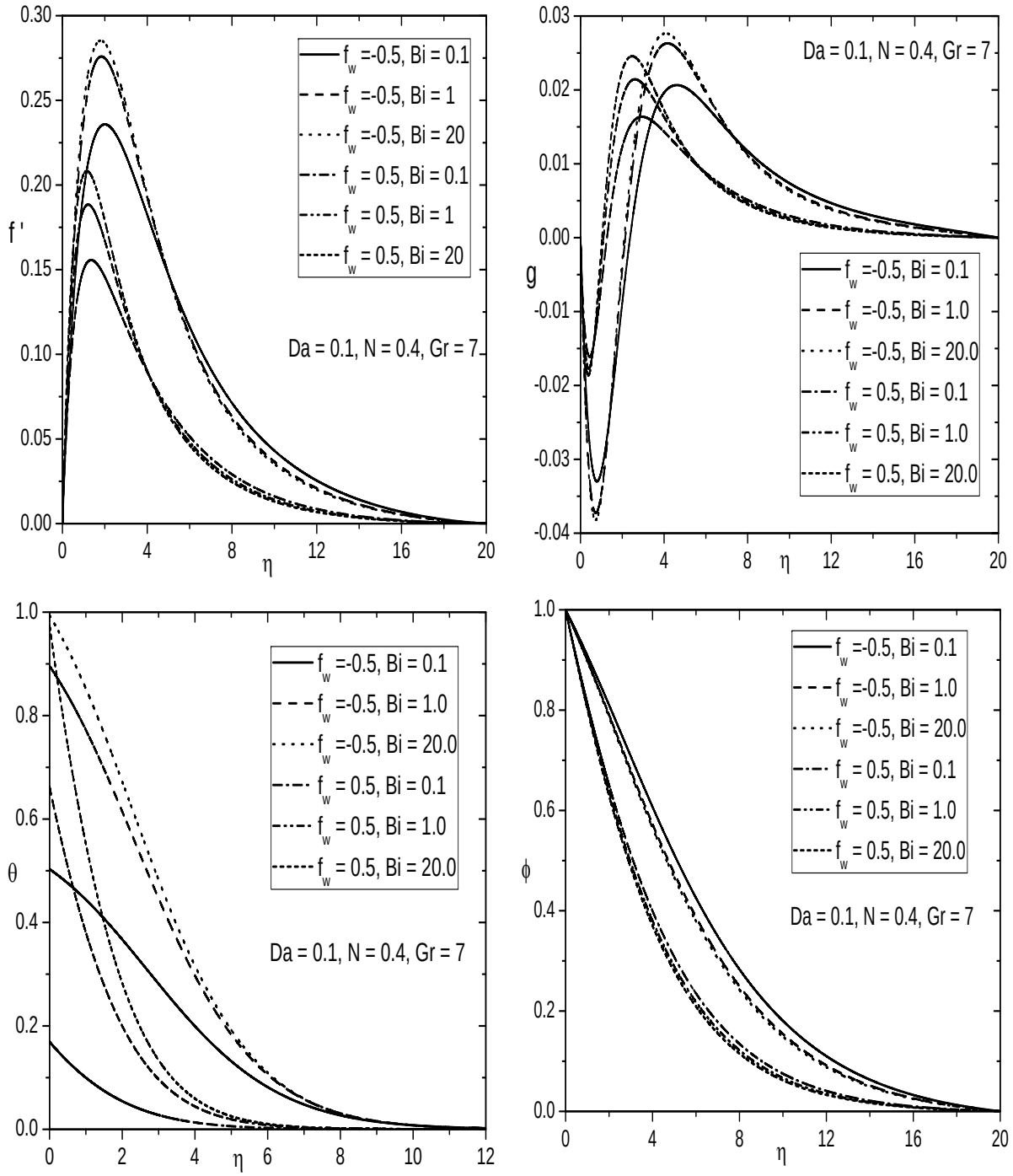

Figure 3.4: *Variation of Bi on (a)Velocity, (b)Microrotation, (c)Temperature and (d)Concentration profiles.*

3.2.2 Case(b): Mixed Convection

Consider the flow to be a mixed convection, which arises from an external flow with velocity $[\bar{u_e}(x)]$ and buoyancy forces. We introduce the following dimensionless variables

$$x = \frac{\overline{x}}{L},\ y = \frac{\overline{y}}{L}Re^{1/2},\ u = \frac{\overline{u}}{U_\infty},\ v = \frac{\overline{v}}{U_\infty}Re^{1/2}, \tag{3.21}$$
$$u_e = \frac{\overline{u}_e}{U_\infty},\ \omega = \frac{L^2}{\nu Re^{3/2}}\overline{\omega},\ \theta = \frac{T - T_\infty}{T_f - T_\infty},\ \phi = \frac{C - C_\infty}{C_w - C_\infty}$$

In view of the continuity equation (3.1), we introduce the stream function ψ as follows

$$u = \frac{\partial \psi}{\partial y}, \quad v = -\frac{\partial \psi}{\partial x} \tag{3.22}$$

Using (3.21) and (3.22) in Eqs.(3.2)-(3.5), we get the following momentum, angular momentum, energy and concentration equations

$$\frac{1}{\epsilon^2}\left(\frac{\partial \psi}{\partial y}\frac{\partial^2 \psi}{\partial x \partial y} - \frac{\partial \psi}{\partial x}\frac{\partial^2 \psi}{\partial y^2}\right) - \frac{1}{\epsilon}\left(\frac{1}{1-N}\right)\frac{\partial^3 \psi}{\partial y^3} - \left(\frac{N}{1-N}\right)\frac{\partial \omega}{\partial y} - \frac{g^*\beta_T(T_f - T_\infty)}{\nu^2 Re^2}\,\theta$$
$$-\frac{g^*\beta_C(C_w - C_\infty)}{\nu^2 Re^2}\,\phi - u_e\frac{du_e}{dx} + \frac{1}{DaRe}\left(\frac{\partial \psi}{\partial y} - u_e\right) = 0 \tag{3.23}$$
$$\frac{1}{\epsilon}\left(\frac{\partial \psi}{\partial y}\frac{\partial \omega}{\partial x} - \frac{\partial \psi}{\partial x}\frac{\partial \omega}{\partial y}\right) - \left(\frac{2-N}{2-2N}\right)\frac{\partial^2 \omega}{\partial y^2} + \left(\frac{N}{1-N}\right)\left(2\omega + \frac{1}{\epsilon}\frac{\partial^2 \psi}{\partial y^2}\right) = 0 \tag{3.24}$$
$$\frac{\partial \psi}{\partial y}\frac{\partial \theta}{\partial x} - \frac{\partial \psi}{\partial x}\frac{\partial \theta}{\partial y} - \frac{1}{Pr}\frac{\partial^2 \theta}{\partial y^2} = 0 \tag{3.25}$$
$$\frac{\partial \psi}{\partial y}\frac{\partial \phi}{\partial x} - \frac{\partial \psi}{\partial x}\frac{\partial \phi}{\partial y} - \frac{1}{Sc}\frac{\partial^2 \phi}{\partial y^2} = 0 \tag{3.26}$$

Now, the boundary conditions (3.6) become

$$\frac{\partial \psi}{\partial y} = 0,\ \ \frac{\partial \psi}{\partial x} = f_w,\ \ \omega = -n\frac{\partial^2 \psi}{\partial y^2},\ \ \frac{\partial \theta}{\partial y} = -Bi(1-\theta),\ \ \phi = 1 \quad \text{at} \quad y = 0 \tag{3.27a}$$
$$\frac{\partial \psi}{\partial y} = u_e,\ \ \omega = 0,\ \ \theta = 0,\ \ \phi = 0 \quad \text{as} \quad y \to \infty \tag{3.27b}$$

Proceeding same as in case(a) of the chapter-2, the following similarity transformations are

attained using Lie group scaling transformations.

$$\eta = y,\ \psi = xf(\eta),\ \omega = xg(\eta),\ u_e = x,\ \beta_T = x\beta_{T_0},\ \beta_C = x\beta_{C_0},\ \theta = \theta(\eta),\ \phi = \phi(\eta) \tag{3.28}$$

Using (3.28) in Eqs. (3.23)-(3.26), we get the following system of similarity equations

$$\frac{1}{\epsilon}\left(\frac{1}{1-N}\right)f''' + \frac{1}{\epsilon^2}ff'' + 1 - \frac{1}{\epsilon^2}f'^2 + \left(\frac{N}{1-N}\right)g' + \lambda(\theta + \mathcal{B}\phi) + \frac{1}{Da\,Re}(1-f') = 0 \tag{3.29}$$

$$\left(\frac{2-N}{2-2N}\right)g'' + \frac{1}{\epsilon}fg' - \frac{1}{\epsilon}f'g - \left(\frac{N}{1-N}\right)\left(2g + \frac{1}{\epsilon}f''\right) = 0 \tag{3.30}$$

$$\frac{1}{Pr}\theta'' + f\theta' = 0 \tag{3.31}$$

$$\frac{1}{Sc}\phi'' + f\phi' = 0 \tag{3.32}$$

Boundary conditions (3.27) in terms of f, g, θ and ϕ become

$$f(0) = f_w,\ f'(0) = 0,\ g(0) = -nf''(0),\ \theta'(0) = -Bi[1-\theta(0)],\ \phi(0) = 1 \tag{3.33a}$$

$$f'(\infty) = 1,\ g(\infty) = 0,\ \theta(\infty) = 0,\ \phi(\infty) = 0 \tag{3.33b}$$

The non-dimensional skin friction C_f, wall couple stress M_w, local Nusselt number $Nu_{\overline{x}}$ and Sherwood number $Sh_{\overline{x}}$, are given by

$$\left.\begin{aligned} &C_f Re_{\overline{x}^{1/2}} = 2\left(\frac{1-nN}{1-N}\right)f''(0),\ M_w Re_{\overline{x}} = \left(\frac{2-N}{2-2N}\right)g'(0), \\ &\frac{Nu_{\overline{x}}}{Re_{\overline{x}^{1/2}}} = -\theta'(0),\ \frac{Sh_{\overline{x}}}{Re_{\overline{x}^{1/2}}} = -\phi'(0) \end{aligned}\right\} \tag{3.34}$$

Results and Discussion

The system of Eqs.(3.29)-(3.32) along with the boundary conditions (3.33) are solved numerically using the spectral quasi-linearization method, which is clearly discussed in the chapter-2. In order to validate the code generated, for the special case of $N = 0$, $n = 0$, $\lambda = 0$, $Bi \to \infty$, $Da \to \infty$ and $f_w = 0$, the results of the present problem have been compared with those of Merkin [58] and Nazar *et al.* [73] and it is found that they are in good agreement (Tab. (2.4)). The effects of coupling number N, Darcy number Da, Biot number Bi and suction/injection parameter f_w on

the physical quantities of the flow, heat and mass transfer rates have been carried out explicitly for both opposing and aiding flow situations by taking $\mathcal{B} = 1.0$, $n = 0$, $\epsilon = 1.0$, $Pr = 0.71$ and $Sc = 0.22$. Further, it is noticed that the value of the mixed convection parameter λ is taken as positive in the aiding flow situation and negative in the opposing flow situation. However, in the case of opposing flow, the flow field becomes more complex.

Opposing flow

The effects of coupling number N on the non-dimensional velocity, microrotation, temperature and concentration profiles are displayed in Figs. 3.5(a)-3.5(d) for both the cases of suction and injection. In the absence of N, the fluid behaves as non-polar fluid with a loss of the micropolarity. As N increases, it is found from Fig. 3.5(a) that the maximum velocity decreases. It is observed from Fig. 3.5(b) that as N increases, the microrotation profile tends to become flat, and then approaches to their free stream values far away from the wall. It is seen from Figs. 3.5(c) and 3.5(d) that the temperature and concentration of the fluid increase with the increase of coupling number N. It is important to note that the velocity in case of the micropolar fluid is less but, the temperature and concentration are more when compared to those of viscous fluids. The above results are true for both suction and injection cases.

Figs. 3.6(a)-3.6(d) illustrate the influence of Darcy number Da on the non-dimensional velocity, microrotation, temperature and concentration profiles for both suction and injection cases. As Darcy number increases, the velocity decreases in both the cases of suction and injection [Fig. 3.6(a)]. The porous matrix structure becomes less and less prominent with the increase of permeability and in the point of accumulation, as $Da \to \infty \left(i.e., -\dfrac{1}{Da\, Re}\, f' \to 0 \right)$ and $\epsilon = 1$, the porous medium vanishes and reduces to mixed convective flow of micropolar fluid. From Fig. 3.6(b), it is explored that the microrotation reduces with the enhancement of Darcy number and converges to their free stream values. It is seen from Fig. 3.6(c) that the temperature of the fluid increases with the increase of Darcy number for both suction and injection cases. Also, Fig. 3.6(d) shows that as Darcy number increases, the concentration profile enhances for both suction and injection cases.

The variations of non-dimensional velocity, microrotation, temperature and concentration profiles for different values of Biot number for both suction and injection cases are depicted in Figs. 3.7(a)-3.7(d). As Biot number Bi increases, the fluid velocity decreases within the momentum

boundary layer in both the cases of suction and injection [Fig. 3.7(a)]. Fig. 3.7(b) shows that as the Biot number increases, the microrotation profile slightly decreases within the range $(0 < \eta < 1)$ after that, it increases in the injection case. However, in the suction case, there is no significant effect up to $\eta = 0.65$ approximately and then it increases with the increase of Biot number. Fig. 3.7(c) reveals that for both suction and injection cases, the fluid temperature is high at the plate surface and decreases exponentially to zero value far away from the plate satisfying the boundary conditions. As a result, an increase in Biot number leads to increase in the fluid temperature efficiency. Fig. 3.7(d) illustrates that as Biot number Bi increases, there is no significant effect on the concentration boundary layer thickness in the case of suction, but slightly increases in the injection case.

The variations of the skin-friction, wall couple stress, heat and mass transfers rate are shown in Tab.(3.2) in both the cases of suction and injection for different values of the coupling number, Biot number and Darcy number. Tab.(3.2) indicates that the skin friction is higher for the micropolar fluid when compared to the viscous fluid ($n = 0$, $N = 0$). The wall couple stress, heat and mass transfer rates decrease but, the skin friction increases with the increase of coupling number. From Tab.(3.2), it can be observed that the skin-friction, heat and mass transfer rates decrease, but the wall couple stress increases with the increase of Da. It is also noticed that the skin-friction and mass transfer rate reduce, but the wall couple stress and heat transfer rate enhances with Biot number Bi enhancement.

Aiding flow

The influence of coupling number N on the dimensionless velocity, microrotation, temperature and concentration profiles is displayed in Figs. 3.8(a)-3.8(d) in both the cases of suction and injection for fixed values of other parameters. As coupling number N increases, it is found from Fig. 3.8(a) that the velocity decreases in both suction and injection cases. Fig. 3.8(b) exhibits that initially, the microrotation profile tends to become flat, and then converges to their free stream values far away from the wall with an increase in coupling number. For both suction and injection, the temperature and concentration increase with the increase of coupling number as shown in Figs. 3.8(c) and 3.8(d).

Figs. 3.9(a)-3.9(d) exhibit the effects of Darcy number Da, on the non-dimensional velocity,

microrotation, temperature and concentration profiles in both the cases of suction and injection. Fig. 3.9(a) indicates that an increase in Da reduces the velocity of the micropolar fluid near the wall and its behaviour reverses far away from the wall. From Fig. 3.9(b), it can be noticed that as Darcy number increases the microrotation profile shows reverse rotation. From Figs. 3.9(c) and 3.9(d), it can be concluded that the temperature and concentration increase with the increase of Darcy number. The above results are same in both the cases of suction and injection.

The variation of Biot number Bi on the dimensionless velocity, microrotation, temperature and concentration profiles is depicted in Figs. 3.10(a)-3.10(d) in both the cases of suction and injection for fixed values of other parameters. It is interesting to observe from Fig. 3.10(a) that an increase in Biot number Bi produces a substantial enhancement in the fluid velocity within the momentum boundary layer. As Bi increases, initially, there is no significant effect in the case of suction, but slightly decreases in the injection case and then it increases for both suction and injection [Fig. 3.10(b)]. Fig. 3.10(c) interprets that for both suction and injection cases, the temperature of the fluid enhances with the enhancement of Biot number. As the value of Biot number increases, the concentration decreases slightly in the injection case, but it does not show significant effect in the suction case [Fig.3.10(d)].

The variations of skin-friction, wall couple stress, heat and mass transfer rates are shown in Tab.(3.2) in both the cases of suction and injection for different values of coupling, Biot and Darcy numbers. From Tab. (3.2), it can be seen that the skin friction $C_f Re_{\overline{x}^{1/2}}$ is higher for the micropolar fluid when compared to the viscous fluid ($n = 0$, $N = 0$) for both suction as well as injection cases. Further, the wall couple stress, heat and mass transfer rates decrease with the increase of coupling number in both suction and injection cases. It can be observed from table that the skin-friction, heat and mass transfer rates decrease but, the wall couple stress increases with the increase of Da in the presence of suction and injection. It can be noticed that the skin-friction, heat and mass transfer rates increase, but the wall couple stress decreases with an increase in Biot number Bi for both suction and injection cases.

Table 3.2: *Variations of skin friction, wall couple stress, heat and mass transfer coefficients for varying values of coupling number, Darcy number, Biot number, mixed convection and suction/injection parameters*

λ	fw	N	Da	Bi	$C_f Re_{\overline{x}^{1/2}}$	$M_w Re_{\overline{x}}$	$\frac{Nu_{\overline{x}}}{Re_{\overline{x}^{1/2}}}$	$\frac{Sh_{\overline{x}}}{Re_{\overline{x}^{1/2}}}$
-0.5	-0.5	0	0.1	0.1	4.200684	0	0.077355	0.258083
-0.5	-0.5	0.5	0.1	0.1	6.028993	-0.5016	0.076054	0.247237
-0.5	-0.5	0.8	0.1	0.1	9.279943	-1.45206	0.073841	0.23027
-0.5	0.5	0	0.1	0.1	5.237084	0	0.088676	0.400173
-0.5	0.5	0.5	0.1	0.1	7.109759	-0.59758	0.088259	0.387192
-0.5	0.5	0.8	0.1	0.1	10.44195	-1.66538	0.087611	0.367259
1	-0.5	0	0.1	0.1	5.393751	0	0.079244	0.279211
1	-0.5	0.5	0.1	0.1	7.689083	-0.59422	0.077944	0.266581
1	-0.5	0.8	0.1	0.1	11.7283	-1.73555	0.075727	0.246983
1	0.5	0	0.1	0.1	6.443151	0	0.089099	0.417337
1	0.5	0.5	0.1	0.1	8.672207	-0.67155	0.088656	0.40257
1	0.5	0.8	0.1	0.1	12.58159	-1.89275	0.087967	0.38009
-0.5	-0.5	0.3	0.01	0.1	16.45829	-0.33854	0.080276	0.286325
-0.5	-0.5	0.3	0.1	0.1	5.086925	-0.24007	0.076725	0.252733
-0.5	-0.5	0.3	0.5	0.1	2.477442	-0.17672	0.073133	0.224628
-0.5	0.5	0.3	0.01	0.1	17.47235	-0.36032	0.08941	0.424335
-0.5	0.5	0.3	0.1	0.1	6.143973	-0.28831	0.08847	0.393731
-0.5	0.5	0.3	0.5	0.1	3.624604	-0.24647	0.08782	0.373152
1	-0.5	0.3	0.01	0.1	17.01112	-0.34663	0.080535	0.289739
1	-0.5	0.3	0.1	0.1	6.506748	-0.28201	0.078613	0.272964
1	-0.5	0.3	0.5	0.1	4.615073	-0.258	0.077737	0.2663
1	0.5	0.3	0.01	0.1	17.99893	-0.36673	0.089477	0.427263
1	0.5	0.3	0.1	0.1	7.523803	-0.32081	0.08888	0.409995
1	0.5	0.3	0.5	0.1	5.67869	-0.30557	0.088653	0.403908
-0.5	-0.5	0.3	1	0.1	1.977417	-0.15929	0.071856	0.215988
-0.5	-0.5	0.3	1	1	1.618677	-0.14356	0.193142	0.207599
-0.5	-0.5	0.3	1	3	1.533433	-0.13967	0.218255	0.205485
-0.5	0.5	0.3	1	0.1	3.169636	-0.23637	0.087648	0.367902
-0.5	0.5	0.3	1	1	2.903577	-0.2296	0.412412	0.364319
-0.5	0.5	0.3	1	3	2.77322	-0.22623	0.56625	0.362526
1	-0.5	0.3	1	0.1	4.327651	-0.25371	0.07757	0.265113
1	-0.5	0.3	1	1	4.86199	-0.27045	0.265047	0.27263
1	-0.5	0.3	1	3	5.022161	-0.27534	0.32533	0.274796
1	0.5	0.3	1	0.1	5.404291	-0.30306	0.088614	0.402902
1	0.5	0.3	1	1	5.836549	-0.31223	0.440615	0.407301
1	0.5	0.3	1	3	6.05778	-0.31686	0.626829	0.409502

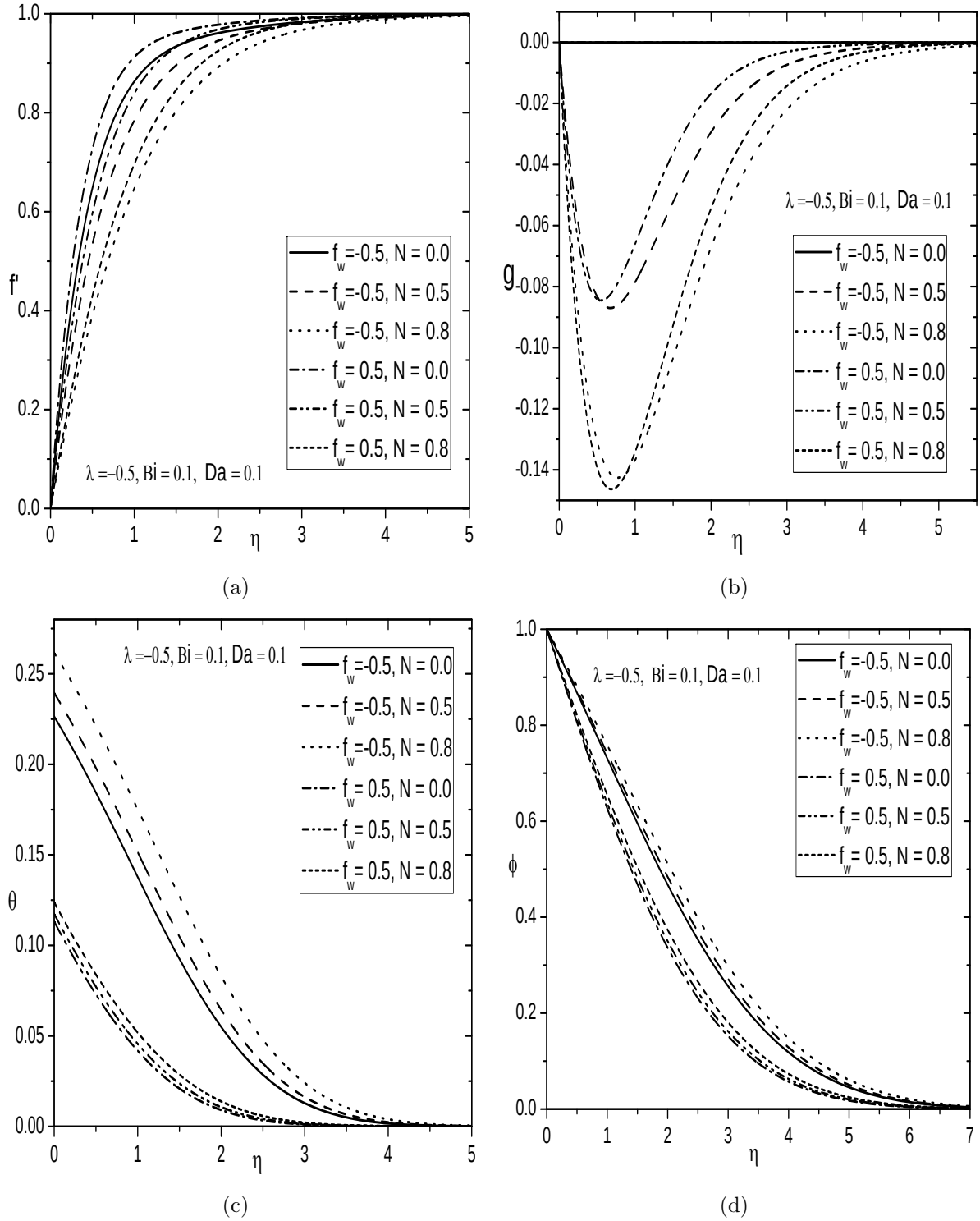

Figure 3.5: *Variation of N on (a)Velocity, (b)Microrotation, (c)Temperature and (d)Concentration profiles* (Opposing flow case)

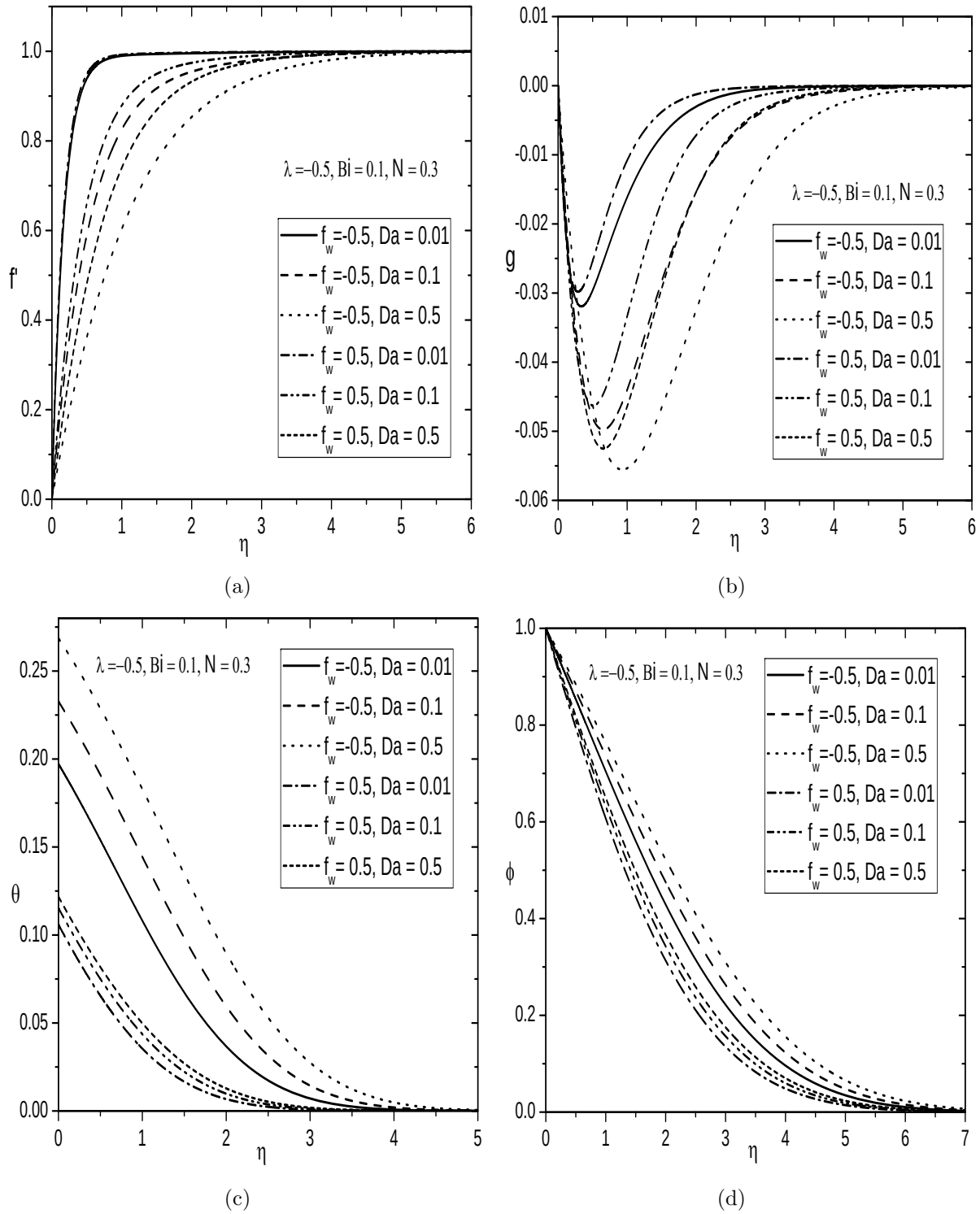

Figure 3.6: *Variation of Da on (a)Velocity, (b)Microrotation, (c)Temperature and (d)Concentration profiles* (Opposing flow case)

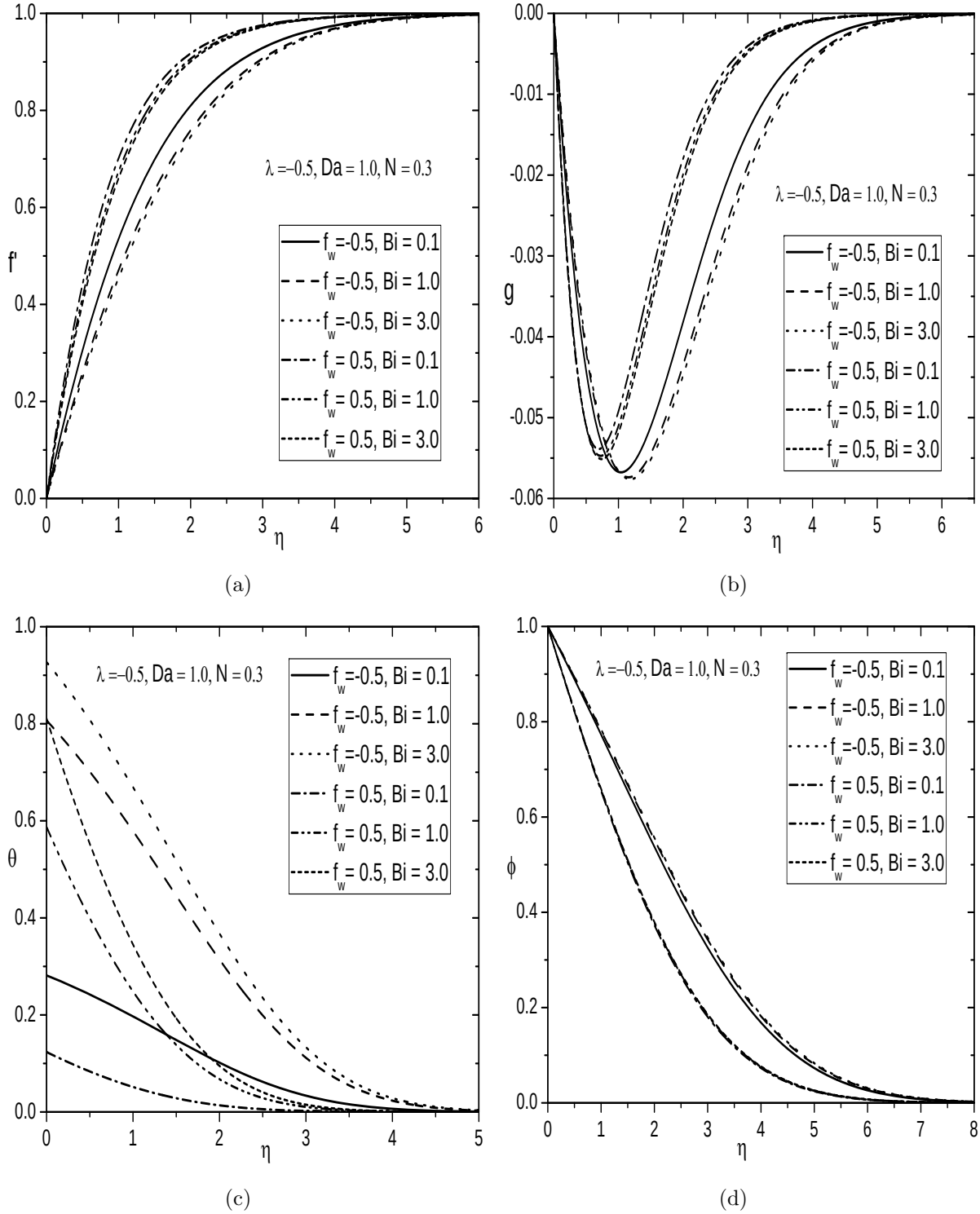

Figure 3.7: *Variation of Bi on (a)Velocity, (b)Microrotation, (c)Temperature and (d)Concentration profiles* (Opposing flow case)

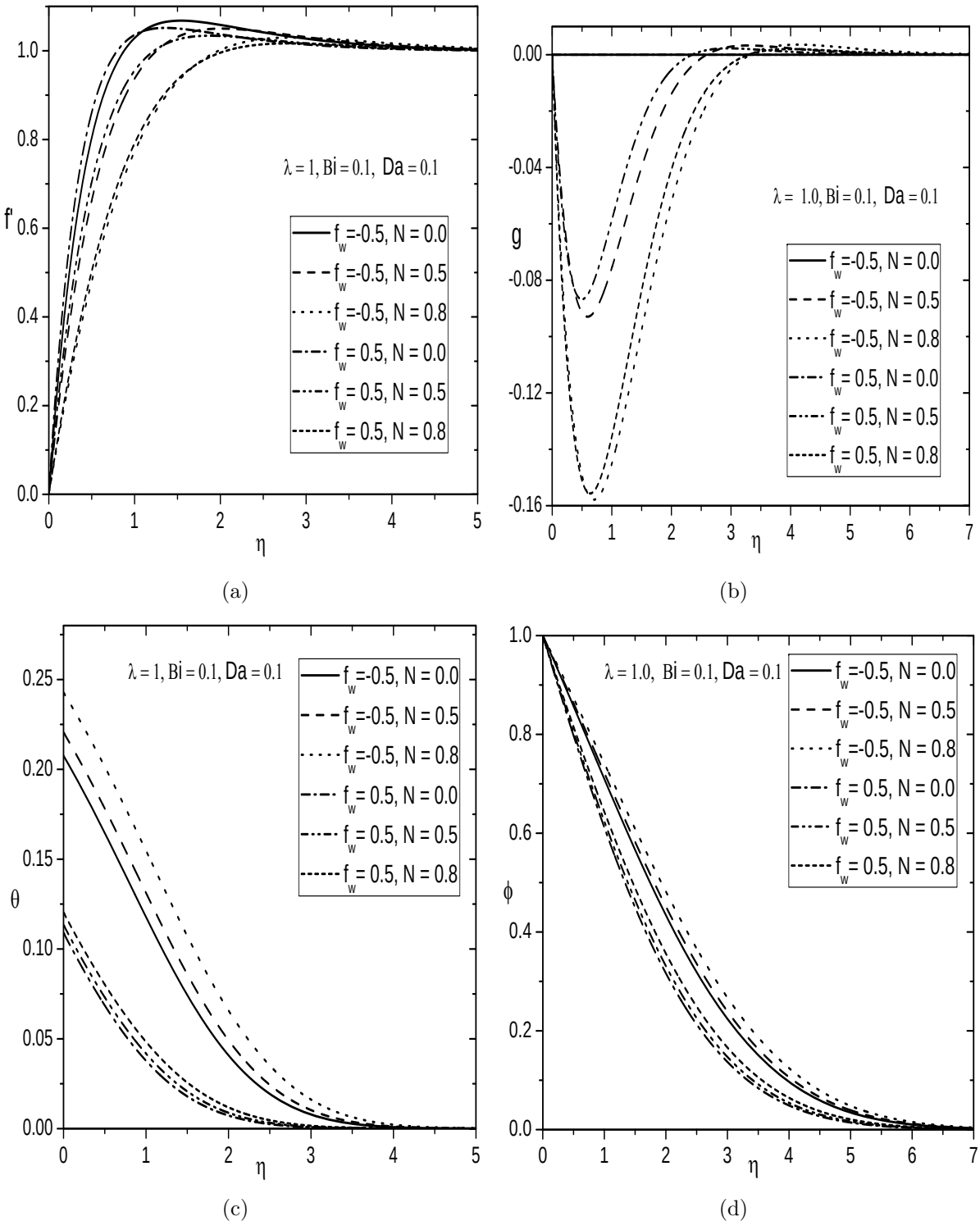

Figure 3.8: *Variation of N on (a)Velocity, (b)Microrotation, (c)Temperature and (d)Concentration profiles* (Aiding flow case)

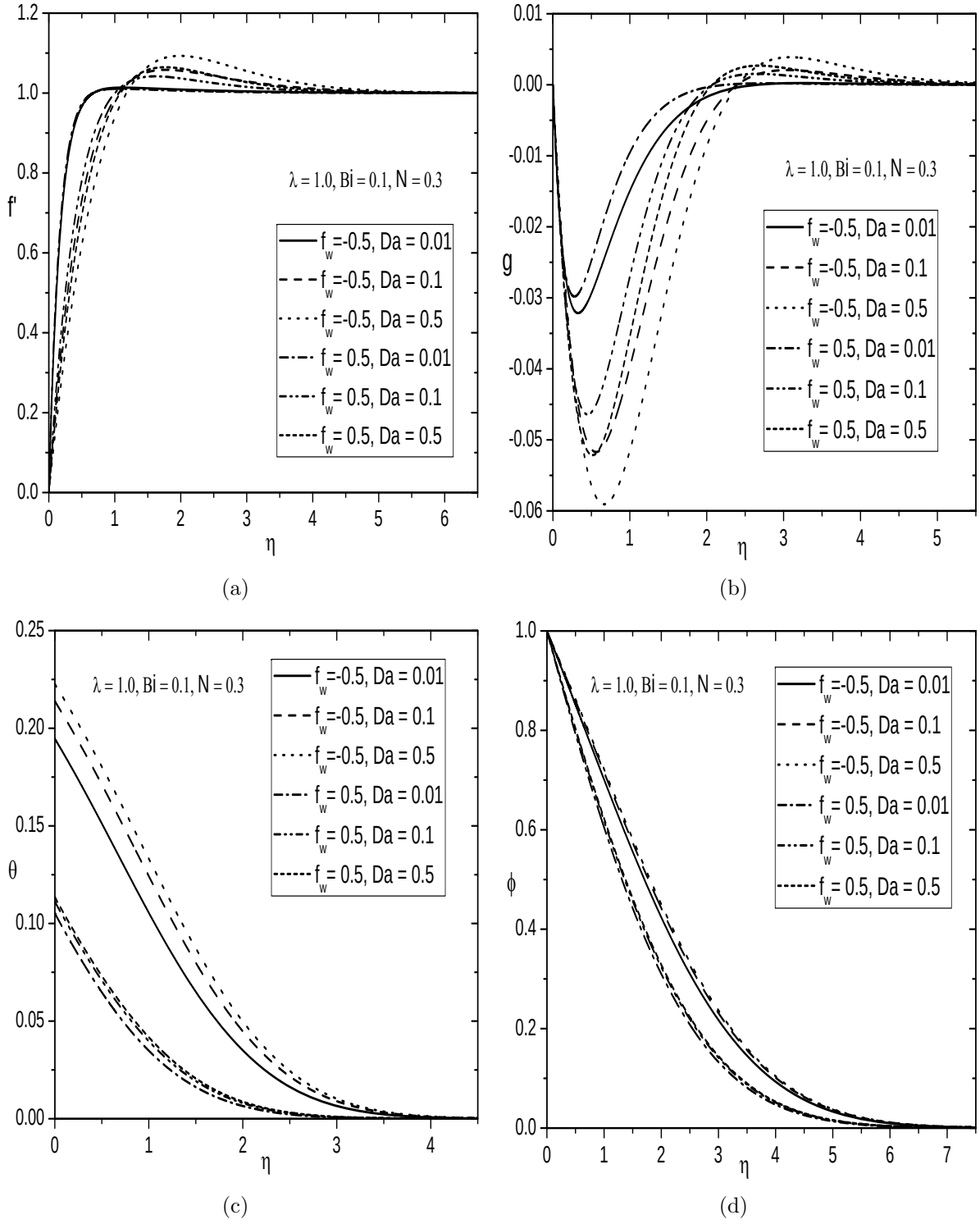

Figure 3.9: *Variation of Da on (a)Velocity, (b)Microrotation, (c)Temperature and (d)Concentration profiles* (Aiding flow case)

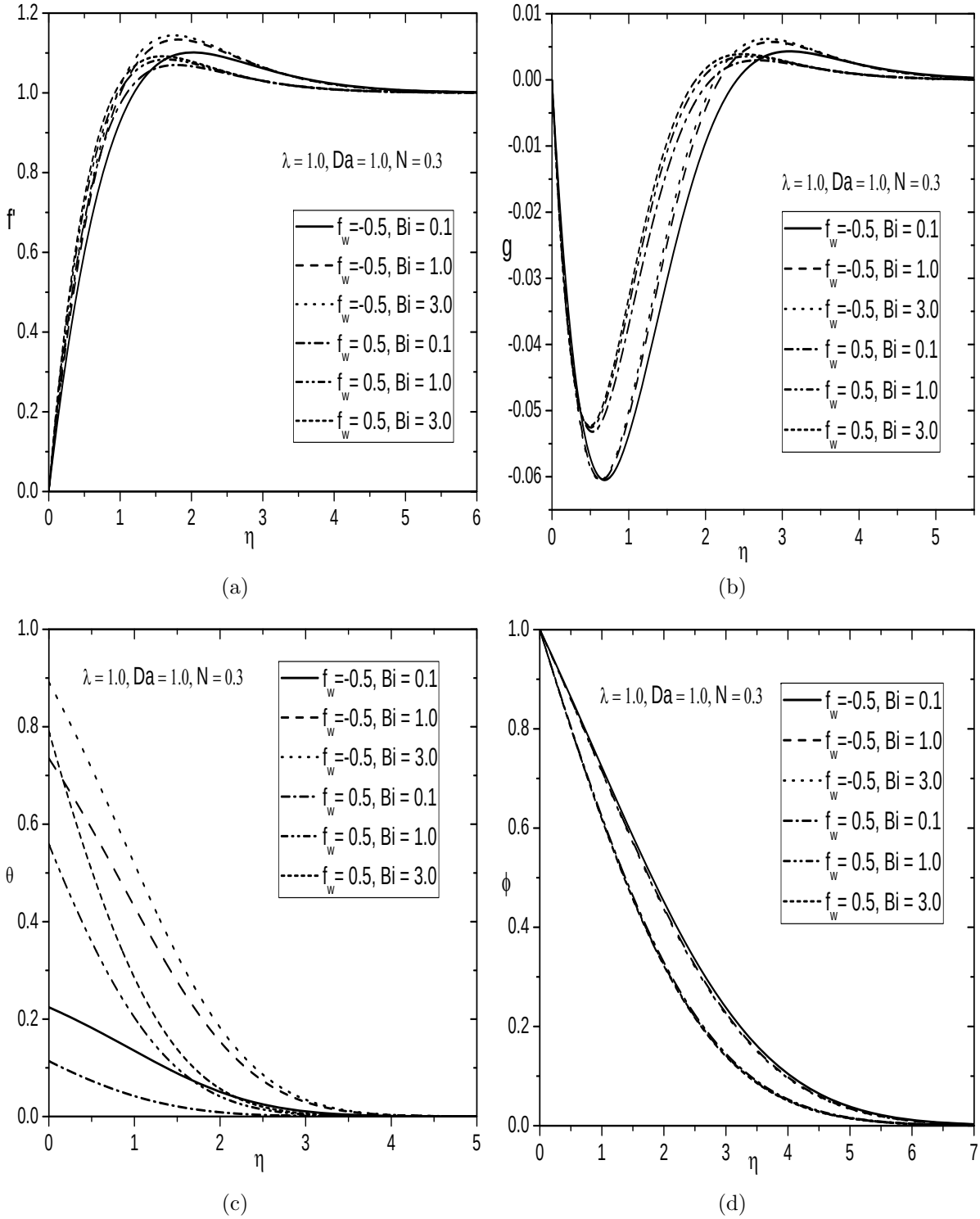

Figure 3.10: *Variation of Bi on (a)Velocity, (b)Microrotation, (c)Temperature and (d)Concentration profiles* (Aiding flow case)

3.3 Conclusions

In this chapter, free and mixed convective heat and mass transfer along a permeable vertical plate embedded in a porous medium saturated with a micropolar fluid subject to the convective boundary condition is analyzed. From this computational analysis, the following conclusions are drawn in the presence of suction/injection for both case (a) and case (b).

Case (a) Free Convection: The higher values of the coupling number N results in a lower velocity distribution compared to the Newtonian fluid case ($N = 0$). The numerical results indicate that the skin friction is higher and wall couple stresses is lower for the micropolar fluid in comparison with the Newtonian fluid. Likewise, non-dimensional heat and mass transfer rates decrease with the increase of the coupling number. An increase in N leads to increase in the temperature and concentration distributions for both the injection and suction. Also, the microrotation shows reverse rotation near the two boundaries. For both the cases of suction and injection, an increase in Biot number Bi, results in decrease of concentration and wall couple stress accompanied by an increase in the temperature, skin friction, heat and mass transfer rates within the boundary layers. It is observed that the wall couple stress decreases, but the skin friction, heat and mass transfer rates increase with an increase in Darcy parameter Da for both suction and injection cases.

Case (b) Mixed Convection: The larger values of the coupling number results in a lower velocity, wall couple stress, heat and mass transfer rates, but higher temperature, concentration and skin friction for both the aiding and opposing flow situations. For both aiding and opposing flows: the velocity, skin friction, heat and mass transfer rates decrease, but the temperature, concentration and wall couple stresses increase with an increase in the value of Darcy number Da in the presence of suction and injection. For both opposing and aiding flows, the temperature and heat transfer rate increase with the increase of Biot number. In opposing flow situation: the velocity, skin-friction and mass transfer rate decrease, but the wall couple stress and concentration increase with the increase of Bi in both the cases of suction and injection. These profiles and physical quantities show reverse trend in the case of aiding flow situation.

Chapter 4

Homogeneous-Heterogeneous Reactions on Nonlinear Convective Flow of a Micropolar Fluid with Radiation Effect [1]

4.1 Introduction

Considerable attention has been paid to study the combined heat and mass transfer problems with the effect of chemical reaction in the recent past. As it plays a crucial role in diverse applications such as drying, energy transfer in the wet cooling surface, evaporation at the surface of the water body, etc. Two types of chemical reactions, namely, homogeneous and heterogeneous reactions in different fluid flows over various surface geometries have been attracted by several researchers. Further, the homogeneous reaction arises constantly throughout a given phase, while the heterogeneous reaction occurs in a bounded region or within the boundary of phase. In view of the above said applications, a mathematical model has been proposed by Chaudhary and Merkin [20] to study the homogeneous-heterogeneous reactions in boundary layer flow with the effect of loss of autocat-

[1] Case(a):Published in "**Nonlinear Engineering**" 5(3) (2016) 193–204.,
Case(b) Accepted in "**Proc. Natl. Acad. Sci., India, Sect. A Phys. Sci**"

alyst. Khan and Pop[49] studied the viscoelastic fluid along a stretching sheet in the presence of homogeneous-heterogeneous reactions. Nandkeolyar *et al.* [71] investigated the influence of internal heat generation in a nanofluid flow with homogeneous-heterogeneous reactions.

The analysis of nonlinear thermal convection (i.e., may be treated as nonlinear relationship between the density and temperature) is of great interest owing to their numerous applications in engineering, astrophysics, geophysics and industrial manufacturing processes such as cooling of electronic components, doping processes, pore water convection near salt domes, etc. Few researchers have aimed at this point and tried to explore various aspects in this direction. Barrow and Rao [11] discussed the effect of variable thermal expansion coefficient on free convection. Nandkeolyar *et al.* [70] analyzed the effect of viscous dissipation on a stagnation point flow of a nanofluid along a stretching sheet by considering the nonlinear convection (For more details, see the citations therein).

In this chapter, the significance of nonlinear temperature-dependent density relation in an incompressible micropolar fluid flow along a vertical plate with the convective boundary condition, is studied in two cases, namely, free and mixed convections. In addition, the homogeneous-heterogeneous reactions and thermal radiation are incorporated in the present analysis. To our best knowledge, this problem in a micropolar fluid has not been reported in the literature. The influence of pertinent parameters on physical quantities of the flow are examined and exhibited through graphs. The numerical values of the skin friction, wall couple stress and heat transfer rate for different values of governing parameters are also tabulated. The results are compared with relevant results in the existing literature and found to be in good agreement.

4.2 Mathematical Formulation

Consider the steady, two dimensional and laminar convective flow of an incompressible micropolar fluid along a vertical plate. Choose the coordinate system such that the $\overline{x}$-axis is along the vertical plate and $\overline{y}$-axis normal to the plate. The physical model and coordinate system is shown in Fig. (4.1). The temperature difference between the plate and the medium is assumed to be large, so that the convection region is thick. The fluid is considered to be a gray, absorbing and emitting radiation, but non-scattering medium and the Rosseland approximation is used to describe the

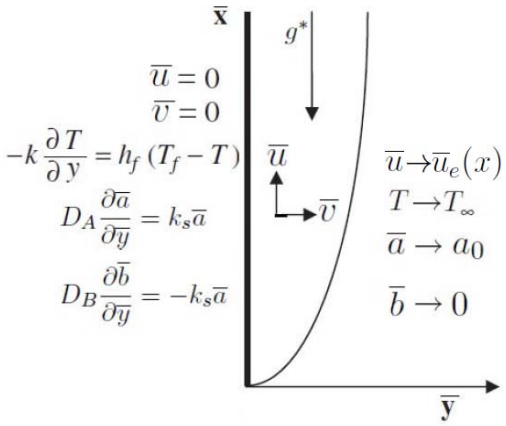

Figure 4.1: *Physical model and coordinate system*

radiative heat flux in the energy equation. Assume that the velocity of the outer flow is $\overline{u}_e(x)$ and the free stream temperature is T_∞ . The plate is either heated or cooled from left by convection from a fluid of temperature T_f with $T_f > T_\infty$ corresponding to a heated surface and $T_f < T_\infty$ corresponding to a cooled surface respectively.

It is assumed that a simple homogeneous-heterogeneous reaction model exists as proposed by Chaudhary and Merkin [20] in the following form:

For the homogeneous reaction, cubic autocatalysis is chosen as follows:

$$A + 2B \to 3B, \qquad \text{rate} = k_c\overline{a}\,\overline{b}^2$$

while on the catalyst surface, the single isothermal first order reaction is taken as

$$A \to B, \qquad \text{rate} = k_s\overline{a}$$

By employing nonlinear Boussinesq approximation and making use of the standard boundary layer assumptions, the governing equations for the micropolar fluid [59, 43, 103] are given by

$$\frac{\partial \overline{u}}{\partial \overline{x}} + \frac{\partial \overline{v}}{\partial \overline{y}} = 0 \tag{4.1}$$

$$\rho\left(\overline{u}\frac{\partial \overline{u}}{\partial \overline{x}} + \overline{v}\frac{\partial \overline{u}}{\partial \overline{y}}\right) = (\mu + \kappa)\frac{\partial^2 \overline{u}}{\partial \overline{y}^2} + \rho\overline{u}_e\frac{d\overline{u}_e}{d\overline{x}} + \kappa\frac{\partial \overline{\omega}}{\partial \overline{y}} + \rho g^*\left[\beta_1(T - T_\infty) + \beta_2(T - T_\infty)^2\right] \tag{4.2}$$

$$\rho j\left(\overline{u}\frac{\partial\overline{\omega}}{\partial\overline{x}}+\overline{v}\frac{\partial\overline{\omega}}{\partial\overline{y}}\right)=\gamma\frac{\partial^2\overline{\omega}}{\partial\overline{y}^2}-\kappa\left(2\overline{\omega}+\frac{\partial\overline{u}}{\partial\overline{y}}\right) \tag{4.3}$$

$$\overline{u}\frac{\partial T}{\partial\overline{x}}+\overline{v}\frac{\partial T}{\partial\overline{y}}=\alpha\frac{\partial^2 T}{\partial\overline{y}^2}+\frac{4\alpha\,\sigma^*}{3k\,k^*}\frac{\partial^2}{\partial\overline{y}^2}\left(4T_\infty^3T-3T_\infty^4\right) \tag{4.4}$$

$$\overline{u}\frac{\partial\overline{a}}{\partial\overline{x}}+\overline{v}\frac{\partial\overline{a}}{\partial\overline{y}}=D_A\frac{\partial^2\overline{a}}{\partial\overline{y}^2}-k_c\overline{a}\,\overline{b}^2 \tag{4.5}$$

$$\overline{u}\frac{\partial\overline{b}}{\partial\overline{x}}+\overline{v}\frac{\partial\overline{b}}{\partial\overline{y}}=D_B\frac{\partial^2\overline{b}}{\partial\overline{y}^2}+k_c\overline{a}\,\overline{b}^2 \tag{4.6}$$

where $\overline{a}$ and $\overline{b}$ are concentrations of the chemical species A and B, D_A and D_B are the respective diffusion coefficients of species A and B, β_1 and β_2 are the coefficients of thermal expansion, σ^* is the Stefan-Boltzmann constant and k^* is the mean absorption coefficient. In the Eq.(4.4), the last term is obtained by assuming that the temperature differences within the flow are sufficiently small and the power function is expressed as a linear function of temperature by neglecting the higher-order terms of the expansion.

The associated boundary conditions are

$$\overline{u}=0,\ \overline{v}=0,\ \overline{\omega}=-n\frac{\partial\overline{u}}{\partial\overline{y}},\ -k\frac{\partial T}{\partial\overline{y}}=h_f(T_f-T),\ D_A\frac{\partial\overline{a}}{\partial\overline{y}}=k_s\overline{a},\ D_B\frac{\partial\overline{b}}{\partial\overline{y}}=-k_s\overline{a}\ \text{at}\ \overline{y}=0 \tag{4.7a}$$

$$\overline{u}=\overline{u}_e(x),\ \overline{\omega}=0,\ T=T_\infty,\ \overline{a}=a_0,\ \overline{b}=0\ \ \text{as}\ \ \ \overline{y}\to\infty \tag{4.7b}$$

where a_0 is a positive constant and k_s is the rate constant. In this chapter also, two types (cases) of problems are considered: (a) free/natural convection and (b) mixed convection.

4.2.1 Case(a): Natural Convection

The flow is assumed to be a natural convection which is caused by buoyancy forces only without any external agent, and hence the velocity of the external flow becomes zero $(ie., \overline{u}_e=0)$. We introduce the following dimensionless variables

$$x=\frac{\overline{x}}{L},\ y=\frac{\overline{y}}{L}Gr^{1/4},\ u=\frac{L}{\nu Gr^{1/2}}\overline{u},\ v=\frac{L}{\nu Gr^{1/4}}\overline{v},\ \omega=\frac{L^2}{\nu Gr^{3/4}}\overline{\omega},\ \theta=\frac{T-T_\infty}{T_f-T_\infty},\ h=\frac{\overline{a}}{a_0},\ h_1=\frac{\overline{b}}{a_0} \tag{4.8}$$

In view of the continuity equation (4.1), we introduce the stream function ψ by

$$u = \frac{\partial \psi}{\partial y}, \quad v = -\frac{\partial \psi}{\partial x} \tag{4.9}$$

Using (4.8) and (4.9) in Eqs.(4.2)-(4.6), we get the following momentum, angular momentum, energy, and concentration equations of species A and B

$$\frac{\partial \psi}{\partial y}\frac{\partial^2 \psi}{\partial x \partial y} - \frac{\partial \psi}{\partial x}\frac{\partial^2 \psi}{\partial y^2} - \left(\frac{1}{1-N}\right)\frac{\partial^3 \psi}{\partial y^3} - \left(\frac{N}{1-N}\right)\frac{\partial \omega}{\partial y} - \frac{\beta_1}{\beta_{T_0}}\,\theta\left(1 + \frac{\beta_2}{\beta_1}\theta(T_f - T_\infty)\right) = 0 \tag{4.10}$$

$$\frac{\partial \psi}{\partial y}\frac{\partial \omega}{\partial x} - \frac{\partial \psi}{\partial x}\frac{\partial \omega}{\partial y} - \left(\frac{2-N}{2-2N}\right)\frac{\partial^2 \omega}{\partial y^2} + \left(\frac{N}{1-N}\right)\left(2\omega + \frac{\partial^2 \psi}{\partial y^2}\right) = 0 \tag{4.11}$$

$$\frac{\partial \psi}{\partial y}\frac{\partial \theta}{\partial x} - \frac{\partial \psi}{\partial x}\frac{\partial \theta}{\partial y} - \frac{1}{Pr}\left(1 + \frac{4}{3}R\right)\frac{\partial^2 \theta}{\partial y^2} = 0 \tag{4.12}$$

$$\frac{\partial \psi}{\partial y}\frac{\partial h}{\partial x} - \frac{\partial \psi}{\partial x}\frac{\partial h}{\partial y} - \frac{1}{Sc}\frac{\partial^2 h}{\partial y^2} + K\,h\,{h_1}^2 = 0 \tag{4.13}$$

$$\frac{\partial \psi}{\partial y}\frac{\partial h_1}{\partial x} - \frac{\partial \psi}{\partial x}\frac{\partial h_1}{\partial y} - \frac{\delta}{Sc}\frac{\partial^2 h_1}{\partial y^2} - K\,h\,{h_1}^2 = 0 \tag{4.14}$$

In usual definitions, $Sc = \dfrac{\nu}{D_A}$ is the Schmidt number, $R = \dfrac{4\sigma^* T_\infty^3}{kk^*}$ is the radiation parameter, $K = \dfrac{k_c {a_0}^2 L}{\nu Gr^{1/2}}$ is the strength of homogeneous reaction and $\delta = \dfrac{D_B}{D_A}$ is the ratio of diffusion coefficient.

Now, the boundary conditions (4.7) become

$$\frac{\partial \psi}{\partial y} = 0,\ \frac{\partial \psi}{\partial x} = 0,\ \omega = -n\frac{\partial^2 \psi}{\partial y^2},\ \frac{\partial \theta}{\partial y} = -Bi(1-\theta),\ \frac{\partial h}{\partial y} = K_s h,\ \delta\frac{\partial h_1}{\partial y} = -K_s h \text{ at } y = 0 \tag{4.15a}$$

$$\frac{\partial \psi}{\partial y} = 0,\ \omega = 0,\ \theta = 0,\ h = 1,\ h_1 = 0 \quad \text{as} \quad y \to \infty \tag{4.15b}$$

where $K_s = \dfrac{k_s L G r^{-1/4}}{D_A}$ is the strength of heterogeneous (surface) reaction.

In order to get the similarity represenatation of the system of Eqs. (4.10) - (4.14), a one-parameter scaling group of transformations, which is a simplified form of Lie group transformation, is selected as (Seddeek *et al.* [90])

$$\begin{aligned} &\Gamma : x^* = x\,e^{\varepsilon\,\alpha_1},\ y^* = y\,e^{\varepsilon\,\alpha_2},\ \psi^* = \psi\,e^{\varepsilon\,\alpha_3},\ \omega^* = \omega\,e^{\varepsilon\,\alpha_4},\ \theta^* = \theta\,e^{\varepsilon\,\alpha_5}, \\ &h^* = h\,e^{\varepsilon\,\alpha_6},\ h_1^* = h_1\,e^{\varepsilon\,\alpha_7},\ \beta_1^* = \beta_1\,e^{\varepsilon\,\alpha_8},\ \beta_2^* = \beta_2\,e^{\varepsilon\,\alpha_9} \end{aligned} \tag{4.16}$$

Using the procedure of Lie scaling group transformations as explained in the case(a) of second chapter, the similarity transformations are obtained as

$$\eta = y,\ \psi = xf(\eta),\ \omega = xg(\eta),\ \beta_1 = x\beta_{T_0},\ \beta_2 = x\beta_{T_1},\ \theta = \theta(\eta),\ h = h(\eta),\ h_1 = h_1(\eta) \tag{4.17}$$

where β_{T_0} and β_{T_1} are the constant coefficients of thermal expansion.

Using (4.17) in Eqs. (4.10) - (4.14), the following similarity equations are attained

$$\left(\frac{1}{1-N}\right) f''' + ff'' - f'^2 + \left(\frac{N}{1-N}\right) g' + \theta(1+\chi\theta) = 0 \tag{4.18}$$

$$\left(\frac{2-N}{2-2N}\right) g'' + fg' - f'g - \left(\frac{N}{1-N}\right)(2g + f'') = 0 \tag{4.19}$$

$$\frac{1}{Pr}\left(1 + \frac{4}{3}R\right)\theta'' + f\theta' = 0 \tag{4.20}$$

$$\frac{1}{Sc}h'' + fh' - Khh_1{}^2 = 0 \tag{4.21}$$

$$\frac{\delta}{Sc}h_1'' + fh_1' + Khh_1{}^2 = 0 \tag{4.22}$$

where $\chi = \dfrac{\beta_{T_1}}{\beta_{T_0}}(T_f - T_\infty)$ is the nonlinear density temperature (NDT) parameter.

Boundary conditions (4.15) in terms of f, g, θ, h and h_1 become

$$f(0) = 0,\ f'(0) = 0,\ f'(\eta) = 0 \quad as\ \ \eta \to \infty \tag{4.23a}$$

$$g(0) = -nf''(0),\ g(\eta) = 0 \quad as\ \ \eta \to \infty \tag{4.23b}$$

$$\theta'(0) = -Bi[1 - \theta(0)],\ \theta(\eta) = 0 \quad as\ \ \eta \to \infty \tag{4.23c}$$

$$h'(0) = K_s h(0),\ h(\eta) = 1 \quad as\ \ \eta \to \infty \tag{4.23d}$$

$$\delta h_1'(0) = -K_s h(0),\ h_1(\eta) = 0 \quad as\ \ \eta \to \infty \tag{4.23e}$$

It is expected that the diffusion coefficients of chemical species A and B are of comparable size, which undergo further assumption that the diffusion coefficients D_A and D_B are equal, i.e., $\delta = 1$ (See Ref.[20]). This assumption leads to the following relation

$$h(\eta) + h_1(\eta) = 1 \tag{4.24}$$

Thus, the two Eqs. (4.21) and (4.22) reduce into the single equation as given below

$$\frac{1}{Sc}h'' + fh' - Kh(1-h)^2 = 0 \tag{4.25}$$

and the associated boundary conditions are simplified as follows

$$h'(0) = K_s\, h(0), \;\; h(\eta) = 1 \quad as \;\; \eta \to \infty \tag{4.26}$$

The shear stress, wall couple stress and heat transfer rate from the plate, are defined as

$$\tau_w = \left[(\mu+\kappa)\frac{\partial \overline{u}}{\partial \overline{y}} + \kappa\overline{\omega}\right]_{\overline{y}=0},\; m_w = \gamma\left[\frac{\partial \overline{\omega}}{\partial \overline{y}}\right]_{\overline{y}=0} \text{ and } q_w = -k\left[\left(\frac{\partial T}{\partial \overline{y}}\right) + \frac{4\alpha\,\sigma^*}{3k\,k^*}\frac{\partial}{\partial \overline{y}}\left(4T_\infty^3 T - 3T_\infty^4\right)\right]_{\overline{y}=0} \tag{4.27a}$$

The quantities of physical interest are the non-dimensional skin friction $C_f = \dfrac{2\tau_w}{\rho\overline{u}_*^2}$, wall couple stress $M_w = \dfrac{m_w}{\rho\overline{u}_*^2\overline{x}}$ and local Nusselt number $Nu_{\overline{x}} = \dfrac{q_w\overline{x}}{k(T_f - T_\infty)}$, which are given by

$$C_f Gr^{1/4} = 2\left(\frac{1-nN}{1-N}\right)f''(0),\; M_w Gr^{1/2} = \left(\frac{2-N}{2-2N}\right)g'(0) \text{ and } \frac{Nu_{\overline{x}}}{Gr_{\overline{x}}^{1/4}} = \left(1+\frac{4}{3}R\right)\theta'(0) \tag{4.28}$$

where $Gr_{\overline{x}} = \dfrac{g^*\beta_{T_0}(T_f - T_\infty)\overline{x}^3}{\nu^2}$ is the local Grashof number and $\overline{u}_*$ is the characteristic velocity.

Results and Discussion

The coupled nonlinear Eqs.(4.18)-(4.20) and (4.25) along with the boundary conditions (4.23)(a) - (4.23)(c) and (4.26) are solved numerically using the spectral quasi-linearisation method, which is explained clearly in the case(a) of chapter-2. In order to assess the accuracy of the code generated, for $N = 0$, $R = 0$, $n = 0$, $Pr = 1$, $\chi = 0$ and $Bi \to \infty$, the results of the present problem in the absence of homogeneous and heterogeneous reactions, have been compared with those of Merkin [57], Nazar *et al.* [72] and Molla *et al.* [60] and found that they are in good agreement [Tab. (2.1)]. Also, the values of heat transfer rate, for $n = 0.5$, $R = 0$, $Pr = 1$, $Bi \to \infty$ and $\chi = 0$, agree well with that of Nazar *et al.* [72] as shown in Tab. (2.2). The investigation is carried out to analyze the nonlinear convection parameter χ, Biot number Bi, homogeneous and heterogeneous reaction

parameters K and K_s, for fixed values of $n = 0$, $Pr = 0.71$ and $Sc = 0.22$.

The influence of coupling number N on the dimensionless velocity, microrotation, temperature and species concentration is illustrated in Figs. 4.2(a)-4.2(d) for fixed values of other parameters. As N increases, it is found from Fig. 4.2(a) that the maximum velocity decreases in amplitude and the location of the maximum velocity moves farther away from the wall. Since $N \to 0$ corresponds to a viscous fluid, the velocity in the case of micropolar fluid is less compared to that of the viscous fluid case. From Fig. 4.2(b), it can be observed that as N increases, the microrotation tends to become flat initially, and then approaches to their free stream values far away from the wall. This is due to the fact that with an increase in N, the vortex viscosity of fluid increases and hence, it promotes the microrotation of micropolar fluid. It is seen from Fig. 4.2(c) that the thickness of thermal boundary layer of the fluid increases with the increase of coupling number N. Fig. 4.2(d) shows that an increase in coupling number N causes to decrease of the species concentration.

Figs. 4.3(a) - 4.3(d) depict the variation of non-dimensional velocity f', microrotation g, temperature θ and species concentration h across the boundary layers with the influence of Biot number. Physically, the case of $Bi = 0$ (i,e., the plate is completely insulated) indicates that the internal thermal resistance of the plate is very high and no convective heat transfer to the cold fluid on the upper part of the plate. It is also interesting to notice that an increase in Biot number Bi leads to increase of the fluid velocity within the momentum boundary layer [Fig. 4.3(a)]. Fig. 4.3(b) brings out the behavior of microrotation that, as the value of Bi increases, the microrotation shows reverse rotation near the two boundaries. The physical behaviour of Bi, (i.e., the convective heating increases with the Biot number, and the limiting case of $Bi \to \infty$ gives the isothermal surface), is clearly seen in Fig. 4.3(c), where $\theta(0) = 1$. Hence, the fluid temperature is maximum at the plate surface and decreases exponentially to zero value far away from the plate satisfying the boundary conditions with Biot number. Finally, the outcome of varying Biot number is seen to be qualitatively same on both the temperature and species concentration.

The variations of non-dimensional velocity f', microrotation g, temperature θ and species concentration h across the boundary layers for different values of the nonlinear convection parameter or nonlinear density-temperature (NDT) parameter χ, are displayed in Figs.4.4(a) - 4.4(d). The nonlinear convection (NDT) parameter χ measures the nonlinearity in a density-temperature relationship. Physically, the case of $\chi > 0$ indicates that the fluid temperature is higher than the ambient temperature and hence, there is a supply of heat to the flow region from the wall. Further,

$\chi = 0$ is used to represent the case of linear convection. Fig. 4.4(a) explores that the velocity increases in amplitude and moves far away from the wall with the increase of NDT parameter. From Fig. 4.4(b), it can be noticed that the microrotation shows reverse rotation near the two boundaries with the increase of nonlinear convection parameter. Fig.4.4(c) and 4.4(d) display that the temperature of the fluid reduces, but the the species concentration enhances with the enhancement of NDT parameter.

Figs.4.5(a)-4.5(d) illustrate the effects of radiation on the non-dimensional velocity f', microrotation g, temperature θ and species concentration h across the boundary layers. The velocity of the fluid increase in amplitude with the increase of radiation parameter [Fig. 4.5(a)]. This is due to the fact that, when heat is absorbed, the buoyancy force accelerates the flow and hence, the fluid velocity enhances. Fig. 4.5(b) depicts that initially, the microrotation reduces up to some range and then enhances with the increase of radiation parameter. As the value of radiation parameter enhances, the temperature and species concentration enhance as displayed in Figs.4.5(c) and 4.5(d).

The variations of species concentration and mass transfer rate for different values of the homogeneous and heterogeneous reaction parameters, are presented in Figs. 4.6(a)-4.6(b). As we know that an increase in the value of K corresponds to increase in the strength of homogeneous reaction rate. It is noticed that by increasing the homogeneous reaction parameter, both the species concentration and rate of mass transfer decrease. If the heterogeneous reaction parameter K_s increases, then the strength of heterogeneous reaction rate increases. It is clear from Figs. 4.7(a) and 4.7(b) that the species concentration and rate of mass transfer decrease with the increase of heterogeneous reaction parameter K_s. Also noticed that the influence of heterogeneous reaction on species concentration is more as compared with that of the homogeneous reaction.

Table (4.1) displays the variations of $C_f Gr^{1/4}$, $M_w Gr^{1/2}$, and $\frac{Nu_{\overline{x}}}{Gr_{\overline{x}}^{1/4}}$ with different combinations of coupling number N, Biot number Bi, NDT parameter χ and radiation parameter R for fixed values of K and K_s parameters. It can be observed from Tab.(4.1) that the skin friction factor is higher for micropolar fluid than that of the viscous fluid ($N = 0$). Since micropolar fluids offer a more resistance (resulting from vortex viscosity) to the fluid movement and cause larger skin friction factor compared to viscous fluid. The results as well suggest that for larger values of the coupling number N, results in lower wall couple stresses and heat transfer coefficient but, higher skin friction coefficient. The skin-friction as well as heat transfer rate increase, but the wall couple stress decreases with an increase in the values of Bi. From Tab.(4.1), it can be noticed that the

Table 4.1: *Variations of skin friction, wall couple stress and heat transfer rate for varying values of micropolar parameter N, Biot numbers Bi, nonlinear convection parameter χ and radiation parameter R with $K = 1$ and $K_s = 0.5$.*

N	Bi	χ	R	$C_f Gr^{1/4}$	$M_w Gr^{1/2}$	$\frac{Nu_{\overline{x}}}{Gr_{\overline{x}}^{1/4}}$
0	1	0.2	1	1.756493	0	0.480086
0.3	1	0.2	1	2.015974	-0.123739	0.467144
0.5	1	0.2	1	2.267649	-0.245410	0.454613
0.8	1	0.2	1	3.026412	-0.575191	0.417755
0.5	0.1	0.2	1	1.122521	-0.142904	0.153756
0.5	1	0.2	1	2.267649	-0.245410	0.454613
0.5	5	0.2	1	2.614438	-0.272738	0.562262
0.5	20	0.2	1	2.698133	-0.279139	0.589131
0.5	1	0	1	2.074777	-0.231944	0.447202
0.5	1	1	1	2.975747	-0.292284	0.479211
0.5	1	3	1	4.475145	-0.381480	0.521647
0.5	1	5	1	5.756038	-0.449982	0.551059
0.5	1	0.2	1	2.267649	-0.245410	0.454613
0.5	1	0.2	3	2.588761	-0.291111	0.770213
0.5	1	0.2	5	2.756319	-0.315331	1.022012
0.5	1	0.2	7	2.865031	-0.331128	1.239710

skin friction and heat transfer rate increase, but the wall couple stress decreases with the increase of NDT parameter. It can be seen from the Tab.(4.1) that as the radiation parameter increases, the skin friction and heat transfer rate increase, whereas the wall couple stress decreases.

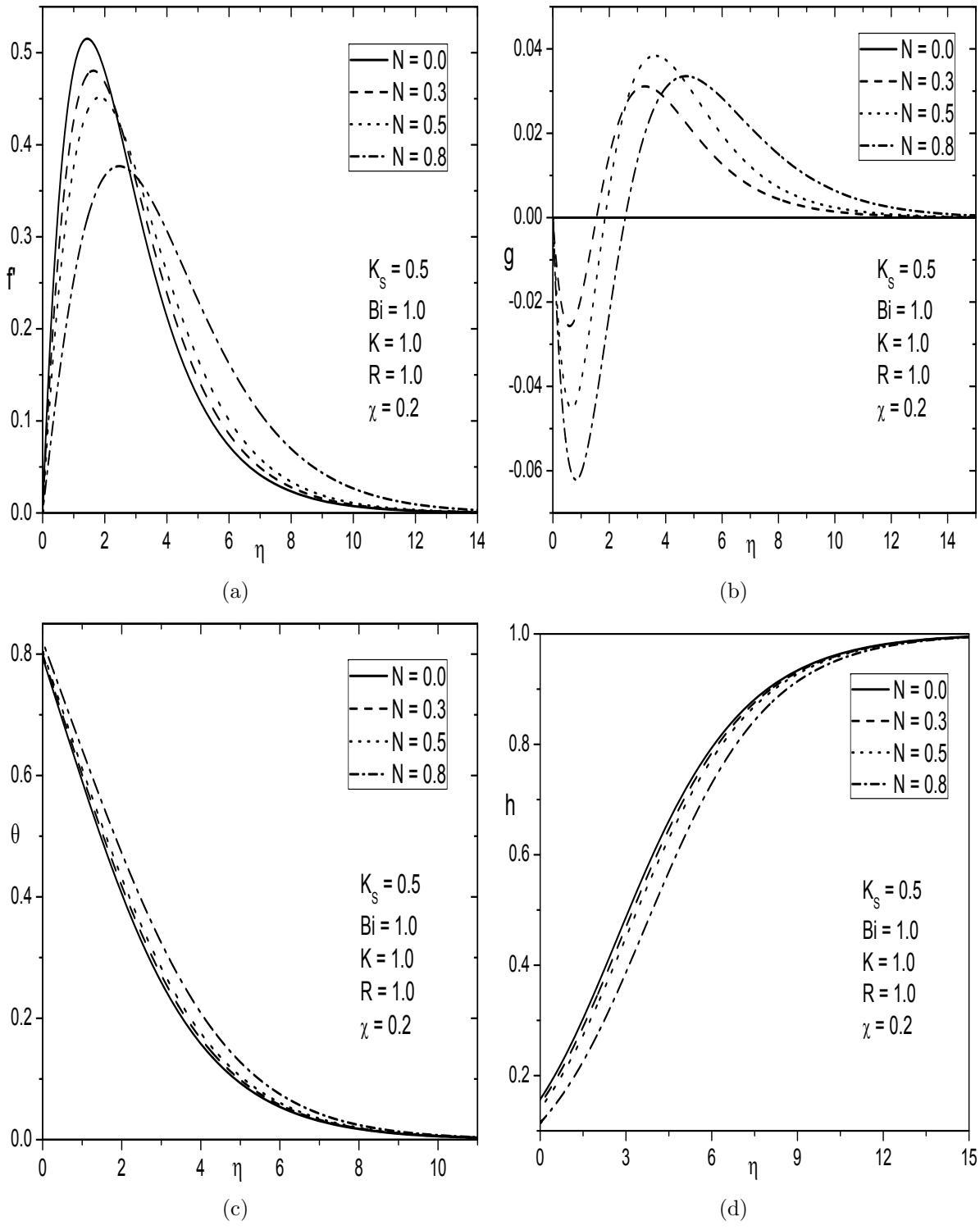

Figure 4.2: *Variation of N on (a)Velocity, (b)Microrotation, (c)Temperature and (d)Concentration profiles.*

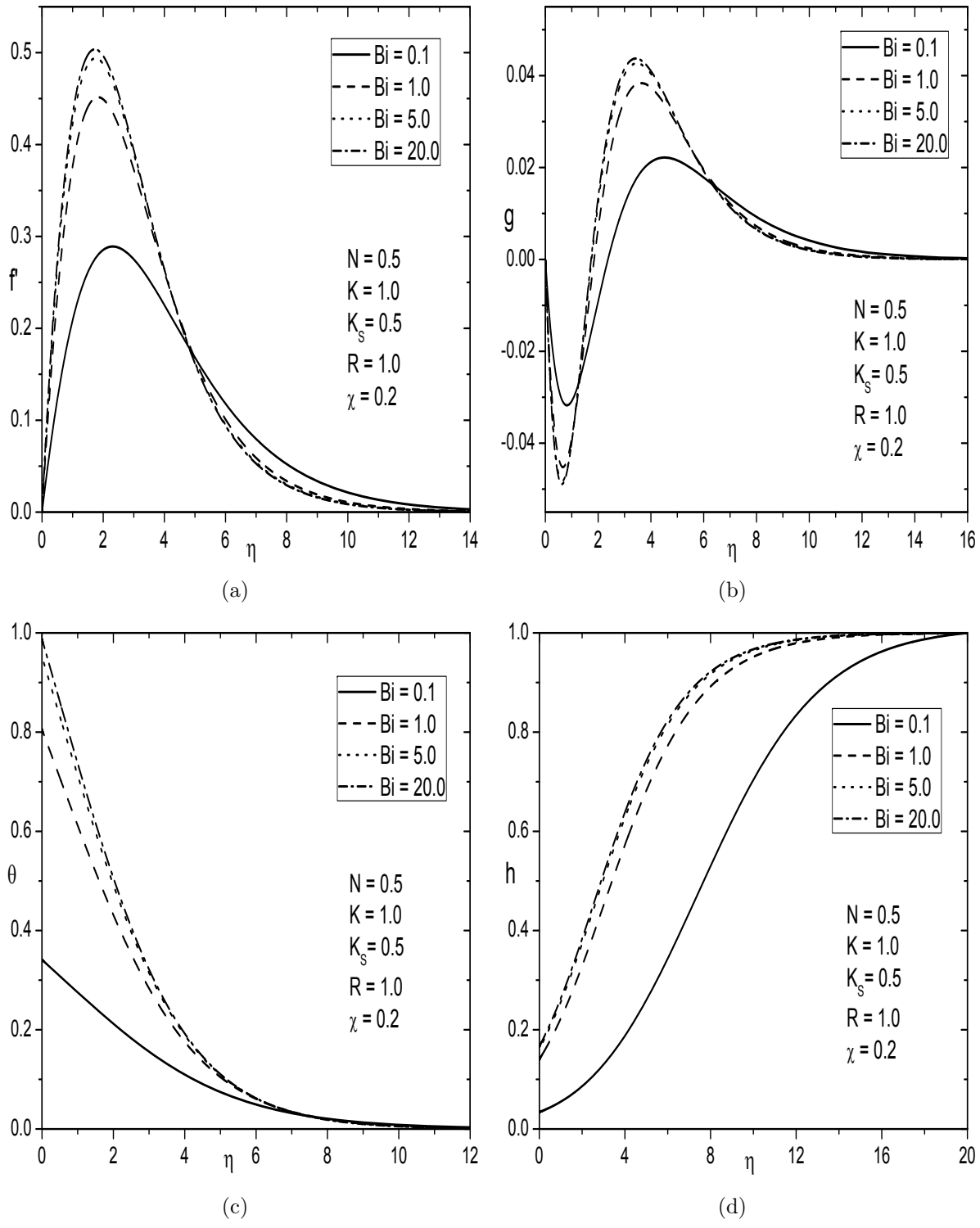

Figure 4.3: *Variation of Bi on (a)Velocity, (b)Microrotation, (c)Temperature and (d)Concentration profiles.*

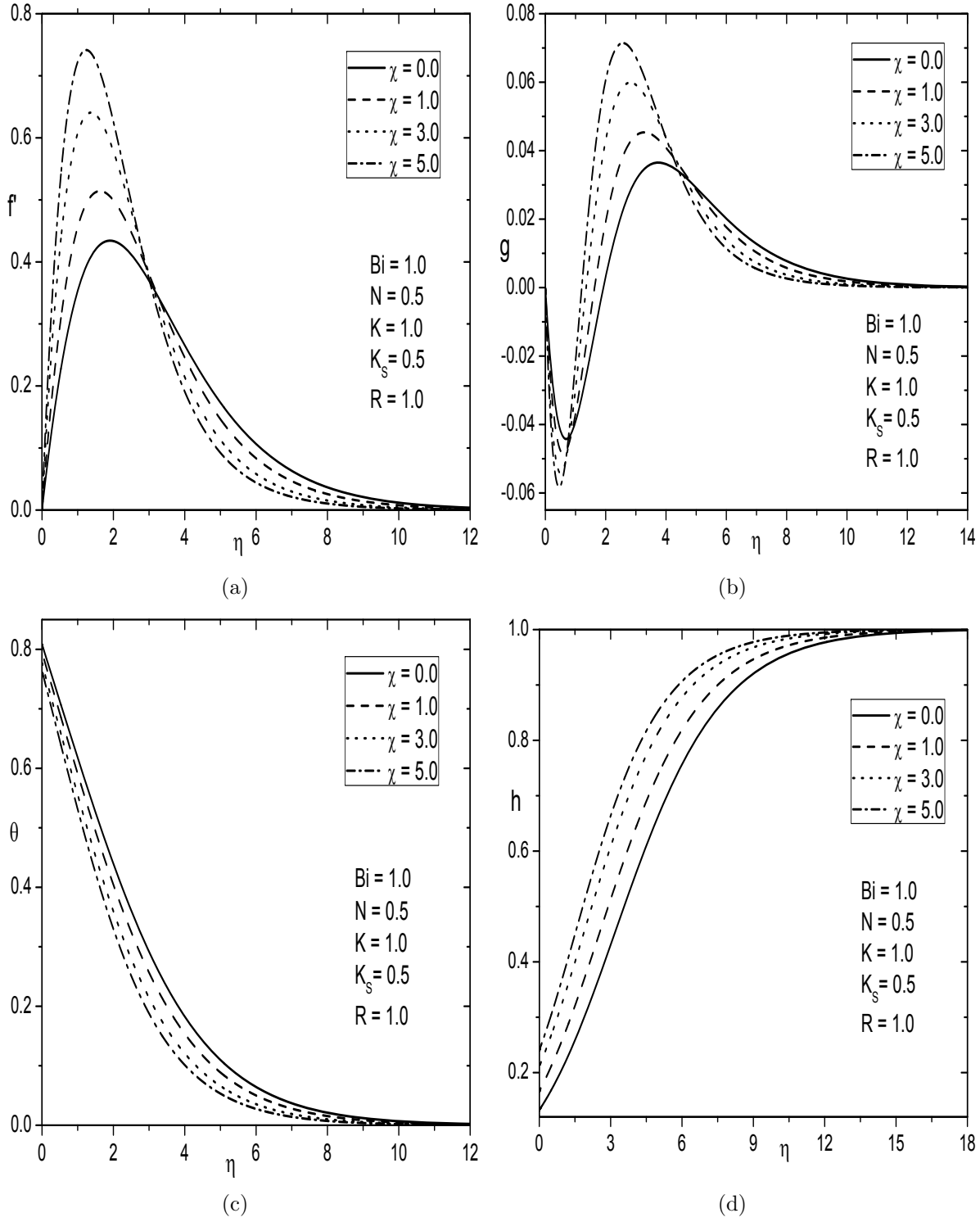

Figure 4.4: *Variation of χ on (a)Velocity, (b)Microrotation, (c)Temperature and (d)Concentration profiles.*

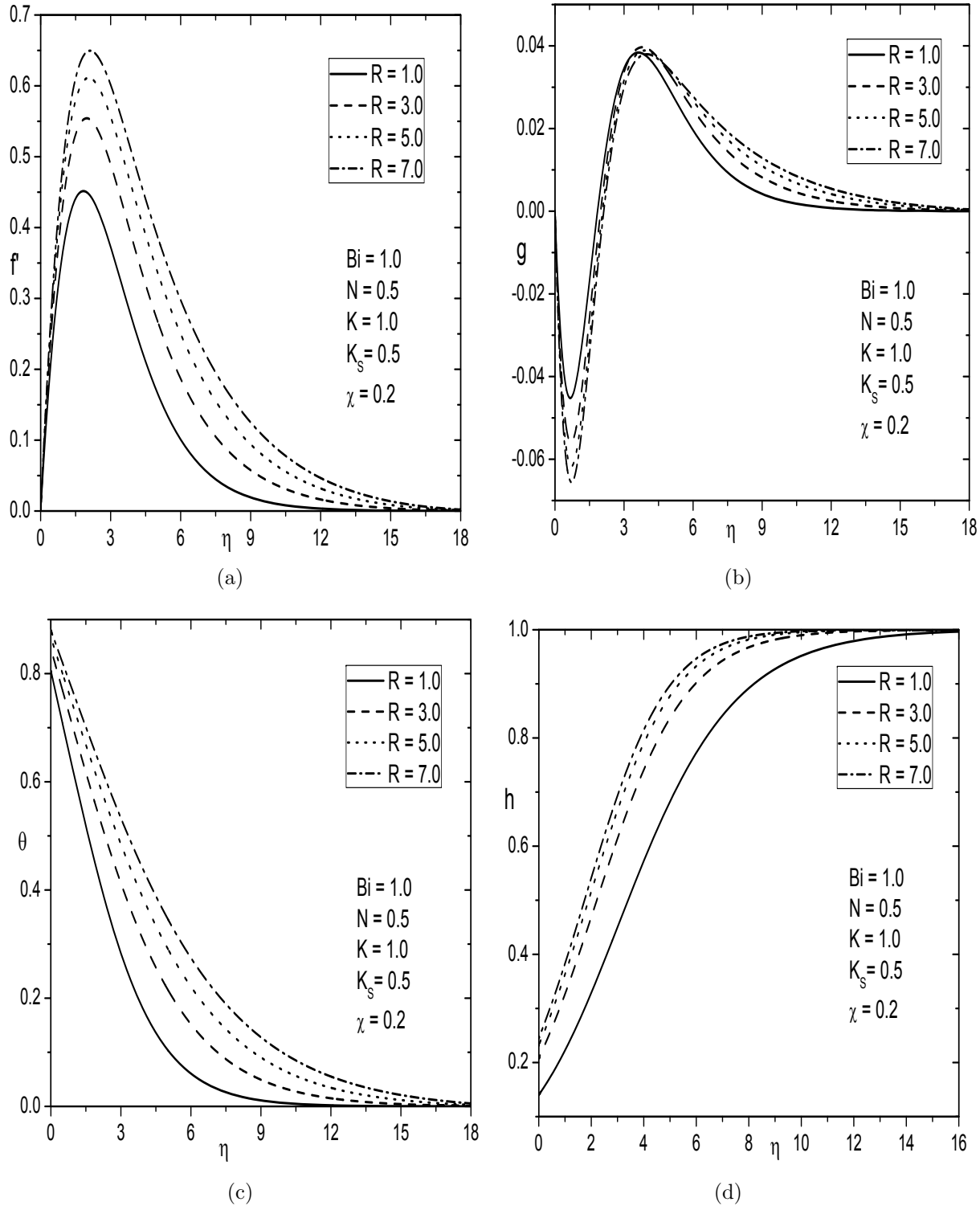

Figure 4.5: *Variation of R on (a)Velocity, (b)Microrotation, (c)Temperature and (d)Concentration profiles.*

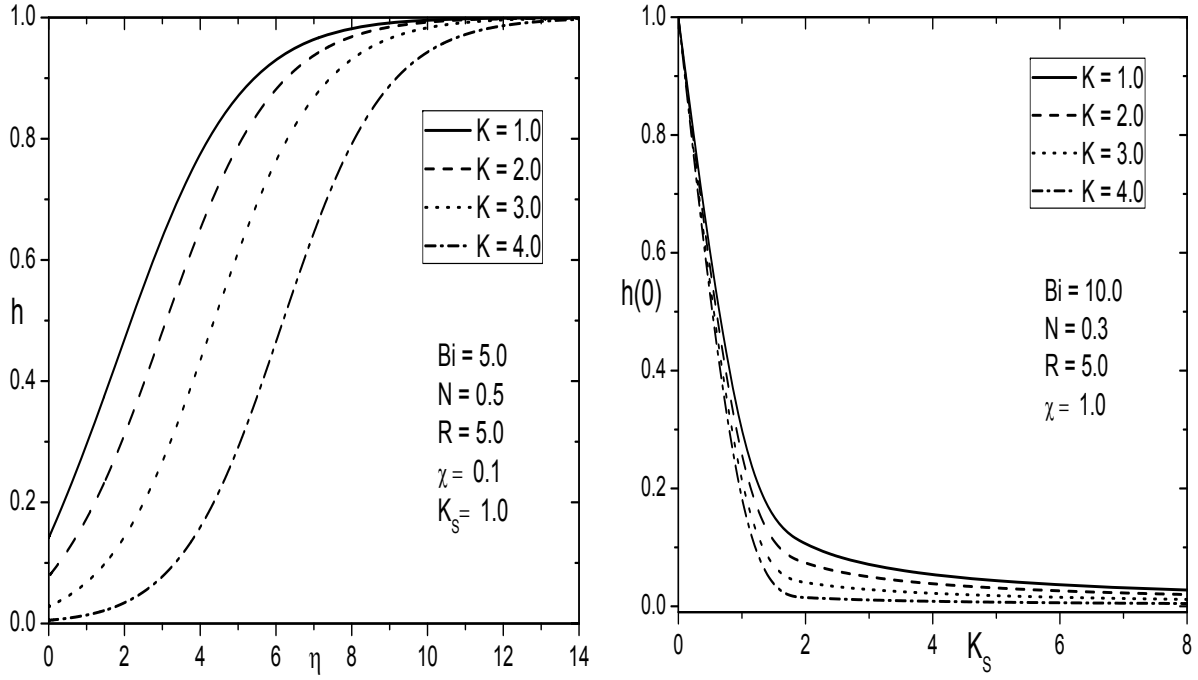

(a) (b)

Figure 4.6: *Variation of K on (a)Concentration profile h and (b) Mass transfer rate $h(0)$.*

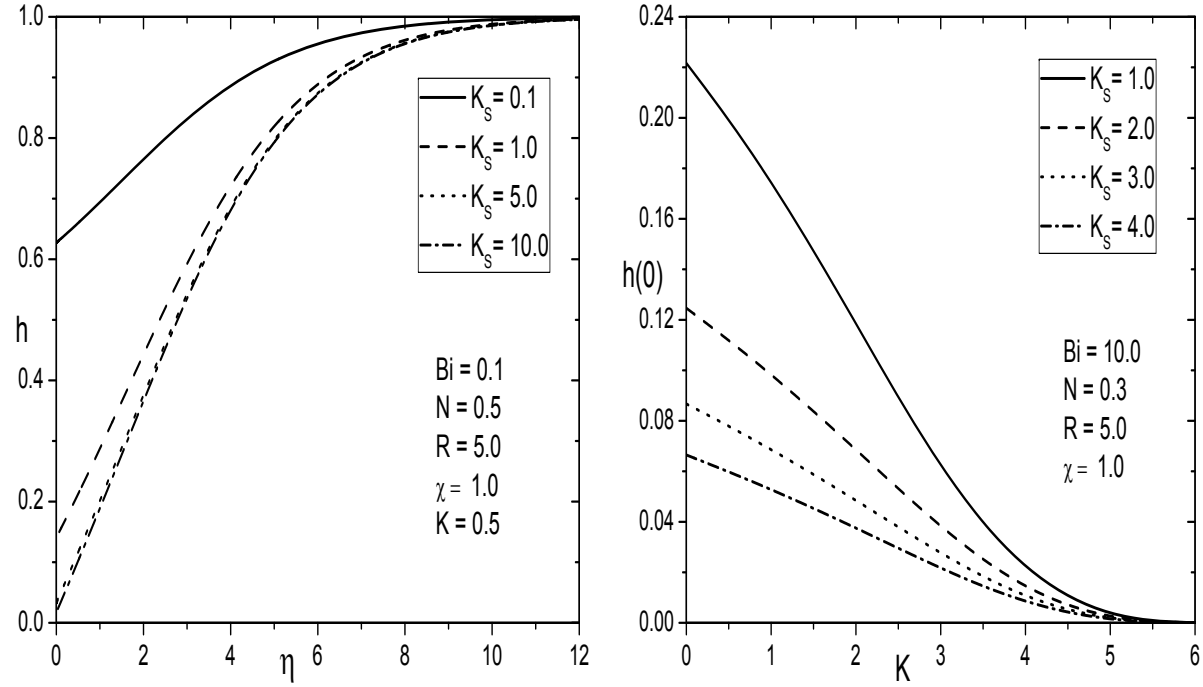

(a) (b)

Figure 4.7: *Variation of K_s on (a)Concentration profile h and (b) Mass transfer rate $h(0)$.*

4.2.2 Case(b): Mixed Convection

Consider the flow to be a mixed convection, which arises from an external flow with velocity $[\bar{u_e}(x)]$ and buoyancy forces. We introduce the following dimensionless variables

$$\left.\begin{aligned} &x = \frac{\overline{x}}{L},\ y = \frac{\overline{y}}{L}Re^{1/2},\ u = \frac{\overline{u}}{U_\infty},\ v = \frac{\overline{v}}{U_\infty}Re^{1/2}, \\ &u_e = \frac{\overline{u}_e}{U_\infty},\ \omega = \frac{L^2}{\nu Re^{3/2}}\overline{\omega},\ \theta = \frac{T - T_\infty}{T_f - T_\infty},\ h = \frac{\overline{a}}{a_0},\ h_1 = \frac{\overline{b}}{a_0}. \end{aligned}\right\} \tag{4.29}$$

Using (4.9) and (4.29) in Eqs.(4.2)-(4.6), we get the momentum, angular momentum, energy and concentration equations of species A and B as follows

$$\frac{\partial\psi}{\partial y}\frac{\partial^2\psi}{\partial x\partial y} - \frac{\partial\psi}{\partial x}\frac{\partial^2\psi}{\partial y^2} - \left(\frac{1}{1-N}\right)\frac{\partial^3\psi}{\partial y^3} - \left(\frac{N}{1-N}\right)\frac{\partial\omega}{\partial y} - u_e\frac{du_e}{dx} - \frac{g^*\beta_1(T_f - T_\infty)}{\nu^2 Re^2}\,\theta\left(1 + \frac{\beta_2}{\beta_1}\theta(T_f - T_\infty)\right) = 0 \tag{4.30}$$

$$\frac{\partial\psi}{\partial y}\frac{\partial\omega}{\partial x} - \frac{\partial\psi}{\partial x}\frac{\partial\omega}{\partial y} - \left(\frac{2-N}{2-2N}\right)\frac{\partial^2\omega}{\partial y^2} + \left(\frac{N}{1-N}\right)\left(2\omega + \frac{\partial^2\psi}{\partial y^2}\right) = 0 \tag{4.31}$$

$$\frac{\partial\psi}{\partial y}\frac{\partial\theta}{\partial x} - \frac{\partial\psi}{\partial x}\frac{\partial\theta}{\partial y} - \frac{1}{Pr}\left(1 + \frac{4}{3}R\right)\frac{\partial^2\theta}{\partial y^2} = 0 \tag{4.32}$$

$$\frac{\partial\psi}{\partial y}\frac{\partial h}{\partial x} - \frac{\partial\psi}{\partial x}\frac{\partial h}{\partial y} - \frac{1}{Sc}\frac{\partial^2 h}{\partial y^2} + K\,h\,{h_1}^2 = 0 \tag{4.33}$$

$$\frac{\partial\psi}{\partial y}\frac{\partial h_1}{\partial x} - \frac{\partial\psi}{\partial x}\frac{\partial h_1}{\partial y} - \frac{\delta}{Sc}\frac{\partial^2 h_1}{\partial y^2} - K\,h\,{h_1}^2 = 0 \tag{4.34}$$

where $K = \dfrac{k_c {a_0}^2 L}{U_\infty}$ is the strength of homogenous reaction and $\delta = \dfrac{D_B}{D_A}$ is the ratio of diffusion coefficient.

Now, the boundary conditions (4.7) become

$$\frac{\partial\psi}{\partial y} = 0,\ \frac{\partial\psi}{\partial x} = 0,\ \omega = -n\frac{\partial^2\psi}{\partial y^2},\ \frac{\partial\theta}{\partial y} = -Bi(1-\theta),\ \frac{\partial h}{\partial y} = K_s h,\ \delta\frac{\partial h_1}{\partial y} = -K_s h \text{ at } y = 0 \tag{4.35a}$$

$$\frac{\partial\psi}{\partial y} = u_e,\ \omega = 0,\ \theta = 0,\ h = 1,\ h_1 = 0 \text{ as } y \to \infty \tag{4.35b}$$

where $K_s = \dfrac{k_s L Re^{-1/2}}{D_A}$ is the strength of heterogeneous (surface) reaction.

Using the procedure of the Lie group transformations as explained in the case(a) of second

chapter, the following similarity transformations are obtained

$$\eta = y,\ \psi = xf(\eta),\ \omega = xg(\eta),\ u_e = x, \beta_1 = \beta_{T_0}x, \beta_2 = \beta_{T_1}x,\ \theta = \theta(\eta),\ h_1 = h_1(\eta),\ h_2 = h_2(\eta) \tag{4.36}$$

Substituting (4.36) into Eqs. (4.30)-(4.34), and making use of the assumption that diffusion coefficients D_A and D_B are equal as explained in the previous case, the resulting system of similarity equations takes the following form:

$$\left(\frac{1}{1-N}\right) f''' + ff'' + 1 - f'^2 + \left(\frac{N}{1-N}\right) g' + \lambda\theta(1+\chi\theta) = 0 \tag{4.37}$$

$$\left(\frac{2-N}{2-2N}\right) g'' + fg' - f'g - \left(\frac{N}{1-N}\right)(2g + f'') = 0 \tag{4.38}$$

$$\frac{1}{Pr}\left(1 + \frac{4}{3}R\right)\theta'' + f\theta' = 0 \tag{4.39}$$

$$\frac{1}{Sc}h'' + fh' - Kh(1-h)^2 = 0 \tag{4.40}$$

The associated boundary conditions (4.35) become

$$f(\eta) = 0,\ f'(\eta) = 0,\ g(\eta) = -nf''(\eta),\ \theta'(\eta) = -Bi[1-\theta(\eta)],\ h'(\eta) = K_s\, h(0) \,\text{at}\, \eta = 0 \tag{4.41a}$$

$$f'(\eta) = 1,\ g(\eta) = 0,\ \theta(\eta) = 0,\ h(\eta) = 1 \ \ as\ \eta \to \infty \tag{4.41b}$$

The quantities of physical interest are the non-dimensional skin friction $C_f = \dfrac{2\tau_w}{\rho\overline{u}_e^2}$, wall couple stress $M_w = \dfrac{m_w}{\rho\overline{u}_e^2\overline{x}}$ and the local Nusselt number $Nu_{\overline{x}} = \dfrac{q_w\overline{x}}{k(T_f - T_\infty)}$, are given by

$$C_f Re_{\overline{x}^{1/2}} = 2\left(\frac{1-nN}{1-N}\right) f''(0),\ M_w Re_{\overline{x}} = \left(\frac{2-N}{2-2N}\right) g'(0),\ \frac{Nu_{\overline{x}}}{Re_{\overline{x}^{1/2}}} = -\left(1 + \frac{4}{3}R\right)\theta'(0) \tag{4.42}$$

Results and Discussion

The governing non-linear ordinary differential equations (4.37) - (4.40) along with the boundary conditions (4.41) are solved numerically using the spectral quasi-linearization method. In order to validate the code generated, for the special case of $N = 0$, $n = 0$, $Pr = 1$, $R = 0$, $\chi = 0$

and $Bi \to \infty$, the results of the present problem have been compared with those of Merkin [58] and Nazar *et al.* [73] in the absence of homogeneous and heterogeneous reactions and found that they are in good agreement, as shown in Tab. (2.4). To study the effects of nonlinear convection parameter χ, Biot number Bi, strength of homogeneous and heterogeneous reaction parameters K and K_s, computations have been carried out for $n = 0$, $Pr = 0.71$ and $Sc = 0.22$.

Figs. 4.8(a)-4.8(d) illustrate the effect of coupling number N on the dimensionless velocity, microrotation, temperature and species concentration for fixed values of other parameters. As the coupling number N increases, it is found from Fig. 4.8(a) that the velocity decreases within the momentum boundary layer. From Fig. 4.8(b), it can be observed that the microrotation is flat for $N = 0$, and it shows reverse rotation near two boundaries with the increase of coupling number. This is due to the fact that an increment in N indicates a higher vortex viscosity of fluid and hence it promotes the microrotation of micropolar fluids. It is seen from Fig. 4.8(c) that the thermal boundary layer of the fluid increases with the increase of coupling number N. Fig. 4.8(d) shows that an enhancement in coupling number N causes to reduction of the species concentration. The above results are true in both the cases of aiding and opposing flow situations.

Figs. 4.9(a) - 4.9(d) displayed the influence of Biot number on the non-dimensional velocity f', microrotation g, temperature θ and species concentration h across the boundary layers for both opposing and aiding flows. It is interesting to note that an increase in the intensity of convective surface heat transfer Bi produces a significant enhancement in the fluid velocity within the momentum boundary layer for aiding flow situation, but the reverse is true for opposing flow situation [Fig. 4.9(a)]. Fig. 4.9(b) illustrates that as the Biot number Bi increases, the microrotation shows reverse rotation near the two boundaries and moreover, it is observed that the microrotation in aiding and opposing flows shows opposite trend. The outcome of temperature with the increase of Biot number is seen to be qualitatively same for both aiding and opposing flow situations as displayed in Fig. 4.9(c). From Fig. 4.9(d), it can be noticed that the species concentration reduces in opposing flow situation, but it enhances in aiding flow situation. Physically, the aiding flow ($\lambda > 0$) implies favourable pressure gradient and thus fluid gets accelerated, but in the case of opposing flow ($\lambda < 0$), the fluid gets decelerated. Hence, the concentration enhances in aiding flow, but reduces in opposing flow with the increase of Biot number.

In Figs. 4.10(a) - 4.10(d), the variation of nonlinear convection parameter(NDT) on the non-dimensional velocity f', microrotation g, temperature θ and species concentration h across the

boundary layers, are depicted. The nonlinear convection (NDT) parameter χ measures the nonlinearity in a density-temperature relationship. With an increase in NDT parameter, the velocity of the fluid increases in aiding flow, but decreases in opposing flow [Fig. 4.10(a)]. From Fig. 4.10(b), it can be perceived that the microrotation shows reverse rotation near two boundaries with the increase of NDT parameter and it is found that the microrotation in opposing and aiding flows depicts the reverse nature. From Fig. 4.10(c), it is seen that the fluid temperature reduces in aiding flow, but it enhances in opposing flow. It is observed from Fig. 4.10(d) that the concentration profile shows a reverse behaviour to the temperature profile for both opposing and aiding flow situations.

The effects of radiation on the non-dimensional velocity f', microrotation g, temperature θ and species concentration h across the boundary layers, are explored in Figs. 4.11(a)-4.11(d). Fig. 4.11(a) shows that the velocity of the fluid increases in aiding flow, but it reduces in opposing flow with the increase of radiation parameter. Fig.4.11(b) reveals that the microrotation first decreases up to certain range and then increases in the case of aiding flow, but coming to the opposing flow situation, it shows reverse behaviour with the increase of radiation parameter. As the radiation parameter enhances, the temperature enhances for both opposing and aiding flow cases as displayed in Fig.4.11(c). Fig.4.5(d) exhibits that the species concentration diminishes in opposing flow, but it raises in aiding flow.

Figs. 4.12(a) - 4.13(b) display effects of homogeneous and heterogeneous reaction parameters on the species concentration h and mass transfer rate $h(0)$ for fixed values of other parameters. Generally, an increase in the values of K and K_s correspond to an increase in the strength of homogeneous and heterogeneous reaction rates. For both aiding and opposing flow situations, Figs. 4.12(a) - 4.13(b) shows that the species concentration and rate of mass transfer decrease with the increase of homogeneous and heterogeneous reaction parameters. Also, it can be noticed that the influence of heterogeneous reaction is more about the species concentration as compared with that of homogeneous reaction.

For both opposing and aiding flow situations, Tab. (4.2) displays the variations of $C_f Re_{\overline{x}^{1/2}}$, $M_w Re_{\overline{x}}$, and $\frac{Nu_{\overline{x}}}{Re_{\overline{x}^{1/2}}}$ with different combinations of the coupling number N, Biot number Bi, NDT parameter χ and radiation parameter R for fixed values of K and K_s parameters. For $Bi = 1$, $\chi = 0.2$ and $R = 1$, it can be seen from Tab.(4.2) that the skin friction is more for the micropolar fluid than that of the viscous fluid ($N = 0$). Because micropolar fluids offer more resistance to

the fluid movement and causes higher skin friction factor compared to that of the viscous fluid. The results reveal that for larger values of coupling number N, lower the wall couple stresses and heat transfer coefficient, but higher the skin friction coefficient for both opposing and aiding flows. In the presence of opposing and aiding flow situations, the skin-friction and wall couple stress coefficients show opposite trend, but the heat transfer rate increases with the increase of Bi. It can be noticed that with the increase of NDT parameter for fixed $N = 0.5$, $Bi = 1$ and $R = 1$, the skin friction and heat transfer rate increase, but the wall couple stress decreases in aiding flow situation and these show opposite behaviour in opposing flow. It can be noticed that by increasing the values of radiation parameter, the skin friction and wall couple stress show reverse trend, but the heat transfer rate increases for both opposing and aiding flow situations for $N = 0.5$, $Bi = 1$ and $\chi = 0.2$.

Table 4.2: *Variations of skin friction, wall couple stress and heat transfer rate for varying values of mixed convection parameter λ, micropolar parameter N, Biot numbers Bi, nonlinear convection parameter χ and radiation parameter R with $K = 1$ and $K_s = 0.5$.*

λ	N	Bi	χ	R	$C_f Re_{\overline{x}^{1/2}}$	$M_w Re_{\overline{x}}$	$\frac{Nu_{\overline{x}}}{Re_{\overline{x}^{1/2}}}$
-0.5	0	1	0.2	1	1.90338	0	0.58773
-0.5	0.5	1	0.2	1	2.64177	-0.377	0.56254
-0.5	0.8	1	0.2	1	3.89651	-0.92115	0.52662
1	0	1	0.2	1	3.45320	0	0.64195
1	0.5	1	0.2	1	4.64805	-0.51521	0.61203
1	0.8	1	0.2	1	6.59057	-1.30285	0.56908
-0.5	0.5	0.1	0.2	2	3.115025	-0.41039	0.26830
-0.5	0.5	1	0.2	2	2.548011	-0.36657	0.76384
-0.5	0.5	10	0.2	2	2.321203	-0.34859	0.92608
1	0.5	0.1	0.2	2	3.832294	-0.46378	0.27124
1	0.5	1	0.2	2	4.802345	-0.53067	0.84178
1	0.5	10	0.2	2	5.201253	-0.55668	1.07891
-0.5	0.5	1	0	1	2.720552	-0.38201	0.56437
-0.5	0.5	1	1	1	2.316535	-0.35591	0.55473
-0.5	0.5	1	3	1	1.408176	-0.29323	0.53042
1	0.5	1	0	1	4.52312	-0.50851	0.60991
1	0.5	1	1	1	5.133435	-0.5408	0.62003
1	0.5	1	3	1	6.264075	-0.59791	0.63730
-0.5	0.5	1	0.2	1	2.641779	-0.377	0.56254
-0.5	0.5	1	0.2	3	2.483645	-0.35907	0.93739
-0.5	0.5	1	0.2	5	2.398495	-0.34875	1.23928
1	0.5	1	0.2	1	4.648059	-0.51521	0.61203
1	0.5	1	0.2	3	4.907605	-0.54162	1.04180
1	0.5	1	0.2	5	5.047856	-0.55666	1.38941

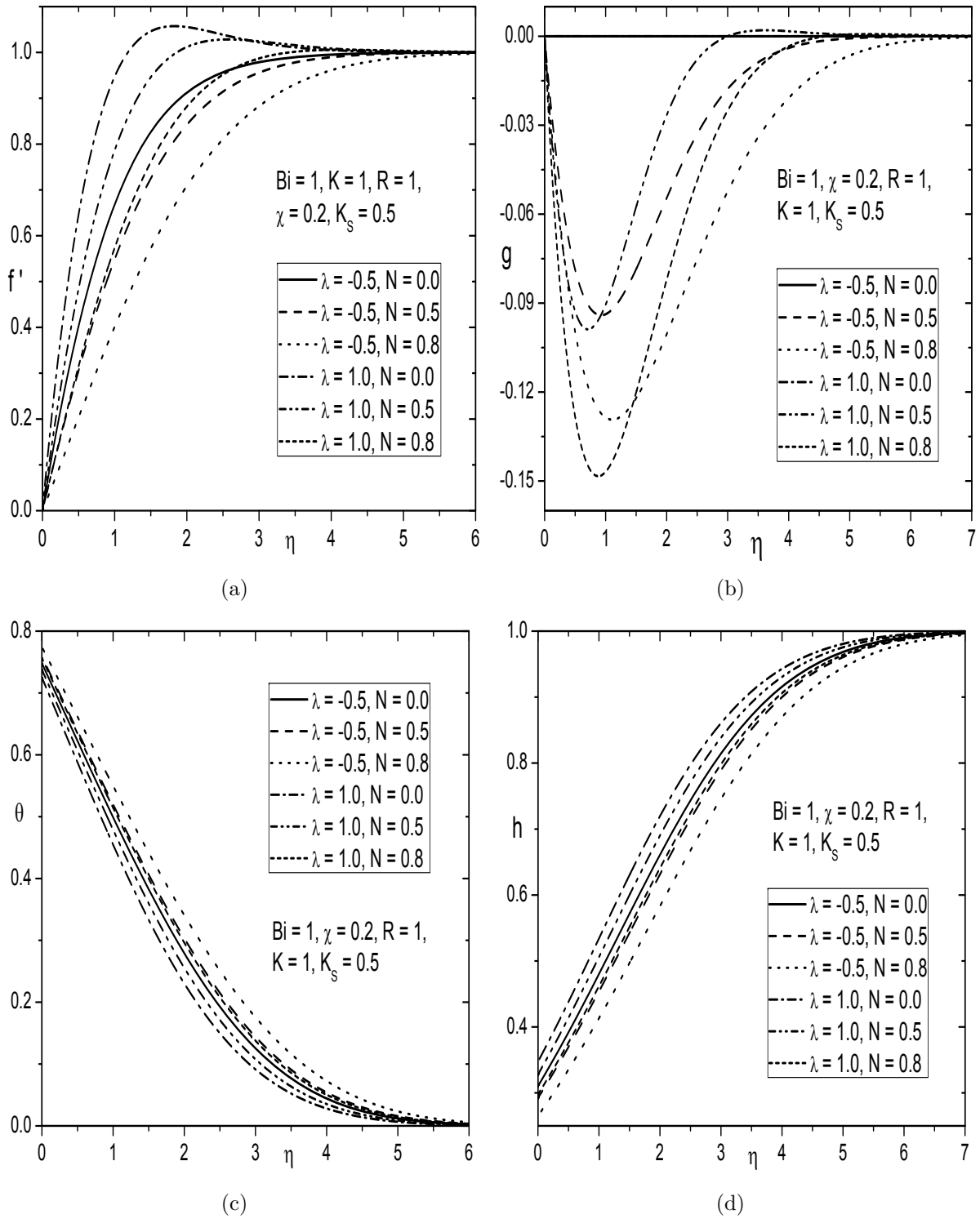

Figure 4.8: *Variation of N on (a)Velocity, (b)Microrotation, (c)Temperature and (d)Concentration profiles.*

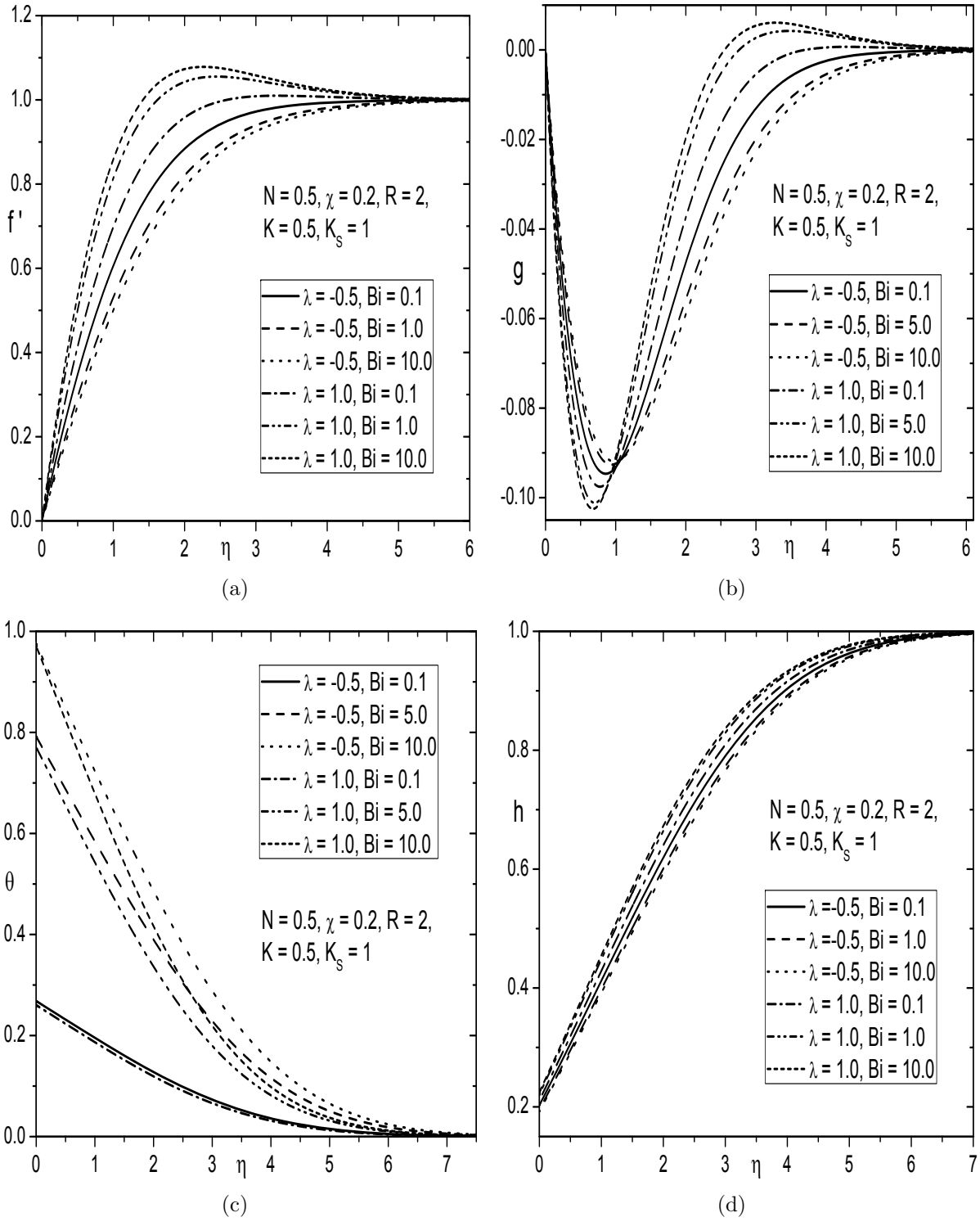

Figure 4.9: *Variation of Bi on (a)Velocity, (b)Microrotation, (c)Temperature and (d)Concentration profiles*

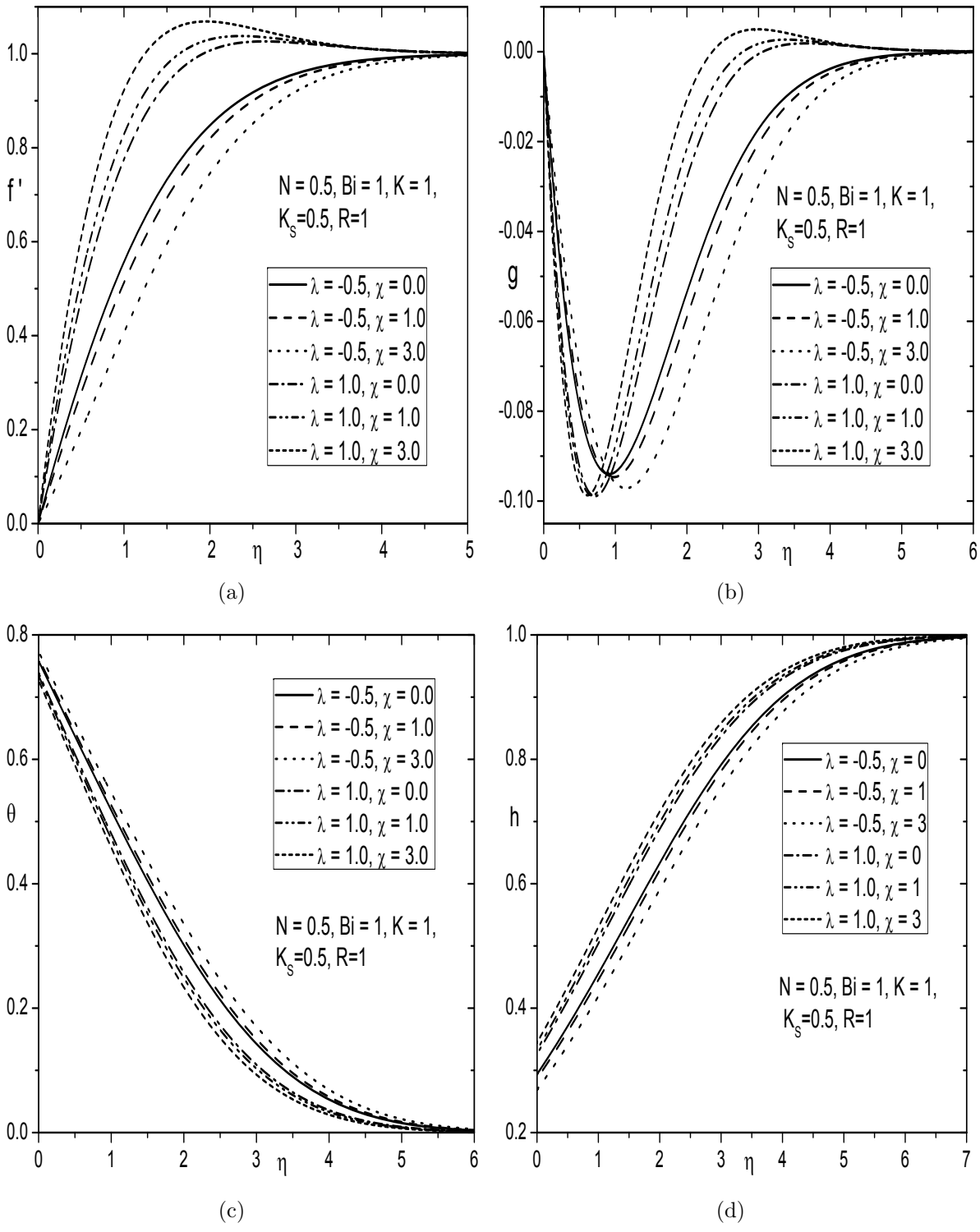

Figure 4.10: *Variation of χ on (a)Velocity, (b)Microrotation, (c)Temperature and (d)Concentration profiles*

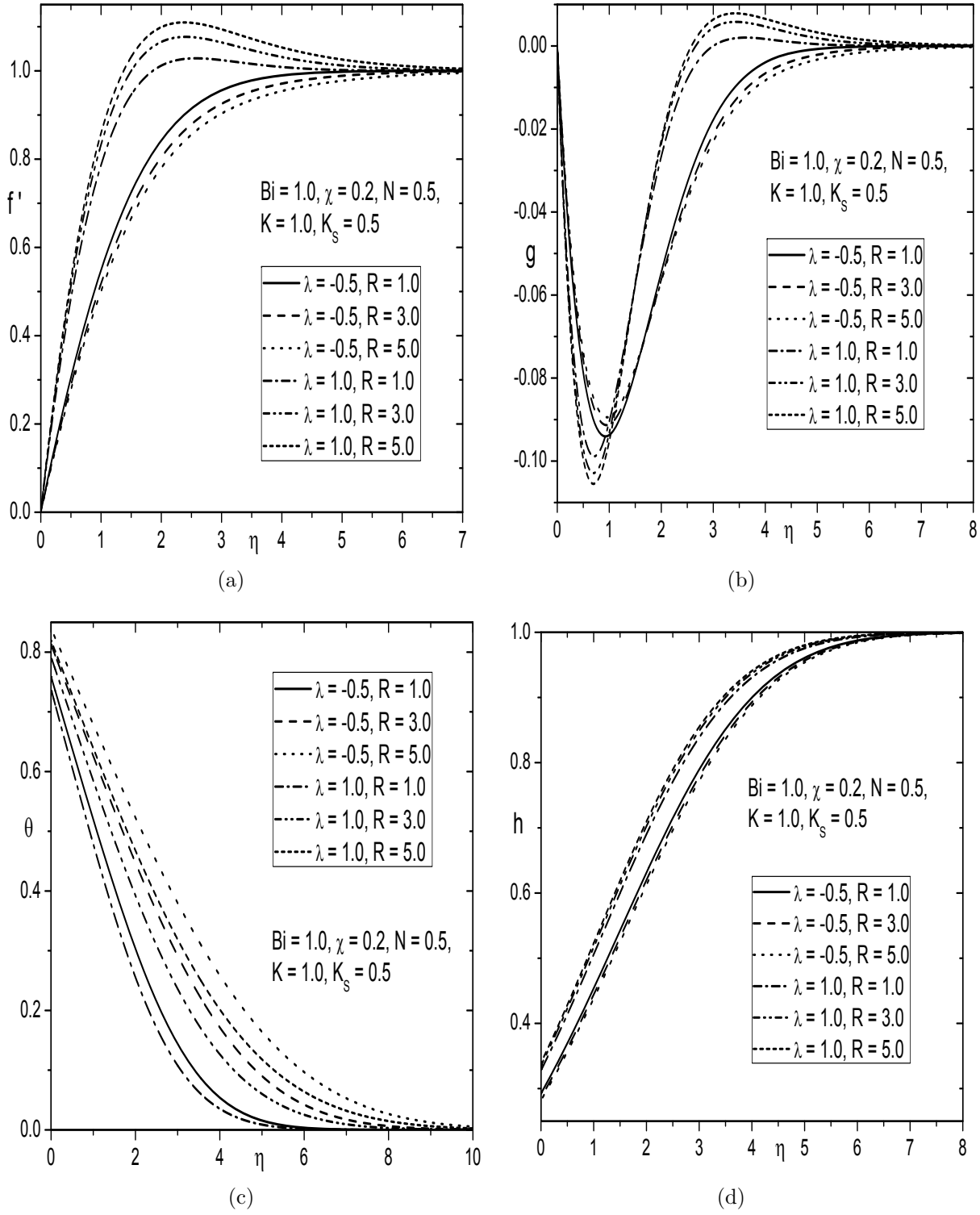

Figure 4.11: *Variation of R on (a)Velocity, (b)Microrotation, (c)Temperature and (d)Concentration profiles*

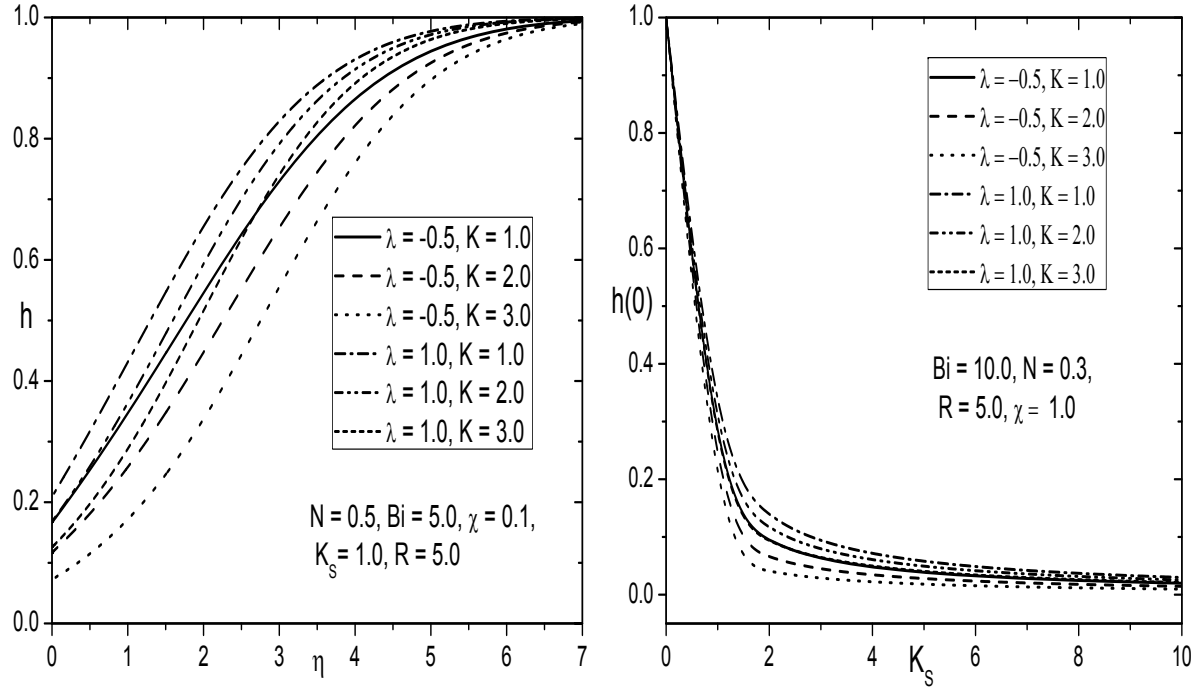

(a) (b)

Figure 4.12: *Variation of K on (a)Concentration profile h and (b) Mass transfer rate $h(0)$*

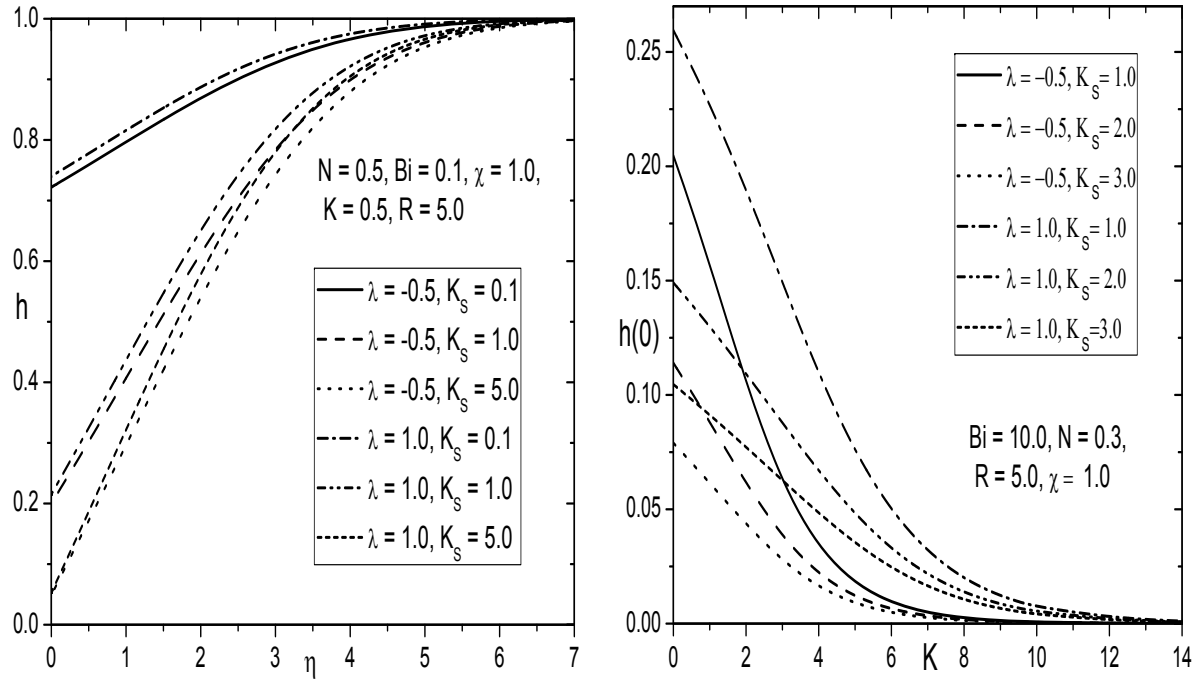

(a) (b)

Figure 4.13: *Variation of K_s on (a)Concentration profile h and (b) Mass transfer rate $h(0)$*

4.3 Conclusions

In this chapter, the influence of radiation and homogeneous and heterogeneous reactions on non-linear convective flow of a micropolar fluid in the preence of the convective boundary condition, is studied. The resulting equations are solved numerically by the spectral quasi-linearization method. The main findings are summarized as follows:

As in the previous chapters, the behavior of coupling number N is found to be similar on various profiles, except for the species concentration. As Biot number Bi increases, the wall couple stress coefficient decreases, but the skin friction, velocity distribution and species concentration increase for both case (a) and aiding flow (i,e. in case (b)). However, these show reverse trend in opposing flow (i,e., case(b)). For both cases (a) and (b), the temperature and heat transfer rate increases with the increase of Biot number. The higher values of nonlinear convection parameter χ results in lower temperature and wall couple stress coefficient, but higher velocity, species concentration, skin friction and heat transfer rate for both case(a) and aiding flow (i,e. in case (b)). Further, the velocity, skin friction and heat transfer rate decrease, but the temperature and wall couple stress enhances in opposing flow (i,e. in case(b)) with the enhancement of nonlinear convection parameter. It is observed that with an increase in strength of homogeneous and heterogeneous reaction parameters K and K_s, the species concentration and mass transfer rate decrease for both case(a) and case(b). Finally, we conclude that the effect of heterogeneous reaction is more on species concentration as compared with that of homogeneous reaction.

Chapter 5

Nonlinear Convective Flow of a Micropolar Fluid in a Darcy Porous Medium with Homogeneous - Heterogeneous Reactions [1]

5.1 Introduction

The convection in a fluid saturated porous media received much attention in recent times due to its significant role in various engineering, scientific and industrial applications. Since, Darcy′s law gives a linear empirical relationship between the Darcian velocity and the pressure drop across the porous medium, and it is valid for slow flows with the low permeability. The study of convective flows embedded in a Darcy′s porous medium saturated with a micropolar fluid has been attracted by several researchers (to mention few, see Refs. [14]; [29]; [96]). Most of the chemical reactions comprise of both homogeneous and heterogeneous reactions. The homogeneous reaction takes place in the bulk of the fluid, while heterogeneous reaction occurs on some catalytic surfaces. Several investigators discussed the significance of homogeneous-heterogeneous reactions in Newtonian fluid,

[1]Case(a): Published in "**Frontiers in Heat and Mass Transfer**" (2017) DOI: 10.5098/hmt.8.6, Case(b) Published in "**Open Engineering**", 6 (2016) 106–119

but very few authors noticed these effects in non-Newtonian fluids. For instance, Shaw *et al.* [91] analyzed the effects of homogeneous-heterogeneous reactions on the micropolar fluid flow from a permeable stretching or shrinking sheet, including the influence of permeability. Kameswaran *et al.* [46] discussed the stagnation point flow over a shrinking or stretching sheet placed in a saturated porous medium, considering the effects of homogeneous-heterogeneous reactions.

As mentioned in introduction part (i.e., in Chapter-1), most of the works dealing with the linear convective flows in Newtonian and non-Newtonian fluids have been reported in the literature. But, the nonlinear variation in buoyancy due to the nonlinear thermal convection may affect on the flow and heat transfer characteristics (for more details, see Vajravelu *et al.* [103] and refer the citations therein). In order to explore this physical situation, Kameswaran *et al.* [47] studied the effect of thermophoretic on nonlinear convective flow in a non-Darcy porous medium. Later, Nandkeolyar *et al.* [71] analyzed the nonlinear convection in a nanofluid saturated porous medium in the presence of viscous dissipation and Newtonian heating effects.

The objective of this chapter is to analyze the effects of homogeneous and heterogeneous reactions on nonlinear free and mixed convective flows of a micropolar fluid embedded in a porous medium under the convective boundary condition. To our best knowledge and from the literature, to date, there is no study which considers this problem in a micropolar fluid with homogeneous-heterogeneous reactions and nonlinear convection effects. As in the previous Chapter, here also the governing equations and their associated boundary conditions are solved numerically using the spectral quasi-linearization method. The results are compared with the relevant results in the existing literature and are found to be in good agreement. Also, the physical quantities of the flow, and heat and mass transfer rates are analyzed for various parameters namely, the micropolar parameter, nonlinear convection parameter, Darcy parameter and Biot number.

5.2 Mathematical Formulation

Consider the steady, laminar, two dimensional convective flow of a micropolar fluid along a vertical plate embedded in Darcy porous medium. Choose the coordinate system such that $\overline{x}$-axis is along the vertical plate and $\overline{y}$-axis is normal to the plate as shown in Fig. (5.1). This chapter is an extension of the chapter - 4 by considering the fluid saturated porous medium in the absence of

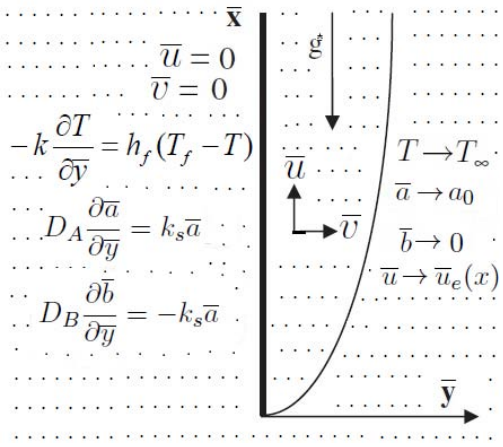

Figure 5.1: *Physical model and coordinate system*

radiation effect. In addition to assumptions made in chapter - 4, the following assumptions are taken into account in the analysis: (i) the porous medium is isotropic and homogeneous, (ii) the properties of the fluid and porous medium are constant except for the nonlinear density-temperature variation required by the nonlinear Boussinesq approximation (i.e., this will be achieved by assuming that the sufficiently large temperature differences between the plate and the medium), and (iii) the fluid and porous medium are in local thermodynamic equilibrium.

Under the above assumptions, and using the Darcy model and Dupuit-Forchheimer relationship [74], the governing equations describing the micropolar fluid are given by

$$\frac{\partial \overline{u}}{\partial \overline{x}} + \frac{\partial \overline{v}}{\partial \overline{y}} = 0 \tag{5.1}$$

$$\frac{\rho}{\epsilon^2}\left(\overline{u}\frac{\partial \overline{u}}{\partial \overline{x}} + \overline{v}\frac{\partial \overline{u}}{\partial \overline{y}}\right) = \frac{1}{\epsilon}(\mu+\kappa)\frac{\partial^2 \overline{u}}{\partial \overline{y}^2} + \rho\overline{u}_e\frac{d\overline{u}_e}{d\overline{x}} + \kappa\frac{\partial \overline{\omega}}{\partial \overline{y}} + \rho g^*\left[\beta_1(T-T_\infty) + \beta_2(T-T_\infty)^2\right] - \frac{\mu}{K_p}(\overline{u}-\overline{u}_e) \tag{5.2}$$

$$\frac{\rho j}{\epsilon}\left(\overline{u}\frac{\partial \overline{\omega}}{\partial \overline{x}} + \overline{v}\frac{\partial \overline{\omega}}{\partial \overline{y}}\right) = \gamma\frac{\partial^2 \overline{\omega}}{\partial \overline{y}^2} - \kappa\left(2\overline{\omega} + \frac{1}{\epsilon}\frac{\partial \overline{u}}{\partial \overline{y}}\right) \tag{5.3}$$

$$\overline{u}\frac{\partial T}{\partial \overline{x}} + \overline{v}\frac{\partial T}{\partial \overline{y}} = \alpha\frac{\partial^2 T}{\partial \overline{y}^2} \tag{5.4}$$

$$\overline{u}\frac{\partial \overline{a}}{\partial \overline{x}} + \overline{v}\frac{\partial \overline{a}}{\partial \overline{y}} = D_A\frac{\partial^2 \overline{a}}{\partial \overline{y}^2} - k_c\overline{a}\,\overline{b}^2 \tag{5.5}$$

$$\overline{u}\frac{\partial \overline{b}}{\partial \overline{x}} + \overline{v}\frac{\partial \overline{b}}{\partial \overline{y}} = D_B\frac{\partial^2 \overline{b}}{\partial \overline{y}^2} + k_c\overline{a}\,\overline{b}^2 \tag{5.6}$$

where $\overline{u}$ and $\overline{v}$ are the Darcy velocity components in $\overline{x}$ and $\overline{y}$ directions respectively.

The boundary conditions are

$$\overline{u}=0,\ \overline{v}=0,\ \overline{\omega}=-n\frac{\partial\overline{u}}{\partial\overline{y}},\ -k\frac{\partial T}{\partial\overline{y}}=h_f(T_f-T),\ D_A\frac{\partial\overline{a}}{\partial\overline{y}}=k_s\overline{a},\ D_B\frac{\partial\overline{b}}{\partial\overline{y}}=-k_s\overline{a}\ \text{at}\ \overline{y}=0 \tag{5.7a}$$

$$\overline{u}=\overline{u}_e(x),\ \overline{\omega}=0,\ T=T_\infty,\ \overline{a}=a_0,\ \overline{b}=0\ \text{as}\ \overline{y}\to\infty \tag{5.7b}$$

In this chapter also, two types (cases) of problems are considered: (a) free/natural convection and (b) mixed convection.

5.2.1 Case(a): Natural Convection

The flow is assumed to be a natural convection which is caused by buoyancy forces only without any external agent, and hence the velocity of the external flow becomes zero. We introduce the following dimensionless variables

$$x=\frac{\overline{x}}{L},\ y=\frac{\overline{y}}{L}Gr^{1/4},\ u=\frac{L}{\nu Gr^{1/2}}\overline{u},\ v=\frac{L}{\nu Gr^{1/4}}\overline{v},\ \omega=\frac{L^2}{\nu Gr^{3/4}}\overline{\omega},\ \theta=\frac{T-T_\infty}{T_f-T_\infty},\ h=\frac{\overline{a}}{a_0},\ h_1=\frac{\overline{b}}{a_0} \tag{5.8}$$

The following stream function ψ has been introduced to satisfy the continuity equation (5.1) identically

$$u=\frac{\partial\psi}{\partial y},\quad v=-\frac{\partial\psi}{\partial x}. \tag{5.9}$$

Substituting (5.8) and (5.9) into Eqs. (5.2)-(5.6), the momentum, angular momentum, energy, and concentration equations of species A and B can be written as

$$\frac{1}{\epsilon^2}\left(\frac{\partial\psi}{\partial y}\frac{\partial^2\psi}{\partial x\partial y}-\frac{\partial\psi}{\partial x}\frac{\partial^2\psi}{\partial y^2}\right)-\frac{1}{\epsilon}\left(\frac{1}{1-N}\right)\frac{\partial^3\psi}{\partial y^3}-\frac{\beta_1(T_f-T_\infty)}{\beta_{T_0}}\,\theta\left(1+\frac{\beta_2}{\beta_1}\theta(T_f-T_\infty)\right) \tag{5.10}$$

$$-\left(\frac{N}{1-N}\right)\frac{\partial\omega}{\partial y}+\frac{1}{Da\,Gr^{1/2}}\frac{\partial\psi}{\partial y}=0$$

$$\frac{1}{\epsilon}\left(\frac{\partial\psi}{\partial y}\frac{\partial\omega}{\partial x}-\frac{\partial\psi}{\partial x}\frac{\partial\omega}{\partial y}\right)-\left(\frac{2-N}{2-2N}\right)\frac{\partial^2\omega}{\partial y^2}+\left(\frac{N}{1-N}\right)\left(2\omega+\frac{1}{\epsilon}\frac{\partial^2\psi}{\partial y^2}\right)=0 \tag{5.11}$$

$$\frac{\partial\psi}{\partial y}\frac{\partial\theta}{\partial x}-\frac{\partial\psi}{\partial x}\frac{\partial\theta}{\partial y}-\frac{1}{Pr}\frac{\partial^2\theta}{\partial y^2}=0 \tag{5.12}$$

$$\frac{\partial\psi}{\partial y}\frac{\partial h}{\partial x}-\frac{\partial\psi}{\partial x}\frac{\partial h}{\partial y}-\frac{1}{Sc}\frac{\partial^2 h}{\partial y^2}+K\,h\,{h_1}^2=0 \tag{5.13}$$

$$\frac{\partial\psi}{\partial y}\frac{\partial h_1}{\partial x}-\frac{\partial\psi}{\partial x}\frac{\partial h_1}{\partial y}-\frac{\delta}{Sc}\frac{\partial^2 h_1}{\partial y^2}-K\,h\,{h_1}^2=0 \tag{5.14}$$

Now, the boundary conditions (5.7) become

$$\frac{\partial\psi}{\partial y}=0,\ \ \frac{\partial\psi}{\partial x}=0,\ \ \omega=-n\frac{\partial^2\psi}{\partial y^2},\ \ \frac{\partial\theta}{\partial y}=-Bi(1-\theta),\ \frac{\partial h}{\partial y}=K_s\,h,\ \ \delta\frac{\partial h_1}{\partial y}=-K_s\,h\ \text{at}\ y=0 \tag{5.15a}$$

$$\frac{\partial\psi}{\partial y}=0,\ \ \omega=0,\ \ \theta=0,\ \ h=1,\ \ h_1=0\quad\ \text{as}\quad\ y\to\infty \tag{5.15b}$$

Using the procedure explained in the earlier chapter (i.e., in case(a) of the Chapter-2), the following similarity transformations are obtained

$$\eta=y,\ \psi=xf(\eta),\ \omega=xg(\eta),\ \beta_1=x\beta_{T_0},\ \beta_2=x\beta_{T_1},\ \theta=\theta(\eta),\ h=h(\eta),\ h_1=h_1(\eta) \tag{5.16}$$

Using (5.16) in Eqs. (5.10)-(5.14), and making use of the assumption that diffusion coefficients D_A and D_B are equal as explained in previous chapter of case(a), the resultant similarity representation of system of equations is obtained in the following form

$$\frac{1}{\epsilon}\left(\frac{1}{1-N}\right)f'''+\frac{1}{\epsilon^2}ff''-\frac{1}{\epsilon^2}f'^2+\left(\frac{N}{1-N}\right)g'+\theta(1+\chi\theta)-\frac{1}{DaGr^{1/2}}f'=0 \tag{5.17}$$

$$\left(\frac{2-N}{2-2N}\right)g''+\frac{1}{\epsilon}fg'-\frac{1}{\epsilon}f'g-\left(\frac{N}{1-N}\right)\left(2g+\frac{1}{\epsilon}f''\right)=0 \tag{5.18}$$

$$\frac{1}{Pr}\theta''+f\theta'=0 \tag{5.19}$$

$$\frac{1}{Sc}h''+fh'-Kh(1-h)^2=0 \tag{5.20}$$

along with the modified boundary conditions

$$f'(0)=0,\ g(0)=-nf''(0),\ \theta'(0)=-Bi[1-\theta(0)],\ h'(0)=K_s\,h(0) \tag{5.21a}$$

$$f'(\infty)\to 0,\ g(\infty)\to 0,\ \theta(\infty)\to 0,\ h(\infty)\to 1 \tag{5.21b}$$

The non-dimensional skin friction $C_f = \dfrac{2\tau_w}{\rho\overline{u}_*^2}$, wall couple stress $M_w = \dfrac{m_w}{\rho\overline{u}_*^2\overline{x}}$ and local Nusselt number $Nu_{\overline{x}} = \dfrac{q_w\overline{x}}{k(T_f - T_\infty)}$, are given by

$$C_f Gr_{\overline{x}}^{1/4} = 2\left(\frac{1-nN}{1-N}\right) f''(0),\ M_w Gr_{\overline{x}}^{1/2} = \left(\frac{2-N}{2-2N}\right) g'(0) \text{ and } \frac{Nu_{\overline{x}}}{Gr_{\overline{x}}^{1/4}} = -\theta'(0) \tag{5.22}$$

where $Gr_{\overline{x}} = \dfrac{g^*\beta_{T_0}(T_f - T_\infty)\overline{x}^3}{\nu^2}$ is the local Grashof number.

Results and Discussion

The resultant Eqs. (5.17) - (5.20) along with the boundary conditions (5.21) have been solved numerically using the spectral quasi-linearization method. In order to assess the accuracy of the code generated, for $N = 0$, $\epsilon = 1$, $n = 0$, $Pr = 1$, $\chi = 0$, $Da \to \infty$ and $Bi \to \infty$, the results of the present problem in the absence of homogeneous and heterogeneous reactions, have been compared with those of Merkin [57], Nazar *et al.* [72] and Molla *et al.* [60] and found that they are in good agreement [Tab. (2.1)]. Also, the values of heat transfer rate, for $n = 0.5$, $\epsilon = 1$, $Pr = 1$, $Bi \to \infty$, $Da \to \infty$ and $\chi = 0$, agree well with that of Nazar *et al.* [72] as shown in Tab. (2.2). To study the effects of nonlinear convection parameter χ, Darcy number Da, Biot number Bi, strength of homogeneous and heterogeneous reaction parameters K and K_s, computations have been carried out in the case of $n = 0$, $\epsilon = 0.6$, $Gr = 10$, $Pr = 0.71$ and $Sc = 0.22$.

The effects of coupling number N on the non-dimensional velocity, microrotation, temperature and species concentration are displayed in Figs. 5.2(a)-5.2(d). From Fig. 5.2(a), it can be observed that with the increase of coupling number, the fluid velocity reduces near the surface of the plate and far away from the plate it shows reverse behaviour. As expected, the fluid vortex viscosity increases by increasing the coupling number and thus it promotes the microrotation of micropolar fluids. It is noticed from Fig. 5.2(b) that initially, the microrotation profile is flat and then approaches to their free stream values with the increase of coupling number. By enhancing the coupling number, the thickness of temperature and species concentration boundary layers increase [Figs. 5.2(c) and 5.2(d)]. These results are tuned with the results of earlier chapters for coupling number N.

Figs. 5.3(a) -5.3(d) depict the variation of Biot number Bi on the non-dimensional velocity f',

microrotation g, temperature θ and species concentration h across the boundary layers. From Fig. 5.3(a), it is clear that the fluid velocity is zero at the plate surface and then enhances gradually near the surface of the plate. It is interesting to reveal that the fluid velocity enhances within the momentum boundary layer with the increase of Biot number Bi. As expected, by increasing the value of Biot number, the microrotation profile shows reverse rotation near two boundaries as shown in Fig. 5.3(b). Fig. 5.3(c) depicts that, the temperature of the fluid is extreme at plate surface and diminishes exponentially to zero far away from the plate and moreover, it is observed that the temperature enhances with an increase in Biot number. Fig. 5.3(d) illustrates that the species concentration increases with the increase of Biot number Bi.

The variations of non-dimensional velocity f', microrotation g, temperature θ and species concentration h profiles are displayed in Figs. 5.4(a)-5.4(d) for different values of the nonlinear convection parameter χ. With an increase in χ, the velocity increases, but far away from the plate it shows opposite trend as depicted in Fig. 5.4(a). From Fig. 5.4(b), it can be observed that the microrotation shows reverse rotation near two boundaries with an increase in the values of nonlinear convection parameter. The nonlinear convection parameter χ measures the nonlinearity in density-temperature relationship. From Figs.5.4(c) and 5.4(d), it is clear that the temperature reduces and species concentration enhances with an enhance in nonlinear convection parameter. Finally, it is concluded from the results that the fluid temperature is more and species concentration is less in the case of linear convection ($\chi = 0$) as compared with that of nonlinear convection case ($\chi \neq 0$).

Figs. 5.5(a)-5.5(d) present the influence of Darcy number Da on the non-dimensional velocity, microrotation, temperature and species concentration. From Fig. 5.5(a), it can be noticed that with an increase in Darcy number, the velocity of the fluid increases near the wall and farther from the plate it shows opposite behaviour. With the increase of Darcy number the porous matrix structure becomes less and less prominent. Moreover, as the Darcy number tends to infinity (i,e. $Da \to \infty$) and porosity ϵ =1, the present problem reduces to the classical free convective flow of a micropolar fluid with the convective boundary condition. Fig. 5.5(b) reveals that as the value of Darcy parameter increases, the microrotation show opposite trends within the boundary layer. It is seen from Figs. 5.5(c) and 5.5(d) that the temperature and species concentration of the fluid show qualitatively opposite nature with an increase in Darcy number.

The variations of homogeneous and heterogeneous reaction parameters K and K_s on the species

concentration h and mass transfer rate $h(0)$ across the boundary layers, are plotted in Figs. 5.6(a)-5.7(b). Physically, an increase in the value of K corresponds to increase in the strength of homogeneous reaction rate. Figs. 5.6(a) and 5.6(b) depict that an increase in homogeneous reaction causes to decrease in the species concentration and rate of mass transfer. As the heterogeneous reaction parameter K_s increases, the strength of heterogeneous reaction rate increases. It is clear from Fig. 5.7(a) that with the increase of heterogeneous reaction parameter, the species concentration decreases slightly. From Fig. 5.7(b), it can be noticed that the rate of mass transfer decreases with the increase of heterogeneous reaction parameter K_s.

Table (5.1) displays the variations of skin-friction, wall couple stress and heat transfer rate for different values of coupling number N, Biot number Bi, nonlinear convection parameter χ and Darcy number Da and for fixed K and K_s parameters. From Tab. (5.1), it can be observed that with the enhance of coupling number N, the skin friction enhances, but the wall couple stress and heat transfer rate reduce. The skin-friction as well as heat transfer rate increase, but the wall couple stress decrease with the increase of Biot number Bi. It is noticed that with the increase of nonlinear convection parameter, both the skin friction as well as heat transfer rate enhance and the wall couple stress reduces. It is clear that the skin friction and heat transfer rate enhance, but the wall couple stress reduces with the enhancement of Darcy number.

Table 5.1: *Variations of skin friction, wall couple stress and heat transfer rate for varying values of micropolar parameter N, Biot numbers Bi, nonlinear convection parameter χ and Darcy number Da with $K = 1$ and $K_s = 0.5$.*

N	Bi	χ	Da	$C_f Gr_{\overline{x}}^{1/4}$	$M_w Gr_{\overline{x}}^{1/2}$	$\frac{Nu_{\overline{x}}}{Gr_{\overline{x}}^{1/4}}$
0.0	1.0	1.0	1.0	1.537527	0.000000	0.305228
0.3	1.0	1.0	1.0	1.750517	-0.142651	0.294051
0.5	1.0	1.0	1.0	1.959351	-0.291564	0.283342
0.8	1.0	1.0	1 .0	2.57905	-0.710582	0.253065
0.5	0.1	1.0	1.0	0.649682	-0.127284	0.067754
0.5	1.0	1.0	1.0	1.593042	-0.251223	0.219462
0.5	5.0	1.0	1.0	1.959351	-0.291564	0.283342
0.5	10	1.0	1.0	2.022233	-0.29819	0.294465
0.5	1.0	0.0	1.0	1.106618	-0.198623	0.20424
0.5	1.0	1.0	1.0	1.593042	-0.251223	0.219462
0.5	1.0	3.0	1.0	2.399576	-0.328708	0.239398
0.5	1.0	5.0	1.0	3.086638	-0.388064	0.253076
0.5	5.0	1.0	0.05	1.283075	-0.156822	0.197751
0.5	5.0	1.0	0.1	1.530281	-0.204481	0.231549
0.5	5.0	1.0	0.3	1.813237	-0.261512	0.266797
0.5	5.0	1.0	0.5	1.892408	-0.277765	0.275907

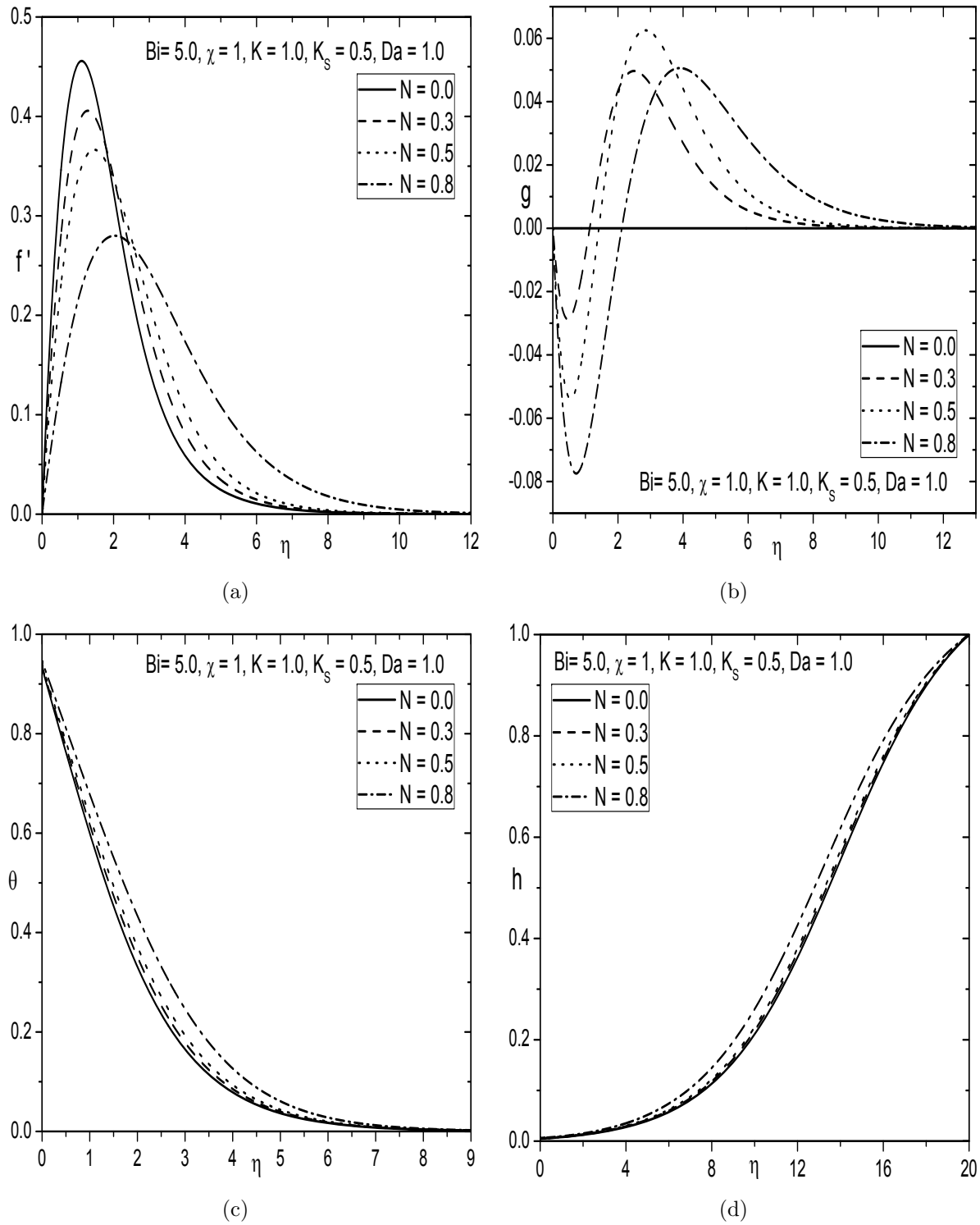

Figure 5.2: *Variation of N on (a)Velocity, (b)Microrotation, (c)Temperature and (d)Concentration profiles.*

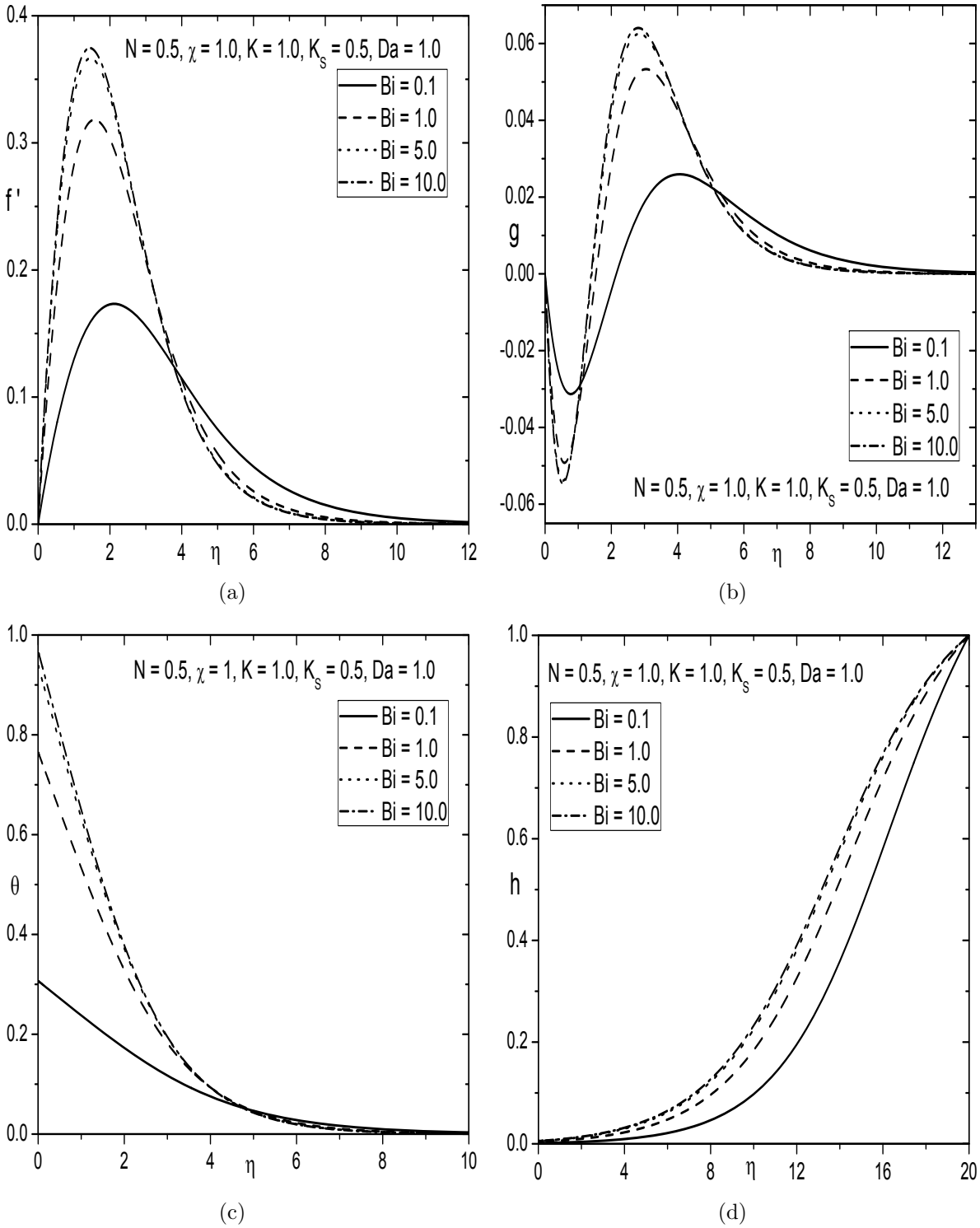

Figure 5.3: *Variation of Bi on (a)Velocity, (b)Microrotation, (c)Temperature and (d)Concentration profiles.*

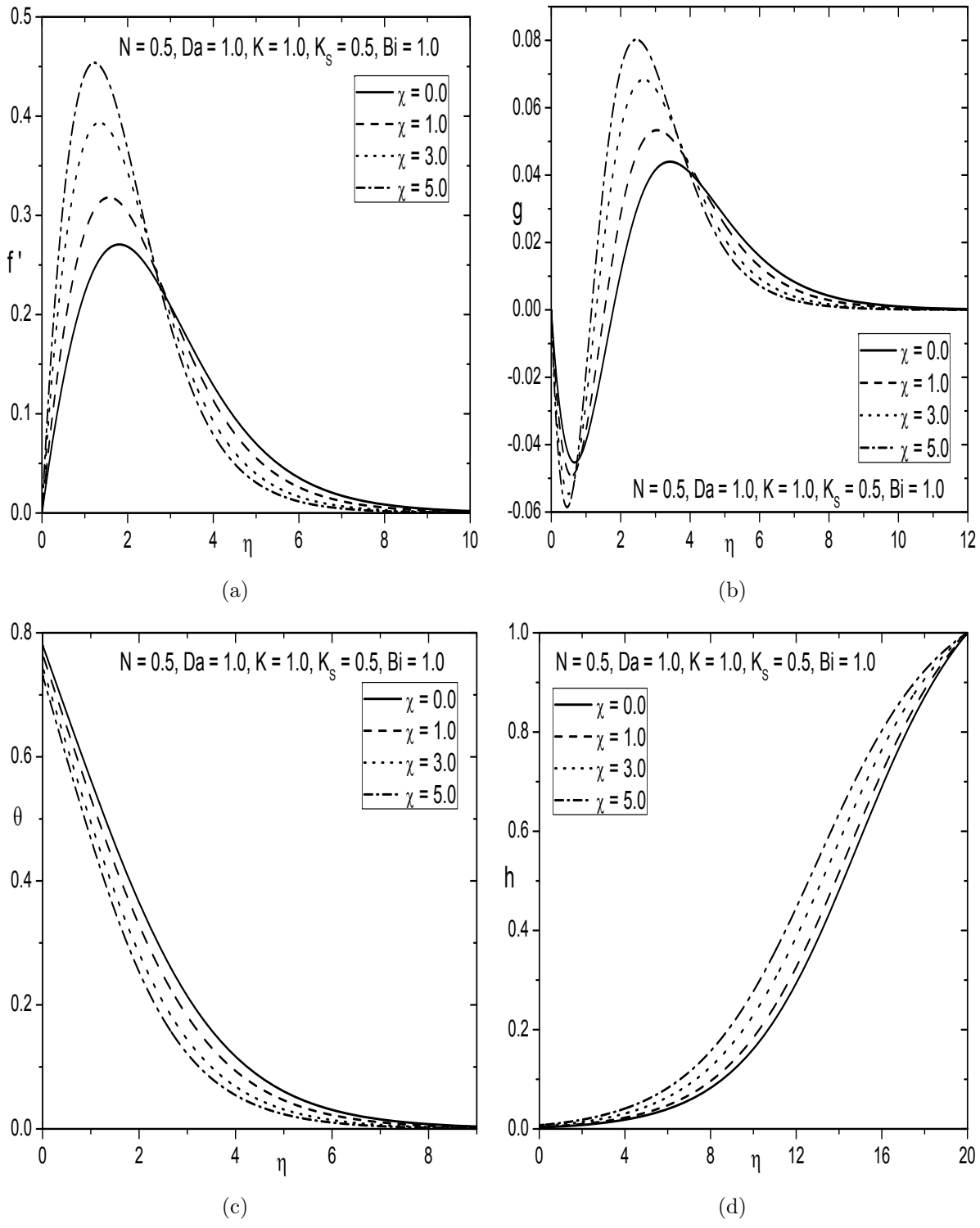

Figure 5.4: *Variation of χ on (a)Velocity, (b)Microrotation, (c)Temperature and (d)Concentration profiles.*

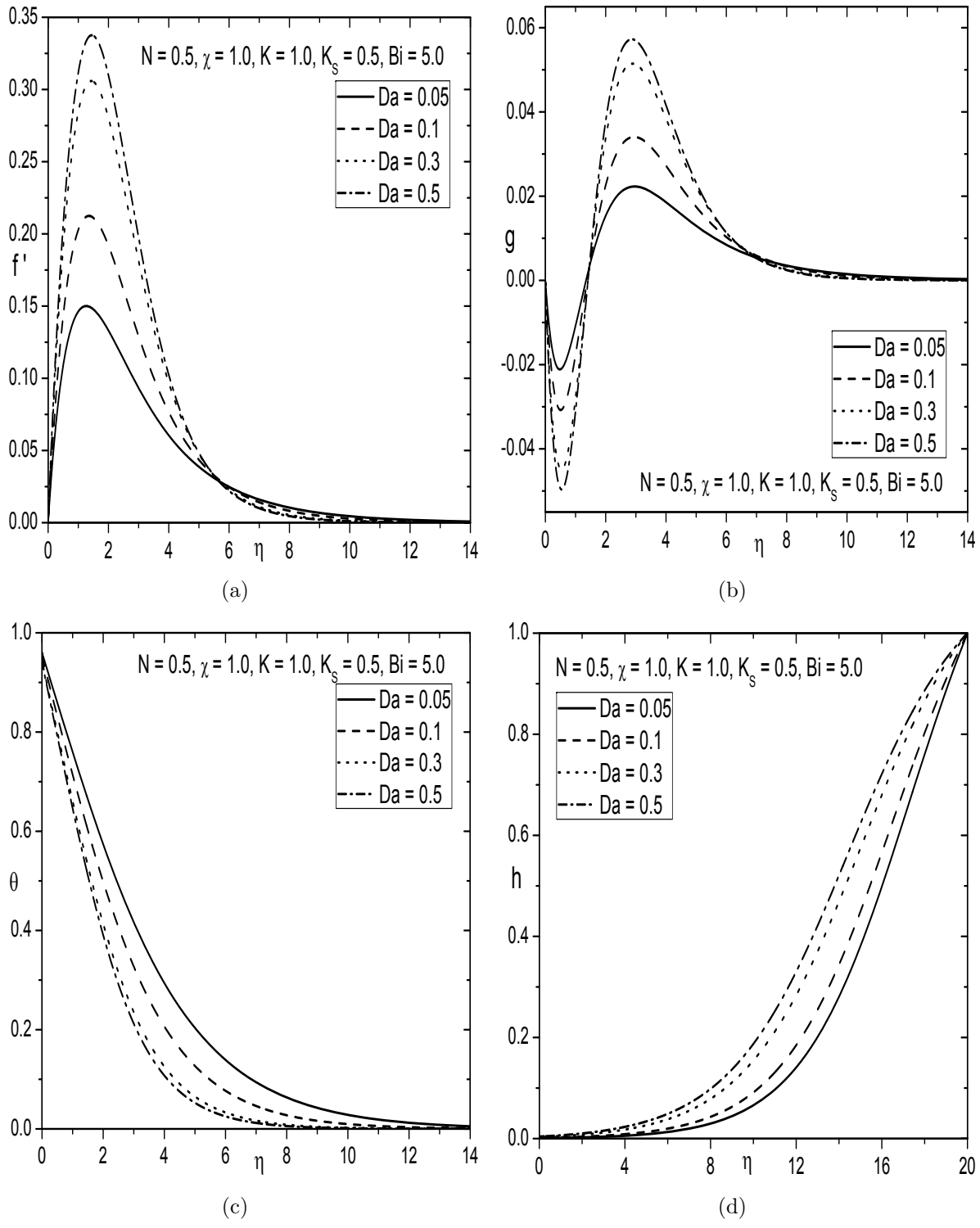

Figure 5.5: *Variation of Da on (a)Velocity, (b)Microrotation, (c)Temperature and (d)Concentration profiles.*

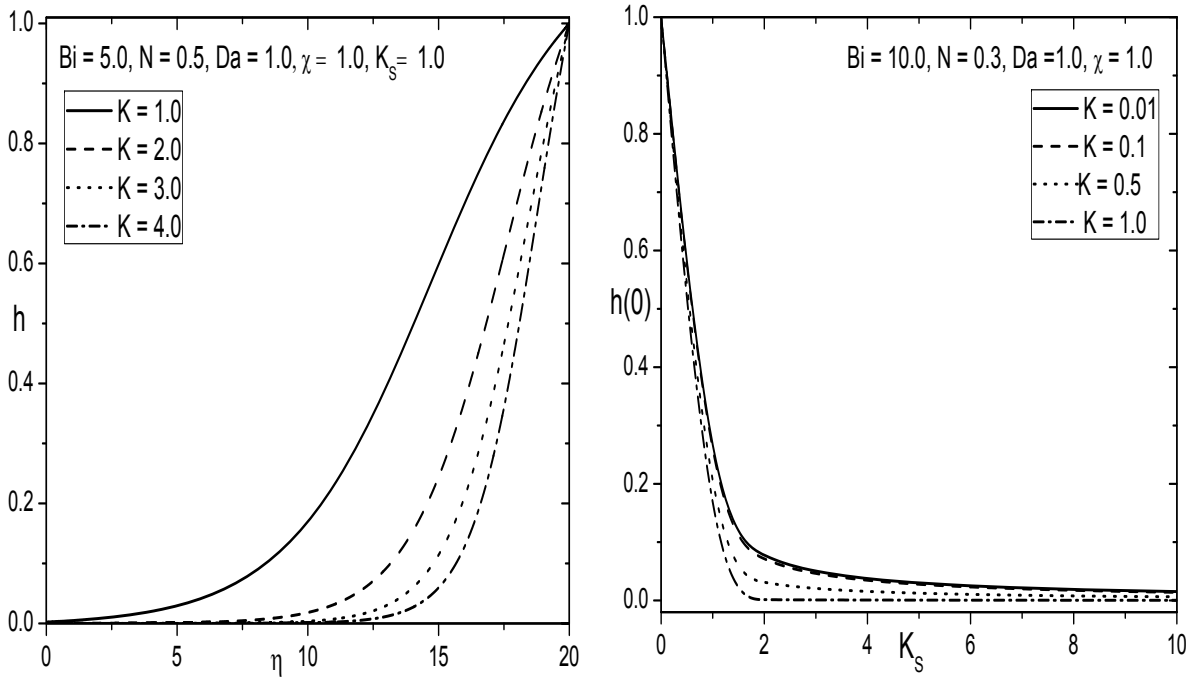

(a) (b)

Figure 5.6: *Variation of K on (a)Concentration profile h and (b) Mass transfer rate $h(0)$.*

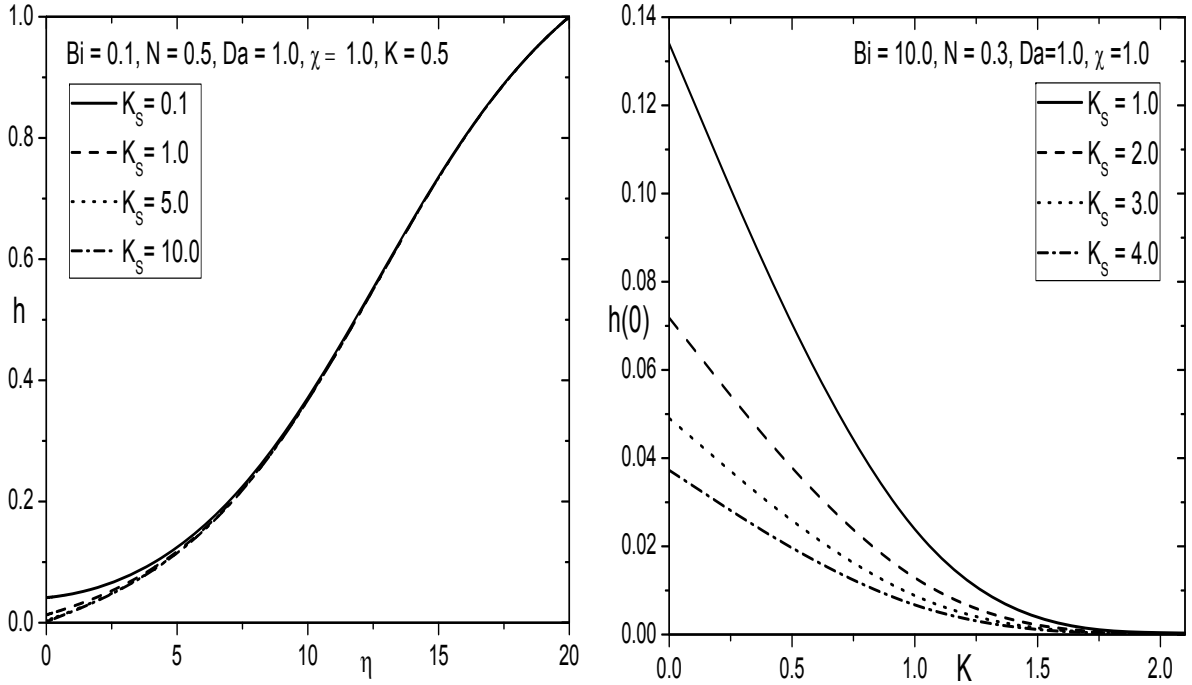

(a) (b)

Figure 5.7: *Variation of K_s on (a)Concentration profile h (b) Mass transfer rate $h(0)$.*

5.2.2 Case(b): Mixed Convection

Consider the flow to be a mixed convection, which arises from an external flow with velocity $[\bar{u_e}(x)]$ and buoyancy forces. We introduce the non-dimensional variables as follows

$$\left.\begin{aligned} x = \frac{\overline{x}}{L},\ y = \frac{\overline{y}}{L}Re^{1/2},\ u = \frac{\overline{u}}{U_\infty},\ v = \frac{\overline{v}}{U_\infty}Re^{1/2}, \\ u_e = \frac{\overline{u}_e}{U_\infty},\ \omega = \frac{L^2}{\nu Re^{3/2}}\overline{\omega},\ \theta = \frac{T-T_\infty}{T_f-T_\infty},\ h = \frac{\overline{a}}{a_0},\ h_1 = \frac{\overline{b}}{a_0} \end{aligned}\right\} \tag{5.23}$$

Using (5.23) and then (5.9) in Eqs.(5.2)-(5.6), we get the following momentum, angular momentum, energy and concentration equations of species A and B

$$\frac{1}{\epsilon^2}\left(\frac{\partial\psi}{\partial y}\frac{\partial^2\psi}{\partial x\partial y} - \frac{\partial\psi}{\partial x}\frac{\partial^2\psi}{\partial y^2}\right) - \frac{1}{\epsilon}\left(\frac{1}{1-N}\right)\frac{\partial^3\psi}{\partial y^3} - \left(\frac{N}{1-N}\right)\frac{\partial\omega}{\partial y} - u_e\frac{du_e}{dx} \tag{5.24}$$

$$-\frac{g^*\beta_1(T_f-T_\infty)}{\nu^2Re^2}\,\theta\left(1+\frac{\beta_2}{\beta_1}\theta(T_f-T_\infty)\right) + \frac{1}{DaRe}\left(\frac{\partial\psi}{\partial y} - u_e\right) = 0$$

$$\frac{1}{\epsilon}\left(\frac{\partial\psi}{\partial y}\frac{\partial\omega}{\partial x} - \frac{\partial\psi}{\partial x}\frac{\partial\omega}{\partial y}\right) - \left(\frac{2-N}{2-2N}\right)\frac{\partial^2\omega}{\partial y^2} + \left(\frac{N}{1-N}\right)\left(2\omega + \frac{1}{\epsilon}\frac{\partial^2\psi}{\partial y^2}\right) = 0 \tag{5.25}$$

$$\frac{\partial\psi}{\partial y}\frac{\partial\theta}{\partial x} - \frac{\partial\psi}{\partial x}\frac{\partial\theta}{\partial y} - \frac{1}{Pr}\frac{\partial^2\theta}{\partial y^2} = 0 \tag{5.26}$$

$$\frac{\partial\psi}{\partial y}\frac{\partial h}{\partial x} - \frac{\partial\psi}{\partial x}\frac{\partial h}{\partial y} - \frac{1}{Sc}\frac{\partial^2 h}{\partial y^2} + K\,h\,{h_1}^2 = 0 \tag{5.27}$$

$$\frac{\partial\psi}{\partial y}\frac{\partial h_1}{\partial x} - \frac{\partial\psi}{\partial x}\frac{\partial h_1}{\partial y} - \frac{\delta}{Sc}\frac{\partial^2 h_1}{\partial y^2} - K\,h\,{h_1}^2 = 0 \tag{5.28}$$

The boundary conditions (5.7) become

$$\frac{\partial\psi}{\partial y} = 0,\ \ \frac{\partial\psi}{\partial x} = 0,\ \ \omega = -n\frac{\partial^2\psi}{\partial y^2},\ \ \frac{\partial\theta}{\partial y} = -Bi(1-\theta), \tag{5.29a}$$

$$\frac{\partial h}{\partial y} = K_s h,\ \ \delta\frac{\partial h_1}{\partial y} = -K_s h \quad \text{at} \quad y = 0$$

$$\frac{\partial\psi}{\partial y} = u_e,\ \ \omega = 0,\ \ \theta = 0,\ \ h = 1,\ \ h_1 = 0 \quad \text{as} \quad y\to\infty \tag{5.29b}$$

Using the procedure explained in case(a) of the second chapter, the following similarity trans-

formations are obtained

$$\eta = y,\ \psi = xf(\eta),\ \omega = xg(\eta),\ u_e = x, \beta_1 = \beta_{T_0}x, \beta_2 = \beta_{T_1}x,\ \theta = \theta(\eta),\ h_1 = h_1(\eta),\ h_2 = h_2(\eta) \tag{5.30}$$

Substituting (5.30) into Eqs. (5.24)-(5.28), and making use of the assumption that diffusion coefficients D_A and D_B are equal as explained in the previous chapter, then the following system of equations in the similarity form is obtained

$$\frac{1}{\epsilon}\left(\frac{1}{1-N}\right)f''' + \frac{1}{\epsilon^2}ff'' - \frac{1}{\epsilon^2}f'^2 + 1 + \left(\frac{N}{1-N}\right)g' + \lambda\theta(1+\chi\theta) + \frac{1}{DaRe}(1-f') = 0 \tag{5.31}$$

$$\left(\frac{2-N}{2-2N}\right)g'' + \frac{1}{\epsilon}fg' - \frac{1}{\epsilon}f'g - \left(\frac{N}{1-N}\right)\left(2g + \frac{1}{\epsilon}f''\right) = 0 \tag{5.32}$$

$$\frac{1}{Pr}\theta'' + f\theta' = 0 \tag{5.33}$$

$$\frac{1}{Sc}h'' + fh' - Kh(1-h)^2 = 0 \tag{5.34}$$

along with the reduced boundary conditions

$$f(0) = 0,\ f'(0) = 0,\ g(0) = -nf''(0),\ \theta'(0) = -Bi[1-\theta(0)],\ h'(0) = K_s\, h(0) \tag{5.35a}$$

$$f'(\infty) \to 1,\ g(\infty) \to 0,\ \theta(\infty) \to 0,\ h(\infty) \to 1 \tag{5.35b}$$

The quantities of physical interest are the non-dimensional skin friction $C_f = \dfrac{2\tau_w}{\rho\overline{u}_e^2}$, wall couple stress $M_w = \dfrac{m_w}{\rho\overline{u}_e^2\overline{x}}$ and local Nusselt number $Nu_{\overline{x}} = \dfrac{q_w\overline{x}}{k(T_f - T_\infty)}$, are given by

$$C_f Re_{\overline{x}^{1/2}} = 2\left(\frac{1-nN}{1-N}\right)f''(0),\ M_w Re_{\overline{x}} = \left(\frac{2-N}{2-2N}\right)g'(0) \text{ and } \frac{Nu_{\overline{x}}}{Re_{\overline{x}^{1/2}}} = -\theta'(0) \tag{5.36}$$

Results and Discussion

The non-linear coupled system of Eqs. (5.31) - (5.34) together with the boundary conditions (5.35) are solved numerically using the spectral quasi-linearization method. In order to validate the code generated, for the special case of $N = 0$, $n = 0$, $Pr = 1$, $Bi \to \infty$, $\epsilon = 1$, $Da \to \infty$ and $\chi = 0$, the results of the present problem have been compared with those of Merkin [58] and Nazar *et al.*

[73] in the absence of homogeneous and heterogeneous reactions and found that they are in good agreement, as shown in Tab. (2.4). To analyze the effects of nonlinear convection χ, Biot number Bi, Darcy number Da, strength of homogeneous and heterogeneous reaction parameters K and K_s, computations have been carried out for $n = 0$, $\epsilon = 1$, $Re = 2$, $Pr = 0.71$ and $Sc = 0.22$.

Figs. 5.8(a)-5.8(d) illustrate the variations of dimensionless velocity, microrotation, temperature and species concentration with the influence of coupling number N. As the coupling number N increases, it is found from Fig. 5.8(a) that the velocity decreases for both aiding and opposing flows. Further, the velocity in the case of micropolar fluid ($N \neq 0$) is less compared to that of the viscous fluid case ($N = 0$). From Fig. 5.8(b), it can be observed that as N increases, initially the microrotation profiles tends to become flat, and then approaches to their free stream values far away from the wall. It is seen from Figs. 5.8(c) and 5.8(d) that the temperature of the fluid enhances, while the species concentration reduces with the increase of coupling number N for both opposing and aiding flow situations.

The variation of Biot number Bi on the non-dimensional velocity f', microrotation g, temperature θ and species concentration h across the boundary layers, is plotted in Figs. 5.9(a) - 5.9(d). It can be noticed from Fig. 5.9(a) that an increase in Biot number Bi causes to increase in the fluid velocity within the momentum boundary layer in aiding flow situation, but it shows the reverse trend in opposing flow situation. From Fig. 5.9(b), it can be found that the microrotation depicts reverse rotation near the two boundaries and also observed that the behaviour of microrotation in aiding flow shows reverse trend when compared to the opposing flow. The increment of Biot number increases the convective heating and hence, $Bi \to \infty$ gives the isothermal surface, which is clearly observed from Fig. 5.9(c), where $\theta(0) = 1$. From this figure it is clear that the temperature of the fluid increases with the increase of Biot number for both aiding and opposing flow situations. Fig. 5.9(d) reveals that the species concentration decreases in the case of opposing flow whereas, it increases in the aiding flow case.

Figs. 5.10(a) - 5.10(d) depict the variation of nonlinear convection parameter χ on the non-dimensional velocity f', microrotation g, temperature θ and species concentration h across the boundary layers. The nonlinear convection (NDT) parameter χ measures the nonlinearity in a density-temperature relationship. From Fig. 5.10(a), it is found that with the increase of NDT parameter, the fluid velocity increases in aiding flow, but decreases in opposing flow. From Fig. 5.10(b), it can be seen that with an increase in the values of χ, the microrotation increases slightly

first and then decreases in opposing flow, but it shows reverse phenomena in aiding flow. The fluid temperature decreases, but the concentration increases in aiding flow while, these show reverse trend in aiding flow [Figs.5.10(c) and 5.10(d)].

The influence of Darcy parameter on the non-dimensional velocity f', microrotation g, temperature θ and species concentration h across the boundary layers, is exhibited in Figs. 5.11(a) - 5.11(d). From Fig. 5.11(a), it is found that the fluid velocity reduces with the increase of Darcy parameter for both aiding and opposing flows. The microrotation profile shows opposite trend within the boundary as shown in Fig. 5.11(b) and it satisfies the free stream values for both aiding and opposing flow situation. It can be seen from Figs. 5.11(c) and 5.11(d) that the temperature enhances and species concentration reduces with the increase of Darcy parameter in both the cases of aiding and opposing flows.

The set of Figs. 5.12(a) - 5.13(b) are prepared to display the influence of K and K_s on the species concentration h and mass transfer rate $h(0)$. An increase in the values of K and K_s correspond to increase in the strength of homogeneous and heterogeneous reaction rates. It is clear from Figs. 5.12(a) and 5.12(b) that the species concentration and mass transfer rate decrease with the increase of homogeneous reaction parameter for both aiding and opposing flows. With the increase of heterogeneous reaction parameter, the species concentration and mass transfer rate decreases in both the cases of opposing and aiding flows [Figs. 5.13(a) and 5.13(b)]. Also noticed that the effect of heterogeneous reaction is more on the species concentration as compared with the homogeneous reaction.

The variations of $C_f Re_{\overline{x}^{1/2}}$, $M_w Re_{\overline{x}}$, and $\frac{Nu_{\overline{x}}}{Re_{\overline{x}^{1/2}}}$ for different combinations of physical parameters, are displayed in Tab. (5.2) for both opposing and aiding flow situations. Generally, the skin friction factor is more for the micropolar fluid than compared with the viscous fluid. It can be noticed that the larger values of coupling number N, results in lower wall couple stresses and heat transfer rate, but higher skin friction for both opposing and aiding flows. It can be observed that in the presence of opposing and aiding flows, the skin-friction and wall couple stress coefficients show opposite trend while, the heat transfer rate enhances with the increase of Bi. It can be revealed that with the increase of NDT parameter the skin friction and heat transfer rate increase, but the wall couple stress decreases for aiding flow and these show reverse behaviour for aiding flow. It can be seen that with the increase of Darcy parameter, the skin friction and heat transfer rate decrease, but the wall couple stress increases for both opposing and aiding flows.

Table 5.2: *Variations of skin friction, wall couple stress and heat transfer rate for different values of mixed convection parameter λ, micropolar parameter N, Biot numbers Bi, nonlinear convection parameter χ and Darcy parameter Da with $K = 1$ and $K_s = 0.5$.*

λ	N	Bi	χ	Da	$C_f Re_{\overline{x}^{1/2}}$	$M_w Re_{\overline{x}}$	$\frac{Nu_{\overline{x}}}{Re_{\overline{x}^{1/2}}}$
-0.5	0	0.1	0.2	0.1	5.05139745	0	0.08471708
-0.5	0.5	0.1	0.2	0.1	7.02948203	-0.57643615	0.08397957
-0.5	0.8	0.1	0.2	0.1	10.52585038	-1.63641876	0.08277617
1	0	0.1	0.2	0.1	5.20029251	0	0.08481064
1	0.5	0.1	0.2	0.1	7.23303374	-0.58533796	0.08407231
1	0.8	0.1	0.2	0.1	10.82520697	-1.66533959	0.08286739
-0.5	0.5	0.1	0.2	0.1	7.02948203	-0.57643615	0.08397957
-0.5	0.5	1	0.2	0.1	6.79463737	-0.56628956	0.34212506
-0.5	0.5	10	0.2	0.1	6.6400254	-0.55969522	0.49188867
1	0.5	0.1	0.2	0.1	7.23303374	-0.58533796	0.08407231
1	0.5	1	0.2	0.1	7.6899358	-0.60466536	0.34881656
1	0.5	10	0.2	0.1	7.9942759	-0.61709627	0.51292588
-0.5	0.5	1	0	0.1	6.82382014	-0.56729995	0.3423021
-0.5	0.5	1	1	0.1	6.67734275	-0.56221764	0.34140988
-0.5	0.5	1	3	0.1	6.38001875	-0.55181666	0.33957065
1	0.5	1	0	0.1	7.63449242	-0.60282032	0.34850487
1	0.5	1	1	0.1	7.9098937	-0.61195218	0.35004251
1	0.5	1	3	0.1	8.44778335	-0.62955653	0.35297148
-0.5	0.5	5	0.2	0.05	9.13996551	-0.62702376	0.49063025
-0.5	0.5	5	0.2	0.1	6.66438295	-0.56073086	0.46917743
-0.5	0.5	5	0.2	0.5	3.73210783	-0.44389793	0.42859056
1	0.5	5	0.2	0.05	10.16478248	-0.66388312	0.5024711
1	0.5	5	0.2	0.1	7.94570088	-0.61513293	0.4872598
1	0.5	5	0.2	0.5	5.5444293	-0.54185965	0.46332811

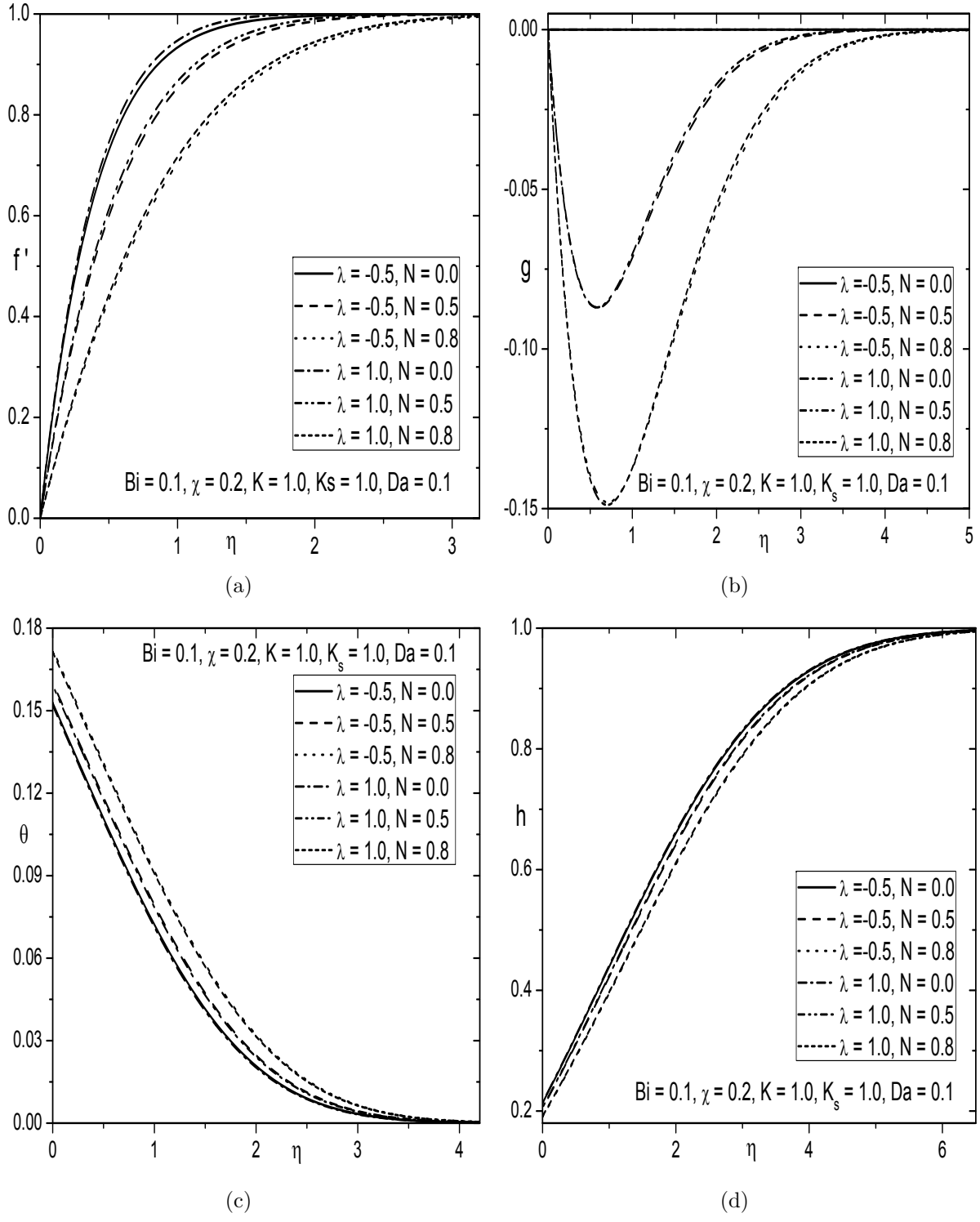

Figure 5.8: *Variation of N on (a)Velocity, (b)Microrotation, (c)Temperature and (d)Concentration profiles*

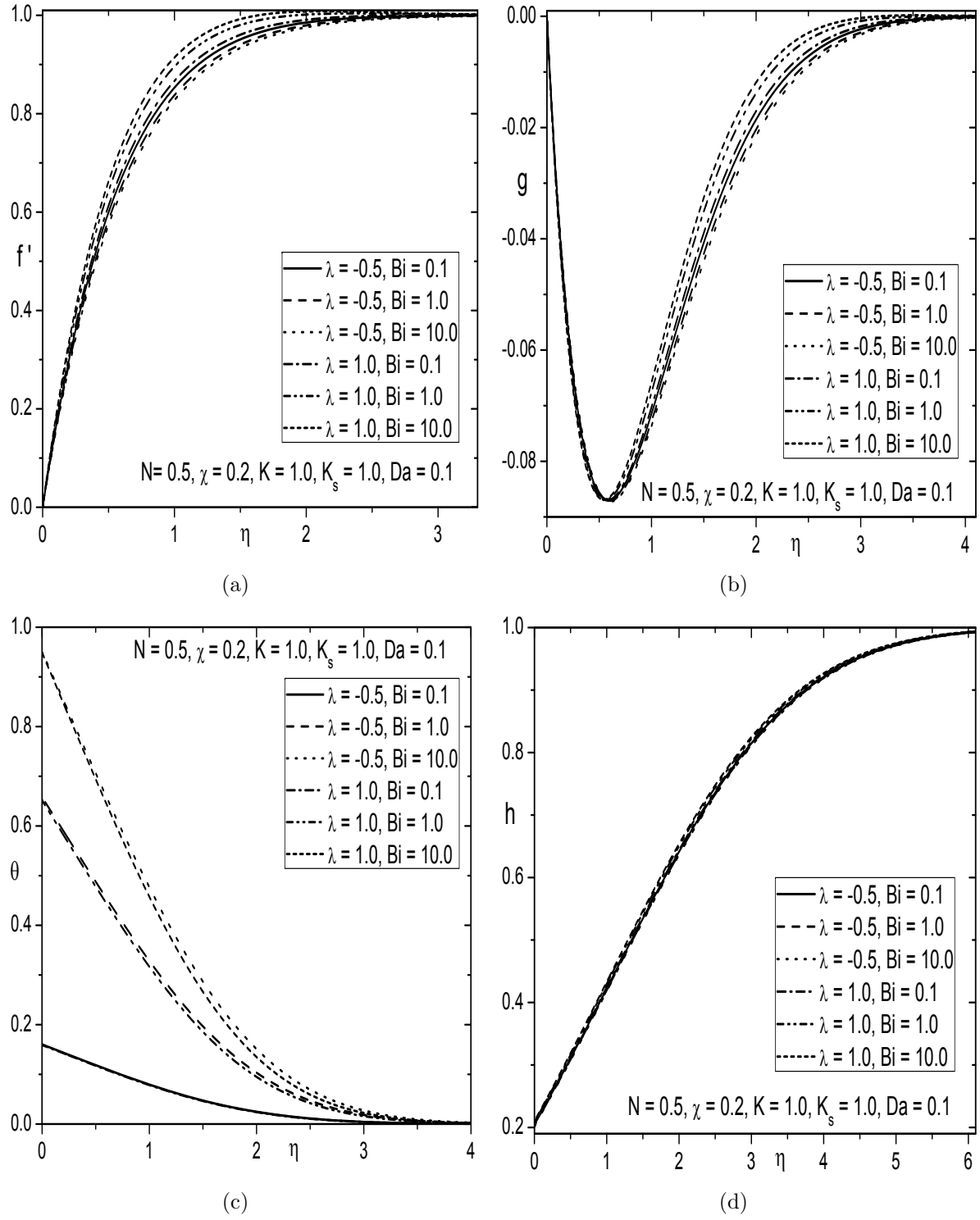

Figure 5.9: *Variation of Bi on (a)Velocity, (b)Microrotation, (c)Temperature and (d)Concentration profiles*

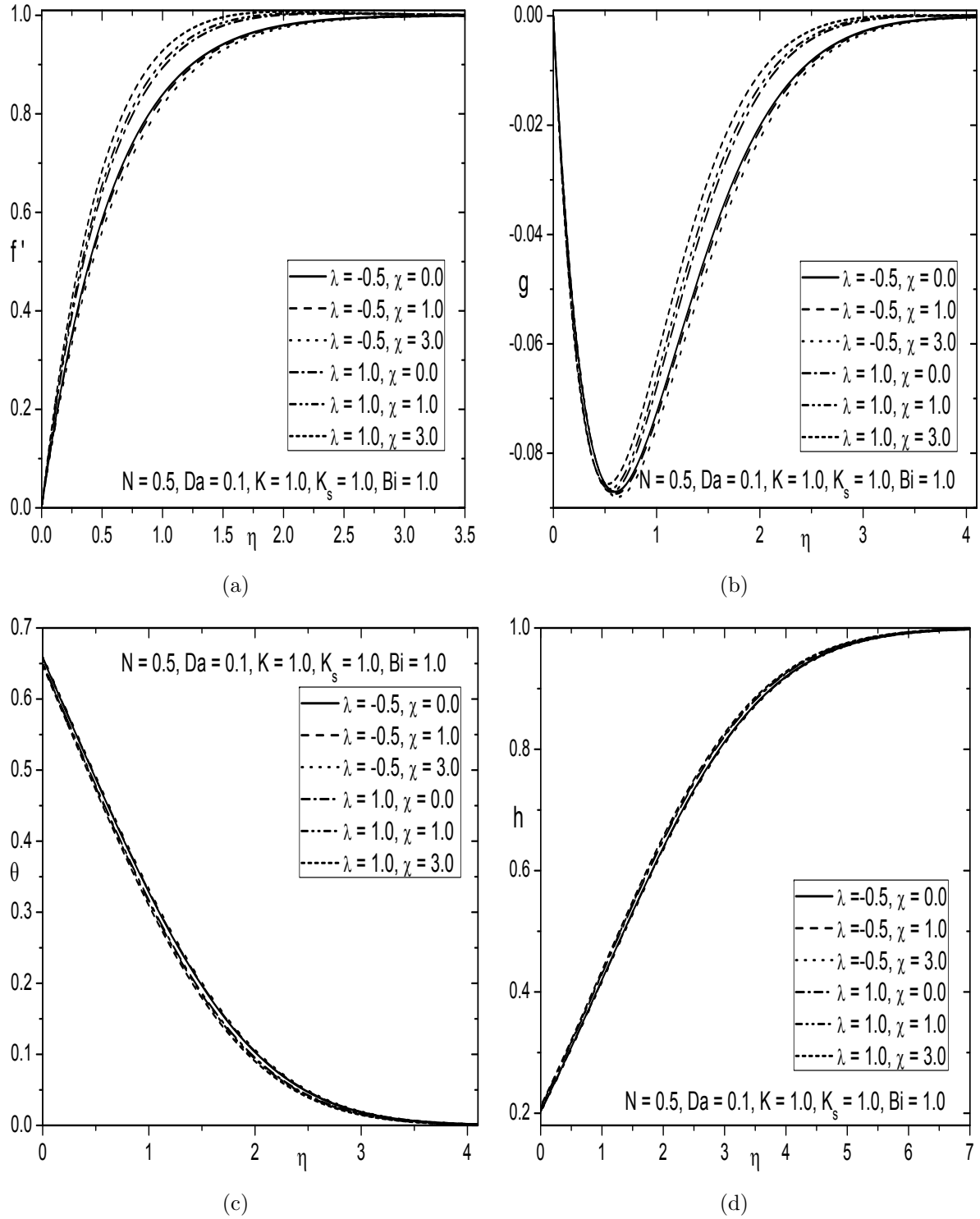

Figure 5.10: *Variation of χ on (a)Velocity, (b)Microrotation, (c)Temperature and (d)Concentration profiles*

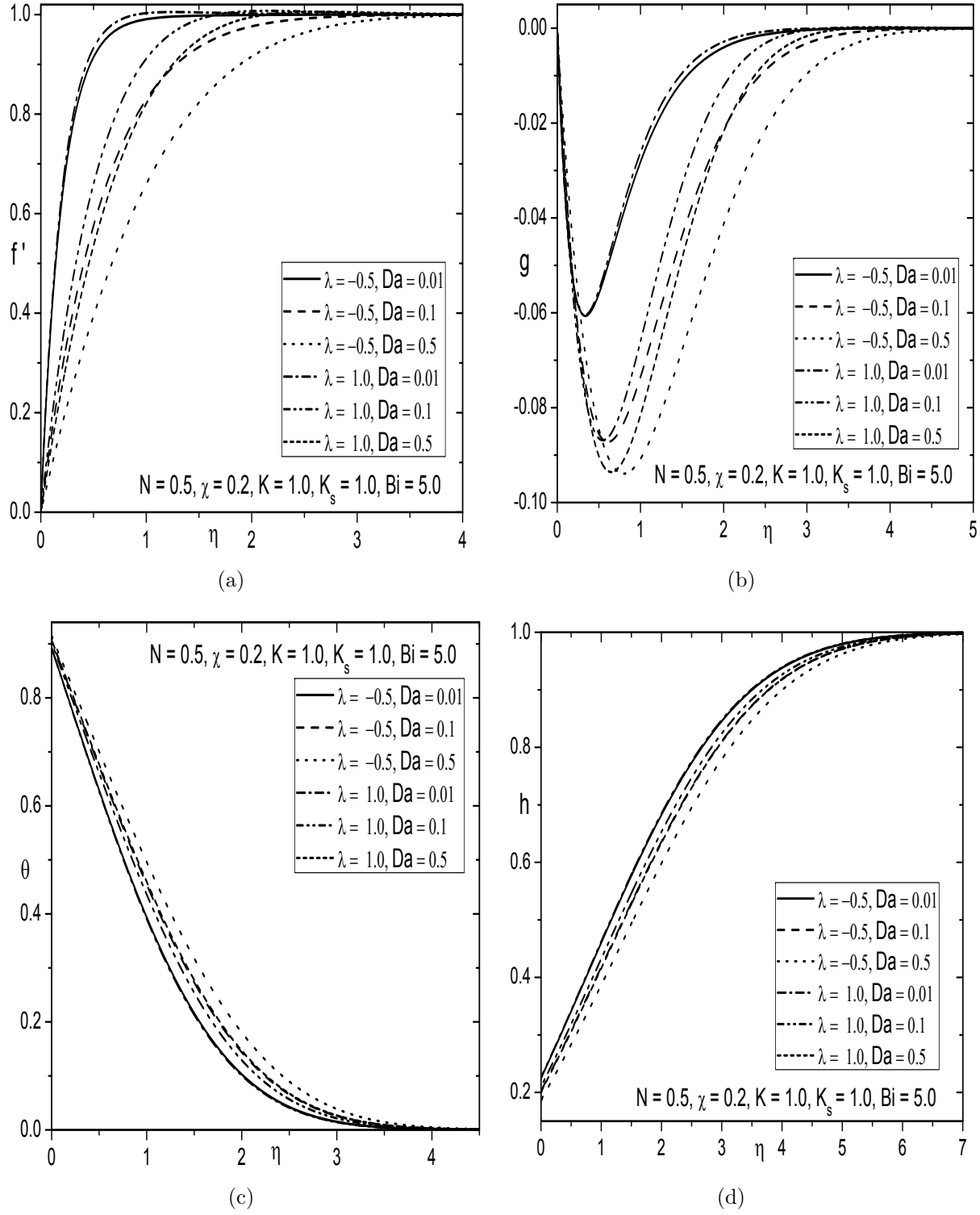

Figure 5.11: *Variation of Da on (a)Velocity, (b)Microrotation, (c)Temperature and (d)Concentration profiles*

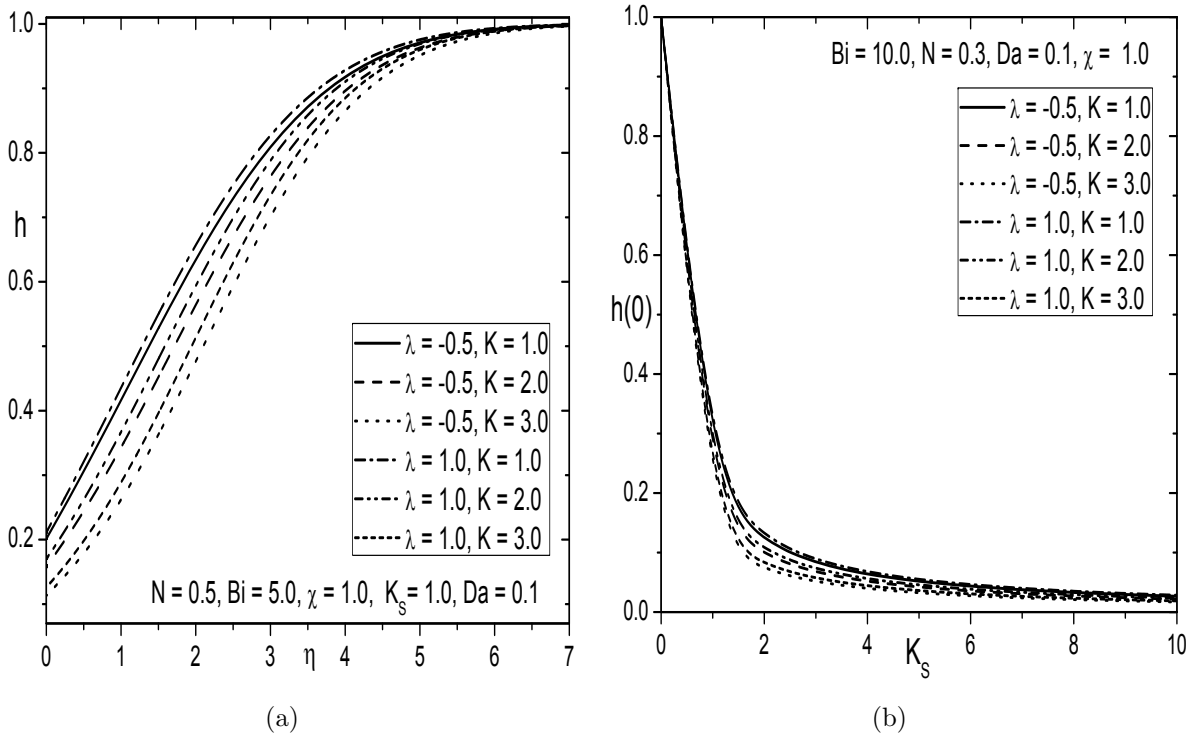

(a) (b)

Figure 5.12: *Variation of K on (a)Concentration profile h and (b) Mass transfer rate $h(0)$*

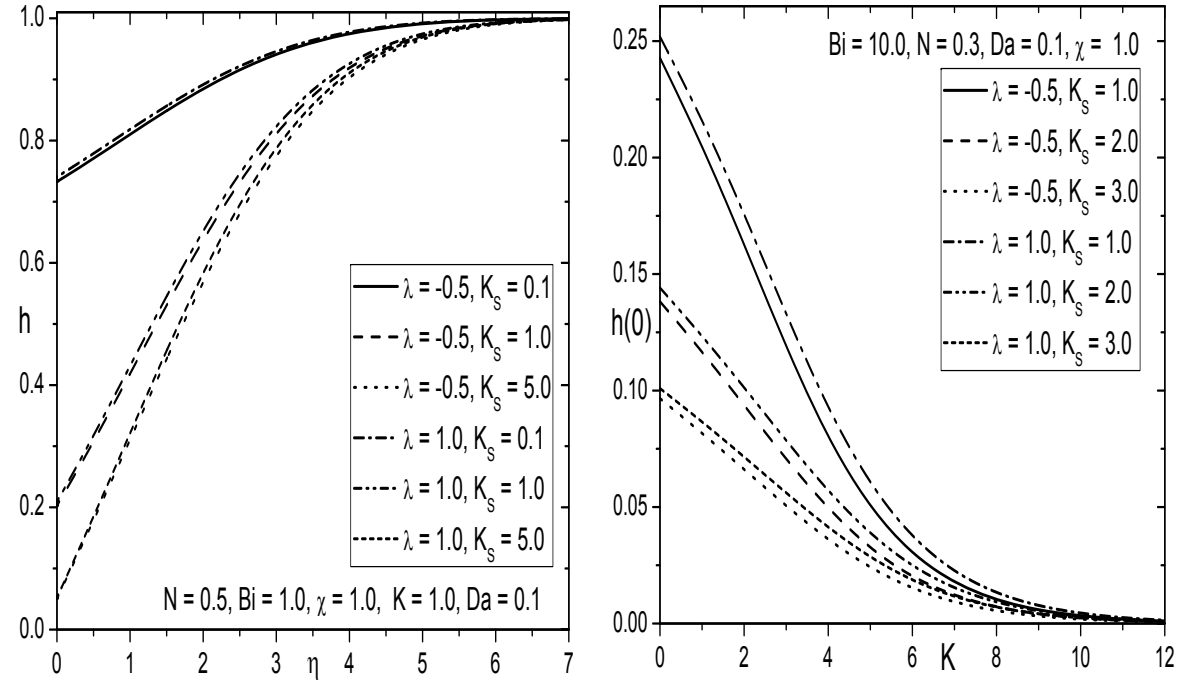

(a) (b)

Figure 5.13: *Variation of K_s on (a)Concentration profile h and (b) Mass transfer rate $h(0)$*

5.3 Conclusions

This chapter investigates the nonlinear convective flow of a micropolar fluid embedded in a Darcy porous medium by taking into an account of homogeneous-heterogeneous reactions with the convective boundary condition. From this study, the conclusions can be drawn in both cases (a) and (b) as follows:

As in the previous chapter, the behavior of nonlinear convection parameter, homogeneous-heterogeneous reaction parameter is found to be similar on various profiles. Case(a): It is found that the skin friction, heat transfer rate, species concentration and velocity (near the plate) increase, but the wall couple stress and temperature decrease with the increase of Darcy number. Case(b): In this case, the flow properties are studied for both opposing and aiding flows. The skin friction coefficient, heat transfer rate, velocity and species concentration enhances, whereas the wall couple stress and temperature reduces with the increase of Darcy parameter. Finally, the microrotation depicts reverse trend.

Part III

FREE AND MIXED CONVECTION OVER THE VERTICAL FRUSTUM OF A CONE IN A MICROPOLAR FLUID

Chapter 6

Convective Flow of a Micropolar Fluid over a Truncated Cone with Soret and Viscous Dissipation Effects [1]

6.1 Introduction

A broad area of research on convective flows over the vertical frustum of a cone in Newtonian /non-Newtonian fluids has gained continuous attention due to its significant engineering applications such as heat exchangers, cooling of electronic devices, etc (for more details, see Hamilton *et al.* [34] and Nakamura *et al.* [69]). Yih [106] discussed the flow and heat transfer characteristics in a free convective boundary layer flow of an optically dense viscous fluid over an isothermal truncated cone in the presence of thermal radiation. Postelnicu [79] provided the non-similar solution for free convective flow of an incompressible micropolar fluid about a truncated cone subjected to a isothermal boundary condition. The boundary layer analysis for micropolar fluid flow over the vertical frustum of a cone with power-law variation in temperature has been studied by Cheng [21]. Recently, Elbashbeshy *et al.* [30] considered the free convective flow over a truncated cone in the presence of thermal radiation and heat generation/absorption effects (for more references, see the

[1] Case(a): Published in "**Int. J. Appl. Comput. Math**", DOI: 10.1007/s40819-016-0227-y (2016)
Case(b) Accepted in "**International Journal of Nonlinear Sciences and Numerical Simulation**"

citaitons therein).

In a fluid flow system, the Soret (thermal-diffusion) effect is a thermodynamic phenomenon in which the molecules in fluids are carried in a multi-component mixture impelled by temperature gradients. It become significant when large density differences exist in a flow regime. For example, the Soret effect can be notable when species are introduced at the surface in a fluid domain with a density lower than the surrounding fluid. From the literature, it seems that a very limited work has been reported on the convective flow of a micropolar fluid over different surface geometries with the Soret effect [7, 98, 99].

Since the viscous dissipation acts as a heat source and initiates substantial temperature in the medium, many investigators have been tried to explore the significance of viscous dissipation in Newtonian and non-Newtonian fluids through various geometries in the recent past. Amin and Mohammadein [27] analyzed the Joule heating and viscous dissipation effects on the magneto-hydromagnetic free convective flow of micropolar fluid with Heimenz slip but, Haque *et al.* [35] considered the same effects with constant heat and mass fluxes in the absence of Heimenz slip. Ahmad *et al.* [2] discussed the micropolar fluid flow over a nonlinearly stretching sheet in the presence of viscous dissipation effect.

In this chapter, the non-similarity solution is provided to analyse the Soret and viscous dissipation effects on a micropolar fluid flow over a truncated cone with the convective boundary condition. According to the author's knowledge, the present study has not been discussed in the literature. For this complex problem, the similarity solution does not exist and hence suitable non-similarity transformations are used to transform the governing equations along with the boundary conditions into non-dimensional form. To find the solution of the present setup, the spectral quasi-linearization method explained in the previous chapters (i.e., Chapters 2 - 5) requires some modification. Hence, the spectral quasi-linearization method has been modified by combining it with implicit finite difference method, named as the extended spectral quasi-linearization method. In this chapter, the system of reduced non-linear partial differential equations are solved by the extended spectral quasi-linearization method. The effects of pertinent parameters on the non-dimensional velocity, microrotation, temperature and concentration profiles as well as, on the surface drag, wall couple stress, heat and mass transfer rates are analyzed.

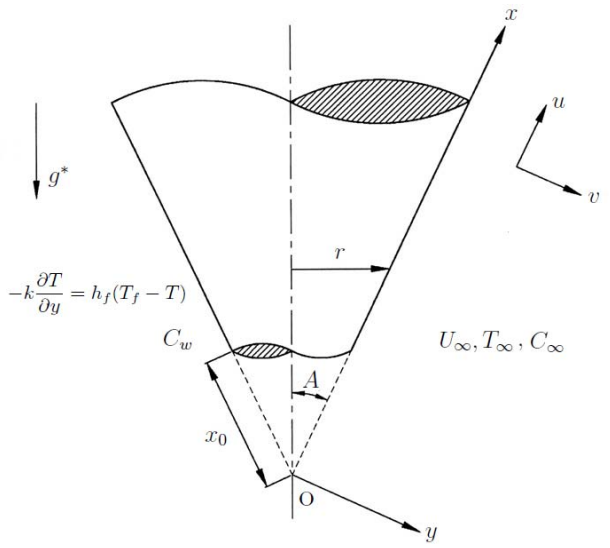

Figure 6.1: *Physical geometry of the problem*

6.2 Mathematical Formulation

Consider the steady, two-dimensional and laminar flow of an incompressible micropolar fluid over a truncated cone. The velocity of the outer flow is assumed to be U_∞. The origin O of the coordinate system is placed at the vertex of a full cone, where x-axis is taken along the surface of the cone measured from the origin and y-axis is normal to the surface [Fig. (6.1)]. The temperature and concentration of the ambient medium are assumed to be T_∞ and C_∞, respectively. The surface of a truncated cone is either cooled or heated by convection from a fluid of temperature T_f with $T_f < T_\infty$ (cooled surface) and $T_f > T_\infty$ (heated surface) respectively. The truncated cone surface is held at constant concentration C_w. The thickness of boundary layer is assumed to be comparatively small in comparison with the radius of a cone and hence the local radius to a point can be approximated by $r = xsinA$ (Ref. Singh *et al.* [92]).

By employing standard boundary layer assumptions and Boussinesq approximation, the governing equations of an incompressible micropolar fluid flow over a truncated cone [68, 79] can be written as

$$\frac{\partial(u\,r)}{\partial x} + \frac{\partial(v\,r)}{\partial y} = 0 \tag{6.1}$$

$$\rho\left(u\,\frac{\partial u}{\partial x} + v\,\frac{\partial u}{\partial y}\right) = (\mu+\kappa)\,\frac{\partial^2 u}{\partial y^2} + \kappa\,\frac{\partial \omega}{\partial y} + \rho g^*\left[\beta_T(T-T_\infty) + \beta_C(C-C_\infty)\right]\cos A \tag{6.2}$$

$$\rho j \left(u \frac{\partial \omega}{\partial x} + v \frac{\partial \omega}{\partial y} \right) = \gamma \frac{\partial^2 \omega}{\partial y^2} - \kappa \left(2\omega + \frac{\partial u}{\partial y} \right) \tag{6.3}$$

$$u \frac{\partial T}{\partial x} + v \frac{\partial T}{\partial y} = \alpha \frac{\partial^2 T}{\partial y^2} + \frac{\mu + \kappa}{\rho C_p} \left(\frac{\partial u}{\partial y} \right)^2 \tag{6.4}$$

$$u \frac{\partial C}{\partial x} + v \frac{\partial C}{\partial y} = D \frac{\partial^2 C}{\partial y^2} + \frac{D K_T}{T_m} \frac{\partial^2 T}{\partial y^2} \tag{6.5}$$

where r is the radius of the vertical frustum of a cone, K_T is the thermal diffusion ratio, T_m is the mean fluid temperature and C_p is the specific heat.

The associated boundary conditions are

$$u = 0,\, v = 0,\, \omega = -n \frac{\partial u}{\partial y},\, -k \frac{\partial T}{\partial y} = h_f (T_f - T),\, C = C_w \text{ at } y = 0 \tag{6.6a}$$

$$u = U_\infty,\, \omega = 0,\, T = T_\infty,\, C = C_\infty \text{ as } y \to \infty \tag{6.6b}$$

Now, we define a stream function ψ, such that it satisfies the continuity equation automatically, defined as

$$u = \frac{1}{r} \frac{\partial \psi}{\partial y},\; v = -\frac{1}{r} \frac{\partial \psi}{\partial x} \tag{6.7}$$

6.2.1 Case(a): Natural Convection

The flow is assumed to be a natural convection which is caused by buoyancy forces only without any external agent, hence the velocity of the external flow become zero ($ie., U_\infty = 0$). We introduce the following transformations

$$\xi = \frac{\overline{x}}{x_0} = \frac{x - x_0}{x_0},\, \eta = \frac{y}{\overline{x}} Gr_x^{1/4},\, \psi = r\nu Gr_x^{1/4} f(\xi, \eta),$$

$$\omega = \frac{\nu Gr_x^{3/4}}{\overline{x}^2} g(\xi, \eta),\, \theta(\xi, \eta) = \frac{T - T_\infty}{T_f - T_\infty},\, \phi(\xi, \eta) = \frac{C - C_\infty}{C_w - C_\infty} \tag{6.8}$$

where $\overline{x} = x - x_0$ and $Gr_x = \dfrac{g^* \beta_T (T_f - T_\infty) \overline{x}^3 cosA}{\nu^2}$ is the local Grashof number.

Substituting (6.7)-(6.8) into Eqs.(6.2)-(6.5), the governing equations reduces to the following

form

$$\left(\frac{1}{1-N}\right) f''' + \left(R+\frac{3}{4}\right) f\, f'' - \frac{1}{2}(f')^2 + \left(\frac{N}{1-N}\right) g' + \theta + \mathcal{B}\phi = \xi\left(f'\,\frac{\partial f'}{\partial \xi} - f''\frac{\partial f}{\partial \xi}\right) \tag{6.9}$$

$$\left(\frac{2-N}{2-2N}\right) g'' + \left(R+\frac{3}{4}\right) f\, g' - \frac{1}{4}\, f'\, g - \xi^{1/2}\left(\frac{N}{1-N}\right)(2g+f'') = \xi\left(f'\,\frac{\partial g}{\partial \xi} - g'\frac{\partial f}{\partial \xi}\right) \tag{6.10}$$

$$\frac{1}{Pr}\theta'' + \left(R+\frac{3}{4}\right) f\,\theta' + \xi\,\varepsilon\left(\frac{1}{1-N}\right)(f'')^2 = \xi\left(f'\,\frac{\partial \theta}{\partial \xi} - \theta'\frac{\partial f}{\partial \xi}\right) \tag{6.11}$$

$$\frac{1}{Sc}\phi'' + \left(R+\frac{3}{4}\right) f\,\phi' + Sr\,\theta'' = \xi\left(f'\,\frac{\partial \phi}{\partial \xi} - \phi'\frac{\partial f}{\partial \xi}\right) \tag{6.12}$$

where the prime represents the partial differentiation with respect to η, $\mathcal{B} = \dfrac{Gc_x}{Gr_x}$ is the buoyancy ratio, $Gc_x = \dfrac{g^*\beta_C(C_w - C_\infty)\overline{x}^3 cosA}{\nu^2}$ is the solutal Grashof number, $Sr = \dfrac{DK_T(T_f - T_\infty)}{\nu T_m(C_w - C_\infty)}$ is the Soret number and $\varepsilon = \dfrac{g^*\,\beta_T x_0 cosA}{C_p}$ is the viscous dissipation parameter.

The corresponding boundary conditions in the non-dimensional form become

$$f(\xi,0) + \frac{\xi}{\left(R+\frac{3}{4}\right)}\frac{\partial f}{\partial \xi} = 0,\ f'(\xi,0) = 0,\ g(\xi,0) = -nf''(\xi,0), \tag{6.13a}$$

$$\theta'(\xi,0) = -\xi^{1/4}\, Bi(1-\theta(\xi,0)),\ \phi(\xi,0) = 1$$

$$f'(\xi,\infty) = 0,\ g(\xi,\infty) = 0,\ \theta(\xi,\infty) = 0,\ \phi(\xi,\infty) = 0 \tag{6.13b}$$

where $\dfrac{g^*\beta_T(T_f - T_\infty){x_0}^3 cosA}{\nu^2}$ is the thermal Grashof number based on x_0, $Bi = \dfrac{h_f\, x_0}{k\, Gr_{x_0}^{1/4}}$ is the Biot number and $R = \dfrac{\xi}{1+\xi}$. When $\xi = 0$, R becomes zero, and hence the current problem reduces to the free convective flow of micropolar fluid along a vertical plate. Since $\xi = (x - x_0)/x_0$, ξ becomes large means x is far down-stream or the cross section radius of the leading edge of truncated cone is very small. Finally, as $\xi \to \infty$, $R \to 1$ (i,e. the geometry of the present problem becomes a full cone).

The wall shear stress, wall couple stress, heat and mass transfer rates over a truncated cone are

$$\tau_w = \left[(\mu+\kappa)\frac{\partial u}{\partial y} + \kappa\omega\right]_{y=0},\ m_w = \gamma\left[\frac{\partial \omega}{\partial y}\right]_{y=0}, q_w = -k\left[\frac{\partial T}{\partial y}\right]_{y=0} \text{and } q_m = -D\left[\frac{\partial C}{\partial y}\right]_{y=0} \tag{6.14}$$

The dimensionless skin friction $C_f = \dfrac{2\tau_w}{\rho u_*^2}$, wall couple stress $M_w = \dfrac{m_w}{\rho u_*^2 x_0}$, local Nusselt number

$Nu_x = \dfrac{q_w \overline{x}}{k(T_f - T_\infty)}$ and local Sherwood number $Sh_x = \dfrac{q_m \overline{x}}{D(C_w - C_\infty)}$, are given by

$$\left.\begin{aligned} &C_f \mathrm{Gr}_x^{1/4} = 2\left(\frac{1-nN}{1-N}\right) f''(\xi,0),\ M_w \mathrm{Gr}_x^{1/2} = \xi^{1/2}\left(\frac{2-N}{2-2N}\right) g'(\xi,0), \\ &\frac{Nu_x}{\mathrm{Gr}_x^{1/4}} = -\theta'(\xi,0),\ \ \frac{Sh_x}{\mathrm{Gr}_x^{1/4}} = -\phi'(\xi,0) \end{aligned}\right\} \tag{6.15}$$

where u_* is the characteristic velocity.

Numerical Solution

In earlier chapters, the spectral quasilinearization method is used to find the solution of system of non-linear ordinary differential equations. In this chapter, the extended SQLM [93] is used to get the non-similarity solution of non-linear and non-homogeneous partial differential equations (6.9)-(6.12) along with the boundary conditions (6.13). Applying QLM on Eqs. (6.9)-(6.12), the nonlinear partial differential equations reduce to the iterative sequence of linearized partial differential equations in the following form

$$\left(\frac{1}{1-N}\right) f'''_{r+1} + \left(\frac{N}{1-N}\right) g'_{r+1} + a_{1,r}\, f''_{r+1} + a_{2,r}\, f'_{r+1} + a_{3,r}\, f_{r+1} + a_{4,r} \tag{6.16}$$

$$+\theta_{r+1} + \mathcal{B}\,\phi_{r+1} = a_{5,r}\frac{\partial f'_{r+1}}{\partial \xi} + a_{6,r}\frac{\partial f_{r+1}}{\partial \xi}$$

$$\left(\frac{2-N}{2-2N}\right) g''_{r+1} + b_{1,r}\, g'_{r+1} + b_{2,r}\, g_{r+1} - \xi^{1/2}\left(\frac{N}{1-N}\right) f''_{r+1} + b_{3,r}\, f'_{r+1} \tag{6.17}$$

$$+b_{4,r}\, f_{r+1} + b_{5,r} = b_{6,r}\frac{\partial g_{r+1}}{\partial \xi} + b_{7,r}\frac{\partial f_{r+1}}{\partial \xi}$$

$$\frac{1}{Pr}\,\theta''_{r+1} + c_{1,r}\,\theta'_{r+1} + c_{2,r}\, f''_{r+1} + c_{3,r}\, f'_{r+1} + c_{4,r}\, f_{r+1} + c_{5,r} = c_{6,r}\frac{\partial \theta_{r+1}}{\partial \xi} + c_{7,r}\frac{\partial f_{r+1}}{\partial \xi} \tag{6.18}$$

$$\frac{1}{Sc}\,\phi''_{r+1} + d_{1,r}\,\phi'_{r+1} + d_{2,r}\, f'_{r+1} + d_{3,r}\, f_{r+1} + Sr\theta''_{r+1} + d_{4,r} = d_{5,r}\frac{\partial \phi_{r+1}}{\partial \xi} + d_{6,r}\frac{\partial f_{r+1}}{\partial \xi} \tag{6.19}$$

where $a_{1,r} = \left(R + \dfrac{3}{4}\right) f_r + \xi\,\dfrac{\partial f_r}{\partial \xi};\ a_{2,r} = -f'_r - \xi\,\dfrac{\partial f'_r}{\partial \xi};\ a_{3,r} = \left(R + \dfrac{3}{4}\right) f''_r;$

$$a_{4,r} = -\left(R + \frac{3}{4}\right) f_r\ f''_r + \frac{1}{2} f'^2_r + \xi f'_r \frac{\partial f'_r}{\partial \xi} - \xi f''_r \frac{\partial f_r}{\partial \xi};\ a_{5,r} = \xi\, f'_r;\ a_{6,r} = -\xi\, f''_r;$$

$$b_{1,r} = \left(R + \frac{3}{4}\right) f_r + \xi \frac{\partial f_r}{\partial \xi};\ b_{2,r} = -\frac{1}{4} f'_r - 2\xi^{1/2} \left(\frac{N}{1-N}\right);$$

$$b_{3,r} = -\frac{1}{4} g_r - \xi \frac{\partial g_r}{\partial \xi};\ b_{4,r} = \left(R + \frac{3}{4}\right) g'_r;\ b_{6,r} = \xi f'_r;\ b_{7,r} = -\xi g'_r;$$

$$b_{5,r} = -\left(R + \frac{3}{4}\right) f_r\, g'_r + \frac{1}{4} f'_r\, g_r + \xi f'_r \frac{\partial g_r}{\partial \xi} - \xi g'_r \frac{\partial f_r}{\partial \xi};\ c_{2,r} = 2\xi\, \varepsilon \left(\frac{1}{1-N}\right) f''_r;$$

$$c_{1,r} = \left(R + \frac{3}{4}\right) f_r + \xi \frac{\partial f_r}{\partial \xi};\ c_{3,r} = -\xi \frac{\partial \theta_r}{\partial \xi};\ c_{4,r} = \left(R + \frac{3}{4}\right) \theta'_r;$$

$$c_{5,r} = -\left(R + \frac{3}{4}\right) f_r\, \theta'_r - \xi\, \varepsilon \left(\frac{1}{1-N}\right) f''^2_r + \xi f'_r \frac{\partial \theta_r}{\partial \xi} - \xi \theta'_r \frac{\partial f_r}{\partial \xi};\ c_{6,r} = \xi f'_r;$$

$$c_{7,r} = -\xi \theta'_r;\ d_{1,r} = \left(R + \frac{3}{4}\right) f_r + \xi \frac{\partial f_r}{\partial \xi};\ d_{2,r} = -\xi \frac{\partial \phi_r}{\partial \xi};\ d_{3,r} = \left(R + \frac{3}{4}\right) \phi'_r;$$

$$d_{4,r} = -\left(R + \frac{3}{4}\right) f_r\, \phi'_r + \xi f'_r \frac{\partial \phi_r}{\partial \xi} - \xi \phi'_r \frac{\partial f_r}{\partial \xi};\ d_{5,r} = \xi f'_r;\ d_{6,r} = -\xi \phi'_r$$

The linearised system of coupled partial differential equations (6.16) - (6.19) with the variable coefficients can be solved iteratively by employing the Chebyshev pseudo-spectral method [18]. Starting from the set of initial approximations f_0, g_0, θ_0, ϕ_0, the iteration scheme (6.16) - (6.19) can be worked out iteratively for $f_{r+1}(\xi, \eta)$, $g_{r+1}(\xi, \eta)$, $\theta_{r+1}(\xi, \eta)$, $\phi_{r+1}(\xi, \eta)$ when r = 0, 1, 2,.... To solve Eqs. (6.16) - (6.19), first we discretize the equations using the Chebyshev spectral collocation method in the η-direction and then we employ the implicit finite difference method in ξ-direction. The basic idea behind the spectral collocation method is that the introduction of a differentiation matrix D, which is used to approximate the unknown variable derivatives at the collocation points as the matrix vector product

$$\frac{df}{d\eta} = \sum_{k=0}^{N_x} D_{lk} f(\tau_k) = \mathbf{DF}, \quad l = 0, 1, ..., N_x \tag{6.20}$$

where N_x+1 is the number of collocation points in η direction, $\mathbf{D} = \dfrac{2\mathcal{D}}{L}$ and $\mathbf{F} = [f(\tau_0), ..., f(\tau_{N_x})]^T$ represents the vector function at the collocation points. In the similar manner, vector functions corresponding to g, θ and ϕ are represented by $\mathbf{G}$, Θ and Φ respectively. Derivatives of higher order are obtained as powers of $\mathbf{D}$,

$$f^{(q)} = \mathbf{D}^q \mathbf{F},\ g^{(q)} = \mathbf{D}^q \mathbf{G},\ \theta^{(q)} = \mathbf{D}^q \Theta,\ \phi^{(q)} = \mathbf{D}^q \Phi \tag{6.21}$$

here q represents the order of the derivative. In the governing problem, the physical region in

the space direction is approximated by truncated domain $[0, \eta_\infty]$, and this truncated domain is transformed into the region $[-1, 1]$ using the mapping $\eta = \dfrac{\eta_\infty(\tau+1)}{2}$, where η_∞ is the finite length selected as numerically large value to approximate the conditions at infinity.

The collocation points on (η, ξ) are defined as

$$\tau_j = \cos\frac{\pi j}{N_x}, \;\; \xi^n = n\Delta\xi \quad\quad j = 0, 1, 2, ..., N_x, \;\; n = 0, 1, 2, ..., N_t \tag{6.22}$$

where $N_x + 1$, $N_t + 1$ are number of grid points in η and ξ directions respectively, and $\Delta\xi$ denotes the spacing in the ξ-direction. The finite difference method with centering about midpoint halfway between ξ^n and ξ^{n+1} is used where the midpoint is defined as $\xi^{n+\frac{1}{2}} = (\xi^{n+1} + \xi^n)/2$. The derivatives with respect to η are defined in terms of the Chebyshev differentiation matrices. In the procedure of applying the centering process about $\xi^{n+\frac{1}{2}}$ to any function, say $f(\xi, \eta)$, its related derivatives can be written as

$$f(\xi^{n+\frac{1}{2}}, \eta_j) = f_j^{n+\frac{1}{2}} = \frac{f_j^{n+1} + f_j^n}{2} \tag{6.23}$$

$$\left(\frac{\partial f}{\partial \xi}\right)_j^{n+\frac{1}{2}} = \frac{f_j^{n+1} - f_j^n}{\Delta\xi} \tag{6.24}$$

Apply the spectral method on Eqs. (6.16) - (6.19), with the finite difference in ξ direction, leads to the system of matrix equation as follows:

$$\begin{bmatrix} A_{11} & A_{12} & A_{13} & A_{14} \\ A_{21} & A_{22} & A_{23} & A_{24} \\ A_{31} & A_{32} & A_{33} & A_{34} \\ A_{41} & A_{42} & A_{43} & A_{44} \end{bmatrix} \begin{bmatrix} F_{r+1}^{n+1} \\ G_{r+1}^{n+1} \\ \Theta_{r+1}^{n+1} \\ \Phi_{r+1}^{n+1} \end{bmatrix} = \begin{bmatrix} B_{11} & B_{12} & B_{13} & B_{14} \\ B_{21} & B_{22} & B_{23} & B_{24} \\ B_{31} & B_{32} & B_{33} & B_{34} \\ B_{41} & B_{42} & B_{43} & B_{44} \end{bmatrix} \begin{bmatrix} F_{r+1}^{n} \\ G_{r+1}^{n} \\ \Theta_{r+1}^{n} \\ \Phi_{r+1}^{n} \end{bmatrix} + \begin{bmatrix} K_1 \\ K_2 \\ K_3 \\ K_4 \end{bmatrix} \tag{6.25}$$

where $A_{11} = \dfrac{1}{2}\left[\left(\dfrac{1}{1-N}\right)\mathbf{D}^3 + a_{1,r}^{n+\frac{1}{2}}\mathbf{D}^2 + a_{2,r}^{n+\frac{1}{2}}\mathbf{D} + a_{3,r}^{n+\frac{1}{2}}\right] - \dfrac{a_{5,r}^{n+\frac{1}{2}}\mathbf{D}}{\Delta\xi} - \dfrac{a_{6,r}^{n+\frac{1}{2}}}{\Delta\xi}$;

$A_{12} = \dfrac{1}{2}\left[\left(\dfrac{N}{1-N}\right)\mathbf{D}\right]$; $A_{13} = \dfrac{1}{2}\mathbf{I}$; $A_{14} = \dfrac{1}{2}B\,\mathbf{I}$;

$A_{21} = \dfrac{1}{2}\left[-(\xi^{1/2})^{n+\frac{1}{2}}\left(\dfrac{N}{1-N}\right)\mathbf{D}^2 + b_{3,r}^{n+\frac{1}{2}}\mathbf{D} + b_{4,r}^{n+\frac{1}{2}}\right] - \dfrac{b_{7,r}^{n+\frac{1}{2}}}{\Delta\xi}$; $A_{24} = \mathbf{0}$;

$A_{22} = \dfrac{1}{2}\left[\left(\dfrac{2-N}{2-2N}\right)\mathbf{D}^2 + b_{1,r}^{n+\frac{1}{2}}\mathbf{D} + b_{2,r}^{n+\frac{1}{2}}\right] - \dfrac{b_{6,r}^{n+\frac{1}{2}}}{\Delta\xi}$; $A_{23} = \mathbf{0}$;

$$A_{31} = \frac{1}{2}\left[c_{2,r}^{n+\frac{1}{2}}\mathbf{D}^2 + c_{3,r}^{n+\frac{1}{2}}\mathbf{D} + c_{4,r}^{n+\frac{1}{2}}\right] - \frac{c_{7,r}^{n+\frac{1}{2}}}{\Delta\xi};\ A_{32} = \mathbf{0};$$

$$A_{33} = \frac{1}{2}\left[\frac{1}{Pr}\mathbf{D}^2 + c_{1,r}^{n+\frac{1}{2}}\mathbf{D}\right] - \frac{c_{6,r}^{n+\frac{1}{2}}}{\Delta\xi};\ A_{34} = \mathbf{0};$$

$$A_{41} = \frac{1}{2}\left[d_{2,r}^{n+\frac{1}{2}}\mathbf{D} + d_{3,r}^{n+\frac{1}{2}}\right] - \frac{d_{6,r}^{n+\frac{1}{2}}}{\Delta\xi};\ A_{42} = \mathbf{0};$$

$$A_{43} = \frac{1}{2}\left[Sr\mathbf{D}^2\right];\ A_{44} = \frac{1}{2}\left[\frac{1}{Sc}\mathbf{D}^2 + d_{1,r}^{n+\frac{1}{2}}\mathbf{D}\right] - \frac{d_{5,r}^{n+\frac{1}{2}}}{\Delta\xi};$$

$$B_{11} = -\frac{1}{2}\left[\left(\frac{1}{1-N}\right)\mathbf{D}^3 + a_{1,r}^{n+\frac{1}{2}}\mathbf{D}^2 + a_{2,r}^{n+\frac{1}{2}}\mathbf{D} + a_{3,r}^{n+\frac{1}{2}}\right] - \frac{a_{5,r}^{n+\frac{1}{2}}D}{\Delta\xi} - \frac{a_{6,r}^{n+\frac{1}{2}}}{\Delta\xi};$$

$$B_{12} = -\frac{1}{2}\left[\left(\frac{N}{1-N}\right)\mathbf{D}\right];\ B_{13} = -\frac{1}{2}\mathbf{I};\ B_{14} = -\frac{1}{2}B\,\mathbf{I};$$

$$B_{21} = -\frac{1}{2}\left[-(\xi^{1/2})^{n+\frac{1}{2}}\left(\frac{N}{1-N}\right)\mathbf{D}^2 + b_{3,r}^{n+\frac{1}{2}}\mathbf{D} + b_{4,r}^{n+\frac{1}{2}}\right] - \frac{b_{7,r}^{n+\frac{1}{2}}}{\Delta\xi};\ B_{23} = \mathbf{0};$$

$$B_{22} = -\frac{1}{2}\left[\left(\frac{2-N}{2-2N}\right)\mathbf{D}^2 + b_{1,r}^{n+\frac{1}{2}}\mathbf{D} + b_{2,r}^{n+\frac{1}{2}}\right] - \frac{b_{6,r}^{n+\frac{1}{2}}}{\Delta\xi};\ B_{24} = \mathbf{0};$$

$$B_{31} = -\frac{1}{2}\left[c_{2,r}^{n+\frac{1}{2}}\mathbf{D}^2 + c_{3,r}^{n+\frac{1}{2}}\mathbf{D} + c_{4,r}^{n+\frac{1}{2}}\right] - \frac{c_{7,r}^{n+\frac{1}{2}}}{\Delta\xi};\ B_{32} = \mathbf{0};$$

$$B_{33} = -\frac{1}{2}\left[\frac{1}{Pr}\mathbf{D}^2 + c_{1,r}^{n+\frac{1}{2}}\mathbf{D}\right] - \frac{c_{6,r}^{n+\frac{1}{2}}}{\Delta\xi};\ B_{34} = \mathbf{0};$$

$$B_{41} = -\frac{1}{2}\left[d_{2,r}^{n+\frac{1}{2}}\mathbf{D} + d_{3,r}^{n+\frac{1}{2}}\right] - \frac{d_{6,r}^{n+\frac{1}{2}}}{\Delta\xi};\ B_{42} = \mathbf{0};$$

$$B_{43} = -\frac{1}{2}\left[Sr\mathbf{D}^2\right];\ B_{44} = -\frac{1}{2}\left[\frac{1}{Sc}\mathbf{D}^2 + d_{1,r}^{n+\frac{1}{2}}\mathbf{D}\right] - \frac{d_{5,r}^{n+\frac{1}{2}}}{\Delta\xi};$$

$$K_1 = -a_{4,r}^{n+\frac{1}{2}};\ K_2 = -b_{5,r}^{n+\frac{1}{2}};\ K_3 = -c_{5,r}^{n+\frac{1}{2}};\ K_4 = -d_{4,r}^{n+\frac{1}{2}}.$$

where A_{ij}, B_{ij}, $(i,j = 1,2,3,4)$, identity matrix $\mathbf{I}$ and zero matrix $\mathbf{0}$ are of size $(N_x+1)\times(N_x+1)$.

Numerical procedure is carried out to obtain approximate solution for the quantities of physical interest. In this chapter, a finite computational domain of extent $\eta_\infty = 30$ is chosen in the η-direction. Through numerical experimentation, this value has been found to give accurate results for all the selected physical parameters used in the generation of results. Moreover, the results have

Table 6.1: Comparison of $f''(0,0)$ and $-\theta'(0,0)$, for various values of Pr between the present method and the results obtained by Yih [106].

Pr	$f''(0,0)$		$-\theta'(0,0)$	
	Yih [106]	Present	Yih [106]	Present
1	0.9084	0.90819	0.4012	0.40103
10	0.5927	0.59283	0.8266	0.82684
100	0.3559	0.35594	1.5493	1.54953

not been changed with the increase of η_∞ to a significant extent. The number of collocation points N_x used in the spectral method for discretization is 100. Note that at each time step, the SQLM algorithm allocated on computation value of some quantity, say F_{r+1}^{n+1}. This is attained by iteration procedure using the quasi-linearization method with a known value at the previous time step n as initial approximation. The iteration calculations are carried until some appropriate tolerance level, ϵ_1 is obtained. In this analysis, the tolerance level has fixed to be 10^{-4}. The tolerance level is defined as the maximum values of the infinity norm of the difference between the values of the calculated quantities. For example, in calculating F_{r+1}^{n+1}, the tolerance level and convergence criteria are defined as

$$\max\{\|f'^{n+1}_{r+1} - f'^{n}_{r+1}\|_\infty, \|g^{n+1}_{r+1} - g^{n}_{r+1}\|_\infty, \|\theta^{n+1}_{r+1} - \theta^{n}_{r+1}\|_\infty, \|\phi^{n+1}_{r+1} - \phi^{n}_{r+1}\|_\infty\} < \epsilon_1 \tag{6.26}$$

To ensure the accuracy of the results, a sufficiently small step size $\Delta\xi$ has been taken. The step size preferred to be small enough such that further reduction did not alter the obtained results for the flow properties of physical interest.

Results and Discussion

In order to assess the accuracy of the present method, for the special case of $N = 0$, $Bi \to \infty$, $\mathcal{B} = 0$, $\varepsilon = 0$ and $Sr = 0$, the results of the present problem have been compared with that of Yih [106] and it seems to be good agreement [Tab. (6.1)]. To study the effects of viscous dissipation parameter, coupling, Soret and Biot numbers, the computations have been carried out for $Pr = 0.71$, $n = 0$, $\xi = 0.5$, and $Sc = 0.22$. These values are fixed in this analysis unless otherwise specified.

Figs. 6.2(a) - 6.2(d) display the effects of coupling number on the non-dimensional velocity f', microrotation g, temperature θ and concentration ϕ in the presence and/or absence of Soret number. The coupling number characterizes the coupling of rotational and linear motion arising from the motion of the fluid particles. The micropolarity is absent in the case of $N = 0$ (i.e., as κ tends to zero) and hence, the fluid becomes non-polar fluid. As the coupling number N increases, the velocity decreases near the vertical frustum of a cone and far away from the surface it increases [Fig. 6.2(a)]. From Fig. 6.2(b), it can be remarked that the microrotation profiles tends to become flat at $N = 0$, and further, the microrotation shows reverse rotation with coupling number N enhancement. It can be perceived from Figs. 6.2(c) and 6.2(d) that the temperature and concentration of the micropolar fluid are higher in comparison with the viscous fluid. It is important to note that the velocity (near the truncated cone surface) and concentration are more in the presence of Soret number as compared with those results in the absence of Soret number. The temperature and microrotation don not show any significant effect with the increase of Soret number.

The variation of Biot number on the dimensionless velocity f', microrotation g, temperature θ and concentration ϕ for both $\varepsilon = 0.0$ and $\varepsilon = 0.2$, is plotted in Fig. 6.3(a) - 6.3(d). From Fig. 6.3(a), it can be observed that the velocity rises near the truncated cone and far away from a truncated cone the velocity diminishes with an increase in Biot number. Fig. 6.3(b) shows that with an increase in Biot number, the microrotation shows reverse rotation within the boundary layer for both $\varepsilon = 0$ and $\varepsilon = 0.2$. The temperature enhances with the enhancement of Biot number, as observed in Fig. 6.3(c). From Fig. 6.3(d), it can be illustrated that as the Biot number increases, the concentration shows reverse behaviour within the boundary. The velocity and temperature increases with the increase of viscous dissipation parameter because, the viscous dissipation acts as a heat source and affects the fluid flow. Hence, it increases the thermal buoyancy effects which causes to increase in the velocity and temperature. As the viscous dissipation parameter ε increases, the concentration shows opposite behaviour within the concentration boundary layer.

The effects of coupling number on the non-dimensional skin friction, wall couple stress, heat and mass transfer rates against the streamwise coordinate ξ, are portrayed in Figs. 6.4(a) - 6.4(d) in the presence and absence of Soret number. From Fig. 6.4(a), it can be observed that the skin friction increases with an increase in the value of coupling number. It is worthy to note that, the skin friction is more for the micropolar fluid in comparison to that of the viscous fluid. As

the coupling number enhances, the wall couple stress reduces nonlinearly for the micropolar fluid [Fig. 6.4(b)]. From Fig. 6.4(c), it can be perceived that with the increase of coupling number N, the Nusselt number reduces nonlinearly. From Fig. 6.4(d), it can be illustrated that for both $Sr = 0.0$ and $Sr = 0.5$, the Sherwood number reduces by enhancing the values of coupling number N. Further, it can be noticed that the Nusselt and Sherwood numbers are lower for a micropolar fluid as compared with those of a viscous fluid. Moreover, the skin friction increases slightly, but the Nusselt number and wall couple stress decrease marginally with the increase of Soret number [Figs. 6.4(a) - 6.4(d)].

Figs. 6.5(a) - 6.5(d) depict the variation of Biot number on the non-dimensional skin friction, wall couple stress, Nusselt and Sherwood numbers against the streamwise coordinate ξ in the presence and absence of viscous dissipation parameter. From Fig. 6.5(a), it can be observed that with the enhancement of Biot number, the skin friction coefficient enhances. As the streamwise coordinate increases from 0 to 1, the wall couple stress coefficient reduces with an increase in Biot number [Fig. 6.5(b)]. Moreover, it can be noticed that the wall couple stress decreases nonlinearly with the increase of Biot number. It can be seen from Fig. 6.5(c) that an increase in Biot number leads to increase in the heat transfer rate. The mass transfer rate reduces with the enhancement of Biot number as shown in Fig. 6.5(d). It can be noticed from Figs. 6.5(a) - 6.5(d) that the skin friction and mass transfer rate are more, but the wall couple stress and heat transfer are less in the presence of viscous dissipation parameter when compared with those results in the absence of viscous dissipation parameter.

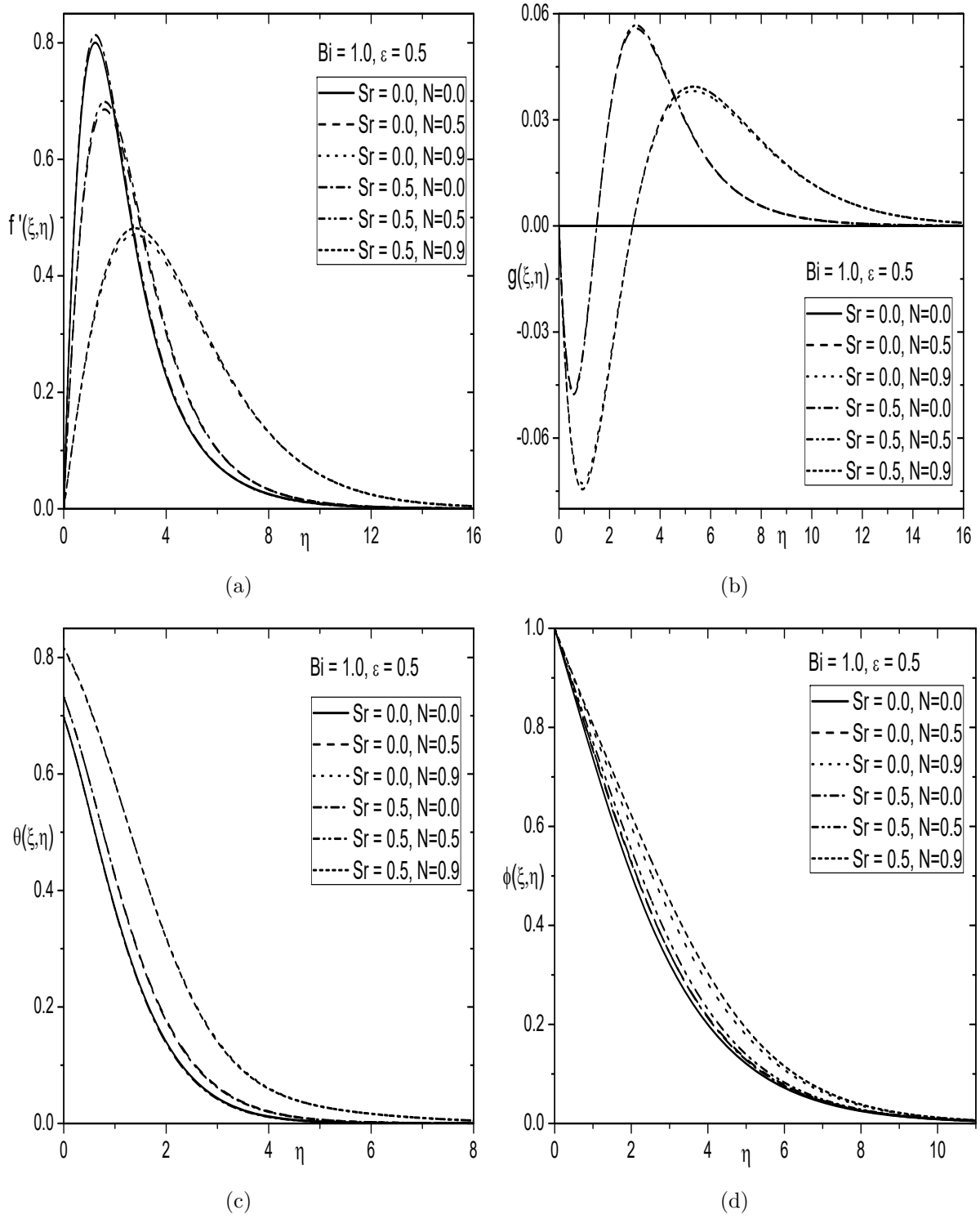

Figure 6.2: *Effects of Sr and N on (a)Velocity, (b)Microrotation, (c)Temperature and (d)Concentration.*

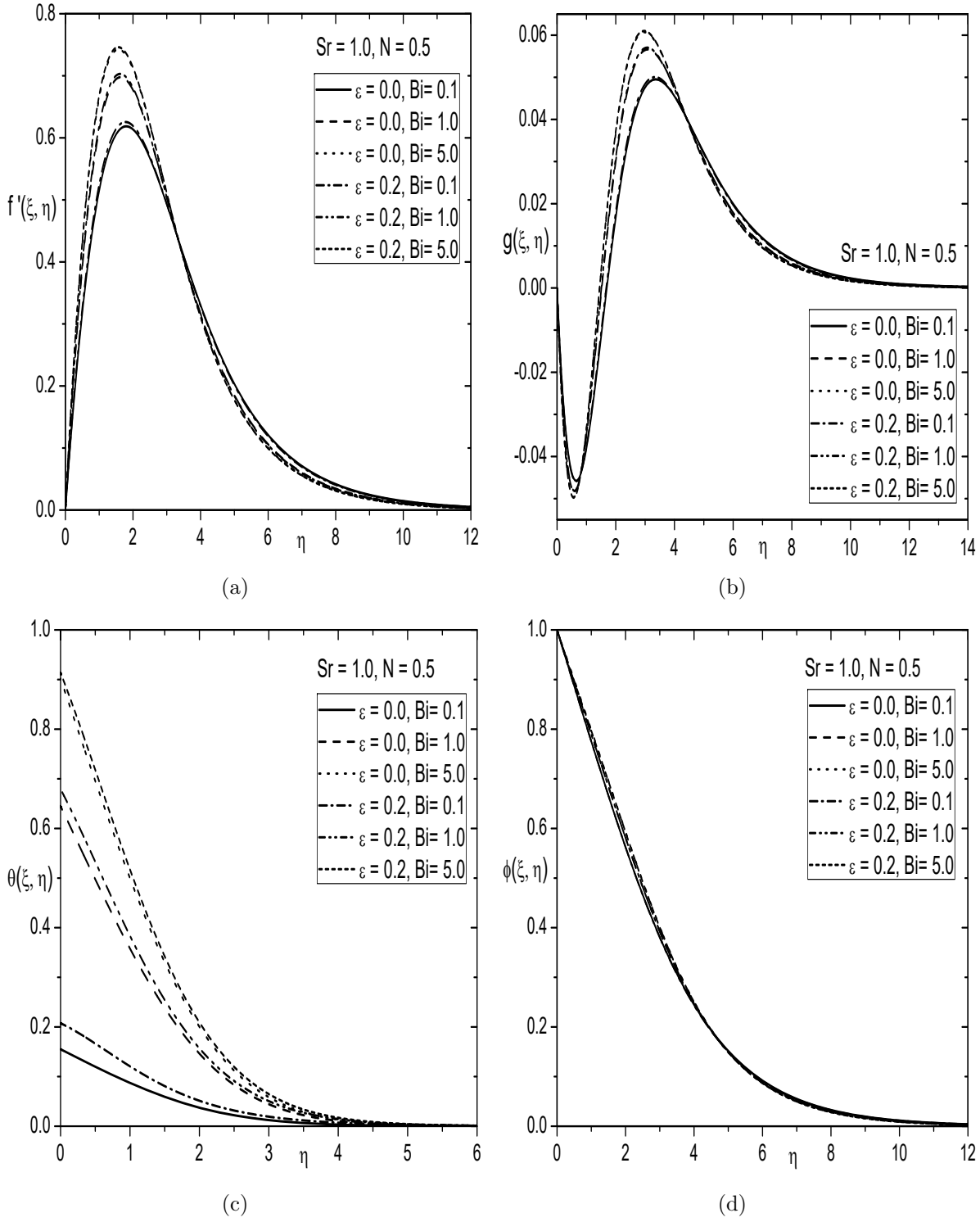

Figure 6.3: *Effects of ε and Bi on (a)Velocity, (b)Microrotation, (c)Temperature and (d)Concentration.*

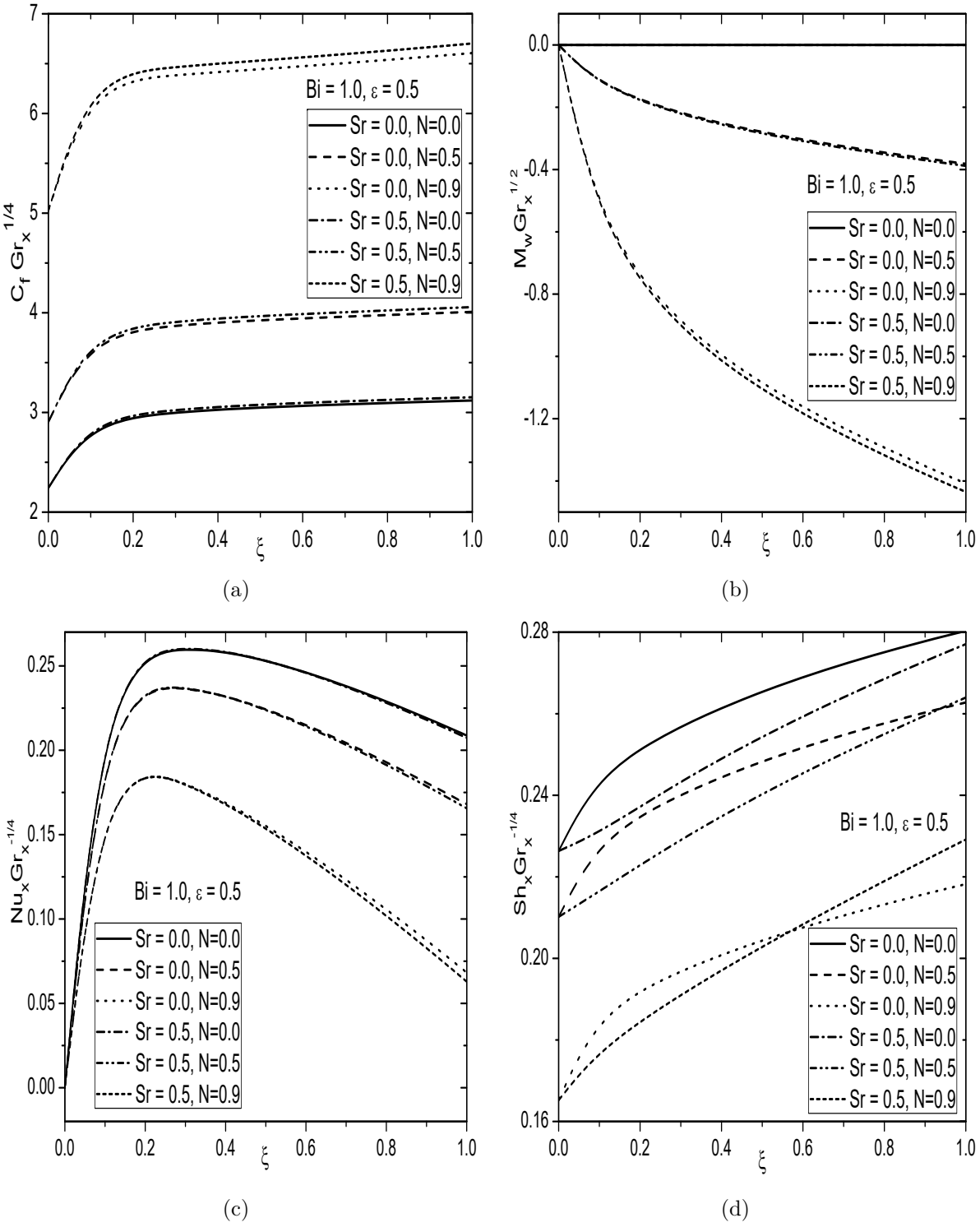

Figure 6.4: *Effects of Sr and N on (a)Skin friction, (b)Wall couple stress, (c)Nusselt number and (d)Sherwood number.*

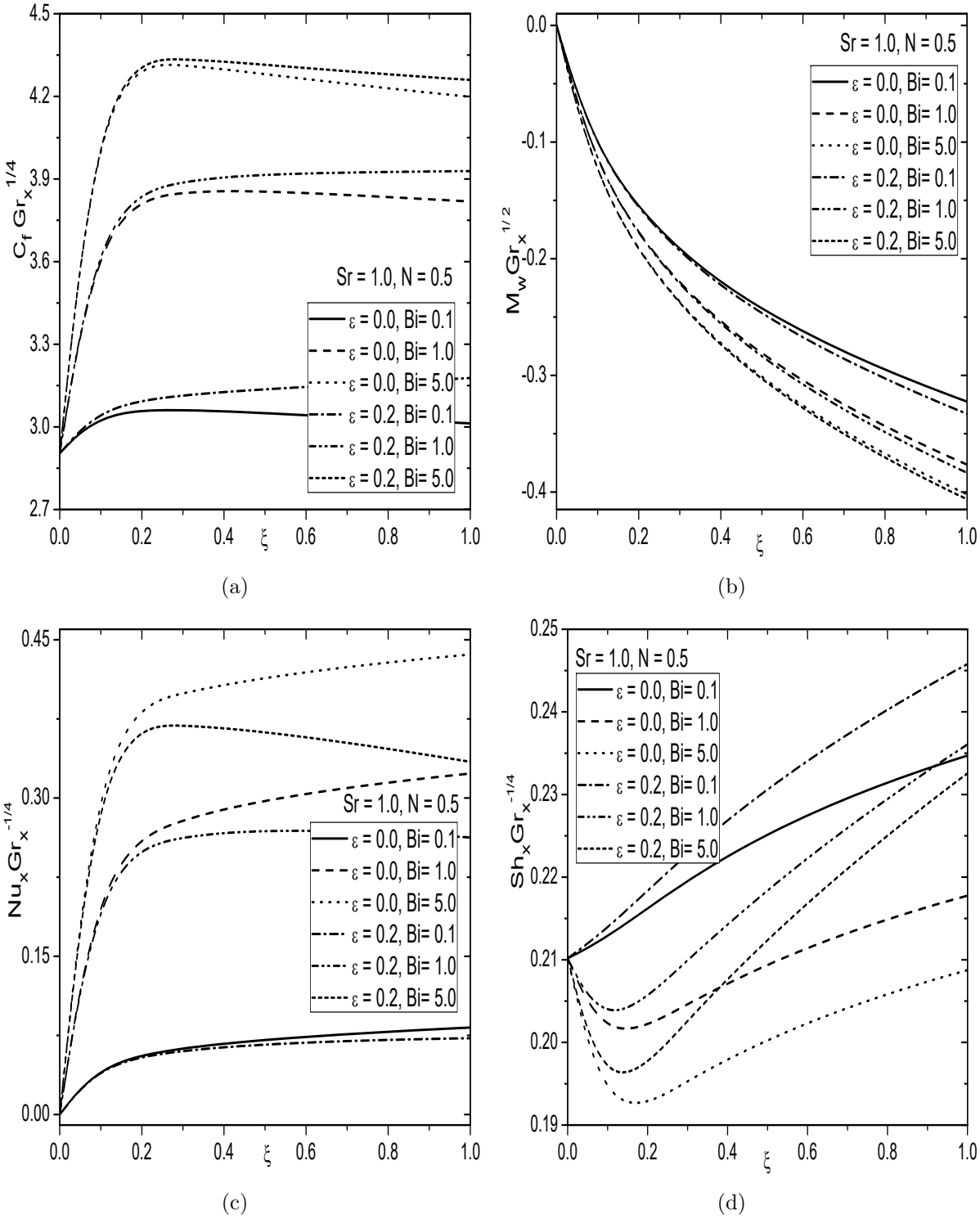

Figure 6.5: *Effects of ε and Bi on (a)Skin friction, (b)Wall couple stress, (c)Nusselt number and (d)Sherwood number.*

6.2.2 Case(b): Mixed Convection

Consider the flow to be mixed convection arises from buoyancy forces and an external flow with velocity (U_∞). We introduce the following transformations

$$\xi = \frac{\overline{x}}{x_0} = \frac{x - x_0}{x_0},\ \eta = \frac{y}{\overline{x}}\, Re_x^{1/2},\ \psi = r\nu Re_x^{1/2} f(\xi,\eta), \tag{6.27}$$

$$\omega = \frac{\nu\, Re_x^{3/2}}{\overline{x}^2}\, g(\xi,\eta),\ \theta(\xi,\eta) = \frac{T - T_\infty}{T_f - T_\infty},\ \phi(\xi,\eta) = \frac{C - C_\infty}{C_w - C_\infty}$$

where $\overline{x} = x - x_0$ and $Re_x = \dfrac{U_\infty\, \overline{x}}{\nu}$ is the local Reynolds number.

Substitution of (6.7) and (6.27) into Eqs.(6.2)- (6.5), gives the following system of differential equations:

$$\left(\frac{1}{1-N}\right) f''' + \left(R + \frac{1}{2}\right) f\, f'' + \left(\frac{N}{1-N}\right) g' + \xi\, \lambda\, (\theta + \mathcal{B}\phi) = \xi \left(f'\, \frac{\partial f'}{\partial \xi} - f''\frac{\partial f}{\partial \xi}\right) \tag{6.28}$$

$$\left(\frac{2-N}{2-2N}\right) g'' + \left(R + \frac{1}{2}\right) f\, g' + \frac{1}{2}\, f'\, g - \xi \left(\frac{N}{1-N}\right)(2g + f'') = \xi \left(f'\, \frac{\partial g}{\partial \xi} - g'\frac{\partial f}{\partial \xi}\right) \tag{6.29}$$

$$\frac{1}{Pr}\theta'' + \left(R + \frac{1}{2}\right) f\, \theta' + \varepsilon \left(\frac{1}{1-N}\right)(f'')^2 = \xi \left(f'\, \frac{\partial \theta}{\partial \xi} - \theta'\frac{\partial f}{\partial \xi}\right) \tag{6.30}$$

$$\frac{1}{Sc}\phi'' + \left(R + \frac{1}{2}\right) f\, \phi' + Sr\, \theta'' = \xi \left(f'\, \frac{\partial \phi}{\partial \xi} - \phi'\frac{\partial f}{\partial \xi}\right) \tag{6.31}$$

where $\varepsilon = \dfrac{U_\infty^2}{C_p(T_f - T_\infty)}$ is the viscous dissipation parameter, $Re_{x_0} = \dfrac{U_\infty\, x_0}{\nu}$ is the Reynolds number based on x_0 and $\lambda = \dfrac{Gr_{x_0}}{Re_{x_0}^2}$ is the mixed convection parameter.

The boundary conditions (6.6) become

$$f(\xi,0) = \frac{-\xi}{\left(R + \frac{1}{2}\right)}\frac{\partial f}{\partial \xi},\ f'(\xi,0) = 0,\ g(\xi,0) = -nf''(\xi,0), \tag{6.32a}$$

$$\theta'(\xi,0) = -\xi^{1/2}\, Bi(1 - \theta(\xi,0)),\ \phi(\xi,0) = 1$$

$$f'(\xi,\infty) = 1,\ g(\xi,\infty) = 0,\ \theta(\xi,\infty) = 0,\ \phi(\xi,\infty) = 0 \tag{6.32b}$$

where $Bi = \dfrac{h_f\, x_0}{k\, Re_{x_0}^{1/2}}$ is the Biot number.

Table 6.2: *Comparison of $-\theta'(0,0)$ for mixed convection flow in Newtonian fluid with the results obtained by Lloyd and Sparrow [50] for different values of Pr.*

	$-\theta'(0,0)$	
Pr	Lloyd and Sparrow [50]	Present
0.03	0.08439	0.08443
0.72	0.2956	0.29564
10	0.7281	0.72814
100	1.572	1.57184

The non-dimensional skin friction $C_f = \dfrac{2\tau_w}{\rho U_\infty^2}$, wall couple stress $M_w = \dfrac{m_w}{\rho U_\infty^2 x_0}$, local Nusselt number $Nu_x = \dfrac{q_w \overline{x}}{k(T_f - T_\infty)}$ and local Sherwood number $Sh_x = \dfrac{q_m \overline{x}}{D(C_w - C_\infty)}$, are given by

$$\left.\begin{aligned} C_f Re_x^{1/2} &= 2\left(\frac{1-nN}{1-N}\right) f''(\xi,0), \quad M_w Re_x = \left(\frac{2-N}{2-2N}\right) g'(\xi,0) \\ \frac{Nu_x}{Re_x^{1/2}} &= -\theta'(\xi,0), \quad \frac{Sh_x}{Re_x^{1/2}} = -\phi'(\xi,0) \end{aligned}\right\} \tag{6.33}$$

Results and Discussion

The reduced non-dimensional partial differential equations (6.28)-(6.31) along with the boundary conditions (6.32) are solved numerically using the extended spectral quasi-linearization method, as explained in the previous case. In order to asses the code generated, for special case of $N = 0$, $\mathcal{B} = 0$, $Bi \to \infty$, $Sr = 0$, $\varepsilon = 0$, $\xi = 0$ and $\lambda = 0$, the results have been compared with those of Lloyd and Sparrow [50] and results seems to be good agreement as shown in Tab. (6.2). To study the effects of coupling number, Biot number, viscous dissipation and Soret number, the computations have been carried out for $Pr = 0.72$, $Sc = 0.22$, $\xi = 0.5$, and $n = 0$.

Figs. 6.6(a)-6.6(d) depict the influence of coupling numbers on the non-dimensional velocity f', microrotation g, temperature θ and concentration ϕ across the boundary layers with or without Soret number. Fig. 6.6(a) shows that the velocity decreases with an increase in coupling number, but it increases slightly with the increase of Soret number. As expected, the velocity in the case of viscous fluid is more as compared with that of the micropolar fluid. Fig. 6.6(b) reveals that the microrotation profiles tend to become flat at $N = 0$, and with the increase of N, it exhibits the

reverse rotation. As the Soret number enhances, the microrotation do not show significant effect. Fig. 6.6(c) displays that the temperature enhances with the increase of coupling number, but it does not show significant effect with the increase of Soret number. The occurrence of diffusion flux due to temperature gradient is treated as Soret effect. This shows that diffusive species with higher values of Soret number accelerates the concentration. Hence, the concentration increases with the enhancement of Soret numbers as depicted in Fig. 6.6(d). Finally, the concentration increases with the increase of coupling number.

The effects of Biot number on the non-dimensional velocity f', microrotation g, temperature θ and concentration ϕ, are displayed in Figs. 6.7(a)-6.7(d) in the presence and absence of viscous dissipation parameter. Fig. 6.7(a) shows that an increase in Biot number leads to increase in the fluid velocity and also, the velocity increases with the increase of viscous dissipation parameter. Fig. 6.7(b) exhibits that the microrotation slightly reduces first and then enhances with the increase of Biot number. The microrotation shows qualitatively same behaviour in the presence and absence of viscous dissipation parameter. Physically, the viscous dissipation acts as a heat source generated due to the viscous stresses acting on it and hence, it increases the temperature of the fluid. Fig. 6.7(c) depicts that the thickness of thermal boundary layer enhances with the increase of both viscous dissipation parameter as well as Biot number. Fig. 6.7(d) illustrates that the solutal boundary layer thickness enhances first and then reduces slightly with the increase of Biot number. Finally, it is noticed that the role of viscous dissipation parameter is very small on the concentration profile.

In Figs. 6.8(a)-6.8(d), the effects of mixed convection parameter λ on the dimensionless velocity, microrotation, temperature and concentration profiles across the boundary layers, are displayed. We know that, $\lambda < 0$ corresponds to the opposing flow, $\lambda = 0$ indicates the forced convective flow and $\lambda > 0$ corresponds to the aiding flow. Fig. 6.8(a) illustrates that the velocity is more in the case of aiding flow, but less in the opposing flow as compared to the forced convective flow case. The microrotation shows reverse rotation within the boundary as displayed in Fig. 6.8(b) for opposing, aiding and forced convective flows. Figs. 6.8(c)-6.8(d) show that the temperature and concentration exhibit qualitatively same behaviour with the influence of mixed convection parameter. In other words, the temperature and concentration are more in the case of opposing flow as compared with those results in the aiding and forced convective flows.

The effects of coupling number on the dimensionless skin friction, wall couple stress, Nusselt and

Sherwood numbers against the streamwise coordinate ξ for $Sr = 0.0$ and $Sr = 0.5$, are portrayed in Figs. 6.9(a)-6.9(d). Fig. 6.9(a) reveals that the skin friction coefficient increases with an increase in coupling number. Further, it can be perceived that the skin friction increases slightly with an increase in Soret number. The wall couple stress coefficient decreases with the increase of coupling number [Fig. 6.9(b)]. As the Soret number enhances, the wall couple stress reduces marginally. Fig. 6.9(c) displays that the Nusselt number reduces nonlinearly with the enhancement of coupling number, whereas, it reduces slightly with an increase in Soret number. Fig. 6.9(d) illustrates that the Sherwood number reduces with the increase of both coupling and Soret numbers. Further, it can be noticed that the Nusselt and Sherwood numbers are lower for the micropolar fluid as compared with those values of the viscous fluid.

Figs. 6.10(a)-6.10(d) depict the variation of Biot number on the non-dimensional skin friction, wall couple stress, Nusselt and Sherwood numbers against the streamwise coordinate ξ in the presence and absence of viscous dissipation. Fig. 6.10(a) reveals that the skin friction coefficient enhances with the enhancing values of Biot number and viscous dissipation parameter. Fig. 6.10(b) explores that the wall couple stress coefficient decreases with the increase of viscous dissipation parameter as well as Biot number. Fig. 6.10(c) reveals that the Nusselt number increases non-linearly with an increase in Biot number, but it decreases with an increase in viscous dissipation parameter. From Fig. 6.10(d), it can be seen that the Sherwood number reduces with the enhancement of Biot number but, it increases with the increase of viscous dissipation parameter.

The influence of mixed convection parameter on skin friction, wall couple stress, Nusselt and Sherwood numbers against the streamwise coordinate ξ , is displayed in Figs. 6.11(a) - 6.11(d). Fig. 6.11(a) portrays that the skin friction in the opposing flow is lower than compared with those of both aiding and forced convective flows. Fig. 6.11(b) depicts that the wall couple stress decreases from opposing flow to aiding flow and moreover, it can be observed that the wall couple stress in the opposing flow is more than that of the aiding flow. Fig. 6.11(c) reveals that the heat transfer rate increases from opposing to aiding flow. Fig. 6.11(d) displays that the mass transfer rate is less in the opposing flow as compared with those of the forced convective and aiding flows.

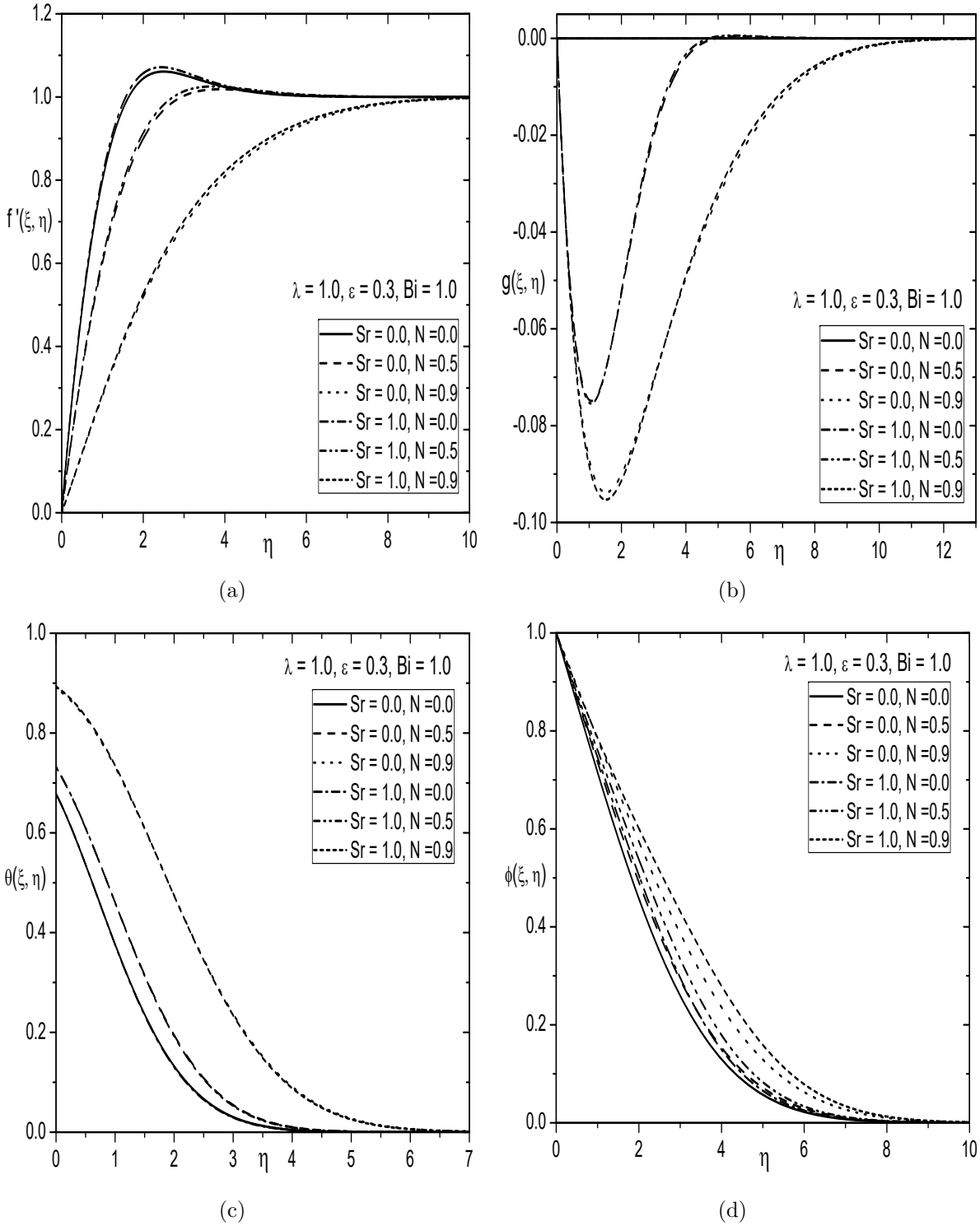

Figure 6.6: *Effects of Sr and N on (a)Velocity, (b)Microrotation, (c)Temperature and (d)Concentration profiles.*

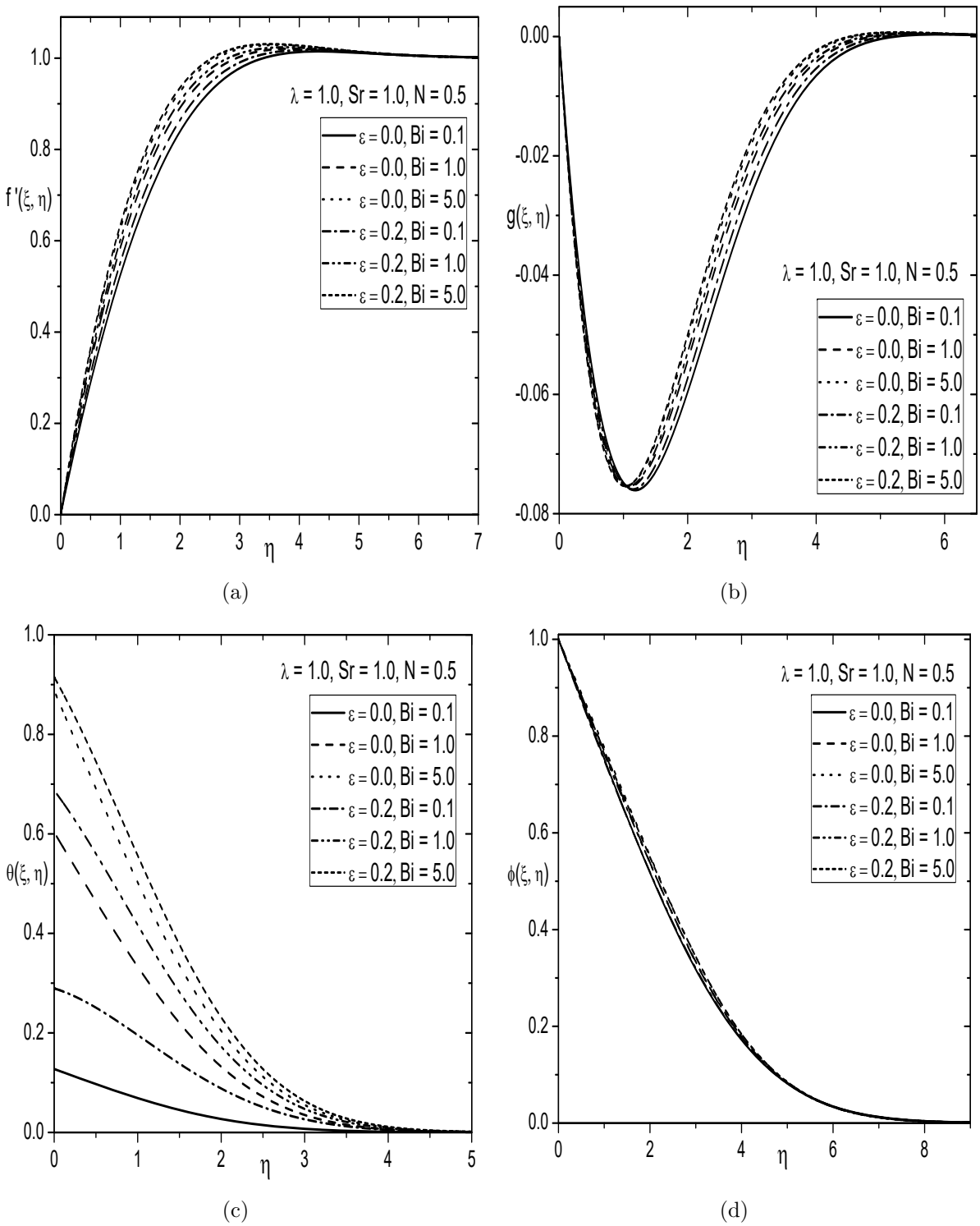

Figure 6.7: *Effects of ε and Bi on (a)Velocity, (b)Microrotation, (c)Temperature and (d)Concentration profiles.*

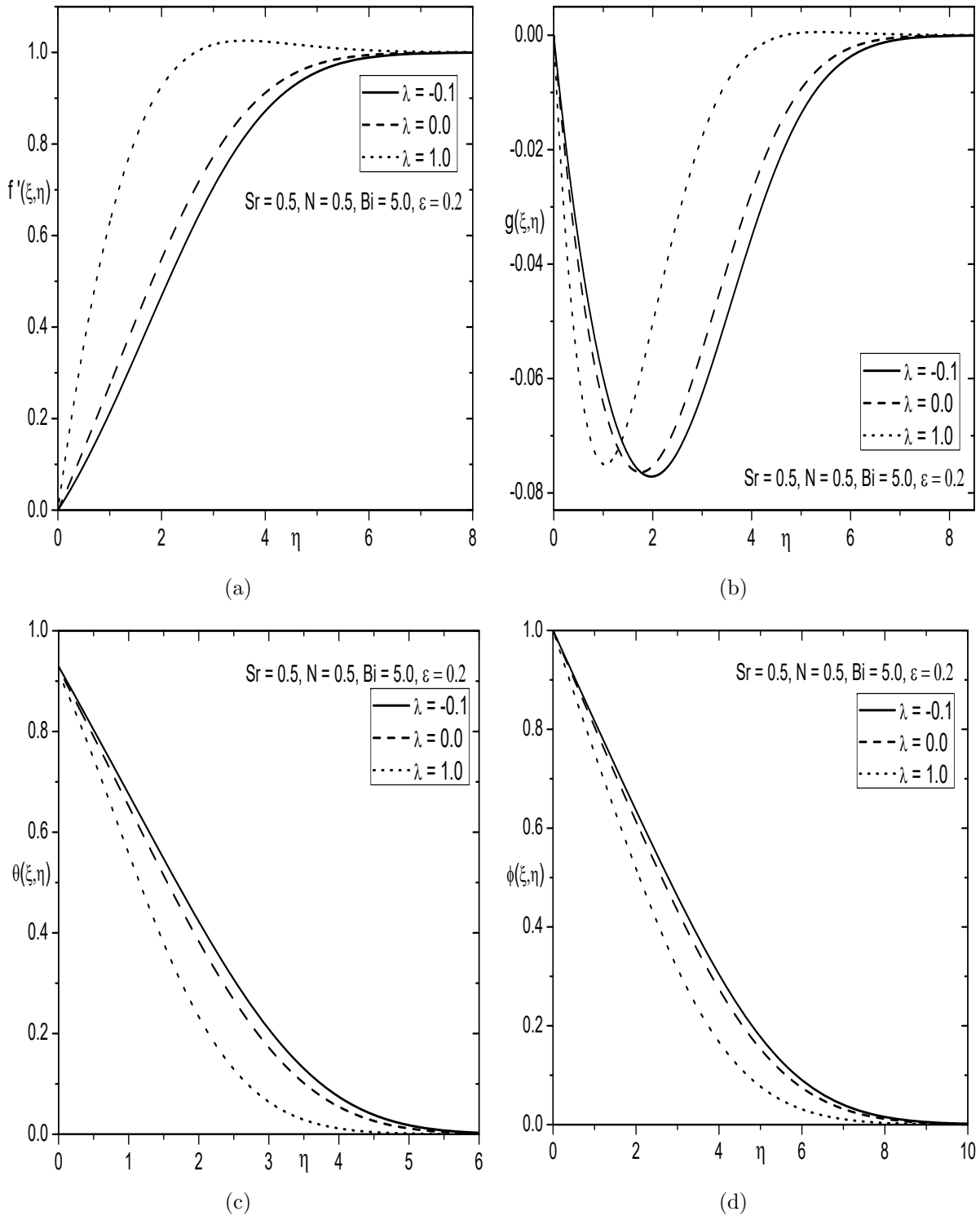

Figure 6.8: *Effect of* λ *on (a)Velocity, (b)Microrotation, (c)Temperature and (d)Concentration profiles.*

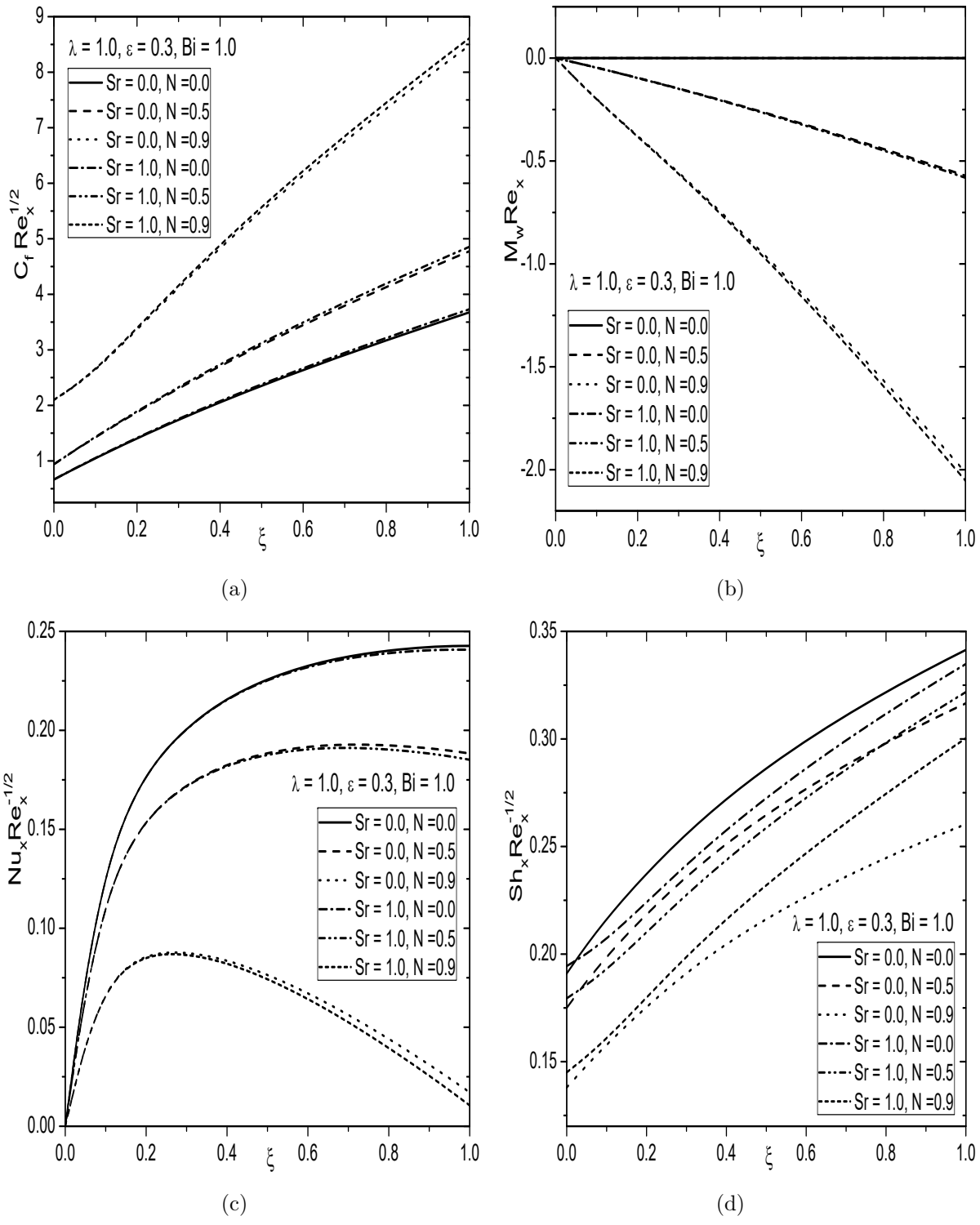

Figure 6.9: *Effects of N and Bi on (a)Skin friction, (b)wall couple stress, (c)Nusselt number and (d)Sherwood number.*

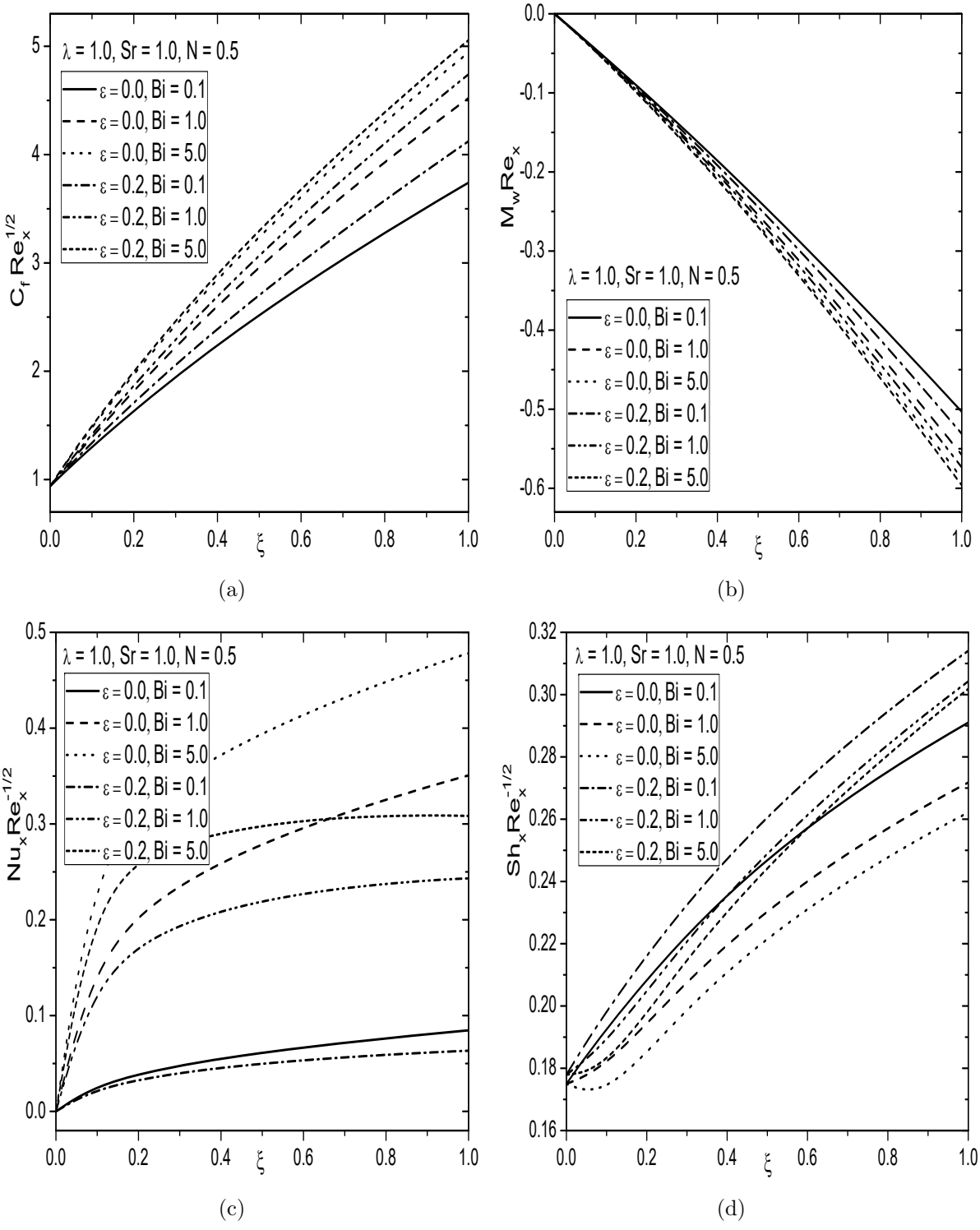

Figure 6.10: *Effects of ε and Bi on (a)Skin friction, (b)wall couple stress, (c)Nusselt number and (d)Sherwood number.*

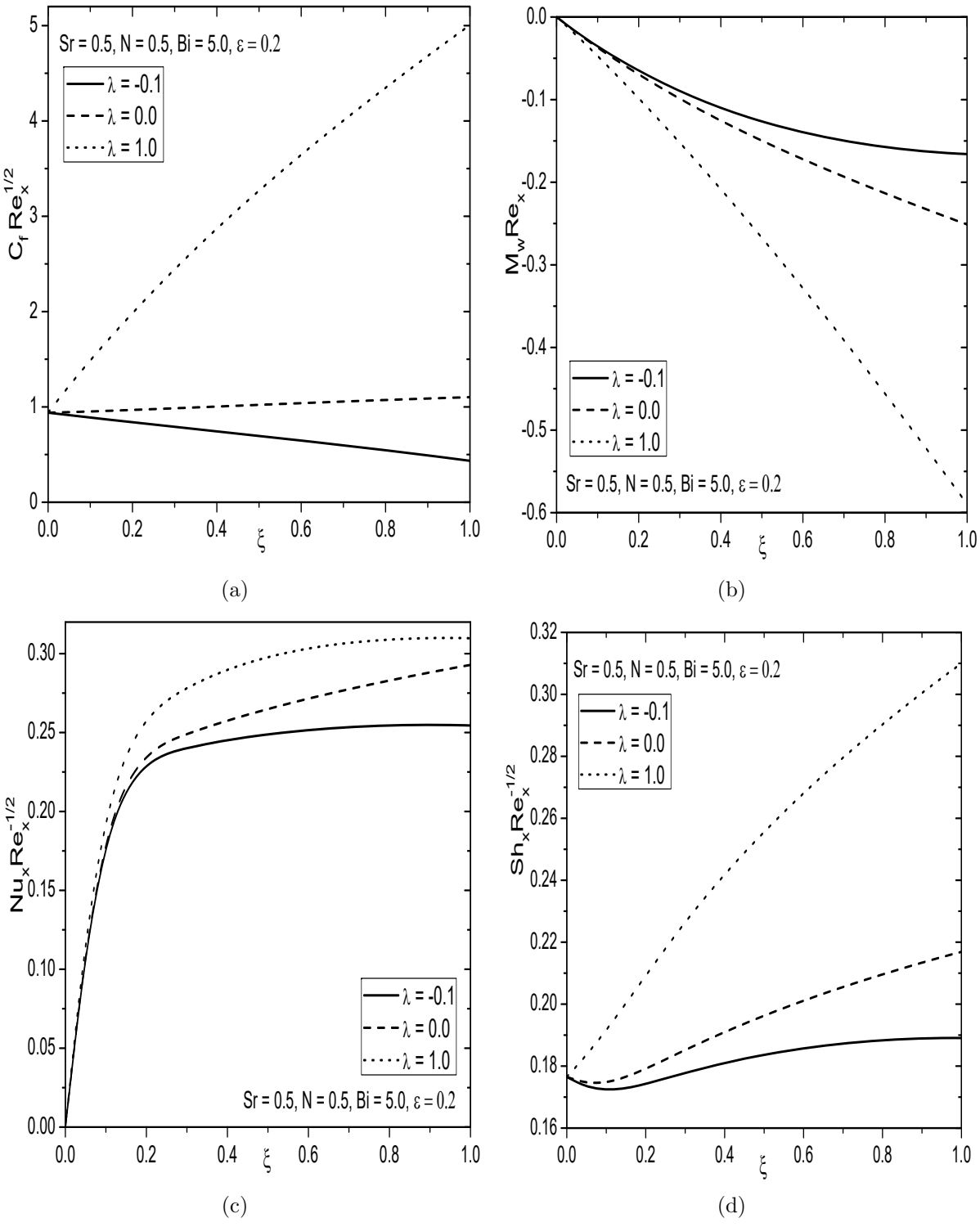

Figure 6.11: *Effect of λ on (a)Skin friction, (b)wall couple stress, (c)Nusselt number and (d)Sherwood number.*

6.3 Conclusions

In erstwhile chapters, the similarity solution for micropolar fluid flow along a vertical plate is obtained numerically using the spectral quasi-linearization method. In this chapter, the non-similarity solution is obtained to analyze the effects of viscous dissipation and Soret on natural and mixed convective flow of a micropolar fluid over the vertical frustum of a cone with the convective boundary condition. From this analysis, the main findings are drawn for both case(a) and case(b) as follows:

An increase in coupling number leads to decrease in the wall couple stress, Nusselt number and Sherwood number, but increase the temperature, concentration and skin friction. Moreover, the velocity decreases in case (a) and (b), but far away from the surface of a truncated cone the velocity shows opposite trend in case(a). The velocity, concentration and skin friction increase, but the wall couple stress, heat and mass transfer rates decrease with the increase of Soret number. By enhancing the Biot number, the skin friction, Nusselt number and temperature enhance, but the wall couple stress and Sherwood number reduce. With the increase of both Biot number and viscous dissipation parameter, the velocity and concentration depicts reverse behaviour within the boundary in case(a) while, the velocity and concentration increase in case(b). As the viscous dissipation parameter increases, the wall couple stress and heat transfer rate decrease, but temperature, skin friction and mass transfer rate increase. Moreover, with the increase of viscous dissipation parameter, the microrotation depicts reverse rotation within the boundary layer. The velocity, skin friction, Nusselt and Sherwood numbers are more in the case of aiding flow as compared with the opposing flow. Further, the temperature and concentration are more in the opposing flow and less in the aiding flow.

Chapter 7

Effects of Soret and Viscous Dissipation on Convective Flow over a Truncated Cone Embedded in a Micropolar Fluid Saturated Non-Darcy Porous Medium [1]

7.1 Introduction

Convective transport phenomena in a porous medium has been the subject of great importance and interest in the recent years owing to its wide range of applications in civil, chemical and mechanical engineering. In many practical situations, the porous medium is bounded by an impermeable surface which has high flow rates, and reveals the non-uniform porosity distribution near the surface region, making Darcy law inapplicable. To model this kind of preferable physical situation, it is therefore, necessary to include the non-Darcian terms in the analysis of convective transport in a porous medium. In brief, the non-Darcy models are extensions of the classical Darcy formulation

[1] Case(a): Accepted in "**Special Topics and Reviews in Porous Media**",
Case(b) Communicated to "**Journal of Engineering Thermophysics**"

to incorporate inertial drag effects, vorticity diffusion, and combinations of these effects. Different models have been proposed in the literature to study the convective transport phenomena in the non-Darcy porous medium. Among these, the Darcy-Forchheimer model is an extension of classical Darcy formulation obtained by adding a squared term of velocity in the momentum equation to account for the inertial effects. Modelling and analysis of dynamics of a micropolar fluid saturated porous medium has been the active field of research from the past few years. This stems from the evidence that this fluid has a large number of industrial and engineering applications. Considerable work has been discussed on the flow, heat and mass transfer characteristics in a Darcy and non-Darcy porous medium [83, 86, 88].

Several investigators analyzed the free convective boundary layer flow over a truncated cone through porous medium saturated with Newtonian and/or non-Newtonian fluids. Mahdy [52] formulated the mathematical model for the double diffusive convective flow over a truncated cone embedded in a porous medium by considering variable viscosity, chemical reaction and heat generation/absorption effects. Cheng [22] analyzed the natural convective flow over a truncated cone in a porous medium saturated with a non-Newtonian nanofluid by incorporating the thermophoresis and Brownian motion effects. The cross-diffusion (Soret and Dufour) effects on free convective flow over the vertical frustum of a cone embedded in a porous medium has been discussed by Rashad and Chamkha [85] (and also see the citations therein).

The objective of this chapter is to examine the viscous dissipation and Soret effects on convective flow over a truncated cone embedded in a micropolar fluid saturated non-Darcy porous medium with the convective boundary condition. From the literature, it seems that the problem under consideration has not been addressed so far. As in the previous chapter, here also, the extended spectral quasi-linearization method has been used to solve the system of reduced non-linear partial differential equations. The influence of pertinent parameters, namely Biot number, Soret number, viscous dissipation, Darcy and Forchheimer numbers on the velocity, microrotation, temperature, concentration, skin-friction, wall couple stress, heat and mass transfer rates over a truncated cone are displayed through graphs and the salient features are discussed.

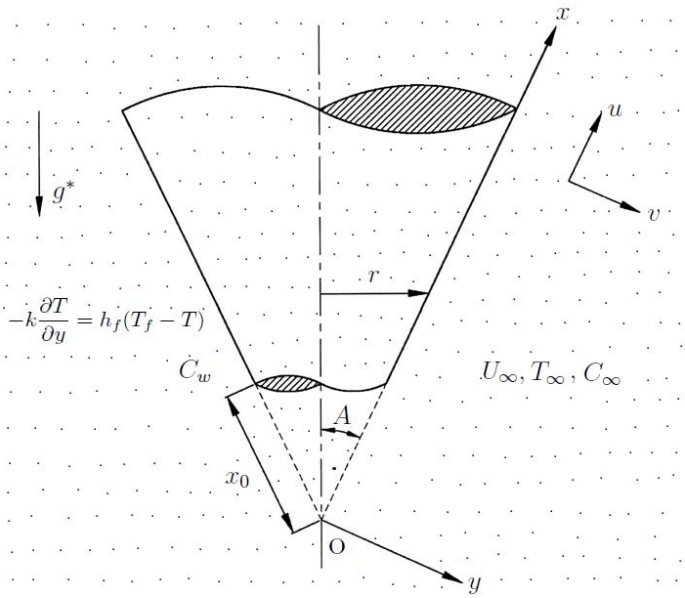

Figure 7.1: *Physical model of the problem*

7.2 Mathematical Formulation

In this chapter, the steady, two dimensional and laminar convective flow over a truncated cone in a micropolar fluid saturated non-Darcy porous medium is considered. Choose the coordinate system such that the x-axis is taken along the vertical frustum of a cone and y-axis is measured normal to it, as shown in Fig. (7.1). This chapter is an extension of chapter-6 by considering the fluid saturated non-Darcy porous medium. In addition to the assumptions made in chapter-6, the following assumptions are taken into account in the analysis: (i) the porous medium is isotropic and homogeneous, (ii) the properties of the fluid and porous medium are constant except for the density variation required by the Boussinesq approximation, and (iii) the fluid and the porous medium are in local thermodynamic equilibrium.

Under the above assumptions, and using the Darcy-Forcheimer model and Dupuit-Forchheimer relationship [74], the governing equations for micropolar fluid saturated non-Darcy porous medium are given by

$$\frac{\partial(u\,r)}{\partial x} + \frac{\partial(v\,r)}{\partial y} = 0 \tag{7.1}$$

$$\frac{\rho}{\epsilon^2}\left(u\,\frac{\partial u}{\partial x} + v\,\frac{\partial u}{\partial y}\right) = \left(\frac{\mu+\kappa}{\epsilon}\right)\frac{\partial^2 u}{\partial y^2} + \kappa\,\frac{\partial \omega}{\partial y} + \rho g^*\left[\beta_T(T-T_\infty) + \beta_C(C-C_\infty)\right]\cos A \tag{7.2}$$

$$-\frac{\mu}{K_p}\,(u-U_\infty)-\frac{\rho\,b}{K_p}\,(u^2-U_\infty^2)$$

$$\frac{\rho j}{\epsilon}\left(u\,\frac{\partial\omega}{\partial x}+v\,\frac{\partial\omega}{\partial y}\right)=\gamma\,\frac{\partial^2\omega}{\partial y^2}-\kappa\,\left(2\omega+\frac{1}{\epsilon}\frac{\partial u}{\partial y}\right) \tag{7.3}$$

$$u\,\frac{\partial T}{\partial x}+v\,\frac{\partial T}{\partial y}=\alpha\,\frac{\partial^2 T}{\partial y^2}+\left(\frac{\mu+\kappa}{\rho\,C_p}\right)\left(\frac{\partial u}{\partial y}\right)^2 \tag{7.4}$$

$$u\,\frac{\partial C}{\partial x}+v\,\frac{\partial C}{\partial y}=D\frac{\partial^2 C}{\partial y^2}+\frac{D\,K_T}{T_m}\,\frac{\partial^2 T}{\partial y^2} \tag{7.5}$$

where b is the Forchheimer constant and K_p is the permeability of the medium.

The associate boundary conditions are

$$u=0,\,v=0,\,\omega=-n\frac{\partial u}{\partial y},\,-k\frac{\partial T}{\partial y}=h_f(T_f-T),\,C=C_w \text{ at } y=0 \tag{7.6a}$$

$$u=U_\infty,\,\omega=0,\,T=T_\infty,\,C=C_\infty \text{ as } y\to\infty \tag{7.6b}$$

Now, we introduce the following stream function ψ, to satisfy the equation of continuity identically, as

$$u=\frac{1}{r}\,\frac{\partial\psi}{\partial y},\;v=-\frac{1}{r}\,\frac{\partial\psi}{\partial x} \tag{7.7}$$

7.2.1 Case(a): Natural Convection

The flow is assumed to be a natural convection which is caused by buoyancy forces only without any external agent and hence, the velocity of the external flow becomes zero ($ie., U_\infty=0$). We introduce the following transformations

$$\xi=\frac{\overline{x}}{x_0}=\frac{x-x_0}{x_0},\,\eta=\frac{y}{\overline{x}}\,Gr_x^{1/4},\,\psi=r\nu Gr_x^{1/4}\,f\,(\xi,\eta)\,,$$

$$\omega=\frac{\nu\,Gr_x^{3/4}}{\overline{x}^2}\,g\,(\xi,\eta)\,,\,\theta\,(\xi,\eta)=\frac{T-T_\infty}{T_f-T_\infty},\,\phi\,(\xi,\eta)=\frac{C-C_\infty}{C_w-C_\infty} \tag{7.8}$$

Substitution of (7.7) - (7.8) into Eqs. (7.2)-(7.5), the system of governing equations become

$$\frac{1}{\epsilon}\left(\frac{1}{1-N}\right)f'''+\frac{1}{\epsilon^2}\left(R+\frac{3}{4}\right)f\,f''-\frac{1}{2\epsilon^2}(f')^2+\left(\frac{N}{1-N}\right)g'+\theta+\mathcal{B}\phi \tag{7.9}$$

$$-\frac{\xi^{1/2}}{Da\,Gr_{x_0}^{1/2}}f'-\xi\frac{Fs}{Da}(f')^2=\frac{\xi}{\epsilon^2}\left(f'\,\frac{\partial f'}{\partial\xi}-f''\frac{\partial f}{\partial\xi}\right)$$

$$\left(\frac{2-N}{2-2N}\right)g''+\frac{1}{\epsilon}\left(R+\frac{3}{4}\right)f\,g'-\frac{1}{4\epsilon}\,f'\,g-\xi^{1/2}\left(\frac{N}{1-N}\right)\left(2g+\frac{1}{\epsilon}f''\right)=\frac{\xi}{\epsilon}\left(f'\,\frac{\partial g}{\partial\xi}-g'\frac{\partial f}{\partial\xi}\right) \quad (7.10)$$

$$\frac{1}{Pr}\theta''+\left(R+\frac{3}{4}\right)f\,\theta'+\xi\varepsilon\left(\frac{1}{1-N}\right)(f'')^2=\xi\left(f'\,\frac{\partial\theta}{\partial\xi}-\theta'\frac{\partial f}{\partial\xi}\right) \quad (7.11)$$

$$\frac{1}{Sc}\phi''+\left(R+\frac{3}{4}\right)f\,\phi'+Sr\,\theta''=\xi\left(f'\,\frac{\partial\phi}{\partial\xi}-\phi'\frac{\partial f}{\partial\xi}\right) \quad (7.12)$$

where $Da=\dfrac{K_p}{x_0^2}$ is the Darcy parameter and $Fs=\dfrac{b}{x_0}$ is the Forchheimer number.

The corresponding boundary conditions (7.6) become

$$f(\xi,0)+\frac{\xi}{\left(R+\frac{3}{4}\right)}\frac{\partial f}{\partial\xi}=0,\ f'(\xi,0)=0,\ g(\xi,0)=-nf''(\xi,0), \quad (7.13a)$$

$$\theta'(\xi,0)=-\xi^{1/4}\,Bi(1-\theta(\xi,0)),\ \phi(\xi,0)=1$$

$$f'(\xi,\infty)=0,\ g(\xi,\infty)=0,\ \theta(\xi,\infty)=0,\ \phi(\xi,\infty)=0 \quad (7.13b)$$

The non-dimensional skin friction ($C_fGr_x^{1/4}$), wall couple stress ($M_wGr_x^{1/2}$), local Nusselt number ($\frac{Nu_x}{Gr_x^{1/4}}$) and local Sherwood number ($\frac{Sh_x}{Gr_x^{1/4}}$), are given by

$$\left.\begin{aligned}&C_f\mathrm{Gr}_x^{1/4}=2\left(\frac{1-nN}{1-N}\right)f''(\xi,0),\qquad M_w\mathrm{Gr}_x^{1/2}=\xi^{1/2}\left(\frac{2-N}{2-2N}\right)g'(\xi,0),\\&\frac{Nu_x}{\mathrm{Gr}_x^{1/4}}=-\theta'(\xi,0),\ \ \frac{Sh_x}{\mathrm{Gr}_x^{1/4}}=-\phi'(\xi,0)\end{aligned}\right\} \quad (7.14)$$

Results and Discussion

As explained in the previous chapter (i,e. chapter 6), here also, the extended spectral quasi-linearization method is employed to solve the non-homogeneous and nonlinear coupled partial differential equations (7.9)-(7.12) along with the boundary conditions (7.13). To verify the accuracy of the code generated, for the special case of $n=0$, $\varepsilon=0$, $\mathcal{B}=0$, $\epsilon=1$, $Fs=0$, $N=0$, $Sr=0$, $Da\to\infty$ and $Bi\to\infty$, the results of the present problem have been compared with those of Yih [106] and it seems to be good agreement [Tab. (6.1)]. To explore the effects of viscous dissipation parameter, coupling, Forchheimer, Soret and Biot numbers, the computations have been carried out for $Pr=0.71$, $\xi=0.5$, $Gr_{x_0}=5$, $Sc=0.22$, $\epsilon=0.9$ and $n=0$. These values are fixed in this

analysis unless otherwise specified.

In Figs.7.2(a) - 7.2(d), effects of Soret and coupling numbers on the non-dimensional velocity f', microrotation g, temperature θ and concentration ϕ, are exhibited. It can be found from Fig. 7.2(a) that with the increase of coupling number N, the velocity reduces near the vertical frustum of a cone, but it enhances far away from the surface. Meanwhile, the velocity increases with the increase of Soret number. From Fig. 7.2(b), it can be noticed that the microrotation profiles tend to become flat initially, and then it shows the reverse rotation with the enhancement of coupling number but, it does not show any significant effect with the increase of Soret number. It can be perceived from Figs. 7.2(c) and 7.2(d) that by enhancing the coupling number N, the temperature and concentration increases with the increase of coupling number. Physically, Soret number is defined as the additional mass diffusion due to the temperature gradients. Therefore, with the increase of Soret number, the concentration increases and the temperature decreases within the respective solutal and thermal boundary layers.

In the presence and absence of viscous dissipation, the variation of Biot number Bi on the non-dimensional velocity f', microrotation g, temperature θ and concentration ϕ, is plotted in Figs. 7.3(a) - 7.3(d). From Fig. 7.3(a), it can be observed that the velocity enhances near the truncated cone and far away from the truncated cone it reduces with the enhancement of both Biot number as well as viscous dissipation parameter. From Fig. 7.3(b), it can be noticed that as the Biot number increases, the microrotation shows qualitatively same behaviour for both $\varepsilon = 0.0$ and $\varepsilon = 0.5$. Generally, the positive values of viscous dissipation parameter represents the fluid heating case (i,e. heat is supplying into the fluid across the surface). Consequently, the temperature of the fluid increases with the enhancement of both Biot number and viscous dissipation parameter [Fig. 7.3(c)]. From Fig. 7.3(d), it can be revealed that the concentration enhances slightly in the initial stage and then reduces with an increase in both Biot number and viscous dissipation parameter.

The influence of both Darcy number Da and Forchhiemer number Fs on the dimensionless velocity f', microrotation g, temperature θ and concentration ϕ, are displayed in Figs. 7.4(a) - 7.4(d). From Fig. 7.4(a), it can be observed that the velocity increases with the increase of Darcy number for both $Fs = 0.0$ and $Fs = 0.5$. As the non-Darcy parameter Fs increases, the porous medium offers more resistance to the fluid flow and hence the velocity is less in the case of non-Darcy porous medium ($Fs = 0.5$) as compared with that of the Darcy porous medium ($Fs = 0.0$). From this figure, it is also clear that the velocity decreases with the increase of Forchheimer number. In

both Darcy ($Fs = 0.0$) and non-Darcy ($Fs \neq 0$) porous media, the microrotation shows reverse rotation with the increase of Darcy parameter [Fig. 7.4(b)]. It can be revealed from Figs. 7.4(c) and 7.4(d) that for both $Fs = 0.0$ and $Fs = 0.5$, the temperature and concentration diminishes with the increase of Darcy parameter. Moreover, it can be noticed that the temperature and concentration are more in the case of non-Darcy porous medium as compared with that of Darcy porous medium case.

The effects of coupling number on the skin friction, wall couple stress, Nusselt and Sherwood numbers against the streamwise coordinate ξ, are portrayed in Figs. 7.5(a) - 7.5(d) for both $Sr = 0.0$ and $Sr = 1.0$. It can be observed from Fig. 7.5(a) that the skin friction enhances with the increase of both coupling and Soret numbers. Moreover, the effect of coupling number shows more prominent than the Soret number on the skin friction. As the coupling number enhances, the wall couple stress coefficient reduces nonlinearly for the micropolar fluid, but it reduces slightly with the increase of Soret number as portrayed in Fig. 7.5(b). From Fig. 7.5(c), it can be perceived that the Nusselt number decreases with the increase of coupling number N but, it increases with the increase of Soret number. It can be observed from Fig. 7.5(d) that by enhancing both coupling number N and Soret number Sr, the Sherwood number reduces. Further, it can be noticed that for both $Sr = 0.0$ and $Sr = 1.0$, the Nusselt and Sherwood numbers are lower for the micropolar fluid as compared with those of the viscous fluid.

Figs. 7.6(a) - 7.6(d) depict the influence of Biot number on the skin friction, wall couple stress, Nusselt and Sherwood numbers against the streamwise coordinate ξ in the presence and absence of viscous dissipation parameter. From Fig. 7.6(a), it can be observed that the skin friction coefficient increases with the increase of both Biot number and viscous dissipation parameter. It can be noticed that the wall couple stress coefficient decreases nonlinearly with an increase in both Bi and ε as displayed in Fig. 7.6(b). From Fig. 7.6(c), it can be observed that the Nusselt number enhances with the increase of Biot number whereas, it decreases with the increase of viscous dissipation. It can be perceived from Fig. 7.6(d) that the Sherwood number reduces nonlinearly with the enhancement of Biot number, but it enhances with the increase of viscous dissipation parameter.

Effects of Forchheimer number and Darcy parameter on the non-dimensional skin friction, wall couple stress, Nusselt and Sherwood numbers against the streamwise coordinate ξ, are portrayed in Figs. 7.7(a) - 7.7(d). Here the Forchheimer number represents the inertial drag in a non-Darcy porous medium and it is applicable for high permeability. As $Fs \to 0$, the non-Darcy porous

medium tends to the Darcy porous medium. It is clear from Fig. 7.7(a) that the resistance to the flow enhances with the increase of Forchheimer number. From Fig. 7.7(a), it can be perceived that the skin friction increases with an increase in Darcy parameter and it decreases with an increase in Forchheimer number. From Fig. 7.7(b), it can be noticed that the wall couple stress reduces with the Darcy parameter enhancement, but it enhances with the Forchheimer number increment. The heat and mass transfer rates increase with the increase of Darcy number, while they decrease with the increase of Forchheimer number [Figs. 7.7(c) and 7.7(d)].

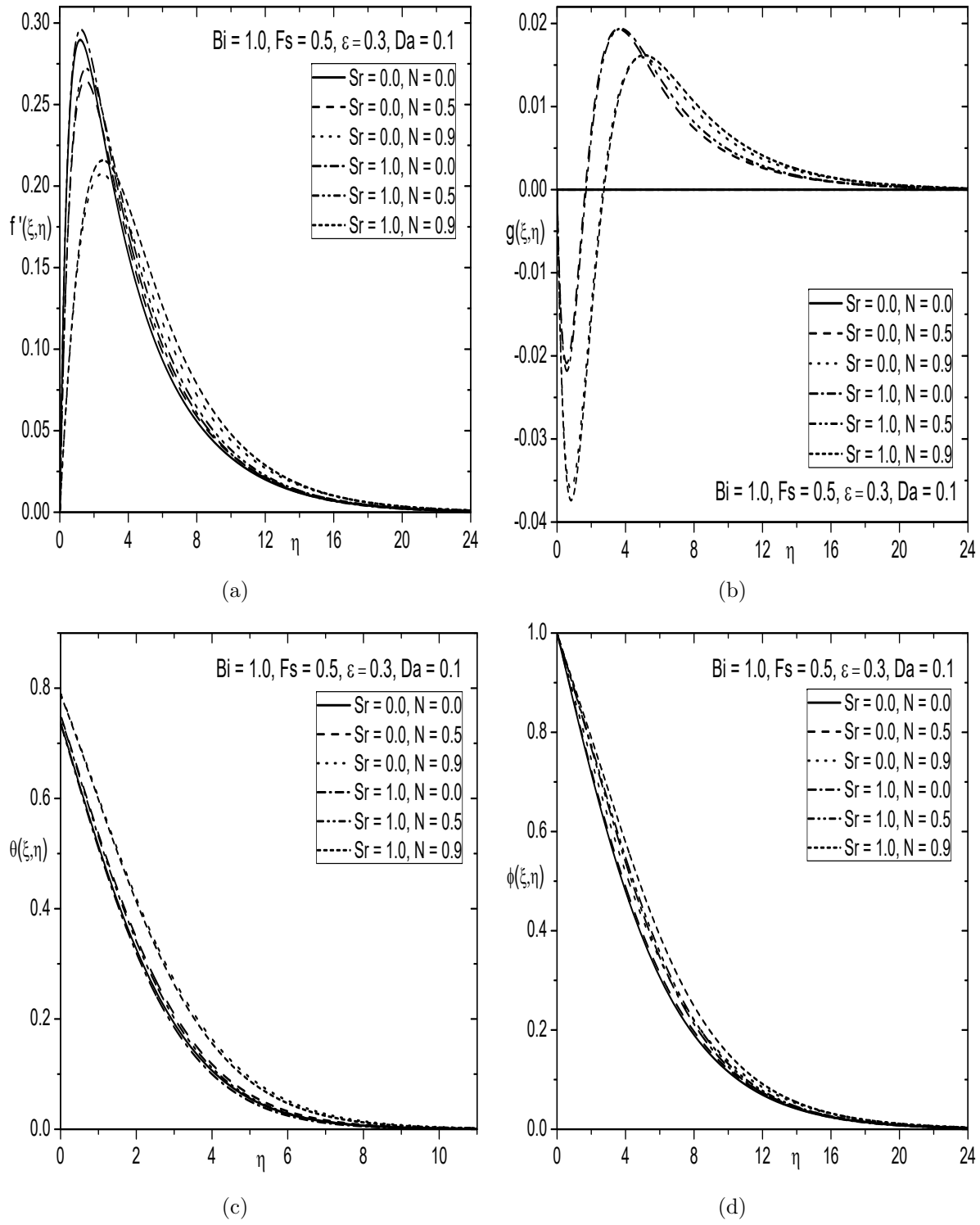

Figure 7.2: *Effects of Sr and N on (a)Velocity, (b)Microrotation, (c)Temperature and (d)Concentration.*

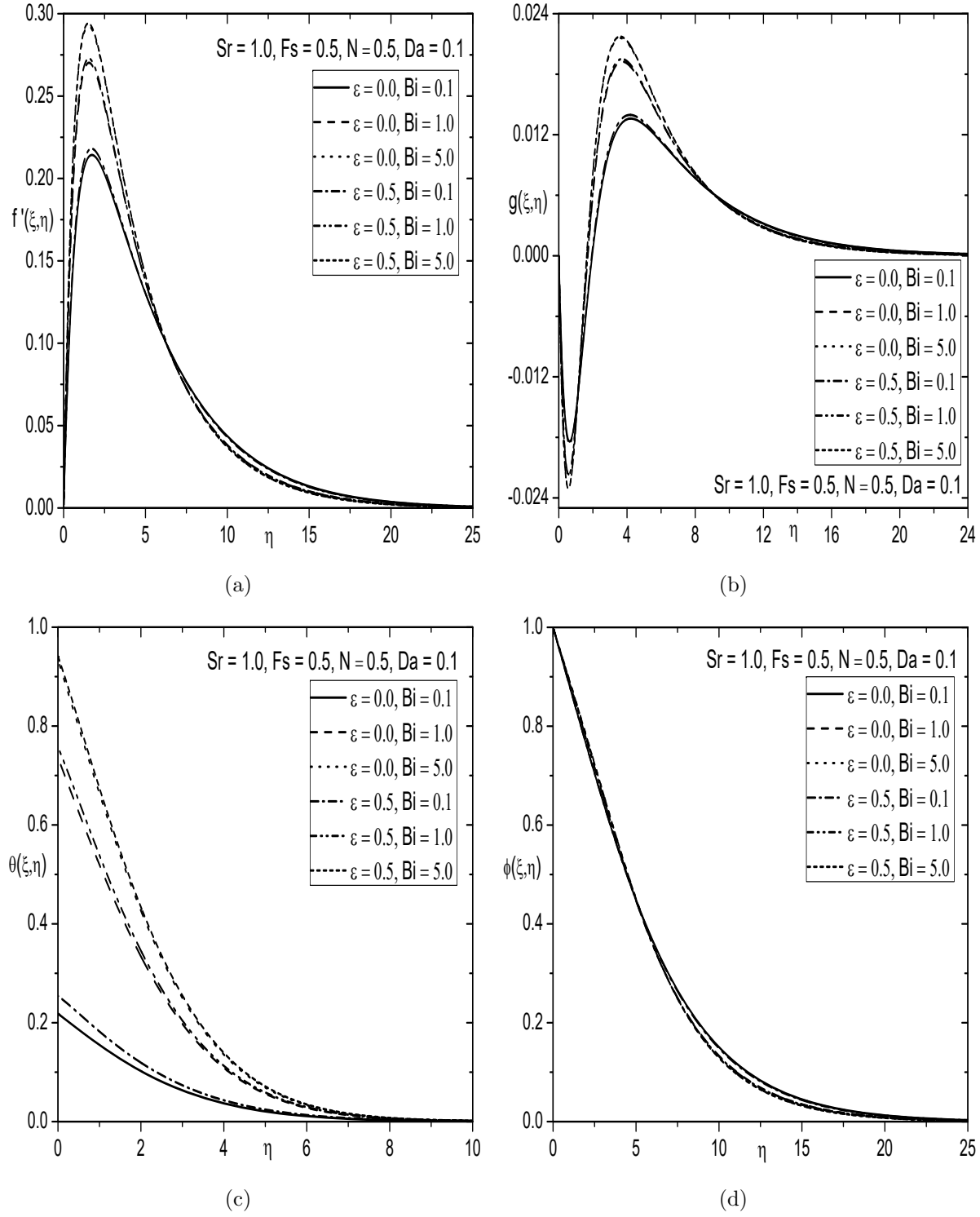

Figure 7.3: *Effects of ε and Bi on (a)Velocity, (b)Microrotation, (c)Temperature and (d)Concentration.*

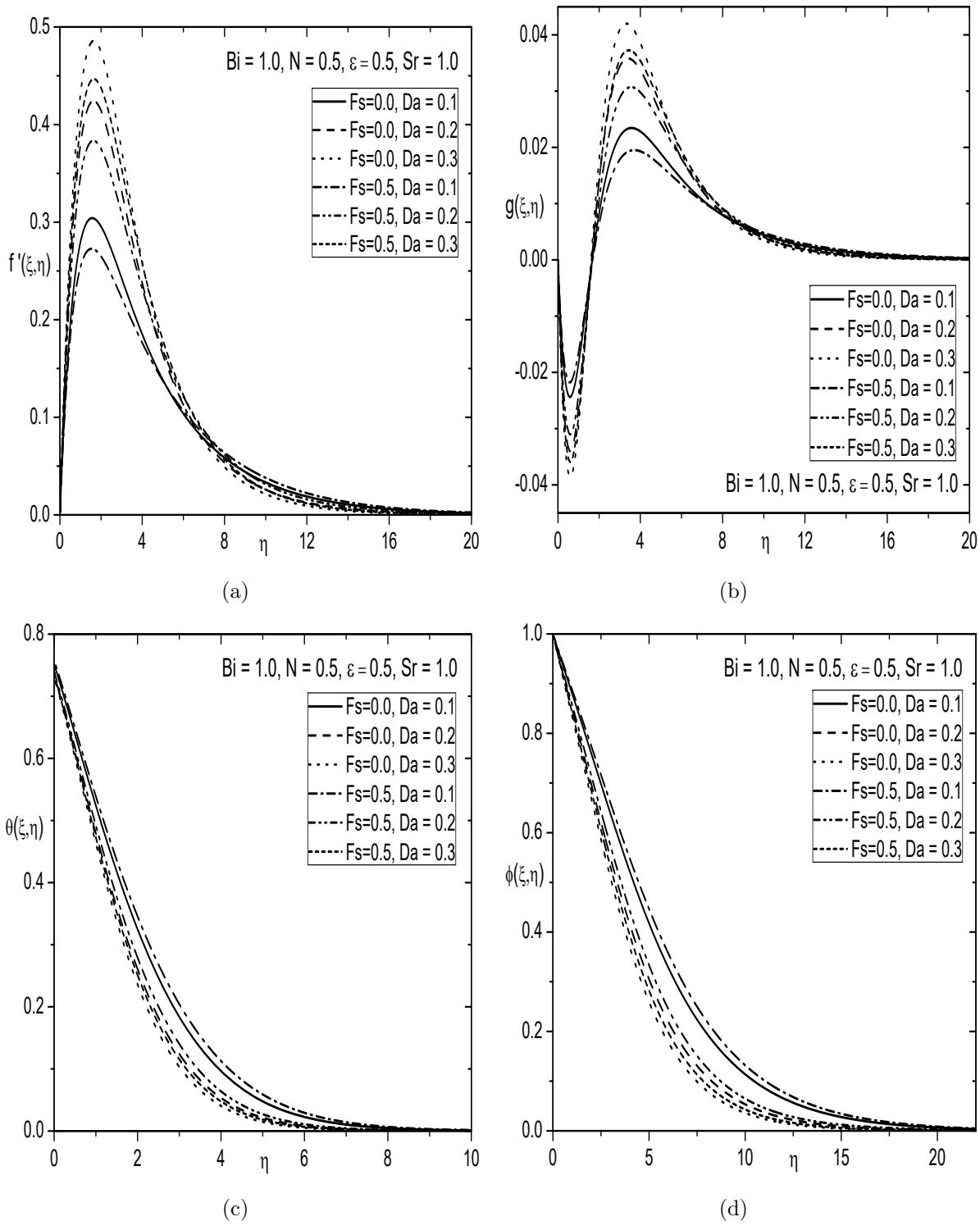

Figure 7.4: *Effects of Fs and Da on (a)Velocity, (b)Microrotation, (c)Temperature and (d)Concentration.*

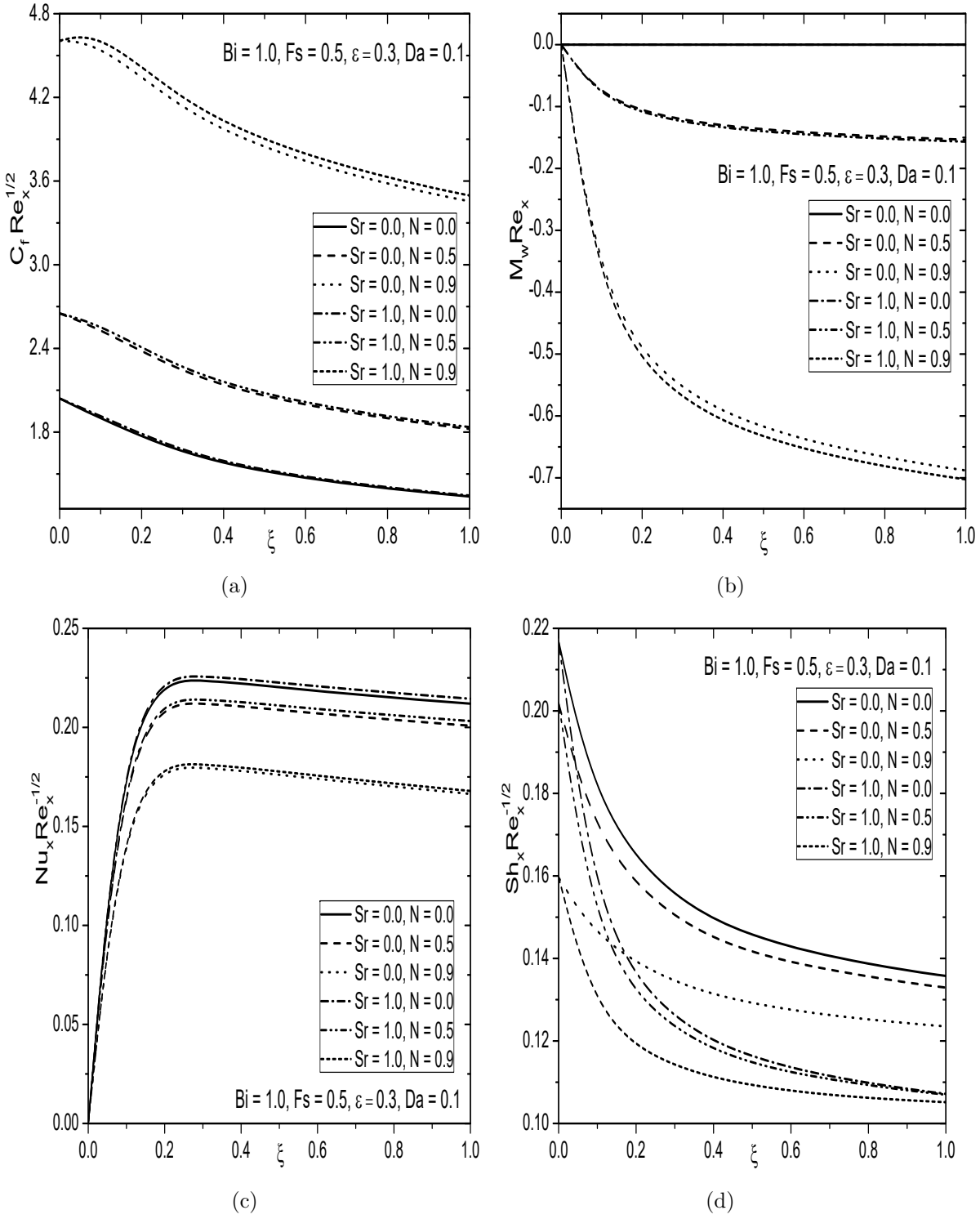

Figure 7.5: *Effects of Sr and N on (a)Skin friction, (b)Wall couple stress, (c)Nusselt number and (d)Sherwood number.*

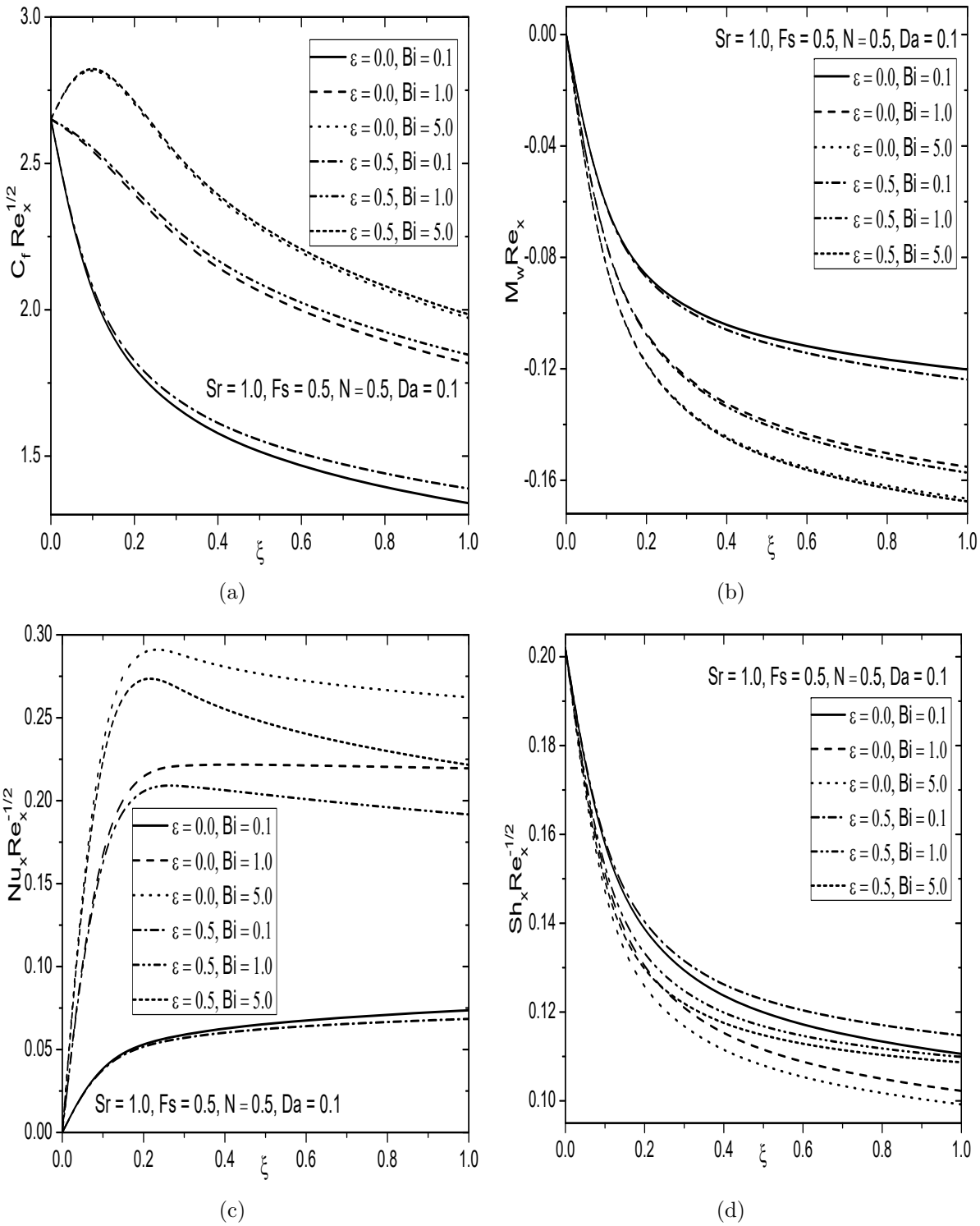

Figure 7.6: *Effects of ε and Bi on (a)Skin friction, (b)Wall couple stress, (c)Nusselt number and (d)Sherwood number.*

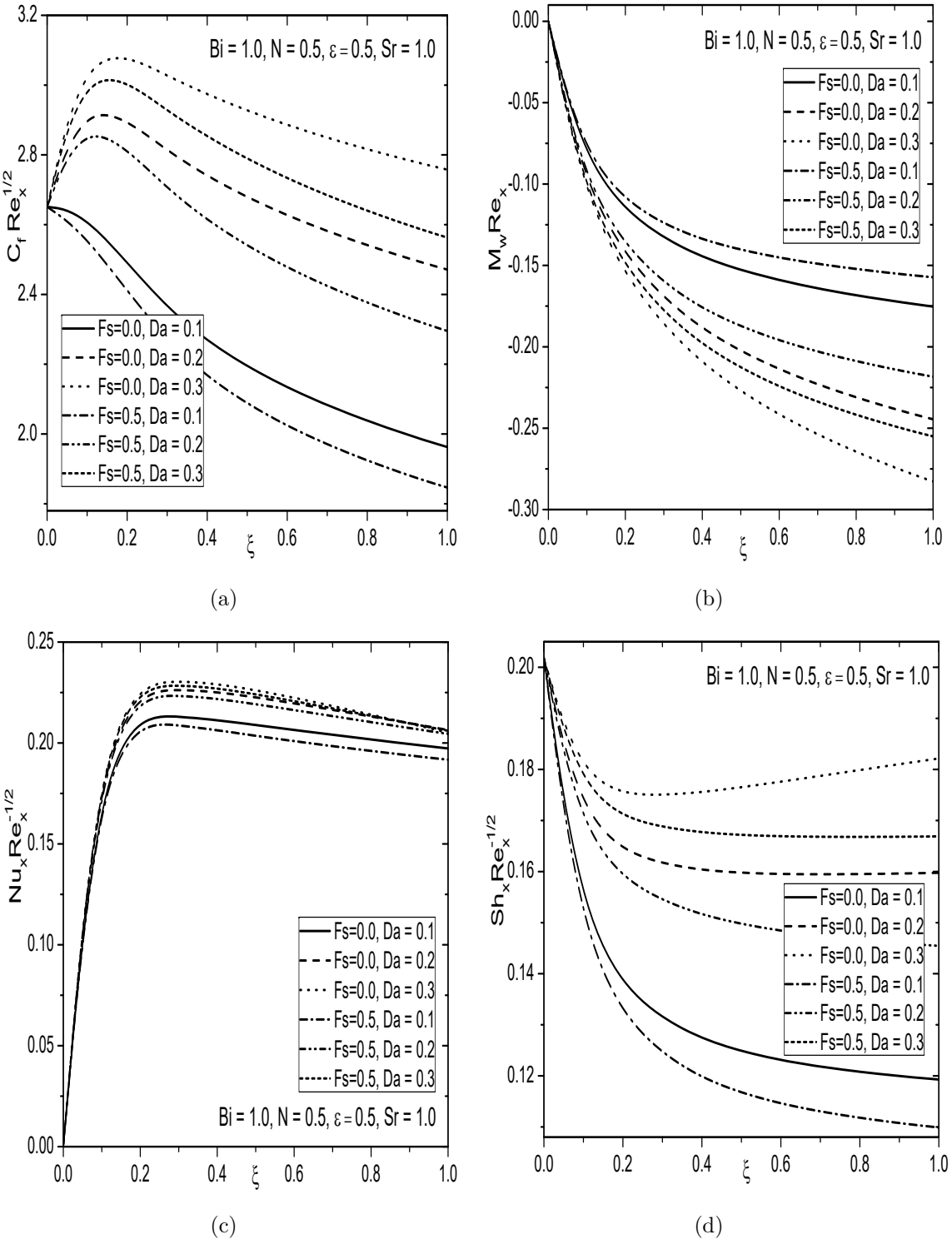

Figure 7.7: *Effects of Fs and Da on (a)Skin friction, (b)Wall couple stress, (c)Nusselt number and (d)Sherwood number.*

7.2.2 Case(b): Mixed Convection

Consider the flow is mixed convective flow arises from an external flow with velocity (U_∞) and buoyancy forces. We introduce the non-similarity transformations in the following form

$$\eta = \frac{y}{\overline{x}}\, Re_x^{1/2},\ \xi = \frac{\overline{x}}{x_0} = \frac{x - x_0}{x_0},\ \psi = r\nu Re_x^{1/2} f\left(\xi, \eta\right), \tag{7.15}$$

$$\omega = \frac{\nu\, Re_x^{3/2}}{\overline{x}^2}\, g\left(\xi, \eta\right),\ \theta\left(\xi, \eta\right) = \frac{T - T_\infty}{T_f - T_\infty},\ \phi\left(\xi, \eta\right) = \frac{C - C_\infty}{C_w - C_\infty}$$

Substitution of (7.7) and (7.15) into Eqs. (7.2)- (7.5), the set of governing equations reduces to the following form

$$\frac{1}{\epsilon}\left(\frac{1}{1-N}\right) f''' + \frac{1}{\epsilon^2}\left(R + \frac{1}{2}\right) f\, f'' + \frac{\xi}{Da\, Re_{x_0}}(1 - f') + \xi\frac{Fs}{Da}\left(1 - (f')^2\right) + \left(\frac{N}{1-N}\right) g' \tag{7.16}$$

$$+\xi\,\lambda\left(\theta + \mathcal{B}\phi\right) = \frac{\xi}{\epsilon^2}\left(f'\,\frac{\partial f'}{\partial \xi} - f''\frac{\partial f}{\partial \xi}\right)$$

$$\left(\frac{2-N}{2-2N}\right) g'' + \frac{1}{\epsilon}\left(R + \frac{1}{2}\right) f\, g' + \frac{1}{2\epsilon}\, f'\, g - \xi\left(\frac{N}{1-N}\right)\left(2g + \frac{1}{\epsilon} f''\right) = \frac{\xi}{\epsilon}\left(f'\,\frac{\partial g}{\partial \xi} - g'\frac{\partial f}{\partial \xi}\right) \tag{7.17}$$

$$\frac{1}{Pr}\theta'' + \left(R + \frac{1}{2}\right) f\,\theta' + \left(\frac{1}{1-N}\right)\varepsilon\,(f'')^2 = \xi\left(f'\,\frac{\partial \theta}{\partial \xi} - \theta'\frac{\partial f}{\partial \xi}\right) \tag{7.18}$$

$$\frac{1}{Sc}\phi'' + \left(R + \frac{1}{2}\right) f\,\phi' + Sr\,\theta'' = \xi\left(f'\,\frac{\partial \phi}{\partial \xi} - \phi'\frac{\partial f}{\partial \xi}\right) \tag{7.19}$$

The associated boundary conditions become

$$f(\xi, 0) = \frac{-\xi}{\left(R + \frac{1}{2}\right)}\frac{\partial f}{\partial \xi},\ f'(\xi, 0) = 0,\ g(\xi, 0) = -n f''(\xi, 0), \tag{7.20a}$$

$$\theta'(\xi, 0) = -\xi^{1/2}\, Bi(1 - \theta(\xi, 0)),\ \phi(\xi, 0) = 1$$

$$f'(\xi, \infty) = 1,\ g(\xi, \infty) = 0,\ \theta(\xi, \infty) = 0,\ \phi(\xi, \infty) = 0 \tag{7.20b}$$

The non-dimensional skin friction $C_f = \dfrac{2\tau_w}{\rho\, U_\infty^2}$, wall couple stress $M_w = \dfrac{m_w}{\rho\, U_\infty^2 x_0}$, local Nusselt

number $Nu_x = \dfrac{q_w \overline{x}}{k(T_f - T_\infty)}$ and local Sherwood number $Sh_x = \dfrac{q_m \overline{x}}{D(C_w - C_\infty)}$, are given by

$$\left.\begin{aligned} C_f Re_x^{1/2} &= 2\left(\frac{1-nN}{1-N}\right) f''(\xi,0), \quad M_w Re_x = \left(\frac{2-N}{2-2N}\right) g'(\xi,0), \\ \frac{Nu_x}{Re_x^{1/2}} &= -\theta'(\xi,0), \quad \frac{Sh_x}{Re_x^{1/2}} = -\phi'(\xi,0) \end{aligned}\right\} \tag{7.21}$$

Results and Discussion

The reduced partial differential equations (7.16)-(7.19) along with the boundary conditions (7.20) are solved numerically using the extended spectral quasi-linearization method. In order to asses the code generated, for special case of $\xi = 0$, $N = 0$, $Bi \to \infty$, $Sr = 0$, $\mathcal{B} = 0$, $Da \to \infty$, $\varepsilon = 0$, $Fs = 0$ and $\lambda = 0$, the results have been compared with those of Lloyd and Sparrow [50] and the agreement is appeared to be good as shown in Tab. (6.2). To study the effects of coupling number, Biot number, viscous dissipation and Soret number, the computations have been carried out for fixed $Pr = 0.71$, $Re_{x_0} = 200$, $\epsilon = 0.9$, $Sc = 0.22$, $\xi = 0.5$ and $n = 0$.

The variation of non-dimensional velocity f', microrotation g, temperature θ and concentration ϕ are displayed in Fig. 7.8 for different values of the coupling number N in the presence and absence of Soret number. It can be noticed from Fig. 7.8(a) that with an increase in the value of coupling number N, decreases the velocity. From Fig. 7.8(b), it can be observed that initially, the microrotation profiles is flat, and then it shows the reverse rotation near the two boundaries with the increase of coupling number. Further, it remarked that there is no significant effect on microrotation profile with the increase of Soret number. It can be perceived from Figs. 7.8(c) and 7.8(d) that with an increase in the values of coupling number N, the temperature and concentration increase. Generally, the diffusive species with higher values of Soret number leads to increase in the concentration. As expected, the temperature and concentration of micropolar fluids are higher as compared with those values of the viscous fluid. Moreover, the velocity and concentration are more in the presence of Soret number, but they are less in the absence of Soret number.

Figs. 7.9(a) - 7.9(d) are prepared to show the variation of non-dimensional velocity f', microrotation g, temperature θ and concentration ϕ for different values of Bi in the presence and absence of ε. From Fig. 7.9(a), it can be observed that the velocity increases with the increase of both Biot number and viscous dissipation parameter. From Fig. 7.9(b), it can be noticed that as the

Biot number increases, the microrotation shows qualitatively same behaviour in the presence and absence of viscous dissipation parameter ε. The temperature enhances with the increase of Biot number as shown in Fig. 7.9(c). The viscous dissipation term in the energy equation acts as an internal distributed heat source generated due to the action of viscous stresses and hence, increases the temperature of the fluid. From Fig. 7.9(d), it can be noticed that the concentration increases with the increase of both Biot number and viscous dissipation parameter.

The influence of Darcy number Da and Forchhiemer number Fs on the dimensionless velocity f', microrotation g, temperature θ and concentration ϕ, is displayed in Figs. 7.10(a) - 7.10(d). It is clear that $Fs = 0.0$ represents the Darcy porous medium. With the increase of permeability, the porous matrix structure becomes less and less prominent and at the point of accumulation, as $Da \to \infty$ and $\epsilon = 1$, the porous medium vanishes. From Fig. 7.10(a), it can be observed that the velocity reduces with the increase of Darcy number in the presence of Forchheimer number, but it does not show significant effect in the absence of Forchheimer number. As the non-Darcy parameter increases, the porous medium offers more resistance to the fluid flow and hence, the velocity is more in the case of non-Darcy porous medium ($Fs = 0.5$) as compared with that of the Darcy porous medium case ($Fs = 0.0$). The microrotation shows reverse rotation with the increase of Darcy parameter in the presence of Forchheimer number [Fig. 7.10(b)]. From Fig. 7.10(c), it can be seen that with the increase of Darcy parameter the temperature shows reverse behaviour within the boundary layer for $Fs = 0.5$, but it depict opposite trend for $Fs = 0.0$. It can be remarked from Fig. 7.10(d) that with the increase of Darcy parameter, the concentration enhances in the case of non-Darcy porous medium, but it does not show significant effect in the Darcy porous medium case.

In Figs. 7.11(a)-7.11(d), the effects of mixed convection parameter λ on the dimensionless velocity, microrotation, temperature and concentration profiles across the boundary layers, are displayed. From Fig. 7.11(a), it can be illustrated that the velocity is more in the aiding flow and less in the opposing flow as compared to the velocity in the forced convective flow. The microrotation shows reverse rotation within the boundary as displayed in Fig. 7.11(b) for opposing, aiding and forced convective flows. The temperature and concentration exhibit qualitatively same behaviour with the influence of mixed convection parameter as shown in Figs. 7.11(c)-7.11(d). In other words, the temperature and concentration are more in the case of opposing flow as compared with those results in the aiding and forced convective flows.

The effects of coupling numbers on the skin friction, wall couple stress, Nusselt and Sherwood numbers against the streamwise coordinate ξ, are portrayed in Figs. 7.12(a) - 7.12(d) for both $Sr = 0.0$ and $Sr = 1.0$. It can be observed from Fig. 7.12(a) that the skin friction enhances with the increase of coupling number, but it enhances slightly with the increase of Soret number. The skin friction coefficient is higher for the micropolar fluid when compared with that of the viscous fluid. As the coupling number enhances, the wall couple stress reduces nonlinearly for the micropolar fluid in the presence and absence of the Soret number [Fig. 7.12(b)]. From Fig. 7.12(c), it can be perceived that the Nusselt number decreases with the increase of coupling number N, but it decreases marginally with the increase of Soret number. It can be observed from Fig. 7.12(d) that by enhancing the coupling number N, the Sherwood number reduces for both $Sr = 0.0$ and $Sr = 1.0$. Further, it can be noticed that the Nusselt and Sherwood numbers are lower for the micropolar fluid as compared with those of the viscous fluid for both $Sr = 0.0$ and $Sr = 1.0$.

Figs. 7.13(a) - 7.13(d) depict the variation of Biot number on the skin friction, wall couple stress, Nusselt and Sherwood numbers against the streamwise coordinate ξ in the presence and absence of viscous dissipation parameter. From Fig. 7.13(a), it can be illustrated that the skin friction coefficient increases with the increase of both Biot number and viscous dissipation parameter. It can be noticed that the wall couple stress coefficient decreases nonlinearly with an increase in both Bi and ε, as shown in Fig. 7.13(b). From Fig. 7.13(c), it can be observed that the Nusselt number enhances with the enhance of Biot number, but it reduces with the enhance of viscous dissipation parameter. From Fig. 7.13(d), it can be perceived that the Sherwood number decreases with an increase in Biot number but, it increases with an increase in viscous dissipation parameter.

Effects of Forchheimer number and Darcy number on the non-dimensional skin friction, wall couple stress, Nusselt and Sherwood numbers against the streamwise coordinate ξ, are depicted in Figs. 7.14(a) - 7.14(d). It is to note that $Fs = 0$ is taken in the analysis to indicate Darcy porous medium and the resistance to the flow is enhanced by increasing the Forchheimer number. It can be perceived from Fig. 7.14(a) that the skin friction decreases in the non-Darcy porous medium and slightly reduces in the Darcy porous medium with the increase of Darcy parameter. From Fig. 7.14(b), it can be noticed that with the increase of Darcy number, the wall couple stress increases for $Fs = 0.5$, but no siginificant effect is found for $Fs = 0.0$. From Fig. 7.14(c), it can be observed that with the increase of Darcy number, the Nusselt number shows more significant effect in the non-Darcy porous medium ($Fs = 0.5$) as compared with that of the Darcy porous medium($Fs = 0.0$).

The mass transfer rate reduces with the increase of Darcy parameter and also noticed that it is more prominent in the presence of Forchheimer number as shown in Fig. 7.14(d). From Figs. 7.14(a) - 7.14(d), it can be observed that the skin friction and mass transfer rate increase, but the wall couple stress and heat transfer rate decrease with the increase of Forchheimer number.

The variation of mixed convection parameter on the skin friction, wall couple stress, Nusselt and Sherwood numbers against streamwise coordinate ξ, is displayed in Figs. 7.15(a) - 7.15(d). From Fig. 7.15(a), it can be noticed that the skin friction in the opposing flow is less as compared with that of both aiding and forced convective flows. Fig. 7.15(b) shows that the wall couple stress decreases from the opposing flow to the aiding flow and moreover, it can be observed that the wall couple stress in the opposing flow is higher than that of the aiding flow. From Fig. 7.15(c), it can be revealed that the heat transfer rate decreases from the opposing flow to the aiding flow. It can be noticed in Fig. 7.15(d) that the mass transfer rate is less in the opposing flow as compared with that of the forced convective and aiding flows.

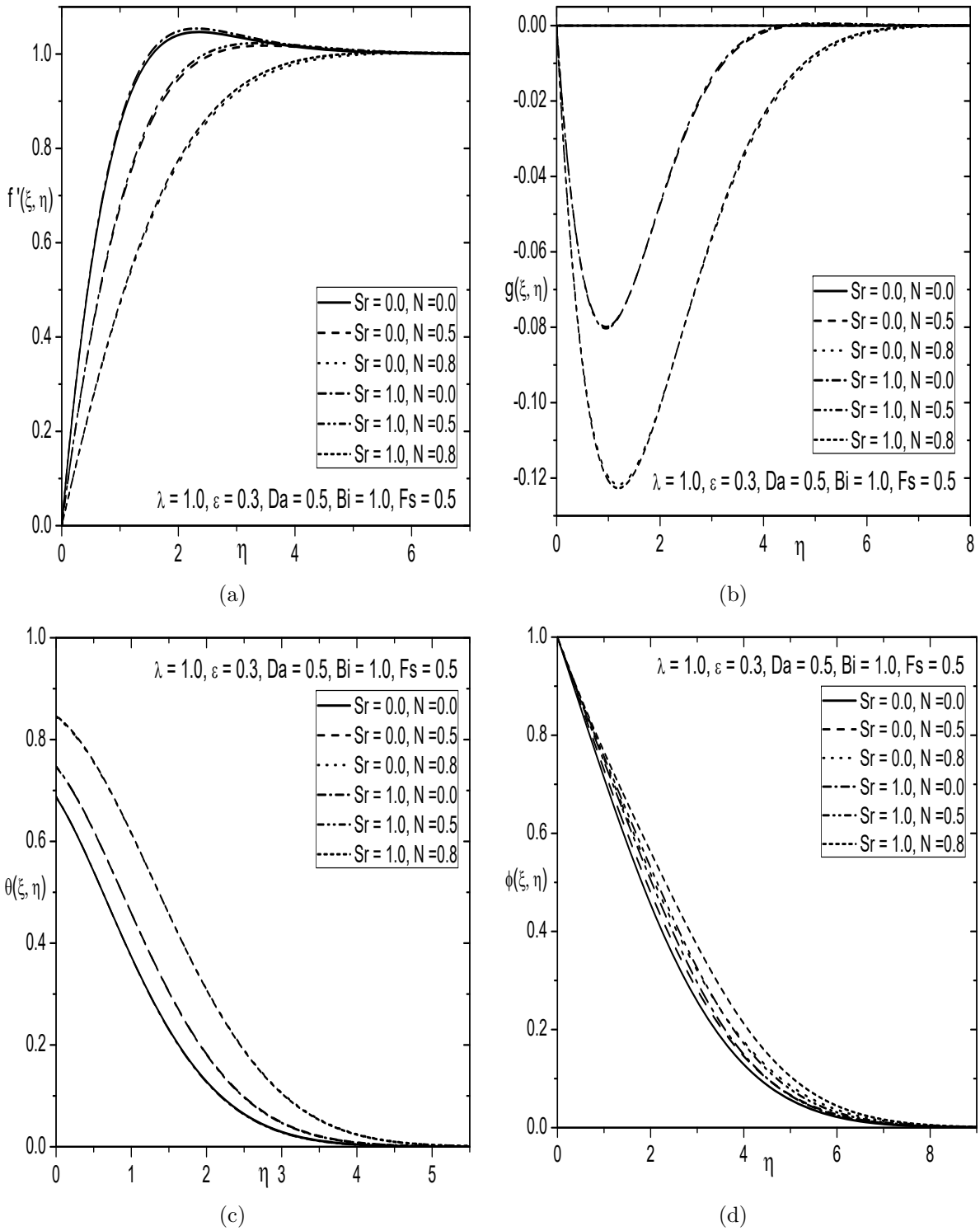

Figure 7.8: *Effects of Sr and N on (a)Velocity, (b)Microrotation, (c)Temperature and (d)Concentration.*

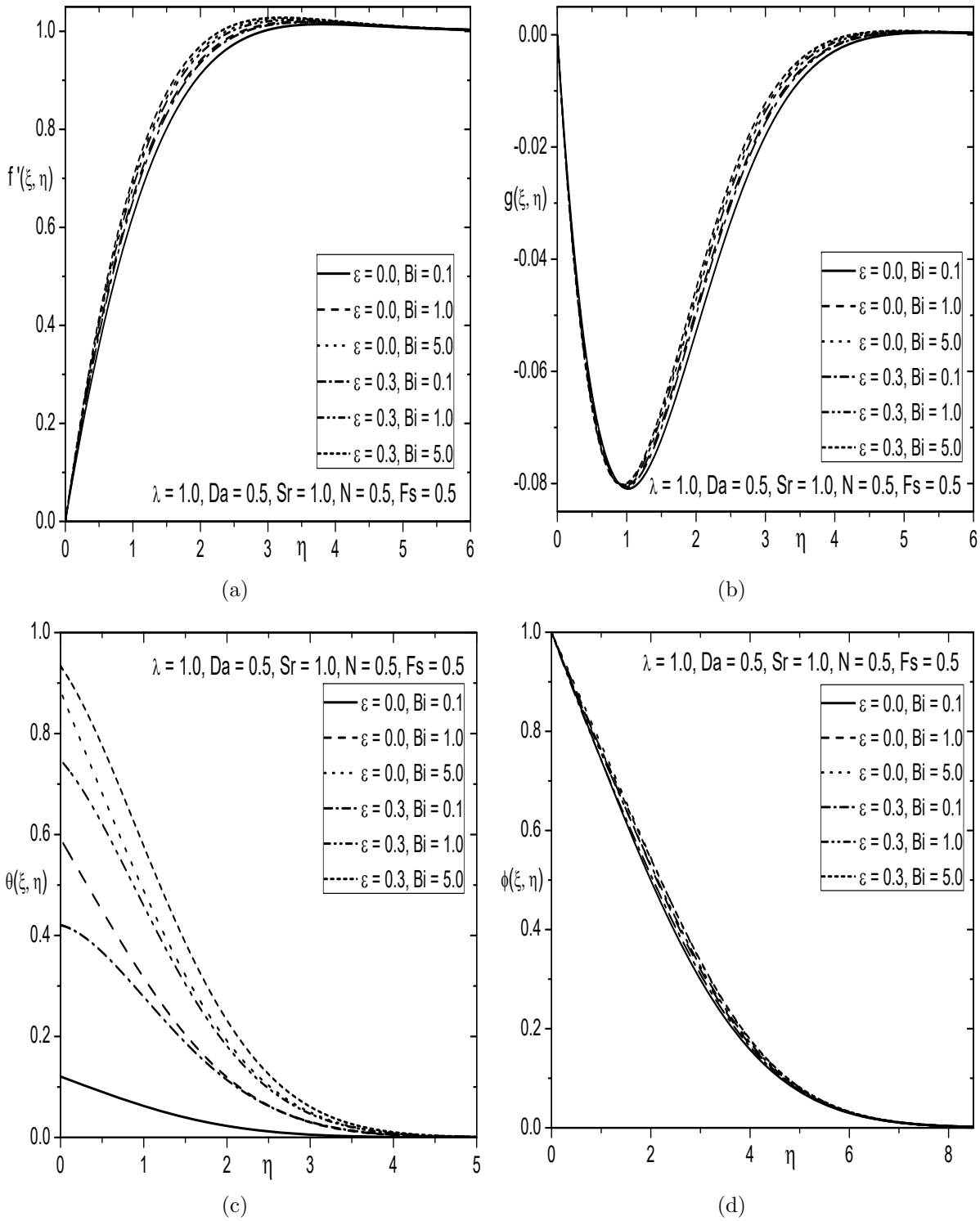

Figure 7.9: *Effects of ε and Bi on (a)Velocity, (b)Microrotation, (c)Temperature and (d)Concentration.*

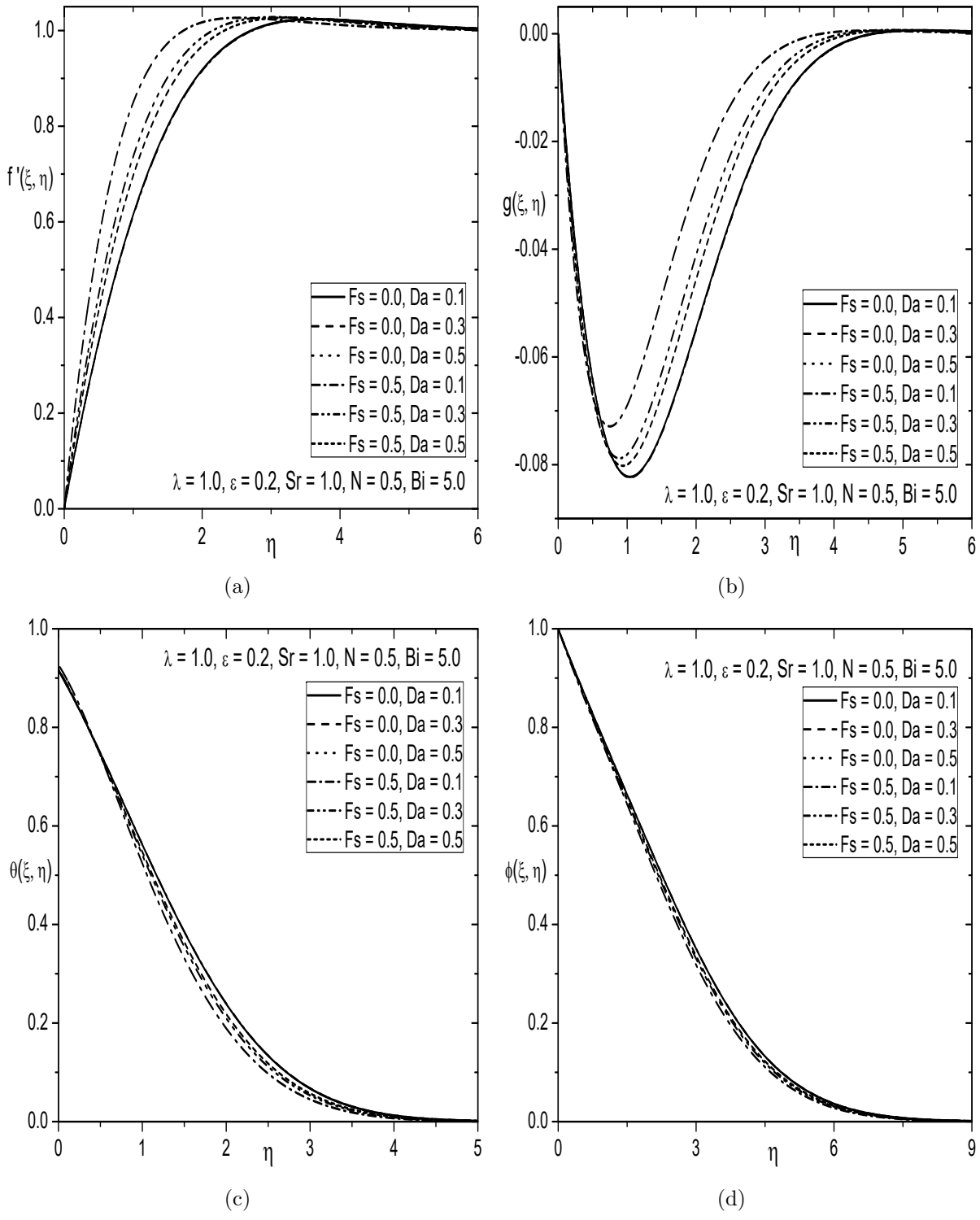

Figure 7.10: *Effects of Fs and Da on (a)Velocity, (b)Microrotation, (c)Temperature and (d)Concentration.*

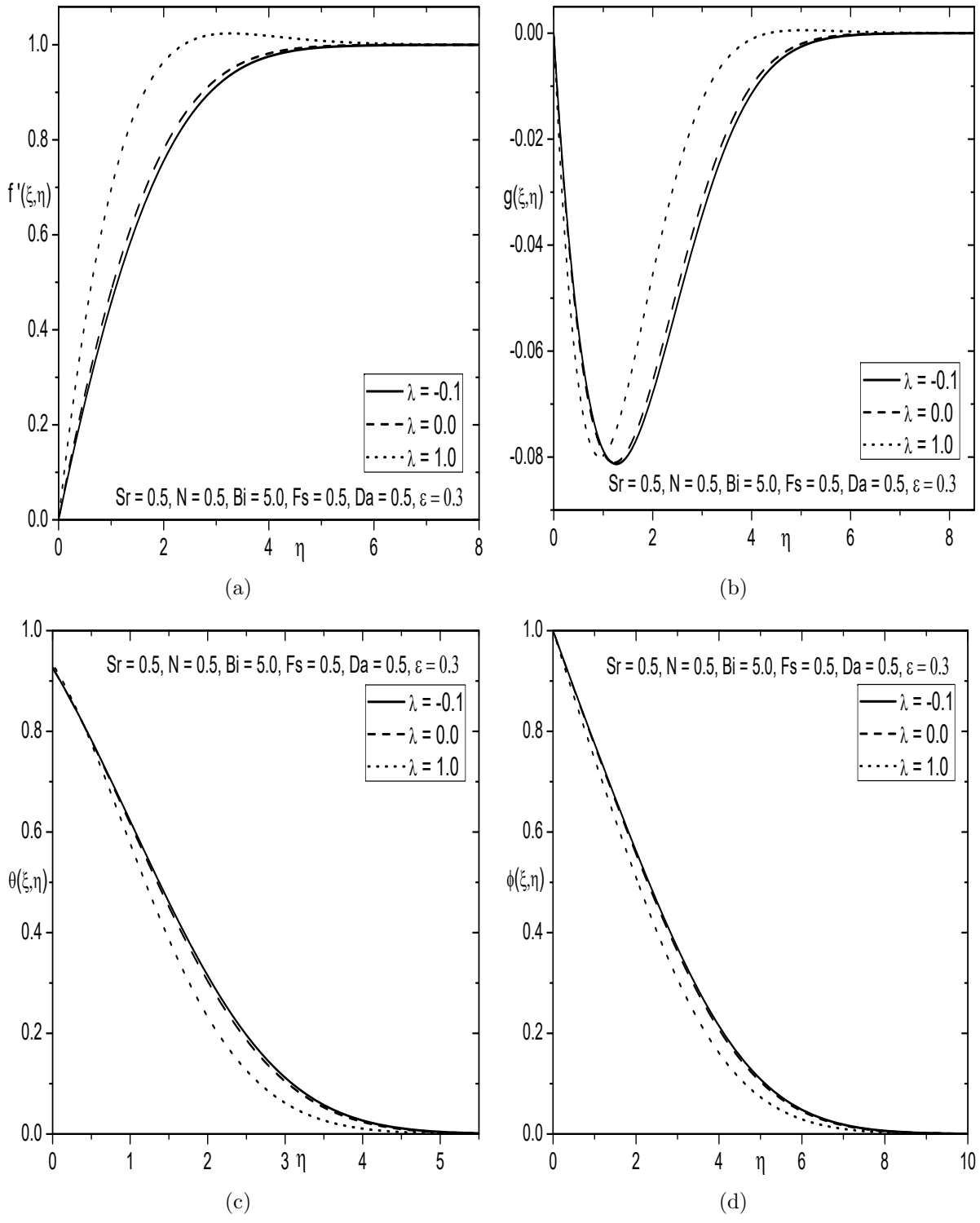

Figure 7.11: *Effects of λ on (a)Velocity, (b)Microrotation, (c)Temperature and (d)Concentration.*

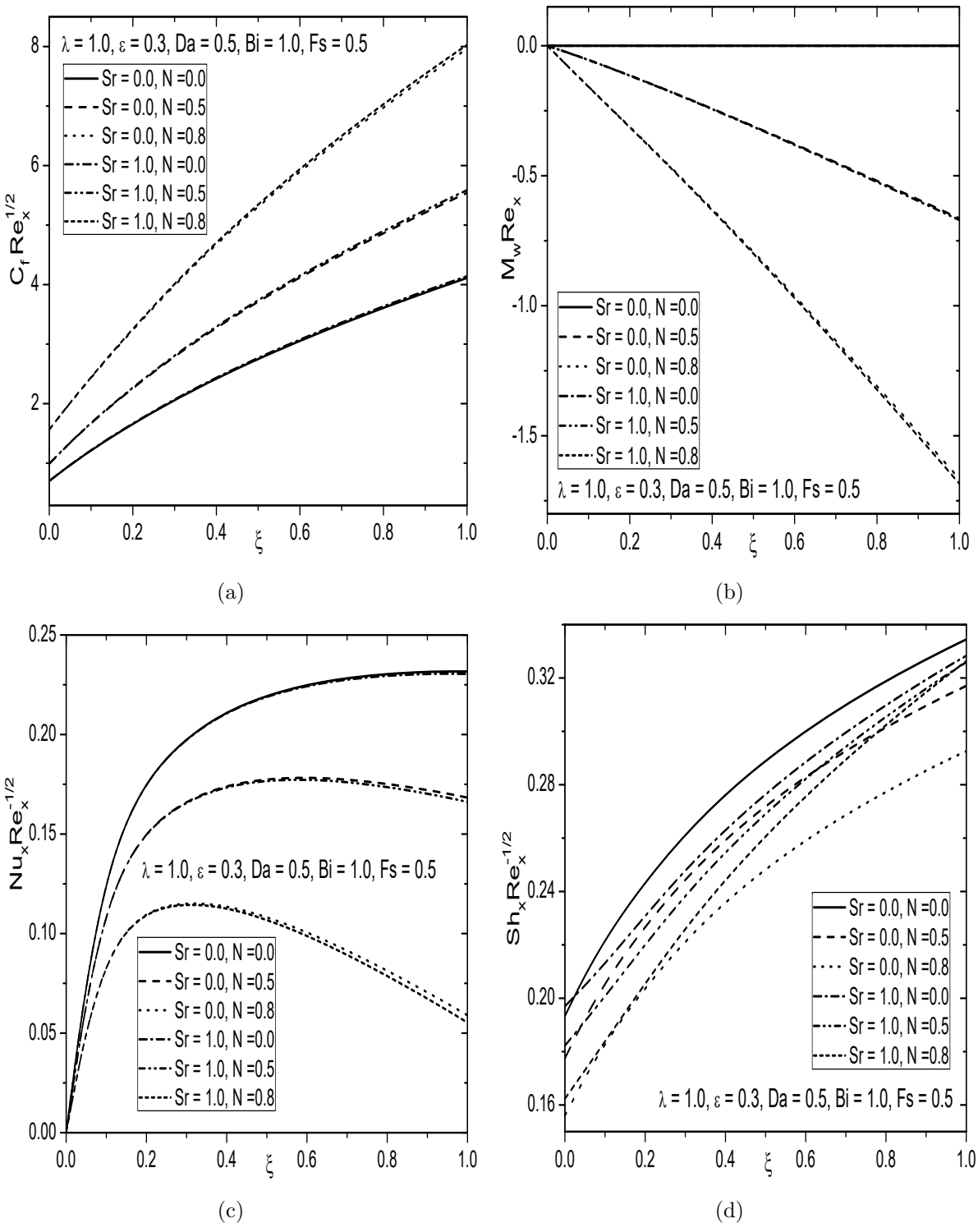

Figure 7.12: *Effects of Sr and N on (a)Skin friction, (b)Wall couple stress (c)Nusselt number and (d)Sherwood number.*

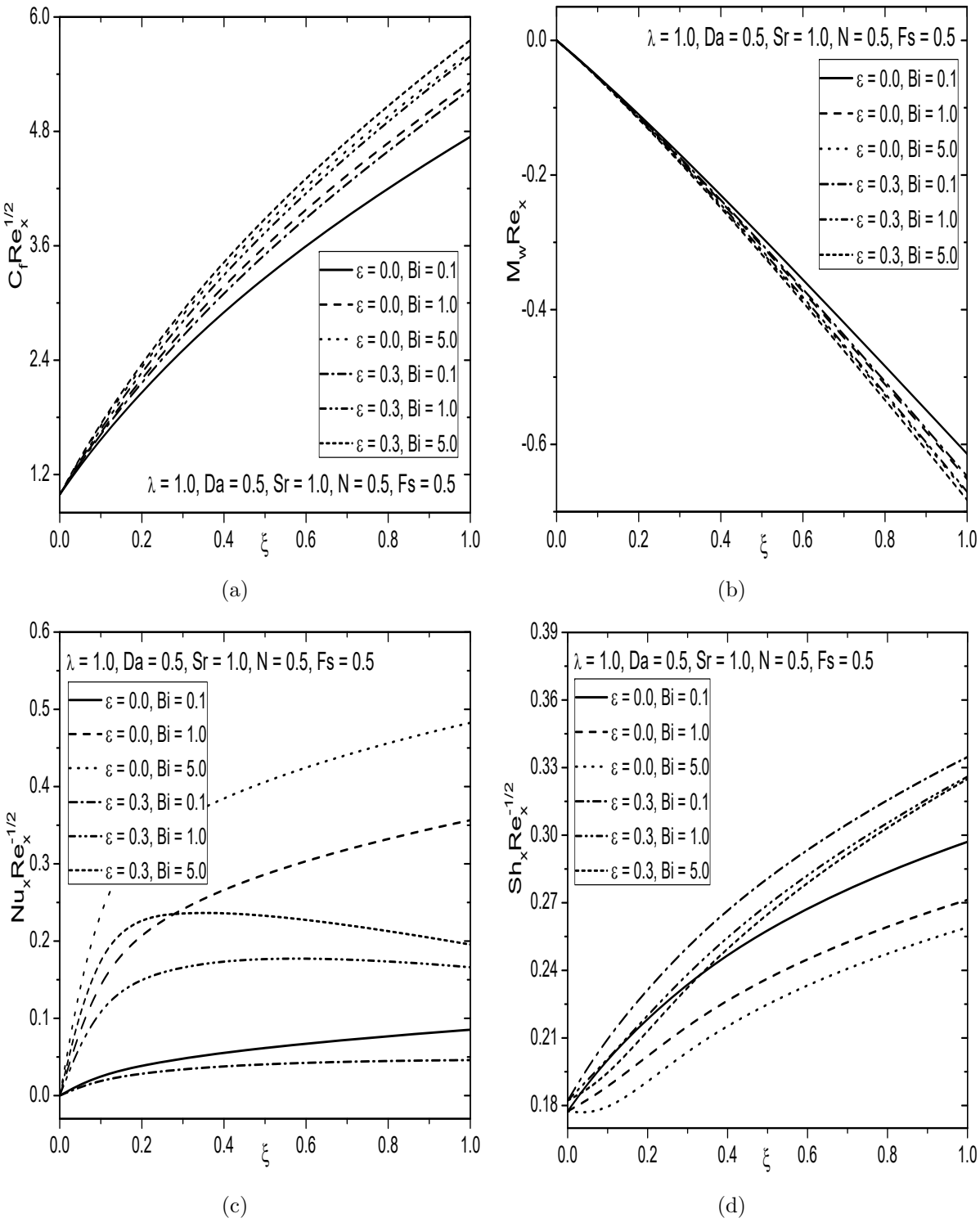

Figure 7.13: *Effects of ε and Bi on (a)Skin friction, (b)Wall couple stress, (c)Nusselt number and (d)Sherwood number.*

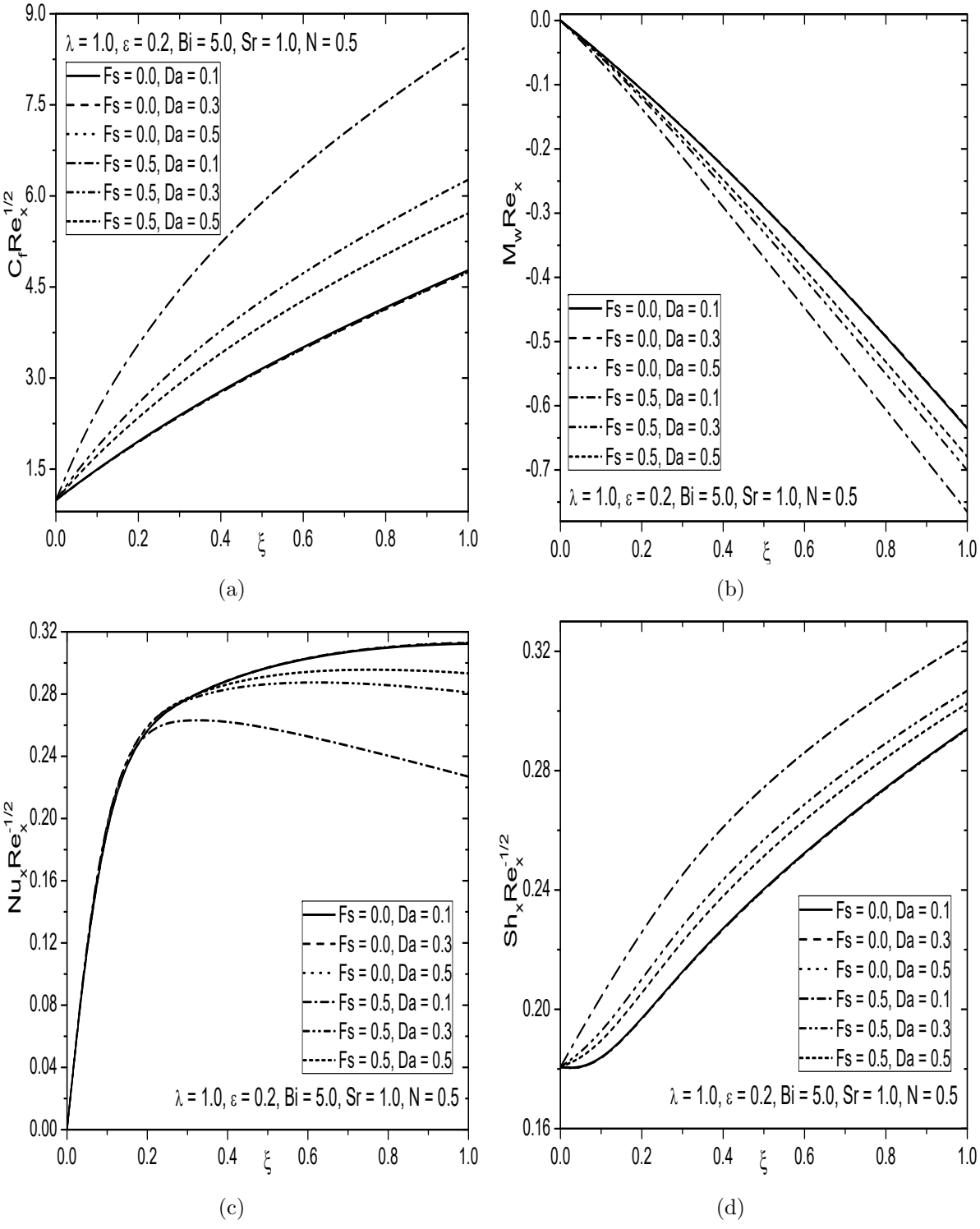

Figure 7.14: *Effects of Fs and Da on (a)Skin friction, (b)Wall couple stress, (c)Nusselt number and (d)Sherwood number.*

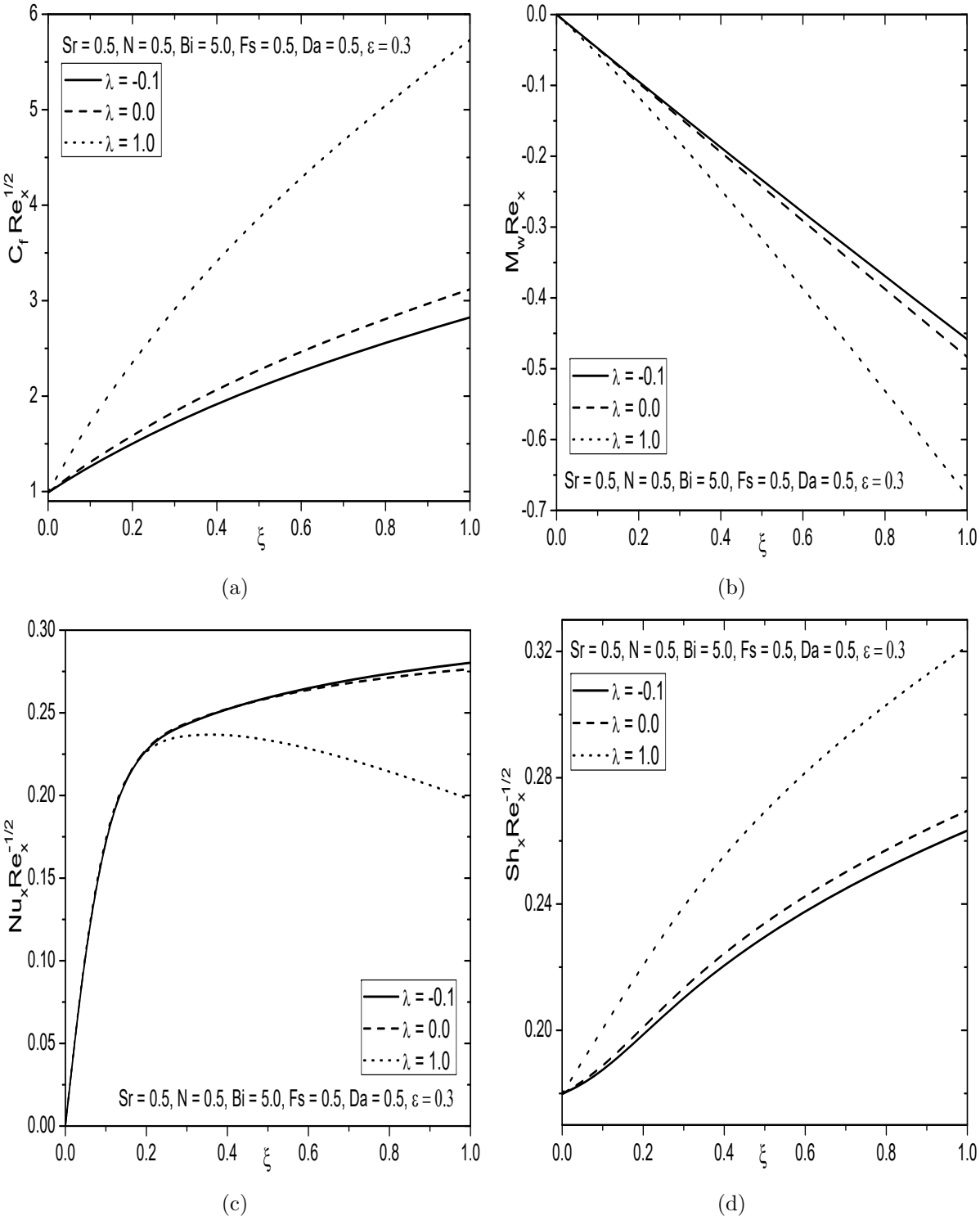

Figure 7.15: *Effect of λ on (a)Skin friction, (b)Wall couple stress, (c)Nusselt number and (d)Sherwood number.*

7.3 Conclusions

In this chapter, the convective flow of an incompressible micropolar fluid over a truncated cone embedded in a saturated porous medium with the viscous dissipation and thermal diffusion effects, is investigated. The resulting non-similarity equations are solved using the extended spectral quasi-linearization method. Based on the analysis carried out, the main conclusions are drawn for both case (a) and case (b) as given below.

As in the previous chapter, the behavior of various parameters namely, N, Sr, Bi are ε are found to be similar on various profiles. Case(a): In the presence and absence of the Forchheimer number, the velocity, skin friction, Nusselt and Sherwood number increase, whereas, the wall couple stress, temperature and concentration decrease with the increase of the Darcy parameter. The velocity, skin friction, heat and mass transfer decrease, but the wall couple stress, temperature and concentration increase with the increase of Forchheimer number. Moreover, the microrotation slightly reduces and then enhances within the boundary layer. Case(b): The velocity, skin friction and Sherwood numbers are more in the aiding flow than compared to that of the opposing flow. Further, the Nusselt number, temperature and concentration are more in the opposing flow and less in the aiding flow. The velocity, skin friction and Sherwood number reduce, but the wall couple stress, Nusselt number, concentration and temperature enhance with the enhance of the Darcy parameter and also, it is observed that these physical quantities are more prominent in the presence of Forchheimer number as compared with the absence of Forchheimer number. The skin friction, mass transfer rate and velocity increase, but the wall couple stress, heat transfer rate, temperature and concentration decrease with the increase of Forchheimer number.

Part IV

SUMMARY AND CONCLUSIONS

Chapter 8

Summary and Conclusions

In this thesis, an analysis of convective heat and mass transfer in a micropolar fluid with/without saturated porous medium subject to the convective boundary condition, is discussed. The study of convective boundary condition has a significant role in heat transfer problems because, it is more realistic in various engineering and industrial processes.

The similarity solution for convective flow along a vertical plate immersed in a micropolar fluid with and without saturated porous medium, is obtained in part-II. The objective of this part is to study the effects of Biot number, micropolar parameter, suction-injection parameter, Darcy parameter, non-linear convection parameter and homogeneous and heterogeneous reactions on free and mixed convective flows. The Lie scaling group of transformations is applied to get the similarity representation of the system of governing partial differential equations and then the resulting system of equations is solved using the spectral quasi-linearization method. The main results indicate the following findings for both (a) free convection and (b) mixed convection in the presence and/or absence of suction-injection parameter:

- An increase in the coupling number N, increases the temperature, concentration and skin friction, but reduces the wall couple stress, heat and mass transfer rates for both free and mixed convective flows. Moreover, the velocity reduces near plate and far away from the plate it shows reverse behaviour in case of free convection, while in mixed convective flow, the velocity decreases for both opposing and aiding flows. In the case of mixed convection flow of chapters 4 and 5, the species concentration reduces.

- The skin friction, mass transfer rate and species concentration (i.e., in chapters 4 and 5) increase whereas, the wall couple stress and concentration decrease with the increase of Biot number in both free convective and aiding flows, but, these show reverse behaviour in opposing flow. The wall couple stress increases for material constant $n = 0.5$ in free convective and aiding flows of chapter 2. Moreover, the velocity enhances in both aiding flow and free convection (near the surface of the plate), whereas it reduces in the opposing flow. The temperature and heat transfer rate enhance for both cases (a) and (b). Microrotation shows reverse rotation within the boundary layer.

- In free convective flow, the skin friction coefficient, heat transfer rate, velocity and species concentration (i,e., in the chapter 5) are more, but the wall couple stress, temperature and concentration (in chapter 3) are less with the increase of Darcy parameter. While, in mixed convective flows, these show reverse behaviour. Further, the microrotation depicts reverse trend.

- The higher values of nonlinear convection parameter results in lower temperature and wall couple stress coefficient, but higher velocity, species concentration, skin friction and heat transfer rate. The behaviour of physical quantities of the flow in the opposing and aiding flow situations show opposite nature.

- The increase in radiation parameter leads to increase in the velocity, species concentration and skin friction for both free convective and aiding flows, but these show reverse behaviour for the opposing flow. For both free and mixed convection, the temperature and heat transfer rate enhance.

- Species concentration and mass transfer rate decreases with the increase of strength of homogeneous and heterogeneous reaction parameters. The effect of heterogeneous reaction on species concentration is more as compared with that of the homogeneous reaction.

Part-III deals with the non-similarity solution for convective flow of a micropolar fluid over the vertical frustum of a cone with Soret and viscous dissipation effects in the presence and absence of non-Darcy porous medium. Studying the influence of pertinent parameters (i.e., like coupling number, Forchheimer number, Biot number, Soret and viscous dissipation) on the velocity, microrotation, temperature and concentration profiles along with the local skin friction, wall couple stress, heat and mass transfer rates are the objectives of this section. Using non-similarity variables, the

governing equations are transformed into non-linear partial differential equations and then solved by using the extended spectral quasi-linearization method. The important observations from these investigations are as follows:

- An increase in coupling number leads to decrease in the wall couple stress, Nusselt number and Sherwood number, but increase in the temperature, concentration and skin friction. Moreover, the velocity decreases in case (a) and (b), but far away from the truncated cone surface, it shows opposite trend in case(a).

- The concentration and skin friction increase, but the wall couple stress and mass transfer rates decrease with the increase of Soret number. Moreover, the heat transfer rate decreases, but it increases in free convective flow (i,e., in chapter 7). Further, the velocity enhances slightly near the vertical frustum of a cone and far away from the surface it shows reverse behaviour in case (a) whereas, it enhances in case (b).

- By enhancing the Biot number, the skin friction, Nusselt number and temperature enhance but, the wall couple stress and Sherwood number reduce. The velocity and concentration depicts reverse behaviour within the boundary layers in case(a) but, they increases in case(b).

- As the viscous dissipation parameter increases, the wall couple stress and heat transfer rate decrease, but the temperature, skin friction and mass transfer rate increase. The velocity and concentration depicts reverse behaviour within the boundary layer in case(a) but, they increase in case(b). Moreover, with the increase of viscous dissipation parameter, the microrotation depicts reverse rotation within the boundary layer.

- In case(a), the velocity, skin friction, Nusselt and Sherwood numbers increase, whereas, the wall couple stress, temperature and concentration decrease with the increase of the Darcy parameter. Moreover, the microrotation slightly reduces and then enhances. In case(b), the velocity, skin friction and Sherwood number reduce, but the wall couple stress, Nusselt number, concentration and temperature increase with the increase of the Darcy parameter. The effect of Darcy parameter is more prominent in the presence of Forchheimer number as compared with those results in the absence of Forchheimer number.

- With the increase of Forchheimer number, the velocity, skin friction, heat and mass transfer decrease, but the wall couple stress, temperature and concentration increase in case(a). The

skin friction, mass transfer rate and velocity increase whereas, the wall couple stress, heat transfer rate, temperature and concentration decrease in case (b).

- As compared to the opposing flow, the skin friction, Sherwood number and velocity are more, but the temperature and concentration are less in the case of aiding flow. The Nusselt number is less in the opposing flow as compared with that of the forced convective and aiding flows in case(a), but it shows opposite trend in case (b).

The work presented in the thesis can be extended to analyze the effects of Joule heating, stratification, double dispersion, MHD, Hall and Ion slip, first and second order slip, etc. Further, this work can be extended by studying the analysis for various non-Newtonian fluids like Couple stress fluids, Casson fluids, nanofluids, etc. Such an exhaustive study can be a rewarding experience though it is challenging as well as time consuming.

Bibliography

[1] E. M. Aboeldahab and E. M. E. Elbarbary. Hall current effect on magnetohydrodynamic free convection flow past semi-infinite vertical plate with mass transfer. *International Journal of Engineering Science*, 39:1641–1652, 2001.

[2] K. Ahmad, A. Ishak, and R. Nazar. Micropolar fluid flow and heat transfer over a nonlinearly stretching plate with viscous dissipation. *Mathematical Problems in Engineering*, 2013:1–5, 2013.

[3] G. Ahmadi. Self-similar solution of incompressible micropolar boundary layer flow over a semi-infinite plate. *Internationl Journal of Engineering Science*, 14:639–646, 1976.

[4] Y. M. Aiyesimi, A. Yusuf, and M. Jiya. A hydromagnetic boundary layer micropolar fluid over a stretching surface in a non-darcy medium with permeability. *Universal Journal of Applied Mathematics*, 1(2):136–141, 2013.

[5] T. Ariman, Turk M.A., and N.D. Sylvester. Microcontinuum fluid mechanics-a review. *Int. J. Engg. Sci.*, 11(8):905–930, 1973.

[6] T. Ariman, Turk M.A., and N.D. Sylvester. Applications of microcontinuum fluid mechanics. *Int. J. Engg. Sci.*, 12(4):273–293, 1974.

[7] F. Awad and P. Sibanda. Dufour and soret effects on heat and mass transfer in a micropolar fluid in a horizontal channel. *WSEAS Trans. Heat Mass Transfer*, 5:165–177, 2010.

[8] A. Aziz. A similarity solution for laminar thermal boundary layer over a flat plate with a convective surface boundary condition. *Communications in Nonlinear Sciences and Numerical Simulations*, 14:1064–1068, 2009.

[9] N. Bachok, A. Ishak, and I. Pop. On the stagnation-point flow towards a stretching sheet with homogeneous heterogeneous reactions effects. *Communications in Nonlinear Sciences and Numerical Simulations*, 16:4296–4302, 2011.

[10] A. Bakier. Natural convection heat and mass transfer in a micropolar fluid saturated non-darcy porous regime with radiation and thermophoresis effects. *Thermal Science*, 15(9):S317–S326, 2011.

[11] H. Barrow and T.L.S. Rao. The effect of variable beta on free convection. *Br. Chem. Eng.*, 16:704–709, 1971.

[12] R.C. Bataller. Radiation effects for the blasius and sakiadis flows with a convective surface boundary condition. *Applied Mathematics and Computation*, 206(2):832–840, 2008.

[13] O. Beg, J. Zueco, and H. Takhar. Laminar free convection from a continuously moving vertical surface in thermally-stratified non-darcian high porosity medium: Network numerical study. *Int. Commun. in Heat and Mass Transfer*, 35:810–816, 2008.

[14] O.A. Beg, R. Bhargava, S. Rawat, H.S. Takhar, and T.A. Beg. Numerical analysis of grashof and darcy number effects on dissipative natural convection boundary layers in micropolar fluid saturated geological porous medium. *International Journal of Fluid Mechanics Research*, 34:287–307, 2007.

[15] A. Bejan. *Convective Heat Transfer*. John Wiley, New York, 2004.

[16] R.E. Bellman and R.E. Kalaba. *Quasilinearisation and Non-Linear Boundary Value Problems*. Elsevier, New York, 1965.

[17] G.W. Bluman and S.C. Anco. *Symmetry and Integration Methods for Differential Equations*. Springer Verlag, 2009.

[18] C. Canuto, M.Y. Hussaini, A. Quarteroni, and T. Zang. *Spectral Methods: Fundamentals in Single Domains, Scientific Computation*. Springer, Berlin, Germany, 2006.

[19] A.J. Chamkha, A. Al-Mudhaf, and J. Al-Yatama. Double-diffusive convective flow of a micropolar fluid over a vertical plate embedded in a porous medium with a chemical reaction. *International Journal of Fluid Mechanics Research*, 31(6):529–551, 2004.

[20] M.A. Chaudhary and J.H. Merkin. Homogeneous-heterogeneous reactions in boundary layer flow: effects of loss of reactant. *Mathl. Comput. Modelling*, 24(3):21–28, 1996.

[21] C.Y. Cheng. Natural convection of a micropolar fluid from a vertical truncated cone with power-law variation in temperature. *International Communications in Heat and Mass Transfer*, 35:39–46, 2008.

[22] C.Y. Cheng. Free convection of non-newtonian nanofluids about a vertical truncated cone in a porous medium. *International Communications in Heat and Mass Transfer*, 39(9):1348–1353, 2012.

[23] S.C. Cowin. Polar fluids. *Physics of Fluids*, 11:1919–1927, 1968.

[24] H.P.G. Darcy. Mles fontaines publiques de la ville de dijon. *Victor Dalmont*, 1856.

[25] W. S. Don and A. Solomonoff. Accuracy and speed in computing the chebyshev collocation derivative. *SIAM J. Sci. Comput.*, 16:1253–1268, 1995.

[26] E. R. G. Eckert and R. M. Drake. *Analysis of Heat and Mass Transfer*. McGraw Hill, New York, 1972.

[27] M.F. El-Amin and A.A. Mohammadein. Effects of viscous dissipation and joule heating on magnetohydrodynamic hiemenz flow of a micropolar fluid. *Heat Transfer Engineering*, 26(6):75–81, 2005.

[28] M.A El-Aziz. Viscous dissipation effect on mixed convection flow of a micropolar fluid over an exponentially stretching sheet. *Canadian Journal of Physics*, 87(4):359–368, 2009.

[29] S.M.M. El-Kabeir and R.S.R. Gorla. Mhd effects on natural convection in a micropolar fluid at a three-dimensional stagnation point in a porous medium. *International Journal of Fluid Mechanics Research,*, 34(2):145–158, 2007.

[30] E.M.A. Elbashbeshy, T.G. Emam, and E.A. Sayed. Effect of thermal radiation on free convection flow and heat transfer over a truncated cone in presence of pressure work and heat generation/absorption. *Thermal Science*, 20(2):555–565, 2016.

[31] V. A. Eremeyev, L.P. Lebedev, and H. Altenbach. *Foundations of Micropolar Mechanics*. Springer, Heidelberg New York, 2013.

[32] A. C. Eringen. Theory of micropolar fluids. *Thermal Science*, 20:555–565, 2016.

[33] B. Gebhart. Effect of viscous dissipation in natural convection. *Journal of Fluid Mechanics*, 14:225–235, 1962.

[34] R.E Hamilton, T.J. Fagan, and G. Kennedy. Closed loop liquid cooling for semiconductor rf simplifier modules. (US005901037A), 1999.

[35] M.Z. Haque, M.M. Alam, M. Ferdows, and A. Postelnicu. Micropolar fluid behaviors on steady mhd free convection and mass transfer flow with constant heat and mass fluxes, joule heating and viscous dissipation. *Journal of King Saud University Engineering Sciences*, 24:71–84, 2012.

[36] I.A. Hassanien, A.H. Essawy, and N.M. Moursy. Natural convection flow of micropolar fluid from a permeable uniform heat flux surface in porous medium. *Applied Mathematics and Computation*, 152(4):323–335, 2004.

[37] I.A. Hassanien and M.A.A. Hamad. Group theoretic method for unsteady free convection flow of a micropolar fluid along a vertical plate in a thermally stratified medium. *Applied Mathematical Modelling*, 32(6):1099–1114, 2008.

[38] T. Hayat, Z. Abbas, and T. Javed. Mixed convection flow of a micropolar fluid over a non-linearly stretching sheet. *Physics Letters A*, 372:637–647, 2008.

[39] T. Hayat, Z. Hussain, M. Farooq, and A. Alsaedi. Effects of homogeneous and heterogeneous reactions and melting heat in the viscoelastic fluid flow. *Journal of Molecular Liquids*, 215:749–755, 2016.

[40] M. A. Hossain and H. S. Takhar. Radiation effect on mixed convection along a vertical plate with uniform surface temperature. *Heat and Mass Transfer*, 31(4):243–248, 1996.

[41] D.B. Ingham and I. Pop. *Transport Phenomena in Porous Media*. Elsevier, Oxford, 2005.

[42] A. Ishak. Similarity solutions for flow and heat transfer over a permeable surface with convective boundary condition. *Applied Mathematics and Computation*, 217:837–842, 2010.

[43] S.K. Jena and M.N. Mathur. Mixed convection flow of a micropolar fluid from an isothermal vertical plate. *Camp. Maths. with Appls.*, 10:291–304, 1984.

[44] N. G. Kafoussias and E. W. Williams. The effect of temperature-dependent viscosity on free-forced convective laminar boundary layer flow past a vertical isothermal flat plate. *Acta Mechanica*, 110:123–137, 1995.

[45] N. G. Kafoussias and N. G. Williams. Thermal-diffusion and diffusion-thermo effects on mixed free-forced convective and mass transfer boundary layer flow with temperature dependent viscosity. *Int. J. Engng. Sci.*, 33:1369–1384, 1995.

[46] P. K. Kameswaran, S. Shaw, P. Sibanda, and P.V. S. N. Murthy. Homogeneous-heterogeneous reactions in a nanofluid flow due to a porous stretching sheet. *Int. J. Heat and Mass Transfer*, 57:465–472, 2013.

[47] P. K. Kameswaran, P. Sibanda, M. K. Partha, and P.V. S. N. Murthy. Thermophoretic and nonlinear convection in non-darcy porous medium. *Journal of Heat Transfer*, 136(4):042601–1–9, 2014.

[48] R. Kandasamy, K. Gunasekaran, and S.B.H. Hasan. Scaling group transformation on fluid flow with variable stream conditions. *Int. J. Non-Linear Mechanics*, 46(7):976–985, 2011.

[49] W. A. Khan and I. Pop. Effects of homogeneousheterogeneous reactions on the viscoelastic fluid toward a stretching sheet. *J. Heat Transfer*, 134:1–5, 2012.

[50] J. R. Lloyd and E. M. Sparrow. Combined free and forced convective flow on vertical surfaces. *Int. J. Heat and Mass Transfer*, 13:434–438, 1970.

[51] G. Lukaszewicz. *Micropolar fluids - Theory and Applications*. Birkhauser, Basel, Switzerland, 1999.

[52] A. Mahdy. Effect of chemical reaction and heat generation or absorption on double-diffusive convection from a vertical truncated cone in porous media with variable viscosity. *International Communications in Heat and Mass Transfer*, 37:548–554, 2010.

[53] O.D. Makinde. Free convection flow with thermal radiation and mass transfer past a moving vertical porous plate. *International Communications in Heat and Mass Transfer*, 32(10):1411–1419, 2005.

[54] O.D. Makinde. Similarity solution for natural convection from a moving vertical plate with internal heat generation and a convective boundary condition. *Thermal Science*, 15:S137–S143, 2011.

[55] O.D. Makinde and A. Aziz. Mhd mixed convection from a vertical plate embedded in a porous medium with a convective boundary condition. *Int. J. Thermal Sciences*, 49:1813–1820, 2010.

[56] J. H. Merkin. The effect of buoyancy forces on the boundary layer flow over semi-infinite vertical flat plate in a uniform free stream. *Journal of Fluid Mechanics*, 35:439–450, 1969.

[57] J.H. Merkin. Free convection boundary layer on an isothermal horizontal circular cylinders. In *ASME/AIChE, Heat Transfer Conference*, pages 9–11, St. Louis, MO, August 1976.

[58] J.H. Merkin. Mixed convection from a horizontal circular cylinder. *Int. J. Heat and Mass Transfer*, 20:73–77, 1977.

[59] J.H. Merkin. A model for isothermal homogeneous-heterogeneous reactions in boundary layer flow. *Mathl. Comput. Modelling*, 24(8):125–136, 1996.

[60] M.M. Molla, M.A. Hossain, and M.C. Paul. Natural convection flow from an isothermal horizontal circular cylinder in presence of heat generation. *Int. J. Eng. Sci.*, 44:949–958, 2006.

[61] S.S. Motsa. A new spectral local linearization method for nonlinear boundary layer flow problems. *Journal of Applied Mathematics*, 2013:1–15, 2013.

[62] S.S. Motsa, F.G. Awad, Z.G. Makukula, and P. Sibanda. The spectral homotopy analysis method extended to systems of partial differential equations. *Abstract and Applied Analysis*, 2014:1–11, 2014.

[63] S.S. Motsa, P.G. Dlamini, and M. Khumalo. Spectral relaxation method and spectral quasi-linearization method for solving unsteady boundary layer flow problems. *Advances in Mathematical Physics*, 2014:1–12, 2014.

[64] S.S. Motsa, P. Sibanda, J.M. Ngnotchouye, and G.T. Marewo. A spectral relaxation approach for unsteady boundary-layer flow and heat transfer of a nanofluid over a permeable stretching/shrinking sheet. *Advances in Mathematical Physics*, 2014:1–10, 2014.

[65] R. Muthuraj, S. Srinivas, A. K. Shukla, and T. R. Ramamohan. Effects of thermal-diffusion, diffusion-thermo, and space porosity on mhd mixed convective flow of micropolar fluid in a vertical channel with viscous dissipation. *Heat TransferAsian Research*, 43(6):561–576, 2014.

[66] A.A. Mutlag, M.J. Uddin, M.A.A. Hamad, and A.I.M. Ismail. Heat transfer analysis for falkner-skan boundary layer flow past a stationary wedge with slip boundary conditions considering temperature-dependent thermal conductivity,. *Sains Malaysiana*, 42:855–862, 2013.

[67] A.A. Mutlag, M.J. Uddin, and A.I.M. Ismail. Scaling transformation for free convection flow of a micropolar fluid along a moving vertical plate in a porous medium with velocity and thermal slip boundary conditions. *Sains Malaysiana*, 43(8):1249–1257, 2014.

[68] T.Y. Na and J.P. Chiou. Laminar natural convection over a frustum of a cone. *Applied Scientific Research*, 35:409–421, 1979.

[69] J. Nakamura, K. Kusunoki, M. Matsushita, M. Watanabe, I. Sawada, H. Fukada, and S. Tohi. Plate heat exchanger used as evaporator or condenser. (W02010013608), 2010.

[70] R. Nandkeolyar, P.K. Kameswaran, S. Shaw, and P. Sibanda. Heat transfer on nanofluid flow with homogeneous-heterogeneous reactions and internal heat generation. *Journal of Heat Transfer*, 136(12):122001–1–8, 2014.

[71] R. Nandkeolyar, A. Sutradhar, P. V. S. N. Murthy, and P. Sibanda. Viscous dissipation and newtonian heating effects on free non-linear convection in a nanofluid saturated porous media. *Open Journal of Heat Mass and Momentum Transfer*, 2:87–97, 2014.

[72] R. Nazar, N. Amin, and I. Pop. Free convection boundary layer on an isothermal horizontal circular cylinder in a micropolar fluid. In *Proceedings of the* 12^{th} *International Heat Transfer Conference*, Paris: Elsevier, August 2002.

[73] R. Nazar, N. Amin, and I. Pop. Mixed convection boundary-layer flow from a horizontal circular cylinder in micropolar fluids: case of constant wall temperature. *Int. J. Numerical Methods for Heat and Fluid Flow*, 13(1):86–109, 2003.

[74] D.A. Nield and A. Bejan. *Convection in Porous Media.* 4^{th} Ed., Springer-Verlag, New York, 2013.

[75] P.J. Olver. *Application of Lie Group to Differential Equations, Graduate Text in Mathematics*. Springer, New York, 1993.

[76] L.V. Ovsiannikov. *Group Analysis of Differential Equations*. Academic Press, New York, 1982.

[77] M.K. Partha. Nonlinear convection in a non-darcy porous medium. *Appl. Math. Mech. -Engl. Ed.*, 31(5):565–574, 2010.

[78] F. O. Patrulescu, T. Grosan, and I. Pop. Mixed convection boundary layer flow from a vertical truncated cone in a nanofluid. *Int. J. Numerical Methods for Heat and Fluid Flow*, 24(5):1175–1190, 2014.

[79] A. Postelnicu. Free convection about a vertical frustum of a cone in a micropolar fluid. *Int. J. Eng. Sci.*, 44:672–682, 2006.

[80] A. Postelnicu. Free convection from a truncated cone subject to constant wall heat flux in a micropolar fluid. *Meccanica*, 47:1349–1357, 2012.

[81] K.V. Prasad, K. Vajravelu, and R.A. Van Gorder. Non-darcian flow and heat transfer along a permeable vertical surface with nonlinear density temperature variation. *Acta Mechanica*, 220:139–154, 2011.

[82] M. M. Rahman, J. H. Merkin, and I. Pop. Mixed convection boundary layer flow past a vertical flat plate with a convective boundary condition. *Acta Mechanica*, 226:2441, 2015.

[83] M. M. Rahman and T. Sultana. Radiative heat transfer flow of micropolar fluid with variable heat flux in a porous medium. *Nonlinear Analysis: Modelling and Control*, 13:71–87, 2008.

[84] A. Raptis. Radiation and free convection flow through a porous medium. *International Communications in Heat and Mass Transfer*, 25(2):289–295, 1998.

[85] A. Rashad and A.J. Chamka. Heat and mass transfer by natural convection flow about a truncated cone in porous media with soret and dufour effects. *Int. J. Numerical Methods for Heat and Fluid Flow*, 24(3):595–612, 2014.

[86] M.M. Rashidi, S.A. Mohimanian pour, and S. Abbasbandy. Analytic approximate solutions for heat transfer of a micropolar fluid through a porous medium with radiation. *Communications in Nonlinear Science and Numerical Simulation*, 16(4):1874–1889, 2011.

[87] D.A. Rees and I. Pop. Free convection boundary layer flow of a micropolar fluid from a vertical flat plate. *IMA Journal of Applied Mathematics*, 61(2):179–197, 1998.

[88] H. Rosali, A. Ishak, and I. Pop. Micropolar fluid flow towards a stretching/shrinking sheet in a porous medium with suction. *International Communications in Heat and Mass Transfer*, 39(6):826–829, 2012.

[89] B.R. Rout, S.K. Parida, and Panda S. Mhd heat and mass transfer of chemical reaction fluid flow over a moving vertical plate in presence of heat source with convective surface boundary condition. *International Journal of Chemical Engineering*, 2013:1–10, 2013.

[90] M.A. Seddeek, M.Y. Akl, and A.M. Al-Hanaya. Thermal radiation effects on mixed convection and mass transfer flow on vertical porous plate with heat generation and chemical reaction by using scaling group. *J. Natural Sciences and Mathematics*, 4:41–60, 2010.

[91] S. Shaw, P.K. Kameswaran, and P. Sibanda. Homogeneous–eterogeneous reactions in micropolar fluid flow from a permeable stretching or shrinking sheet in a porous medium. *Boundary Value Problems*, 2013:1–10, 2013.

[92] P. Singh, V. Radhakrishnan, and K.A. Narayan. Non-similar solutions of free convection flow over a vertical frustum of a cone for constant wall temperature. *Ingenieur-Archiv*, 59:382–389, 1989.

[93] D. Srinivasacharya, S.S. Motsa, and O. Surender. Numerical study of free convection in a doubly stratified non-darcy porous medium using spectral quasilinearization method. *International Journal of Nonlinear Science and Numerical Simulation*, 16:173–183, 2015.

[94] D. Srinivasacharya and Ch. RamReddy. Free convective heat and mass transfer in a doubly stratified non-darcy micropolar fluid. *Korean J. Chem. Eng.*, 28(9):1824–1832, 2011.

[95] D. Srinivasacharya and Ch. RamReddy. Mixed convection heat and mass transfer in a micropolar fluid with soret and dufour effects. *Adv. Appl. Math. Mech.*, 3(4):389–400, 2011.

[96] D. Srinivasacharya and Ch. RamReddy. Mixed convection in a doubly stratified micropolar fluid saturated non-darcy porous medium. *Canadian J. Chemical Engineering*, 90:1311–132, 2012.

[97] D. Srinivasacharya and Ch. RamReddy. Mixed convection heat and mass transfer in a doubly stratified micropolar fluid. *Computational Thermal Sciences*, 5(4):273–287, 2013.

[98] D. Srinivasacharya and M. Shiferaw. Cross diffusion effects on chemically reacting magnetohydrodynamic micropolar fluid between concentric cylinders. *Journal of Heat Transfer*, 135:122003–1–10, 2013.

[99] D. Srinivasacharya and M. Upendar. Free convection in mhd micropolar fluid with soret and dufour effects. *Int. J. Engng. Sci.*, 33:1369–1384, 1995.

[100] T. Tapanidis, G. Tsagas, and H. P. Mazumdar. Application of scaling group of transformations to viscoelastic second-grade fluid flow. *Nonlinear Functional Analysis and Applications*, 8(3):345–350, 2003.

[101] L. N. Trefethen. *Spectral Methods in MATLAB*. SIAM, 2000.

[102] K. Vafai. *Handbook of Porous Media*. 3^{rd} Ed., CRC Press, Taylor and Francis Group, 2015.

[103] K. Vajravelu, J.R. Cannon, J. Leto, R. Semmoum, S. Nathan, M. Draper, and D. Hammock. Nonlinear convection at a porous flat plate with application to heat transfer from a dike. *J. Math. Anal. Appl.*, 277:609–623, 1971.

[104] N.A. Yacob and A. Ishak. Stagnation point flow towards a stretching/shrinking sheet in a micropolar fluid with a convective surface boundary condition. *Can. J. Chem. Eng.*, 90:621–626, 2012.

[105] K.A. Yih. Coupled heat and mass transfer by free convection over a truncated cone in porous media: Vwt/vwc or vhf/vmf. *Acta Mechanica*, 137:83–97, 1999a.

[106] K.A. Yih. Effect of radiation on natural convection about a truncated cone. *International Journal of Heat and Mass Transfer*, 42:4299–4305, 1999b.